Dynamique climatique de l'océan Pacifique ouest équatorial au cours du Pléistocène récent

Thibault de Garidel-Thoron

UNIVERSITE DE DROIT, D'ECONOMIE ET DES SCIENCES D'AIX-MARSEILLE
(AIX-MARSEILLE III)
ECOLE DOCTORALE SCIENCES DE L'ENVIRONNEMENT

N° attribué par la bibliothèque
|__|__|__|__|__|__|__|__|__|__|__|

T H E S E

pour obtenir le grade de

DOCTEUR DE L'UNIVERSITE DE DROIT, D'ECONOMIE ET DES SCIENCES D'AIX-MARSEILLE

(AIX-MARSEILLE III)

Discipline : Géosciences de l'Environnement

présentée et soutenue publiquement

par

Thibault de GARIDEL-THORON

Le 19 juillet 2002

Titre :

DYNAMIQUE CLIMATIQUE DE L'OCEAN PACIFIQUE OUEST EQUATORIAL AU COURS DU PLEISTOCENE RECENT

_____

Directeur de thèse :

M. Luc BEAUFORT

_____

JURY

M. Edouard BARD, Professeur, Collège de France	Co-directeur
M. Luc BEAUFORT, Chargé de Recherche CNRS, Aix-en-Provence	Directeur de thèse
Mme. Elsa CORTIJO, Chargée de Recherche CNRS, Gif-sur-Yvette	Examinateur
M. Patrick DE DECKKER, Professeur, Australian National University	Rapporteur
M. Dick KROON, Professeur, Vrije Universteit Amsterdam,	Rapporteur
M. Nicolas THOUVENY, Professeur, Université de la Méditerranée	Examinateur

Remerciements :

Je remercie Luc Beaufort de la confiance et de la liberté qu'il m'a accordé au cours de ces quatre dernières années pour mes travaux de recherche. Je voudrais lui témoigner du plaisir que j'ai eu à travailler avec lui, du Marion-Dufresne au CEREGE et lui exprimer toute ma reconnaissance pour son aide enthousiaste.

Je remercie Mme Elsa Cortijo, MM. Edouard Bard, Dick Kroon, Patrick De Deckker, et Nicolas Thouveny d'avoir accepté de participer à l'évaluation de ce travail.

Je remercie parmi les personnes avec qui j'ai eu le plaisir de travailler, Edith Vincent qui m'a fait découvrir la taxonomie des foraminifères planctoniques, Franck Bassinot pour sa vision du monde de la géochimie isotopique, Edouard Bard et sa connaissance indéfectible de la paléocéanographie, Brad Linsley, Alan Mix, Lucas Lourens, Nicolas Thouveny et enfin Patrick De Deckker qui m'a ouvert la piste des Orbulines et m'a permis d'utiliser des données non publiées.

Merci à Philippe Dussouillez pour son travail sur SYRACO qui a permis de rendre opérationnel le système d'acquisition automatique d'images sur la loupe binoculaire.

L'aboutissement (?) de ce travail correspond à la fin d'un séjour de plus de quatre années passées au sein du CEREGE. Je remercie en premier lieu Noelle Buchet de m'avoir supporté dans son bureau sans jamais ciller sur le désordre entourant mon bureau et colonisant le sien progressivement. Merci également à tous les jeunes "étudiants-chercheurs", de l'ancienne génération à la nouvelle croisés au désormais célèbre "chez Brigitte", Olivia, Denis, Delphine, Corinne, Ouassila, Eva, Claire, Gilles, Doriane future partenaire de la French Connection à Rutgers, Yannick, Florian, Anne, Doris, Sarah, Jérôme (le catalan), Julien, Martine, Bruno, Christophe et ceux que j'oublie...

Je voudrais remercier en particulier Yannick pour son soutien amical, particulièrement précieux pendant ces derniers mois, et lui exprimer toute mon amitié.

Car il y a de la vie en dehors de l'Arbois, et plus certainement que sur les météorites martiennes chères à Jérôme et Maria, merci aux extra-CEREGE, Guillemette, Estelle et spécialement Camille rencontrées en mer ou dans les montagnes, dont les conversations scientifiques (ou pas) ont contribué plus ou moins directement à ce manuscrit.

J'exprime ma reconnaissance aux jeunes maîtres de conférences, Yann, Laurence, Pierre-Etienne ainsi qu'aux autres demi-hatères Yannick et Jérôme, qui m'ont aidé dans le montage de mes enseignements et m'ont fait gagner un temps précieux pour la rédaction.

Un grand merci également à mes deux familles, ma famille pour son soutien constant, et ma famille "adoptive", chez qui tout est plus simple.

Et bon courage aux futurs docteurs qui ne liront de cette thèse que les remerciements…
Un dernier et ultime merci à Marion.
The end.

Cette thèse a été financée grâce à une allocation du Ministère de la Recherche, et par un contrat d'ATER à l'université d'Aix-Marseille III.

A mes parents

TABLE DES MATIERES

Dynamique glaciaire-interglaciaire

Morphométrie des foraminifères et paléocéanographie

Introduction :

L'augmentation des températures moyennes de l'hémisphère nord au cours du 20eme siècle a posé la question de la séparation de la variabilité climatique naturelle de celle liée à l'action anthropique. Pour pouvoir déconvoluer l'action humaine, il est nécessaire de décrire et de quantifier les variations climatiques naturelles qui ont affectées le climat terrestre, et d'estimer la part relative des mécanismes associés à ces variations. Ce travail de thèse s'inscrit dans cette vaste problématique de description et de quantification de la variabilité naturelle du climat.

A. Introduction Générale

Au cours des deux derniers millions d'années, la Terre a connu une succession de longues périodes glaciaires pendant lesquelles les hautes latitudes étaient recouvertes de glace, alternant avec de courtes périodes interglaciaires dont font partie les 10 000 dernières années (Holocène). Cette succession de périodes glaciaires et interglaciaires a suivi des périodicités d'environ 100 000 ans au cours des derniers 800 000 ans. Des changements de périodes de 41 000 et environ 21 000 ans marquent également les enregistrements paléoclimatiques. Ces changements climatiques ont été liés aux modifications périodiques de la distribution de l'insolation créées par les oscillations orbitales de la terre, appelées cycles de Milankovitch qui possèdent les mêmes caractéristiques spectrales. Ainsi, le cycle de 100 000 ans correspond-il aux variations de l'excentricité de l'orbite de la terre autour du soleil, le cycle de 41 000 ans à l'obliquité de l'axe de rotation de notre planète et le cycle d'environ 21 000 ans à la précession des équinoxes. Ces deux derniers paramètres influencent la distribution spatiale et saisonnière de l'insolation, alors que l'excentricité module la quantité absolue d'énergie solaire reçue. Depuis la formulation de cette théorie par Milankovitch, et sa confirmation par les travaux des 30 dernières années subsiste la question de l'intervention de fortes boucles de rétroactions positives dans le système climatique, indispensables à l'amplification des faibles variations d'insolation.

Les enregistrements climatiques des carottes de glace polaires ont montré que les variations de concentration en CO_2 atmosphérique suivent ces cycles glaciaires-interglaciaires, variations comprises par exemple entre 280 ppm pour l'Holocène et 180 à 200 ppm pour le dernier maximum glaciaire, il y a environ 21 000 ans (Petit et al., 1999). Le CO_2 étant un gaz à effet de serre, des travaux de modélisation ont permis de mettre en évidence son rôle important dans les changements climatiques à l'échelle glaciaire-interglaciaires. Outre des processus uniquement liés aux modifications physico-chimiques de l'océan, de telles variations du cycle du carbone impliquent (a) l'extraction de carbone de l'océan de surface par l'action de la pompe biologique qui va fixer sous forme de calcite le CO_2

dissous dans la colonne d'eau, et (b) des changements associés dans le budget des carbonates de calcium marins. Dans l'état actuel des connaissances, les pompes biologiques des basses et hautes latitudes ont toutes deux joué un rôle dans ce piégeage du CO_2 (Sigman and Boyle, 2000).

Aux basses latitudes, les sédiments carbonatés attestent du fonctionnement de la pompe biologique au cours du temps. En effet, ces sédiments sont majoritairement constitués de coccolithes et de tests de foraminifères planctoniques. Les coccolithophoridés qui sécrètent les plaques de calcite microscopiques (environ 5 µm) appelées coccolithes sont des organismes phytoplanctoniques, alors que les foraminifères planctoniques (200 à 500 µm environ) font partie du zooplancton. L'étude de ces organismes va permettre de reconstituer au cours du temps les changements d'activité de la pompe biologique. Comme ces organismes vivent dans la zone de mélange océanique, qui est influencée par les conditions atmosphériques de surface, leurs microfossiles vont également être des témoins des conditions paléoclimatiques.

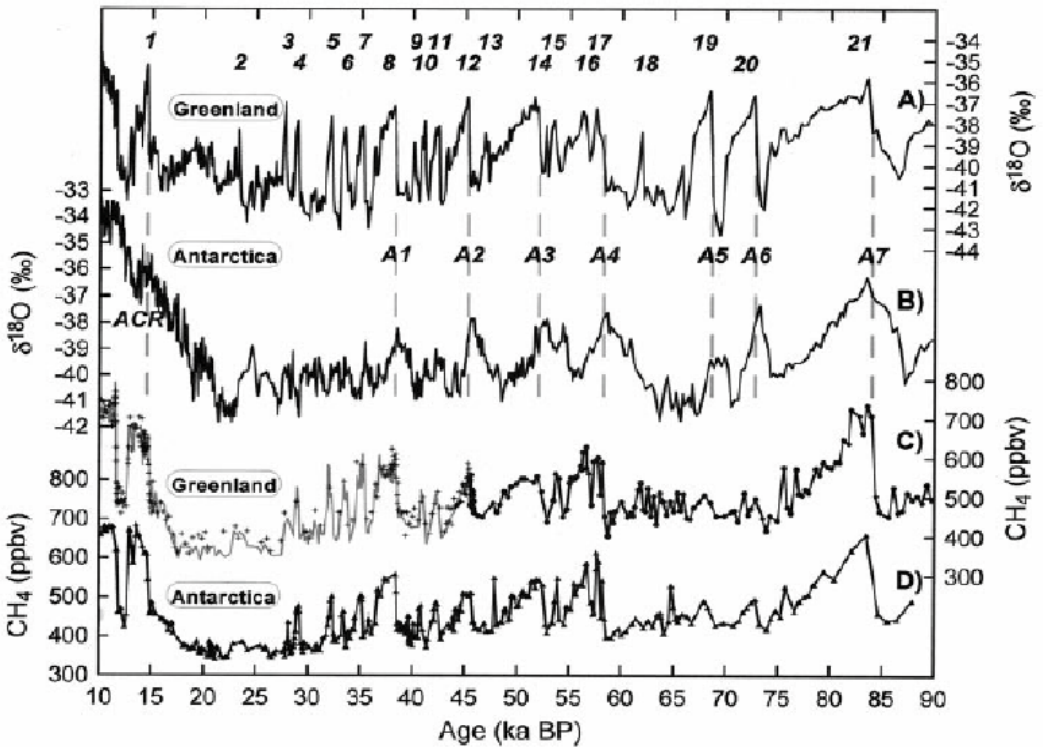

Figure 1 : événements de Dansgaard/Oeschger révélés par les isotopes de l'oxygène dans la carotte de glace GRIP du Groenland (numérotés de 1 à 21). En comparaison figurent les variations observées dans l'Antarctique, et les variations de concentration en méthane atmosphérique (d'après (Blunier and Brook, 2001))

Depuis une dizaine d'années, un nouveau champ de recherches s'est ouvert avec les études paléoclimatiques à haute résolution. Ainsi, l'analyse à haute résolution des isotopes de l'oxygène dans les carottes de glace du Groenland, a permis de mettre en évidence des changements abrupts du climat pendant les 60 000 dernières années (Dansgaard et al., 1993). Ces changements abrupts, les événements de Dansgaard/Oeschger, débutent par un réchauffement abrupt des températures atmosphériques au Groenland de 5-10°C en quelques décennies ou moins, et sont suivis par un

refroidissement graduel sur quelques centaines ou milliers d'années (figure 1.). Le refroidissement accélère pour atteindre la phase la plus froide du cycle (stadiaire). Ces oscillations de température sont également associées à des changements significatifs de la concentration atmosphérique en gaz à effets de serre (le CH_4 par exemple), qui ont sans doute joué un rôle d'amplificateur comme au cours des cycles glaciaire/interglaciaires (Alley et al., 1999). La durée moyenne d'un cycle est d'environ 1500 ans. L'étude des carottes sédimentaires de l'Atlantique Nord montre que ces changements de température sont à mettre en relation avec des modifications de la circulation océanique.

Dans l'Atlantique Nord, le réchauffement différentiel des basses latitudes par rapport aux hautes latitudes tend à accélérer la circulation des eaux de surface vers les pôles, alors que l'évaporation aux basses latitudes, et l'apport d'eaux peu salées aux hautes latitudes tendent inversement à réduire cette circulation. Actuellement, le gradient thermique joue un rôle plus critique que celui du gradient de salinité des eaux de surface. Ainsi, le flux d'eaux de surface chaudes chaudes vers le Nord est contrebalancé par la formation des eaux profondes Nord-Atlantique dans les mers Nordiques qui plongent vers le Sud. Il n'existe pas dans les autres océans de similaires zones de convection. Les eaux profondes Nord-Atlantique vont donc alimenter une boucle de circulation océanique globale, la circulation thermohaline (figure 2).

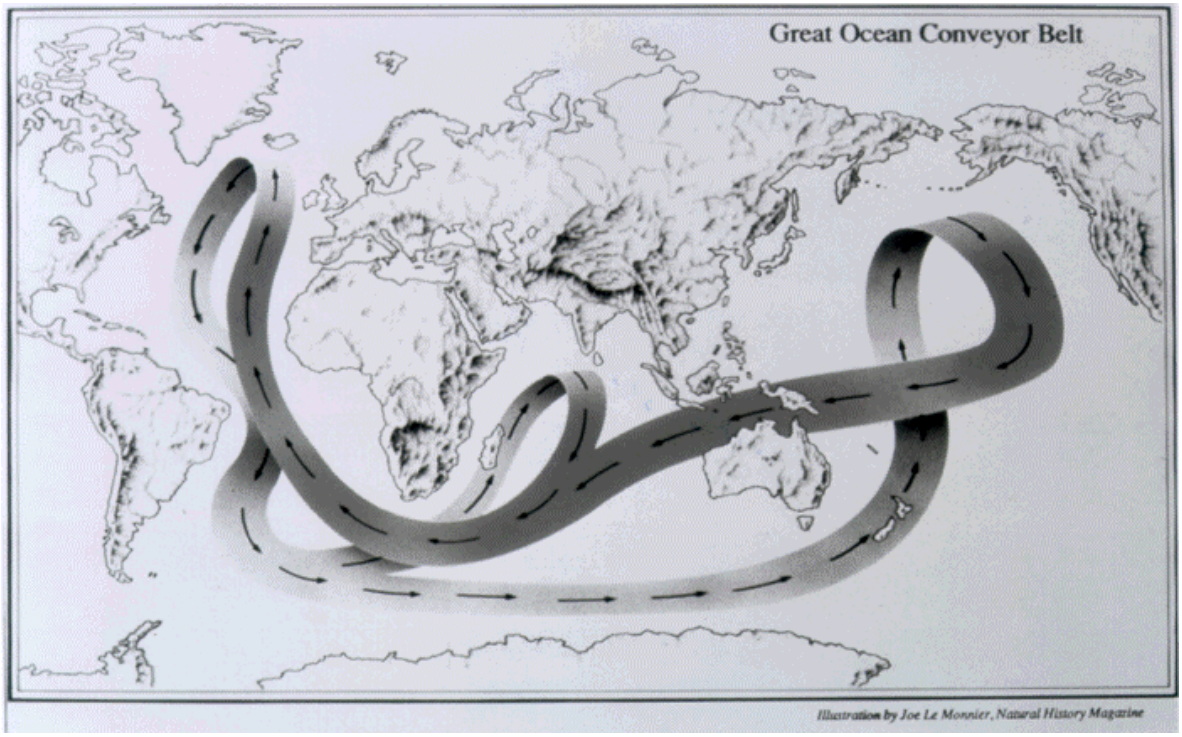

Figure 2 : Schéma de la circulation thermohaline globale (d'après Broecker, 1998)

L'analyse des carottes sédimentaires de l'Atlantique Nord a permis de mettre en évidence l'existence de trois différents régimes de la circulation thermohaline caractérisés par des intensités spécifiques de formation d'eaux profondes et par la localisation des zones de convection

océaniques(Alley et al., 1999). Ces changements d'intensité de la circulation thermohaline sont associés aux événements climatiques de Dansgaard/Oeschger. Schématiquement, les périodes de réchauffement rapide culminant à des températures comparables à celles modernes – les interstadiaires, correspondent à une reprise de la circulation thermohaline, qui suivent des périodes froides pendant lesquelles la circulation thermohaline était plus ou moins ralentie. En particulier, celle-ci était très fortement réduite lors des événements de Heinrich, gigantesques débâcles d'icebergs dans l'Atlantique Nord qui ponctuent certains stadiaires du dernier stade glaciaire.

La variabilité climatique Dansgaard/Oeschger détectée pour la première fois dans les régions circum-Atlantique n'est pas spécifique à cette zone. Les variations de concentration en méthane atmosphérique des carottes de glaces polaires, supportent l'idée d'une dynamique similaire du cycle hydrologique aux basses latitudes, la source principale du méthane étant les zones humides des basses latitudes(Chappellaz et al., 1993). De nombreux enregistrements montrent que les événements de D/O ont été présents aux basses latitudes, même si le phasage précis est encore incertain. Par exemple des enregistrements de mousson indienne sur la marge Pakistanaise (Schulz et al., 1998), d'oxygénation dans le bassin de Santa Barbara(Behl and Kennet, 1996), tous deux à des basses latitudes, montrent également une dynamique de type D/O.

Le cycle hydrologique aux basses latitudes est donc une des questions majeures concernant la variabilité climatique, que ce soit à l'échelle glaciaire-interglaciaire, ou que ce soit pour les événements de type D/O . En effet, la vapeur d'eau est le principal gaz à effet de serre, et peut donc jouer un rôle d'amplificateur dans le système climatique, tout comme le CO_2 et le CH_4. De plus la circulation thermohaline, dont les variations sont reconnues comme ayant un impact global aux échelles de temps glaciaire-interglaciaire et millénnales, est fondamentalement influencée par les gradients de salinité entre les basses latitudes et les hautes.

A l'échelle interannuelle par exemple, des travaux récents ont mis en évidence le lien entre l'intensité de la circulation thermohaline et la distribution spatiale des températures de surface de l'océan Pacifique équatorial. Tout comme de larges débâcles d'icebergs influent la dynamique de la circulation thermohaline, des modifications des quantités d'eau douce transférées entre le Pacifique et l'Atlantique modulent l'intensité de la convection dans l'océan Atlantique Nord (Schmittner et al., 2000) Cette influence du système couplé océan-atmosphère des basses latitudes, a été également démontrée à l'échelle glaciaire-interglaciaire (Schmittner and Clement, 2002).

Le rôle des tropiques est donc fondamental dans la circulation océanique globale, et en particulier la circulation thermohaline. La zone intertropicale étant celle recevant le plus d'énergie solaire, elle est également à l'origine des grands processus atmosphériques. A l'échelle saisonnière, les systèmes de mousson permettent de transférer de très grandes quantités d'énergie d'un hémisphère à l'autre ; que ce soit dans l'océan Indien avec la mousson Indienne, ou que ce soit dans l'océan

Pacifique avec la mousson Est-Asiatique. A l'échelle interannuelle, le phénomène d'El Nino-Oscillation Australe (désigné par l'acronyme ENSO, d' « El Nino-Southern Oscillation ») est la première cause de variabilité climatique globale par le biais des téléconnexions. Ces deux phénomènes prennent leur source dans la zone d'eaux chaudes du Pacifique ouest équatorial (en anglais, « Western Pacific Warm Pool ») qui avec des eaux de surface toujours plus chaudes que 28°C constitue le centre de convection le plus actif de l'atmosphère du globe.

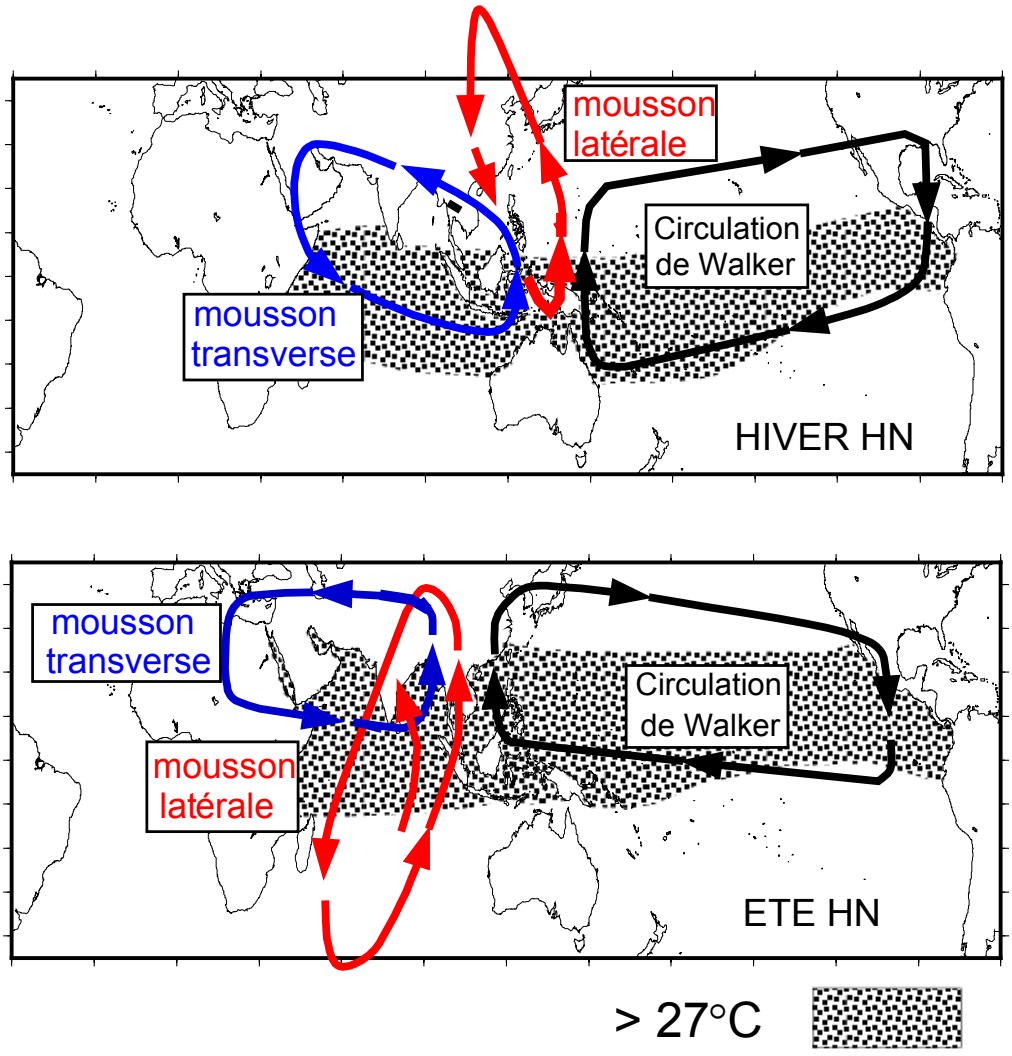

figure 3 : cellules de circulations atmosphériques (d'après Webster, 1998)

Le maintien des températures de surface très chaudes dans le Pacifique ouest est lié à la cellule de Walker zonale (1) qui par la tension des alizés sur les eaux de surface de l'océan Pacifique équatorial empile sur la marge occidentale une lentille d'eau chaude. Cette structure est marqué par un gradient des températures de surface entre le Pacifique ouest et la marge américaine, accompagné d'une pente de la thermocline, la thermocline étant plus profonde dans l'ouest Pacifique. Périodiquement, tous les 3 à 6 ans actuellement, cette structure zonale est perturbée lors des

événements de El Nino. Le centre de convection est déplacé vers l'Est Pacifique, alors que les alizés sont affaiblis, une anomalie positive de température se propage vers l'Est le long de l'équateur. La pente de la thermocline le long de l'équateur est également modifiée, avec un approfondissement significatif vers les marges américaines, et une remontée dans l'Ouest Pacifique.

Deux autres systèmes de circulation atmosphériques sont liés à l'existence de cette zone d'eaux chaudes (Webster et al., 1998). (2) La seconde cellule atmosphérique est méridionale, et correspond au phénomène saisonnier de mousson Asiatique. Cette cellule de mousson latérale, est très active dans le Pacifique ouest pendant l'hiver boréal (mousson d'hiver Est-asiatique). (3) Une troisième cellule transverse relie l'Afrique de l'Ouest à l'archipel Indonésien. Cette cellule constitue un dipôle comparable à la circulation de Walker de l'océan Pacifique, mais elle est également fortement influencée par l'orographie (plateau Tibétain) et la migration de la zone de convergence intertropicale (Saji et al., 1999).

Si le Pacifique équatorial occidental fait l'objet de nombreuses études sur la dynamique climatique actuelle, la variabilité paléoclimatique reste peu étudiée et très discutée. La première raison de la relative absence de travaux sur cette zone, tient à la rareté des enregistrements sédimentaires possédant un taux de sédimentation adapté aux études des derniers cycles climatiques. Cette rareté des enregistrements est elle-même lié à la configuration bathymétrique du Pacifique ouest, la plus grande partie des fonds océaniques étant à une profondeur plus grande que celle de préservation des carbonates. Les meilleurs enregistrements disponibles jusqu'à présents ne possédaient pas de taux de sédimentation suffisants pour offrir une résolution permettant de s'affranchir de l'effet de lissage de la bioturbation. Une deuxième raison des grandes discussions concernant le Pacifique ouest, est liée aux conditions environnementales exceptionnellement chaudes qui sont rarement prises en compte dans les gammes de calibrations des marqueurs (« proxies ») environnementaux.

Les carottes sédimentaires prélevées au cours de la campagne océanographique IMAGES III-IPHIS du Marion-Dufresne dans l'océan Pacifique occidental équatorial (figure 4) nous ont permis d'étudier avec des taux de sédimentation uniques la variabilité paléoclimatique de cette zone. L'abondance en microfossiles carbonatés dans ces sédiments en font des outils adaptés pour tracer la dynamique des eaux superficielles du Pacifique équatorial occidental au cours du Pléistocène récent. Cette thèse décrit la variabilité climatique de cette zone, de l'échelle millénnale à celle des cycles orbitaux.

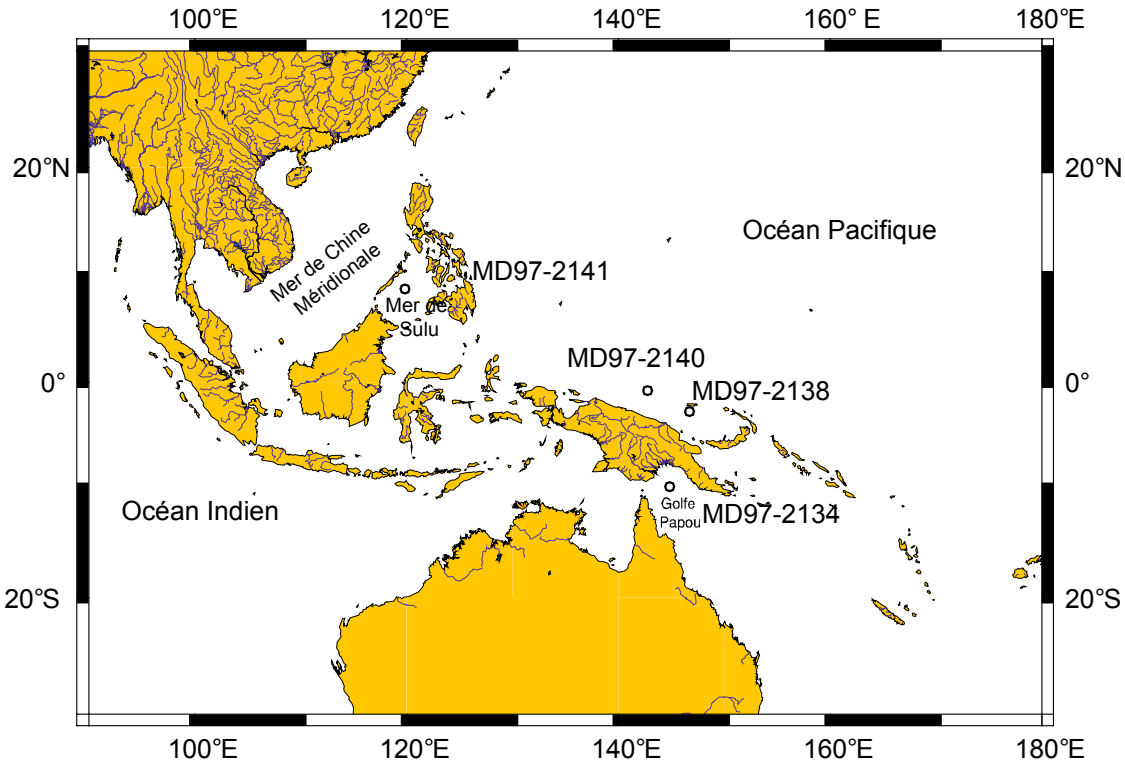

Figure 4 : carte de localisation des carottes étudiées

B. Structure de cette thèse

Formellement, la plus grande partie des résultats obtenus pendant cette thèse ont fait l'objet de rédaction d'articles en anglais. J'ai fait le choix de conserver les articles originaux, en introduisant brièvement chaque article par un exposé de la problématique scientifique, en détaillant les méthodes utilisées dans chaque article, et en résumant les principaux résultats. Les chapitres ont été classés dans trois parties dont la séparation est nécessairement arbitraire, et ne permet pas de s'affranchir des recoupements entre ces différentes parties. La première partie concerne les changements climatiques à l'échelle millénnale du climat dans le Pacifique Ouest. La seconde partie se concentre sur les changements à l'échelle glaciaire-interglaciaire. Et enfin, la dernière partie traite plus spécifiquement des méthodologies concernant les foraminifères planctoniques.

I - Dynamique paléoclimatique rapide :

Le premier chapitre décrit un enregistrement à haute résolution de la Production Primaire en mer de Sulu, un marqueur de la dynamique de la mousson d'hiver. Dans ce chapitre, nous discutons des problèmes de téléconnexions entre la mousson Est-asiatique et les hautes latitudes pour les événements de Dansgaard-Oeschger. Nous nous sommes également attaché à décrire finement les caractéristiques spectrales de cet enregistrement, pour tester la stabilité dans le temps des fréquences suborbitales.

Le deuxième chapitre concernant les changements climatiques rapides décrit un enregistrement à très haute résolution de l'hydrologie de surface du Golfe Papou. Nous montrons que de brusques relargages de méthane se sont produits pendant le dernier stade glaciaire *l.s.* dans la mer de Corail. Ces relargages sont interprétés comme étant liés à la dissociation thermique de gaz hydrates de méthane pendant les bas niveaux marins. Ces relargages peuvent avoir un effet de rétroaction positive important pour le climat global.

II - Dynamique glaciaire/interglaciaire

Le premier chapitre décrit un nouvel enregistrement des températures des eaux de surface dans le cœur du réservoir d'eau chaude du Pacifique Ouest, qui remet en accord les valeurs de températures estimées par les données issues des comptages de foraminifères planctoniques de celles estimées par les alkénones. Une nouvelle fonction de transfert évitant des biais liés selon nous à la structure des écosystèmes a été développée pour toute la bande équatoriale sauf le Pacifique Est. Cet enregistrement confirme les estimations de température au dernier maximum glaciaire de CLIMAP.

Le deuxième chapitre décrit une série d'enregistrements de production primaire le long de l'équateur dans les océans Indo-Pacifiques. La profondeur de la thermocline le long de l'équateur apparaît suivre un balancement entre le Pacifique équatorial occidental d'une part, et le Pacifique Est et l'Ouest de l'océan Indien d'autre part, à l 'échelle de la précession. Ce mécanisme est analogue à celui de l'ENSO, et de la cellule de circulation atmosphérique de la mousson indienne qui actuellement sont présents à l'échelle interannuelle. L'existence d'un cycle à 30 000 ans dans ces enregistrements, similaire à celui observé dans les variations de concentration atmosphériques en CO2, souligne le rôle de la pompe biologique aux basses latitudes.

III – Morphométrie des foraminifères planctoniques :

L'étude du génotype de foraminifères planctoniques a mis en évidence une diversité cryptique insoupçonnée auparavant. Celle-ci nécessite un effort de caractérisation morphométrique. Ce premier chapitre prend l'exemple d'*Orbulina universa* dans le Pacifique ouest. En utilisant les critères de porosité et de taille moyenne du test de ce foraminifère nous caractérisons la diversité morphologique de cette espèce. La calibration des ces deux critères en fonction de divers paramètres environnementaux a été ensuite testée dans deux enregistrements sédimentaires du Pacifique ouest.

La reconnaissance automatique des foraminifères qui permettrait d'étudier en routine la morphométrie des foraminifères, et donc de tester de nouvelles fonctions de transfert basées sur une taxonomie quantitative a fait l'objet d'une étude préliminaire. La méthode des réseaux de neurones a été appliquée avec succès au nannoplancton. Nous montrons dans ce chapitre les résultats préliminaires de cette méthodologie adaptée aux foraminifères planctoniques.

Références :

Alley, R.B., Clark, P.U., Keigwin, L.D., and R.S., W., 1999, Making sense of millennial-scale climate change, Mechanisms of global climate change at millennial time scales, Volume 112: Geophysical Monograph, American Geophysical Union, p. 385-394.

Behl, R., and Kennet, J.P., 1996, Brief interstadial events in the Santa Barbara basin, NE Pacific, during the past 60 kyr: Nature, v. 379, p. 243-246.

Blunier, T., and Brook, E.J., 2001, Timing of millenial-scale climate change in Antarctica and Greenland during the last glacial period: Science, v. 291, p. 109-112.

Chappellaz, J., Blunier, T., Raynaud, D., Barnola, J.-M., Schwander, J., and Stauffer, B., 1993, Synchronous changes in atmospheric methane and Greenland climate between 40 and 8 kyBP: Nature, v. 366, p. 443-445.

Dansgaard, W., Johnsen, S.J., Clausen, H.B., Dahl-Jensen, D., Gundestrup, N.S., Hammer, C.U., Hvidberg, C.S., Steffensen, J.P., Sveinbjörnsdottir, A.E., Jouzel, J., and Bond, G., 1993, Evidence for general instability of past climate from a 250 kyr ice-core record: Nature, v. 364, p. 218-220.

Petit, J.R., Jouzel, J., Raynaud, D., Barkov, N.I., Barnola, J.-M., Basile, I., Bender, M., Chappelaz, J., Davis, M., Delaygue, G., Delmotte, M., Kotlyakov, V., Legrand, M., Lypenkov, V.Y., Lorius, C., Pépin, L., Ritz, C., Saltzman, E., and Stievenard, M., 1999, Climate and atmospheric history of the past 420,000 years from the Vostok ice-core, Antartica: Nature, v. 399, p. 429-436.

Saji, N.H., Goswani, B.N., Vinayachandran, P.N., and Yamagata, T., 1999, A dipole mode in the Indian Ocean: Nature, v. 401, p. 360-362.

Schmittner, A., Appenzeller, C., and Stocker, T., 2000, Enhanced Atlantic freshwater export during El Niño: Geophysical Research Letters, v. 27, p. 1163-1166.

Schmittner, A., and Clement, A.C., 2002, Sensitivity of the thermohaline circulation to tropical and high latitude freshwater forcing during the last glacial-interglacial cycle: Paleoceanography, v. 17, p. 10.1029/2000PA000591.

Schulz, H., von Rad, U., and Erlenkeuser, H., 1998, Correlation between Arabian Sea and Greenland climate oscillations of the past 110,000 years: Nature, v. 393, p. 54-57.

Sigman, D.M., and Boyle, E.A., 2000, Glacial/interglacial variations in atmospheric carbon dioxide: Nature, v. 407, p. 859-869.

Webster, P.J., Magaña, V.O., Palmer, T.N., Shukla, J., Tomas, R.A., Yanai, M., and Yasunari, T., 1998, Monsoons: processes, predictability, and the propects for prediction: Journal of Geophysical Research, v. 103, p. 14451-14510.

Partie I

-

Dynamique Climatique Rapide

Chapitre 1 : Variabilité millénnale de la mousson d'hiver Est-Asiatique

Même si les variations rapides du climat étaient suspectées depuis les années 1970 (e.g. (Pisias et al., 1973)), l'analyse à haute résolution des carottes de glace a révélé l'existence de variations abruptes du climat au cours des 60000 dernières années dans les régions circum-Atlantique (Dansgaard et al., 1993). Ces variations abruptes ont également été décelées dans des enregistrements de basses latitudes, par exemple dans des enregistrements de température dans l'océan Atlantique Nord (Sachs and Lehman, 1999). Des événements similaires ont également été mis en évidence dans enregistrements sédimentaires d'intensité de la mousson indienne (Schulz et al., 1998) ; ou dans le Pacifique Est (Behl and Kennet, 1996). La dynamique de la zone Est-asiatique à l'échelle millénnale restait mal connue. Des changements abrupts de l'intensité de la mousson d'hiver Est-asiatique déduits d'enregistrements granulométriques de séquences de loess-paléosols ont été corrélés aux changements abrupts du Groenland pendant le dernier stade glaciaire (Porter and Zhisheng, 1995). Cependant, l'absence de cadre chronologique bien contraint empêche ces séries d'être interprétée trop en avant. En outre, (Xiao et al., 1999) ont montré l'existence d'événements supplémentaires, à ceux révélés dans l'étude de (Porter and Zhisheng, 1995), indiquant la complexité de la dynamique de la mousson d'hiver, et la nécessité d'enregistrements sédimentaires marins aux taux de sédimentation plus constants.

Des cycles climatiques d'environ 1500 ans ont également fait l'objet de descriptions détaillées dans les reconstructions climatiques déduites de l'analyse des carottes de glace (Mayewski et al., 1997; Stuiver and Braziunas , 1993) ainsi que dans les enregistrements sédimentaires de l'Atlantique Nord (Bianchi and McCave, 1999; Bond et al., 1997). Si une telle cyclicité semble une caractéristique robuste de la circulation thermohaline, son existence potentielle aux basses latitudes n'a pas encore fait l'objet d'études détaillées. Dans cette étude, grâce à un enregistrement à très haute résolution de la productivité primaire déduite de la nannoflore, nous caractérisons dans les domaines temporels et fréquentiels la variabilité climatique millénnale de la mousson d'hiver est-asiatique. Nous avons fait le choix dans cette étude de ne pas utiliser l'ajustement de notre modèle d'âge avec celui des carottes de glace pour éviter la formulation *a priori* d'une relation entre la température au Groenland et le climat dans le Pacifique équatorial.

Méthodes :

Les coccolithophoridés sont des organismes phytoplanctoniques vivants dans les couches océaniques de surface. Ces organismes photosynthétiques sont très sensibles à la luminosité ainsi qu'aux conditions trophiques. Dans les eaux de surface, le principal facteur limitant pour le

développement des coccolithophoridés est la concentration en nutriments. Plus en profondeur, les nutriments sont plus abondants, mais c'est la luminosité qui devient le facteur limitant. La composition spécifique des coccolithophoridés dans la colonne d'eau reflète cette stratification.

Figure 2.1 : Photographie en Microscopie à Balayage Electronique de *Florisphaera profunda*

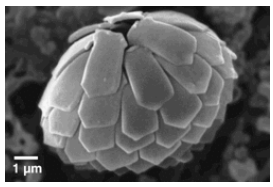

Dans les eaux les plus profondes, l'espèce *Florisphaera profunda* (figure 2.1) domine l'assemblage avec l'espèce *Gladiolithus flabellatus*, alors que dans les eaux superficielles, les autres coccolithophoridés sont plus abondants (Molfino and McIntyre, 1990; Okada and Matsuoka, 1994). Le rapport d'abondance entre *F. profunda* et les autres coccolithes est donc lié à la quantité de nutriments qui peuvent être remontés vers les eaux superficielles. Si les eaux de surface sont riches en nutriments, *F. profunda* sera peu abondante, et inversement (figure 2.2). *F. profunda* sera donc relativement moins abondant dans les eaux à forte production primaire, et plus abondante dans les eaux à faible production primaire.

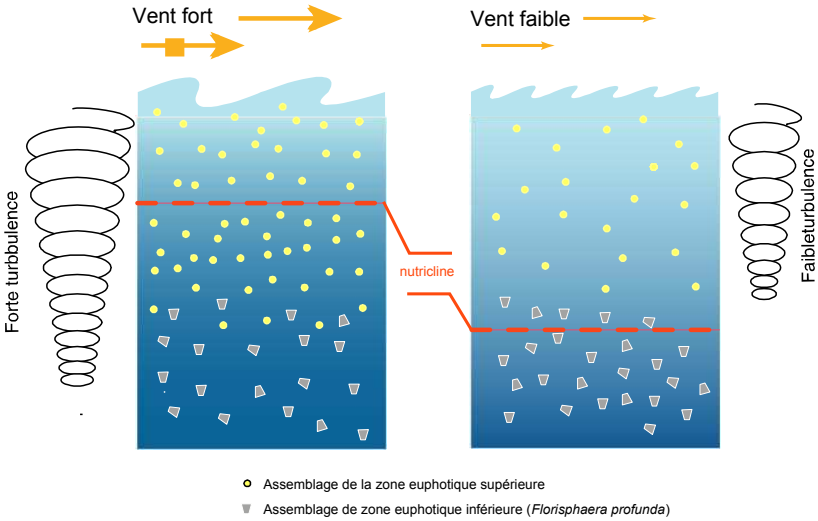

Figure 2.2 : Schéma décrivant la relation entre abondance de Florisphaera profunda et la profondeur de la nutricline. Dans ce schéma, la tension des vents, par pompage d'Ekman est supposé le principal facteur de remontée de nutriments dans la colonne d'eau.

Cette relation a été vérifiée et quantifiée sur des sédiments de surface de l'océan Indien (figure 2.3)(Beaufort et al., 1997). Les données de production primaire sont extraites de l'atlas (Antoine et al., 1995). Ces auteurs ont couplé les images couleurs satellitales, avec des algorithmes permettant d'intégrer la production primaire dans la colonne d'eau.

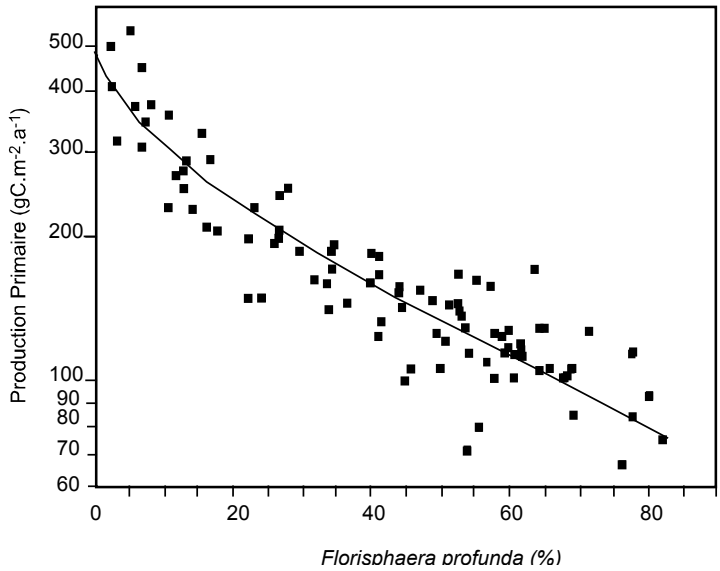

Figure 2.3 : Calibration de la relation entre Florisphaera profunda et la production primaire (d'après (Beaufort et al., 1997)).

Résumé de l'article :

Cette calibration a été appliquée aux comptages de *Florisphaera profunda* effectués à haute résolution dans la carotte MD97-2141 située dans la mer de Sulu qui enregistre les 200 000 dernières années. Actuellement, la production primaire est linéairement reliée à la vitesse des vents de la mousson d'hiver Est-asiatique. Les variations de production primaire dans cette carotte nous indiquent donc les variations dans l'intensité de la mousson d'hiver Est-Asiatique.

A l'échelle glaciaire-interglaciaire, la production primaire est renforcée pendant les stades glaciaires indiquant un renforcement de la mousson d'hiver en période glaciaire. Pendant le dernier stade glaciaire, huit pics de mousson sont recensés, l'occurrence de ces pics étant également enregistrés dans les séquences loessiques de Chine. Ces pics ne sont pas tous liés aux débâcles massives d'icebergs dans l'Atlantique Nord (événements de Heinrich), la moitié seulement des pics décrits en mer de Sulu étant synchrones avec les événements de Heinrich. Néanmoins, une analyse SSA ('Singular Spectrum Analysis'), analyse en composantes principales d'un signal temporel, ainsi que des analyses spectrales révèlent qu'à l'échelle des Dansgaard-Oeschger une dynamique commune existe entre la mousson d'hiver Est-asiatique et les températures au Groenland. Dans cet enregistrement, la mousson d'hiver Est-asiatique oscille à des périodes d'environ 6 ka, 4.2-3.4, 2.3 et 1.5 ka. Ce cycle de 1500 ans est présent du stade isotopique marin 6 jusqu'à l'Holocène, sans que le volume des glaces ne module ce cycle. Ceci suggère que les cycles de 1500 ans ne sont pas forcés par les hautes latitudes comme précédemment supposés.

Références :

Antoine, D., André, J.-M., and Morel, A., 1995, Oceanic primary production 2. Estimation at global scale from satellite (coastal zone color scanner) chlorophyll: Global Biogeochemical Cycles, v. 10, p. 57.

Beaufort, L., Lancelot, Y., Camberlin, P., Cayre, O., Vincent, E., Bassinot, F., and Labeyrie, L., 1997, Insolation cycles as a major control of equatorial Indian ocean primary production: Science, v. 278, p. 1451-1454.

Behl, R., and Kennet, J.P., 1996, Brief interstadial events in the Santa Barbara basin, NE Pacific, during the past 60 kyr: Nature, v. 379, p. 243-246.

Bianchi, G.G., and McCave, I.N., 1999, Holocene periodicity in North Atlantic climate and deep-ocean flow south of Iceland: Nature, v. 397, p. 515-517.

Bond, G., Showers, W., Chezebiet, M., Lotti, R., Almasi, P., deMenocal, P., Priore, P., Cullen, H., Hajdas, I., and Bonani, G., 1997, A pervasive millenial scale cycle in North-Atlantic holocene and glacial climates: Nature, v. 278, p. 1257-1266.

Dansgaard, W., Johnsen, S.J., Clausen, H.B., Dahl-Jensen, D., Gundestrup, N.S., Hammer, C.U., Hvidberg, C.S., Steffensen, J.P., Sveinbjörnsdottir, A.E., Jouzel, J., and Bond, G., 1993, Evidence for general instability of past climate from a 250 kyr ice-core record: Nature, v. 364, p. 218-220.

Mayewski, P.A., Meeker, L.D., Twickler, M.S., Whitlow, S., Yang, Q., Lyons, W.B., and Prentice, M., 1997, Major features and forcing of high-latitude northern hemisphere atmospheric circulation using a 110,000-year long glaciogeochemical series: Journal of Geophysical Research, v. 102, p. 26345-26366.

Molfino, B., and McIntyre, A., 1990, Precessional forcing of nutricline dynamics in the Equatorial Atlantic: Science, v. 249, p. 766-769.

Okada, H., and Matsuoka, M., 1994, Lower-photic nannoflora as an indicator of the late Quaternary monsoonal palaeo-record in the tropical Indian Ocean, O.D.P. and the Marine Biosphere: Aberystwyth, p. 233-245.

Pisias, N.G., Sancetta, C., and Dauphin, P., 1973, Spectral analysis of late Pleistocene-Holocene sediments: Quaternary Research, v. 3, p. 3-9.

Porter, S.C., and Zhisheng, A., 1995, Correlation between climate events in the North Atlantic and China during the last glaciation: Nature, v. 375, p. 305-308.

Sachs, J.P., and Lehman, S.J., 1999, Subtropical North Atlantic temperatures 60,000 to 30,000 years ago: Science, v. 186, p. 756-759.

Schulz, H., von Rad, U., and Erlenkeuser, H., 1998, Correlation between Arabian Sea and Greenland climate oscillations of the past 110,000 years: Nature, v. 393, p. 54-57.

Stuiver, M., and Braziunas , T.F., 1993, Sun, ocean, climate and atmospheric 14CO2: an evaluation of causal and spectral relationships: The Holocene, v. 3, p. 289-305.

Xiao, J.L., An, Z.S., Liu, T.S., Inouchi, Y., Kumai, H., Yoshikawa, S., and Kondo, Y., 1999, East Asian monsoon variation during the last 130,000 years: evidence from the Loess Plateau of central China and Lake Biwa of Japan: Quaternary Science Reviews, v. 18, p. 147-157.

Millennial-scale dynamics of the East Asian winter monsoon during the last 200,000 years

Thibault de Garidel-Thoron and Luc Beaufort
Centre Européen de Recherche et d'Enseignement en Géosciences de l'Environnement (CEREGE), Aix-en-Provence, France

Braddock K. Linsley and Stefanie Dannenmann
Department of Earth and Atmospheric Sciences, University at Albany, State University of New York, Albany, New York, USA

Abstract: The primary productivity dynamics of the last 200,000 years in the Sulu Sea was reconstructed using the abundance of the coccolithophore *Florisphaera profunda* in the IMAGES MD97-2141 core. We find that primary productivity was enhanced during glacial periods, which we suggest is due to a stronger East Asian winter monsoon. During the last 80 kyr, eight significant increases in primary productivity (PP) in the Sulu Sea are similar to East Asian winter monsoon changes recorded in Chinese loess. The PP maxima are not linked with Heinrich events (HE) in the North Atlantic, although four PP peaks are synchronous with HE. The PP oscillations have frequencies near those of the Dansgaard–Oeschger cycles in Northern Hemisphere ice records and indicate a teleconnection of the East Asian winter monsoon with Greenland climate. In this Sulu Sea record the East Asian winter monsoon oscillates with periodicities of ~6, 4.2–3.4, 2.3, and 1.5 kyr. In particular, the 1.5 kyr cycle exhibits a strong and pervasive signal from stage 6 to the Holocene without any ice volume modulation. This stationarity suggests that the 1.5 kyr cycle is not driven by some high-latitude forcing.

1. Introduction

The coupling between the atmosphere and the ocean is fundamental to climate dynamics over seasonal to millennial timescales. Variations in this coupling influence the oceanic biosphere and particularly the phytoplankton of the upper ocean layer. In low-latitude areas the phytoplanktonic activity quantified by primary productivity (PP) is correlated to the wind stress dynamics on the sea surface [*Nair et al.*, 1989]. Previous studies have concentrated on long-term changes in the PP [e.g., *Beaufort et al.*, 1997; *Mix*, 1989], but little is known about the millennial-scale dynamics of PP.

At present, we know that during the last glacial stage our climate system went through rapid changes that are well documented in the North Atlantic area. Two major types of abrupt changes have been described. Heinrich events are documented massive iceberg discharges of ice-rafted debris to the North Atlantic deep-sea sediments occurring with a periodicity of ~6–7 kyr [*Bond et al.*, 1992; *Heinrich*, 1988]. These events are followed by consecutive abrupt warmings on the Greenland continent. Dansgaard–Oeschger (D–O) climatic oscillations with periods of 1000–3000 years have

been described in the Greenland ice cores records [*Dansgaard et al.*, 1993]. These oscillations correspond to ~15°C air temperature shifts between a stadial (cold phase) and an interstadial (warm phase) [*Jouzel*, 1999].

The Heinrich events are correlative with major changes in the climate dynamics recorded worldwide, from the North Atlantic to the Antarctic. In the Asian region the East Asian winter monsoon strengthened during Heinrich events [*Porter and Zhisheng*, 1995; *Xiao et al.*, 1999]. Planktonic foraminifera assemblage in South China Sea recorded these abrupt changes [*Chen and Huang*, 1998; *Wang et al.*, 1999]. In the Sulu Sea the oxygen isotopes ($\delta^{18}O$) of planktonic foraminifera show important rapid oscillations which appear synchronous with some Heinrich events [*Linsley*, 1996].

For the Dansgaard–Oeschger oscillations recorded in ice cores, similar changes are documented in sea surface temperature (SST) reconstructions, percentage of carbonate, magnetic susceptibility, planktonic foraminifera oxygen isotopic composition, and foraminiferal assemblages records from the North Atlantic Ocean (for a review, see *Cortijo et al.* [2000]). The loess-paleosol record in China exhibits comparable shifts [*Chen et al.*, 1997]. In the Santa Barbara basin a bioturbation index records nearly all stadials and interstadials described in the Greenland record [*Behl and Kennet*, 1996]. At low latitudes, organic carbon changes in the Arabian Sea appear to correlate with D-O cycles [*Schulz et al.*, 1998].

To constrain the past millennial variations of low-latitude paleoproductivity, we investigate, at high-resolution, variations in the coccolith assemblages in IMAGES giant piston core MD97-2141 located in the Sulu Sea (Figure 1).

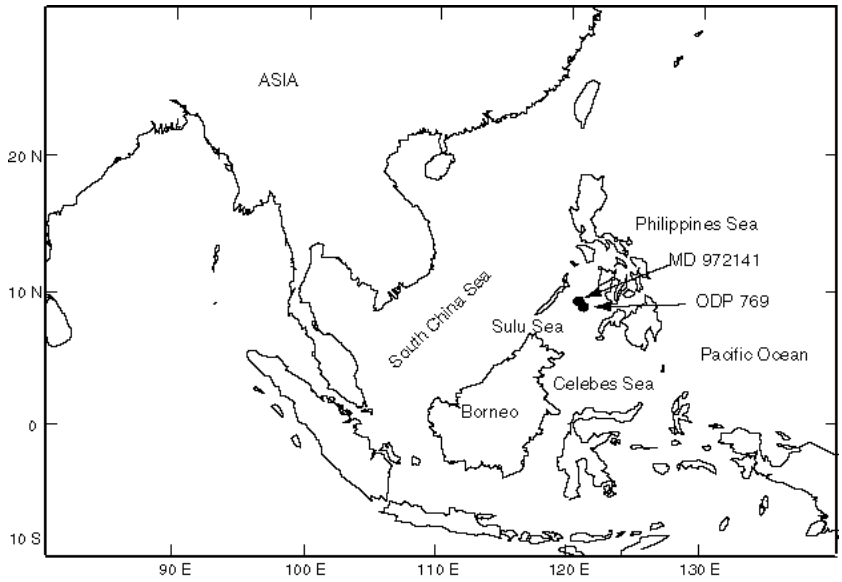

Figure 1. Map of Southeast Asia and of the marginal seas of the western Pacific. Note location of core MD97-2141 in the Sulu Sea.

The Sulu Sea is located between the Asian continent and the "Western Pacific Warm Pool" (WPWP), where annual SST is above 29°C [*Yan et al.*, 1992]. The climate of the Sulu Sea is strongly

influenced by the East Asian monsoon. The East Asian monsoon results from the different potential heating between the WPWP and the Asian continent. During the boreal winter the main heating source is located in the ocean. The latent heat release associated with intense convective precipitation fuels the meridional circulation. Tropical convection in the western equatorial Pacific is connected to the descending branch over the Siberian region, forming a strong local Hadley cell in the East Asian region [*Zhang et al.*, 1997]. The East Asian winter monsoon winds in the Sulu Sea result from the merging of the northerly East Asian monsoon with the Pacific trade winds over the South China Sea [*McGregor and Nieuwolt*, 1998]. East Asian winter monsoon bursts during January to March (Figure 2) can induce blooms of coccolithophorids [*Wiesner et al.*, 1996]. The PP rises correlatively to the wind stress strengthening because of the stronger mixing of the upper ocean (Figure 2) [*Nair et al.*, 1989]. Thus coccolith assemblages record information on both paleoproductivity changes and also on East Asian winter monsoon variations in the Sulu Sea.

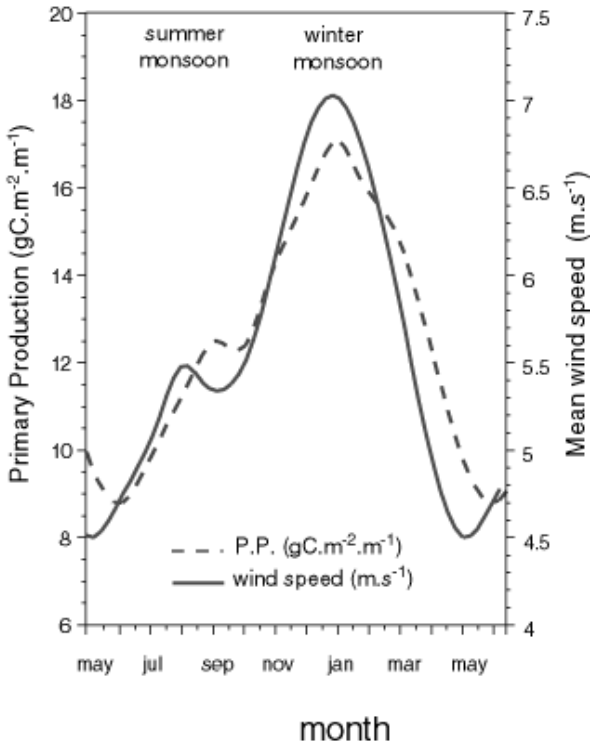

Figure 2. Wind strength in Sulu Sea at 10°N (Comprehensive Ocean-Atmosphere Data Set (COADS) Atlas) and estimated monthly primary production at the same location from *Antoine and Morel* [1996].

2. Material

The 36 m giant piston core IMAGES MD97-2141 (08°47′N, 121°17′E, 3633 m depth) was retrieved during the IPHIS-IMAGES III cruise of the R/V *Marion Dufresne* in May 1997. This position is located in the vicinity of the Ocean Drilling Program (ODP) Site 769 [*Linsley*, 1996]. The core is located on the Cagayan ridge, which protects the site from downslope processes, and above the present lysocline depth (~3800 m), allowing for good preservation of carbonates [*Linsley et al.*, 1985; *Miao et al.*, 1994]. The sediments are composed predominantly of well-preserved nannofossil-foraminifera oozes.

3. Methods

For coccolith counting, the core was sampled every 2 cm in the upper 6 m of the core, allowing for a resolution of ~70 years, and every 3–4 cm in the lower 30 m for a resolution of ~200–500 years. A smear slide was prepared for each sample, and at least 300 coccoliths were counted for each slide (mean of 357 coccoliths) on a Zeiss Axioscop at a 1000× resolution. Percentages of *Florisphaera profunda* (Fp) were computed using the following equation:

$$\%\mathrm{Fp} = 100\ (\text{number Fp})/(\text{total coccoliths})$$

The 95% confidence interval for %Fp varies between ±2 and ±6% depending on the percentage of Fp [*Patterson and Fishbein*, 1989].

Age model for MD97-2141

Depth in core (cm)	AMS ^{14}C Age	Error*	Calendar Age, years	Species/ Age model	Accession Number
1	4 560	± 50	4 798	*G. ruber (white)*	OS-16971
10.5	4 210	± 40	4 286	*G. ruber (white)*	OS-16926
14	4 740	± 40	4 962	*G. ruber (white)*	OS-16410
29	4 700	± 55	4 873	*G. ruber (white)*	OS-16972
59	6 020	± 40	6 416	*G. sacculifer (w/out sac)*	OS-16411
73	6 810	± 55	7 274	*G. sacculifer (w/out sac)*	OS-16973
85	6 830	± 90	7 295	*G. sacculifer (w/out sac)*	OS-18401
94	8 850	± 55	9 455	*G. sacculifer (w/out sac)*	OS-16974
99	10 700	± 90	12 152	*G. sacculifer (w/out sac)*	OS-16975
120	9 380	± 160	10 001	*G. sacculifer (w/out sac)*	OS-16977
150	10 200	± 80	11 045	*G. ruber (white)*	OS-16978
158	10 250	± 120	11 153	*G. sacculifer (w/out sac)*	OS-16980
162	10 750	± 50	12 228	*G. sacculifer (w/out sac)*	OS-16979
205.5	11 750	± 130	13 258	*G. sacculifer (w/out sac)*	OS-17238
212	12 350	± 65	13 931	*G. ruber (white)*	OS-16412
226.5	13 000	± 95	14 796	*G. ruber (white)*	OS-16970
244	14 100	± 70	16 422	*G. ruber (white)*	OS-16413
269	14 750	± 70	17 200	*G. ruber (white)*	OS-16361
282	15 100	± 90	17 591	*G. sacculifer (w/out sac)*	OS-17913
339	17 150	± 140	19 749	*G. ruber (white)*	OS-17914
368	17 650	± 85	20,430†	*G. ruber (white)*	OS-22672
400	18 850	± 140	21847†	*G. sacculifer (w/out sac)*	OS-17916
440	28 000	± 130	32,101†	*G. sacculifer (w/out sac)*	OS-17882
487	30 900	± 260	35,146†	*G. ruber (white)*	OS-17912
506.5	33 000	± 310	37,290†	*G. sacculifer (w/out sac)*	OS-17917
543	33 600	± 590	37,893†	*G. sacculifer (w/out sac)*	OS-17911
553	34 300	± 390	38,790†	*G. sacculifer (w/out sac)*	OS-17915
594	36 900	± 460	41,134†	*G. sacculifer (w/out sac)*	OS-17918
920			59 000	*SPECMAP*	
1150			71 000	*SPECMAP*	
1190			80 000	*SPECMAP*	
1400			99 000	*SPECMAP*	
1450			109 000	*SPECMAP*	
1540			115 000	*SPECMAP*	
1650			131 000	*SPECMAP*	
1790			146 000	*SPECMAP*	
1860			151 000	*SPECMAP*	
2000			171 000	*SPECMAP*	
2200			182 000	*SPECMAP*	
2250			196000	*SPECMAP*	

* Error is given in 1σ

† Calendar ages have been calculated using a 400 year reservoir correction and applying the *Stuiver and Braziunas [1993]* calibration curve for samples younger than 20,000 calendar year in age and a U/Th calibration curve for the samples older than 20,000 calendar years *[Bard et al., 1993]*.

Table 1.

Radiocarbon Ages and Tie Points From the SPECMAP Stack Used in MD97-2141 Chronology[a]

3.1. Age Model

The age model of the core MD97-2141 was developed by *Dannenmann et al.* [1998] and *Oppo et al.* [1998]. It was obtained using 28 accelerator mass spectrometer (AMS) ^{14}C ages on *Globigerinoides ruber* and *G. sacculifer* and by comparison of the planktonic foraminifera $\delta^{18}O$ curve (on *Globigerinoides ruber* and *G. sacculifer* tests) with the SPECMAP stack [*Imbrie et al.*, 1984] (Table 1). The radiocarbon dates were converted to calendar ages using (1) a correction of 400 years, according to the age reservoir of carbon in the ocean [*Bard*, 1988], and then (2) the CALIB3 calibration software [*Stuiver and Reimer*, 1993] to take into account past atmospheric changes in cosmogenic production. All the ages discussed here are calendar ages B.P. The carbon reservoir age in this work is assumed to be invariant with time. We also assumed that the carbon reservoir age changes in the tropical upper oceanic layer where *G. ruber* and *G. sacculifer* live are not varying more than ~200 years [*Duplessy et al.*, 1991]. The last appearance datum of *G. ruber* pink at 1593 cm fits with the Termination II [*Thompson et al.*, 1979], strengthening the validity of the age model (Figure 3). Two ninth-order polynomial regressions were used from the core top to 400 cm and from 440 to 920 cm on the ^{14}C ages and SPECMAP tie points to smooth the sedimentation rate for the last 60 kyr. This smoothing is indispensable for the spectral analyses to avoid spurious peaks linked with sedimentation rates changes.

The average sedimentation rate is ~10.5 cm kyr^{-1}, with maxima during glacial stage 2 of 34 cm kyr^{-1}. For example, the sedimentation rate during the stage 3 is ~30 cm kyr^{-1}, which allows a 70 year resolution (2 cm sampling). A hiatus occurs between 30 and 22 ka (Figure 3). The sedimentation rates are coherent with other records; that is, they are increased during glacial periods and lower during interglacial stages [e.g., *Chen and Huang*, 1998]. Reduced benthic mixing due to dysaerobic conditions in the Sulu Sea lessens the bioturbation smoothing effect [*Kuehl et al.*, 1993]. The sharp transition in the coccolith record at 14.55 ka, occurs within 2 cm, another argument for a weak bioturbation effect.

3.2. Signal analysis

3.2.1. Spectral analysis. To extract the significant periodicities contained in the PP signal, we performed spectral analysis using different algorithms (Blackman-Tukey, maximum entropy, and multitaper methods) provided in the package Analyseries [*Paillard et al.*, 1996]. The comparison of these different methods allows the discrimination of spurious results due to biases of a particular method. We present only the multitaper method (MTM) results here. The MTM is able to detect low-amplitude oscillations in relatively short time series with a high degree of statistical significance [*Thomson*, 1982]. The statistical significance reported in this work is computed using a Fisher test (*F*

test). This *F* test is performed on the amplitude to analyze the harmonic oscillations assuming that the signal contains periodic and separated components [*Yiou et al.*, 1997].

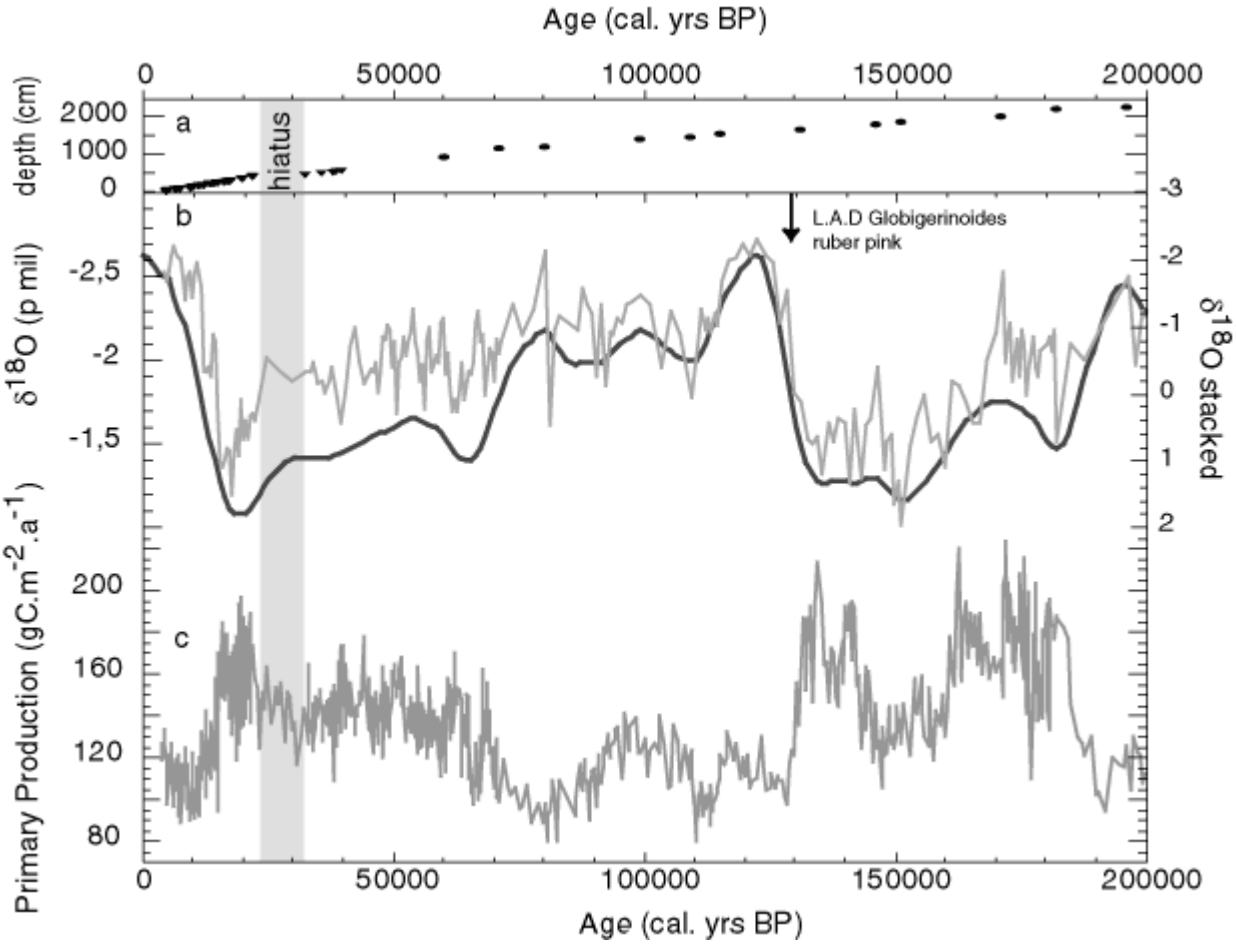

Figure 3. (a) Position of accelerator mass spectrometry (AMS) dates on planktonic foraminifera converted in calendar ages (small triangles) and the SPECMAP tie points used in the stratigraphy (solid circles). Note the hiatus between 400 and 440 cm (shaded area). (b) MD97-2141 $\delta^{18}O$ planktonic foraminifera results at 10 cm intervals (shaded line) compared with the SPECMAP stacked deep-ocean record (thick solid line). (c) MD97-2141 primary productivity (PP) as reconstructed from the coccolithophorid record.

3.2.2. Singular-spectrum analysis. Singular-spectrum analysis (SSA) is designed to extract the information contained in a short, nonstationary, and noisy signal [*Vautard and Ghil*, 1989]. This method is based on the computing of empirical orthogonal functions in the time domain. SSA can give insight into the dynamics of the underlying system that generates the signal. Using data-adaptive filters which are not period dependant, SSA allows the separation of the noise from the trend and the deterministic oscillations of the signal.

3.3. *Florisphaera profunda* : A Paleoproductivity Marker

The coccolithophoridae (Prymnesiophycaea) are phytoplanktonic organisms that live in the oceanic photic zone. They are very sensitive to variations in light and nutrient availability, which are both depth dependent. The lower photic zone is darker and richer in nutrients than the upper photic zone. In the tropical ocean the lower photic zone coccolithophoridae community is dominated by *Florisphaera profunda* associated with *Gladiolithus flabellatus* and *Algirosphaera robusta*, while most of the other species live in the upper photic zone [*Okada and Honjo*, 1973].

When the nutricline is shallow, the upper photic zone species dominate the coccolith community, whereas when the nutricline is deeper, the relative proportion of lower photic community is more important. The depth of the nutricline in the low-latitude open ocean is mainly driven by wind intensity. When winds are strong, the upper layers are well mixed, and the nutrients are upwelled into the upper photic zone. Inversely, when wind stress decreases, the mixing is less effective, and the photic zone is depleted in nutrients. This depth relationship between coccolithophorid communities was successfully used by *Molfino and McIntyre* [1990] to monitor changes in the nutricline depth and has been calibrated to primary productivity by *Beaufort et al.* [1997] for paleoproductivity reconstructions.

The relationship between the *Florisphaera profunda* ratio and primary production has already been quantified by *Beaufort et al.* [1997] with the following equation:

$$y = 617 - [279 \log(x+3)],$$

where y is the yearly PP (g C m^{-2} yr^{-1}) and x is the percent Fp. This equation is based on Indian Ocean low-latitude core tops. We assume that the coccolithophorids' assemblage distributions are homogenous in the intertropical zone. The variations of Fp are in agreement with other paleoproductivity proxies [*Beaufort et al.*, 1997].

4. Results

The present annual PP in the Sulu Sea is 148 g C m^{-2} yr^{-1} [*Antoine and Morel*, 1996], which is close to the average reconstructed PP over the last 200 kyr of 135 g C m^{-2} yr^{-1}. The PP (data are accessible at http://www.cerege.fr and at ftp://ftp.noaa.ngdc.gov/paleo) oscillates during the last 200 kyr between 81 and 223 g C m^{-2} yr^{-1} (Figure 3).

4.1. Glacial-Interglacial Variations

On a glacial-interglacial timescale, PP increases during glacial periods and decreases during interglacials (Figure 3). PP is moderately correlated (r^2 = 0.49) with the ice volume curve (SPECMAP stack of *Imbrie et al.* [1984]). This is shown by the spectral analysis of the paleoproductivity record, which contains orbital frequency peaks of Milankovitch theory (i.e., 1/100 kyr, 1/41 kyr, and ~1/20

kyr) (Figure 4) and confirmed by cross-spectral analysis between the PP time series and the SPECMAP stack (not shown). This orbital forcing explains about half of the variance of the PP record. Half of the variance of the PP remains to be explored in the sub-Milankovitch timescale.

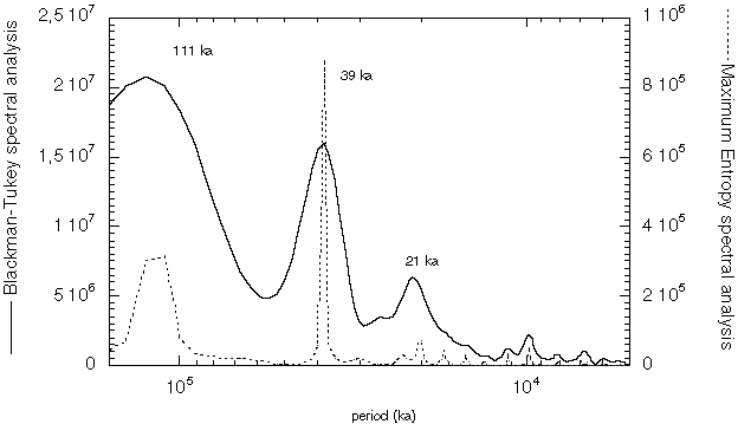

Figure 4. Spectral analysis of the MD97-2141 PP record between 4.1 and 200 ka. Three peaks appear in the spectral analysis computed using the Blackman-Tukey algorithm (solid line) and the maximum entropy algorithm (dotted line), which correspond to orbital frequencies of the Milankovitch theory.

4.2. Sub-Milankovitch Dynamics

4.2.1. Bolling/Allerod and the Younger Dryas event. The last deglaciation is marked by the Younger Dryas event, which interrupts the global warming trend in the Northern Hemisphere. The Younger Dryas seems to be at least hemispheric in extent and has been already described in the Sulu Sea [*Kudrass et al.*, 1991; *Linsley and Thunell*, 1990]. The Younger Dryas event is also present in the MD97-2141 $\delta^{18}O$ record between 13.5 and 11.5 ka (Figure 3). The paleoproductivity record inferred from Fp is characterized by an abrupt decrease at 14.55 ka (from 170 to ~125 g C m^{-2} yr^{-1}) to a plateau until 11.5 ka, followed by another decrease to 100 g C m^{-2} yr^{-1}.

We interpret this PP record to indicate a sharp decrease of the East Asian winter monsoon strength after 14.55 kyr. A similar abrupt transition at 14.5 ka is recorded in the alkenone-sea surface temperature (SST) record of the meridional South China Sea as 1.5°C step [*Pelejero et al.*, 1999a]. Greenland Ice Core Project (GRIP) and Greenland Ice Sheet Project 2 (GISP2) isotopic records also display an abrupt warming at ~14.5 ka. This abrupt warming seems to be at least hemispheric [*Bard et al.*, 1997]. The sea level rise (meltwater pulse (MWP) Ia of *Fairbanks* [1989]) was invoked by *Pelejero et al.* [1999c] to account for the thermal and terrigenous input changes in the South China Sea. However, the abruptness of the PP change (<200 years) is not easily attributable to the flooding of the Sundaland. An abrupt drop in the East Asian winter monsoon intensity can explain this PP change in a more plausible manner.

The interpretation of the Younger Dryas event in the Sulu Sea is still controversial. Two main hypotheses were summarized by *Anderson and Thunell* [1993]: either it reflects a cooling event or it is due to a change in the $\delta^{18}O$ of seawater. Modern analog technique reconstruction of SST with

planktonic foraminifera does not record enough SST difference during the Younger Dryas to account for the observed isotopic shift [*Thunell and Miao*, 1996]. So the enrichment is probably due to changes in seawater isotopic composition during the Younger Dryas. The origin of this change is still being debated as an oceanic source [*Duplessy et al.*, 1991] or an atmospheric variation [*Anderson and Thunell*, 1993].

The PP plateau during the Allerod and the Younger Dryas is similar to the warming recorded by alkenones records from the cores 17961 and 17964 in the South China Sea (SCS) [*Pelejero et al.*, 1999a, 1999b]. The Younger Dryas–Allerod SST difference in the SCS is 0.4°C. This corresponds to an increase of ~0.1‰ of the foraminiferal $\delta^{18}O$, 20% of the 0.5‰ change observed in Sulu Sea sediments [*Linsley*, 1996]. Our PP record strengthens the argument that East Asian winter monsoon dynamics during Younger Dryas were not significantly different from the Allerod because of the small measured change in the PP record between the Allerod and the Younger Dryas. Thus the change in planktonic foraminifera $\delta^{18}O$ composition in the Sulu Sea between the Allerod and the Younger Dryas seems to be mainly due to an isotopic variation in ocean water linked to salinity, after a major change in atmospheric processes 14.5 kyr ago, during the Bolling.

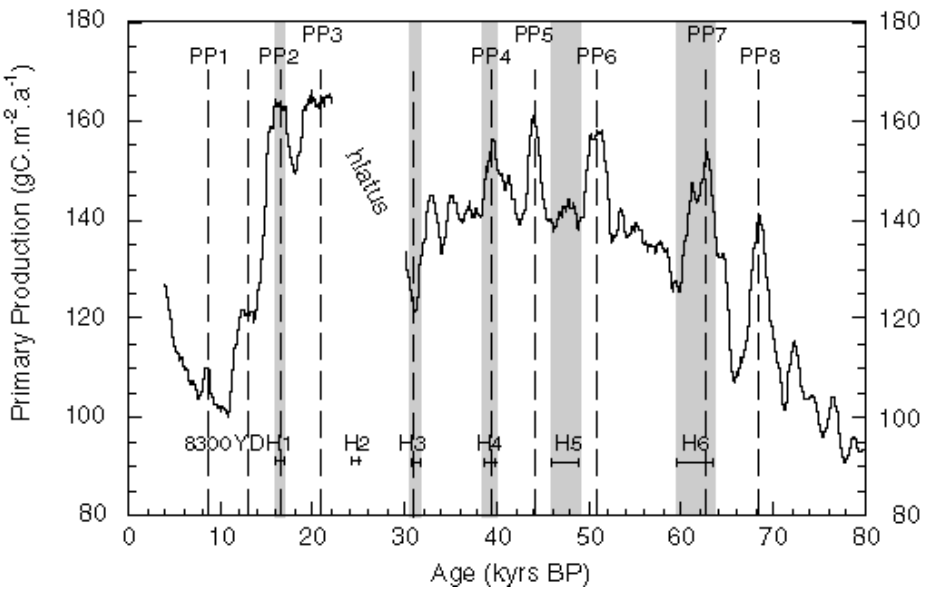

Figure 5. MD97-2141 primary productivity versus calendar age (solid line) smoothed with a 2 kyr moving average window. Between 22 and 30 calendar kyr B.P., a hiatus exists in the sediment record identified with ^{14}C dates (shaded area). The major peaks in PP are numbered from 1 to 8. The Younger Dryas and timing of Heinrich Events in the North Atlantic (shaded area) are shown in toward bottom. The ages for these events are from *Bard* [1998] for the Younger Dryas, *Thouveny et al.* [2000] for North Atlantic Heinrich Events 1–4, and *Chapman and Shackleton* [1998] for the chronology of H5 and H6.

4.2.2. Millennial-scale PP events during MIS 3. The Heinrich events in the North Atlantic have been correlated to short increases of the East Asian winter monsoon dynamics [*Chen et al.*, 1997; *Porter and Zhisheng*, 1995]. In order to compare the millennial variations in the North Atlantic and the PP variations in the Sulu Sea we smoothed the PP record with a 2 kyr average moving window and resampled at a 100 year time step (Figure 5). This 2 kyr window keeps only the variance at the millennial and longer timescales and attenuates the century-scale variations. During the last 80 kyr the

PP record reveals eight events numbered PP1-PP8, some of which may be synchronous with North Atlantic environmental changes (Figure 5). The first one (PP1) at ~8.3 kyr ago is in phase with the early to middle Holocene transition period [*Alley et al.*, 1997]. PP2 matches with Heinrich Event 1 (HE1). PP3 occurs during the Last Glacial Maximum. PP4 seems to correlate with HE4. PP5 and PP6 do not match with any major Heinrich Events, and HE5 is being intercalated between these two PP increases. However, PP5, at ~44 ka is correlated to an increase of the winter monsoon strength recorded in paleoloess from China, dated between 43.3 and 45.2 kyr BP (PL7 of *Chen et al.* [1997]). PP7 could be related to HE6. PP8 does not match any Heinrich Event. *Chen et al.* [1997] also describe two events at 59.2–66.2 ka (PL9) and 68.6–71.2 ka (PL10), which may correlate with PP7 and PP8 given age model uncertainties. In conclusion, all PP maxima in the Sulu Sea can be correlated with Chinese loess events and notably events PP5 and PP8 may correspond only with the Chinese loess record. Therefore we conclude that these regional events are indicative of significant changes in the East Asian winter monsoon dynamics. PP1, PP2, PP4, and PP7 match clearly with North Atlantic Heinrich Events. In stage 3, uncertainties in the age model that cannot be smaller than ±2 kyr may explain the relative discrepancy between PP5 or PP6 and HE5 but cannot account for the occurrence of supplementary peaks (PP5 or PP6 and PP8). Our data indicate that the dynamics of the East Asian winter monsoon is not directly linked with the major iceberg discharges in the North Atlantic as stated by *Porter and Zhisheng* [1995]. The East Asian winter monsoon exhibits higher-frequency dynamics than that of the main HE. However, it remains to be determined if a common dynamic is present between the high- and the low-latitude records that is not linked with major icebergs discharges. We next compare the Dansgaard–Oeschger cycles recorded in the Greenland ice core records with our PP record from the Sulu Sea.

To evaluate Dansgaard–Oeschger scale variability, we performed SSA on the Sulu Sea PP and on the GRIP $\delta^{18}O$ records to examine the relationships between Greenland climate and East Asian winter monsoon dynamics. For this analysis, we resampled the two records at 200 year time intervals after interpolation. We computed SSA with the Vautard-Ghil autocovariance estimator embedded in 20 dimensions corresponding to 2000 years. The first principal component (PC) in the two records describes the long-term trend, and the second PC shows millennial dynamics (Figure 6 and Table 2). There is a good agreement between the two PC2 records of millennial dynamics in PP and temperature in Greenland during the last 70 kyr. PP increases in the Sulu Sea when temperatures in Greenland decrease. Cross-spectral analysis indicates high coherency between the PC2 of PP and the PC2 of GRIP for the ~6 and 3.5 kyr frequency bands with phases of ~160° and of 140°, which is indicative of the opposite phase described above. This phase relationship is well constrained for the deglaciation by ^{14}C ages. The phase cannot be further investigated because of limited synchronization between the ice core records and the marine records inherent to differences in established chronologies.

A strengthening of the East Asian winter monsoon during the glacial stages is compatible with the conclusions of several studies already carried out in this area [*Chen and Huang*, 1998; *Wang et al.*, 1999]. It corresponds to a strengthening of the Hadley cell between the Western Pacific Warm Pool Low and the Siberian High. This mode of atmospheric circulation is compatible with last glacial stage simulations [*Kutzbach et al.*, 1993]. The Siberian Highs are directly connected to the Ferrel cells, which influence the Greenland and Asian climates. This teleconnection should operate via the coupling of these two cells (Ferrel and Hadley) during the winter.

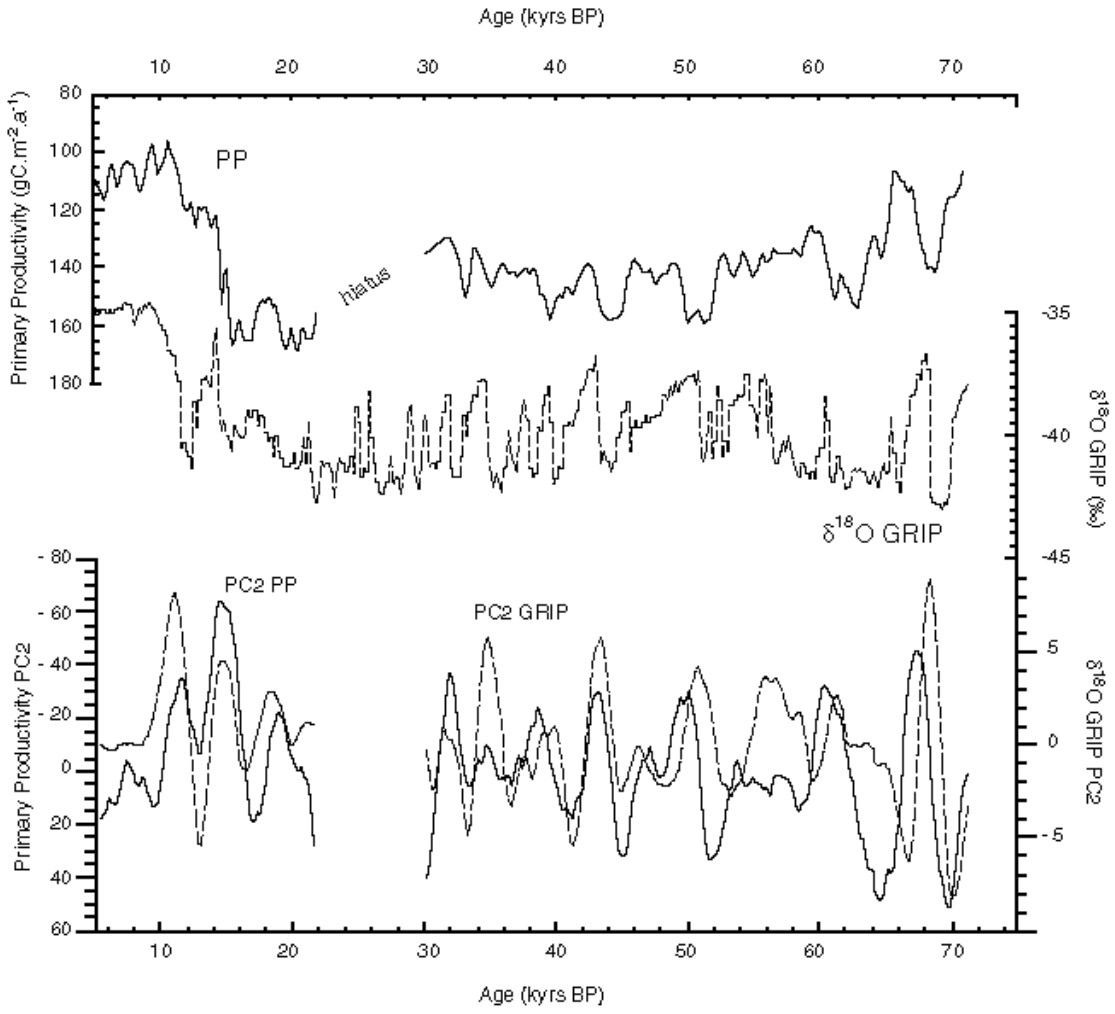

Figure 6. (top) MD97-2141 PP (smoothed; solid line) record versus the $\delta^{18}O$ record of the GRIP ice core (dotted line). (bottom) PC2 of the PP record (solid line) and PC2 of the $\delta^{18}O$ record of GRIP (dotted line) as reconstructed by singular spectrum analysis (SSA), which show similar oscillations. Note that both scales in the bottom panel are inverted compared to the top panel.

In conclusion, the lack of a systematic correlation between the Sulu Sea PP and HE indicates that iceberg discharges in the North Atlantic and the East Asian winter monsoon follow different dynamics. However, the correlation between the Greenland climate PC2 and the East Asian winter monsoon PC2 indicates that similar millennial-scale climate variability affects both the Greenland and the Western Pacific climates.

	PP in Sulu Sea			d18 O GRIP		
	described variance (%)	cumulative variance (%)	mean period (a)	described variance (%)	cumulative variance (%)	mean period (a)
PC1	82.52	82.52	>8000	67.64	67.64	>8000
PC2	6.76	89.29	6200	13.56	81.21	5500
PC3	2.98	92.28	3690	8.4	89.61	3500
PC4	1.67	93.95	2400	3.45	93.06	2760
PC5	1.15	95.10	1870	1.76	94.83	1870
PCs 6 to 20	4.9	100	-	6.07	100	-

Table 2. Percent Variance Described by the Principal Components of the Singular-Spectrum Analysis and Mean Periods of the PCs

4.3. Analysis in the Frequency Domain (Suborbital Frequencies)

Three time slices were defined to explore high-frequency cycles in the PP record. The first one, from 22 to 4.1 ka, spans the whole deglaciation. The second one, from 60 to 30 ka, includes most of stage 3. The third one, from 160 to 130 ka, corresponds to the end of stage 6. The PP records were detrended in each segment using a ninth-order polynomial for the deglaciation, a fourth-order polynomial for stage 6, and a linear detrend for stage 3 (Figure 7c). The three records show variance peaks at periods of ~6, 3.5, and 2.4 kyr and between 1780 and 1200 years with a mean at 1500 years (Figure 7e–7g). The spectral peaks could be related to the age model. However, changing the age model from polynomial fits to linear fits does not change the periods of the peaks >100 years, and the relative timing of the peaks is kept. Thus the spectral peaks seem to be robust features of the signal with this current age model.

4.3.1. The ≈1.5 kyr cycle. For the time slice from 4.1 to 22 ka the most significant peak occurs at 1.38 kyr (significance of 93%). In the 30–60 ka time slice, two peaks occur at 1.54 kyr (98.5%) and 1.2 kyr (99.8%). In the last time slice the peak is at 1.48 ka (99%). The strongest periods are all around 1.4–1.5 kyr, and the occurrence in three different time-slices indicates probably a common origin and an almost stationary signal across different climatic conditions.

4.3.2. The ≈2.4 kyr cycle. In the 4.1–22 ka time slice, two minor peaks occur (2.58 and 2.17 kyr), but they are not significant. In the 30–60 ka time slice the prominent peak occurs at 2.32 kyr (significance of 79.8%). In the 130–160 ka time slice a significant peak is at 2.43 kyr (96%). The period of 2.4 kyr seems also stationary, but its strength varies through time. It is more marked during the glacial stages and may correspond to ice volume forcing.

4.3.3. The ≈4.2-3.3 kyr cycle. In the time slice from 22 to 4.1 ka the peak is at ~4.2 (significance of 97%). The 30–60 ka time slice peaks at 3.6 kyr (97%), and in the 130–160 ka time slice the significant peak is at 3.36 kyr (86%). The strength of this peak is strong in all the time slices, but the period does not seem to be stationary.

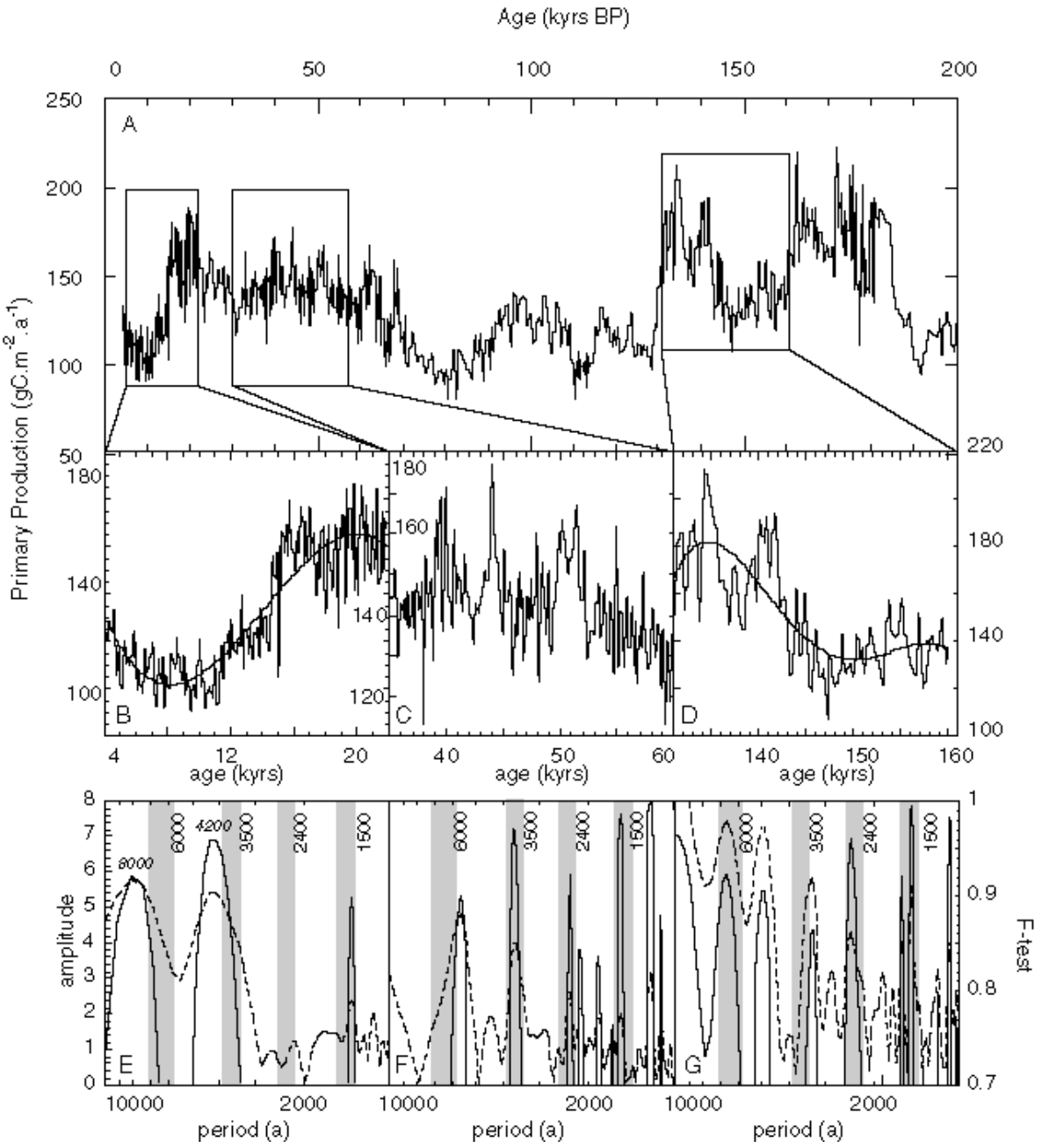

Figure 7. (a) MD97-2141 primary productivity (0–200 ka). Three intervals are enlarged in Figures 7a–7c. (b) From 4 to 22 calendar kyr B.P. A polynomial of third order (thin solid line) was applied to detrend the primary productivity signal (thick solid line) before the multitaper method (MTM) spectral analysis. (c) From 35 to 60 ka. PP (thick solid line) is represented, a linear detrend was performed before spectral analysis. (d) From 130 to 160 ka. A fifth-order polynomial (thin solid line) of the PP (thick solid line) was also subtracted from the PP record before the spectral analysis. (e–g) MTM spectra of the three time windows in Figures 7b, 7c, and 7d, respectively. Line amplitudes (dashed line) and *F* test (estimate of confidence; solid line) are plotted versus period. The shaded areas represent significant frequency bands.

4.3.4. The ≈6 kyr cycle. In the time slice between 4.1 and 22 ka the peak at ~8 kyr is not significant because of the dominant deglaciation signal overprints on the low-frequency band. In the 30–60 ka time slice a peak occurs at 5.7 kyr (significance of 89.9%), and between 130 and 160 ka the significant peak is at 6.7 kyr (92.1%) with another concentration of variance at ~5.06 kyr (90.5%). This frequency is most pronounced during the glacials periods.

5. Discussion: High-Frequency Cycles

Because the frequency of ~6 kyr^{-1} is close to the Heinrich Events' frequency band, we filtered the PP record in this frequency band using a Gaussian filter (bandwidth of 0.1666 kyr^{-1} ± 0.03) (Figure 8a). The resulting PP series clearly shows an amplification during the glacial periods, with minima during interglacials (i.e., Holocene and stage 5: 75–130 ka), and indicates that this frequency seems to be ice volume forced. The amplification could depend on the high-latitude ice volume available for ice rafting events.

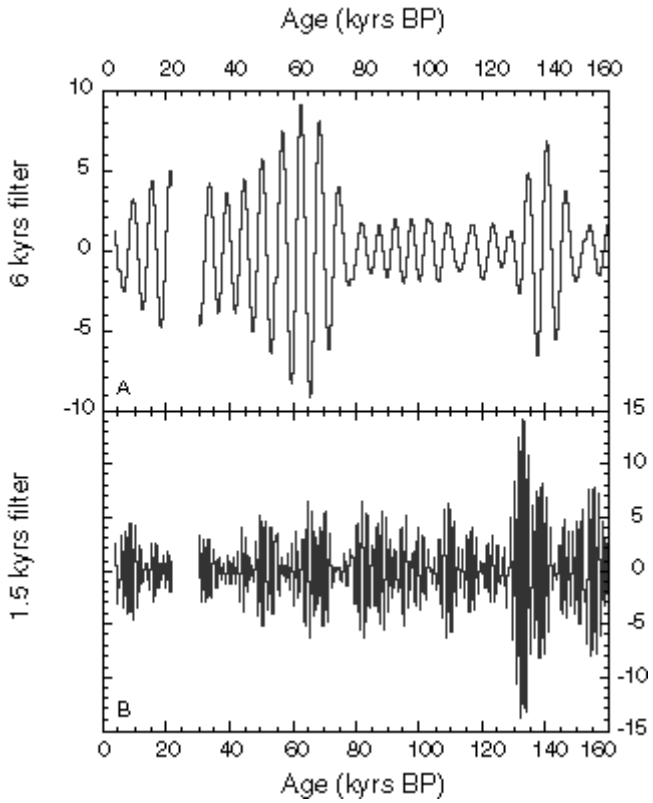

Figure 8. Filtered PP with a Gaussian filter centered on (a) 6000 years and (b) 1500 years. The envelope of the 1500 years filtered signal exhibits a ~20,000 years modulation.

A 3.7 kyr cycle has already been reported by *Pestiaux et al.* [1988] in the Indian Ocean. A similar periodicity of 3.3 kyr was also reported by *Sirocko et al.* [1996] in a production record from the Arabian Sea. These authors attributed this frequency band to combination tones of orbital forcing on monsoon dynamics. In the Sulu Sea this period is significant during the MIS3. This period is not very stable in the PP record, oscillating between 3.62 kyr for stage 3 and 3.36 kyr for stage 6. The identification of this period in several paleomonsoon records seems to indicate that this period is significant in Asian monsoon system dynamics. The hypothesis of combination tone related to precessional and to obliquity frequencies, which forces the climate system like a nonlinear oscillator [*Pestiaux et al.*, 1988], could explain the variations of the spectral peaks contained in this frequency band. Even if a nonlinear climatic oscillator predicts only periods >5 kyr [*Le Treut and Ghil*, 1983],

the monsoon system by its amplification of insolation forcing could probably generate cycles in this frequency band [*Pestiaux et al.*, 1988].

5.1. The 2.4 kyr Cycle

The PP exhibits a strong 2.4 kyr cycle, especially during the last two glacial stages (MIS 2–3 and 6). This period has already been described in oceanic sediments. *Pestiaux et al.* [1988] observe a 2.3 kyr period in the Indian Ocean hydrography, which was interpreted as a combination tone of the precessional and obliquity cycles, representing an internal but nonlinear response of the monsoon system to solar forcing. This cycle is also present in the atmospheric ^{14}C excess record [*Stuiver and Braziunas*, 1993], which depends on the solar flux (Hallstattzeit cycle [*Damon and Jirikowic*, 1992]) and on the oceanic-atmosphere exchange of ^{14}C. A 2.2 kyr periodicity was also reported in a monsoon record from the Oman margin [*Naidu and Malgrem*, 1995], which was attributed to interactions between oceanic circulation changes and atmospheric ^{14}C changes at a 2.3 kyr period. This cycle is not expressed in Termination I of the Sulu Sea PP record. However, it is significant for the glacials stages. The low expression of this cycle in the Sulu Sea during the last termination is perhaps due to the strong overprint of the 1.5 kyr cycle on the PP record. This cycle seems to be stationary throughout this record.

5.2. Pseudo 1.5 kyr Cyclicity

A 1.47 kyr period was first described by *Dansgaard et al.* [1984] in the Camp century $\delta^{18}O$ ice core record. In the Summit ice core (GISP2) the $\delta^{18}O$ and the polar component of a principal component analysis computed on various chemical markers in the ice both show periods ~1.5 kyr [*Mayewski et al.*, 1997]. A 1.47 kyr period was also described by *Bond et al.* [1997] in North Atlantic deep-sea cores during the Holocene and the deglaciation. In Alaska, a lake record contains climatic variations with a 1.5 kyr cycle [*Campbell et al.*, 1998]. These records provide growing evidence for cyclicity of ~1.5 kyr in many high-latitude records. This cycle was also recently linked to fluctuations in continental ice mass during periods of lowered sea level (-45 m below present level) by a simple model of ice dynamics [*Schulz et al.*, 1999]. At lower latitudes the southwest Indian monsoon also shows clear 1.45 kyr cycles in a paleoproductivity record spanning the last deglaciation [*Sirocko et al.*, 1996]. Sirocko et al. speculate that this relationship could be due to subprecessional forcing.

In the Sulu Sea the primary productivity shows clear peaks in a broader 1.5 kyr band (Figure 7). The peak in PP is at 1.38 kyr for the last 22 kyr. For stage 2–3 the major peak is at 1.37 kyr. That ~1.5 kyr cyclicity is also present during stage 6. During the last deglaciation the cycles are well defined. This pseudoperiodicity appears significant in the three time slices, suggesting that it is a pervasive feature of the East Asian winter monsoon dynamics. Our low-latitude record clearly does not record an amplification with increase in the polar continental ice masses (i.e., the sea level does not modulate the

envelope of the 1.5 kyr cycle). During the last 160 kyr, eight maxima in the 1.5 kyr envelope were counted, which correspond roughly to the precession period (160/8 = 20 kyr) (Figure 8b). The East Asian monsoon 1.5 kyr cycle thus could be the climatic expression of a combination tone of the orbital insolation frequencies as already expressed by *Pestiaux et al.* [1988] and *Sirocko et al.* [1996]. The pervasive occurrence of this cycle during both glacial and interglacial periods in the subtropics seems to indicate that if a 1.5 kyr climate oscillator exists, a common origin between high and low latitudes is expected for this cyclicity. We suggest that its presence in the Sulu Sea is not forced by high latitudes, as indicated by its presence during stages 1 and 5 in the Sulu Sea and absence in the intervals in the GRIP record [*Stuiver and Braziunas*, 1993]. Further data are necessary to improve the definition of the frequency bands and the geographical extent of these rapid climate cycles.

6. Conclusions

We reconstructed primary productivity (PP) from coccoliths in the MD97-2141 core, located in the Sulu Sea during the last 200 kyr.

1. We find that PP increased during the glacial stages, whereas the interglacials are times of lower PP. We attribute this PP change to a strengthening of the East Asian winter monsoon in the Sulu Sea during glacial stages.

2. The PP record indicates that an abrupt decrease in the East Asian winter monsoon occurred 14.55 calendar kyr B.P., followed by a ~2 kyr plateau during both Allerod and Younger Dryas. It shows that changes in the $\delta^{18}O$ record from the Sulu Sea during the Younger Dryas are most likely linked with sea surface salinities changes.

3. The PP record exhibits eight rapid oscillations during the last 70 kyr. Only four PP events are synchronous with Heinrich Events. This implies that the East Asian winter monsoon and North Atlantic iceberg discharges follow different dynamics, and that HE are not systematically forcing increases in the East Asian winter monsoon. However, these PP oscillations appear to correlate with peaks of the East Asian monsoon recorded in the Chinese loess. In the timescale close of the pacing of Dansgaard–Oeschger cycles, singular-spectrum analysis reveals that the PP record in the Sulu Sea can be correlated with the Greenland climate. Therefore a common dynamic, which is not forced by icebergs discharges in the North Atlantic, is present in both high- and low-latitude paleoclimatic records.

4. Four dominant frequencies were isolated in the high-frequency pacing of the East Asian winter monsoon. They occur (1) at ~6 kyr, (2) in a 3.3–4.2 kyr frequency band of unknown origin, (3) in a 2.4 kyr frequency band probably resulting from the coupling between solar flux and oceanic processes, and (4) in a 1.5 kyr band. This ~1.5 kyr pseudoperiodicity is a pervasive feature of the East Asian

winter monsoon during the marine stages 1, 3, 5, and 6. The origin of this climatic cyclicity remains unknown, but we suggest that its presence at this site in the low-latitude western Pacific is not forced from the high latitudes.

References

Alley, R. B., P. A. Mayewski, T. Sowers, M. Stuiver, K. C. Taylor, and P. U. Clark, Holocene climatic instability: A prominent, widespread event 8200 yr ago, *Geology*, *25*(6), 483–486, 1997.

Anderson, D. M., and R. C. Thunell, The oxygen-isotope composition of tropical ocean surface water during the last deglaciation, *Quat. Sci. Rev.*, *12*, 456–473, 1993.

Antoine, D., and A. Morel, Oceanic primary production, 2, Estimation at global scale from satellite (coastal zone color scanner) chlorophyll, *Global Biogeochem. Cycles*, *10*, 57–70, 1996.

Bard, E., Correlation of accelerator mass spectrometry ^{14}C ages measured in planktonic foraminifera: Paleoceanographic implications, *Paleoceanography*, *3*(6), 635–645, 1988.

Bard, E., Geochemical and geophysical implications of the radiocarbon calibration, *Geochim. Cosmochim. Acta*, *62*(12), 2025–2038, 1998.

Bard, E., M. Arnold, R. G. Fairbanks, and B. Hamelin, ^{230}Th-^{234}U and ^{14}C ages obtained by mass spectrometry on corals, in *Calibration 1993*, edited by M. Stuiver, A. Long, and R. S. Krea, pp. 191–200, Dep. of Geosci., Univ. of Ariz., Tucson, 1993.

Bard, E., F. Rostek, and C. Sonzogni, Interhemispheric synchrony of the last deglaciation inferred from alkenone palaeothermometry, *Nature*, *385*, 707–710, 1997.

Beaufort, L., Y. Lancelot, P. Camberlin, O. Cayre, E. Vincent, F. Bassinot, and L. Labeyrie, Insolation cycles as a major control of equatorial Indian Ocean primary production, *Science*, *278*, 1451–1454, 1997.

Behl, R., and J. P. Kennet, Brief interstadial events in the Santa Barbara basin, NE Pacific, during the past 60 kyr, *Nature*, *379*, 243–246, 1996.

Bond, G., et al., Evidence for massive discharges of icebergs into the North Atlantic Ocean during the last glacial period, *Nature*, *360*, 245–249, 1992.

Bond, G., W. Showers, M. Chezebiet, R. Lotti, P. Almasi, P. deMenocal, P. Priore, H. Cullen, I. Hajdas, and G. Bonani, A pervasive millennial scale cycle in North-Atlantic Holocene and glacial climates, *Nature*, *278*, 1257–1266, 1997.

Campbell, I. D., C. Campbell, M. J. Apps, N. W. Rutter, and A. B. G. Bush, Late Holocene ca. 1500 yr climatic periodicities and their implications, *Geology*, *26*(5), 471–473, 1998.

Chapman, M. R., and N. J. Shackleton, Millennial-scale fluctuations in North Atlantic heat flux during the last 150,000 years, *Earth Planet. Sci. Lett.*, *159*, 57–70, 1998.

Chen, F. H., J. Bloemendal, J. M. Wang, J. Li, and L. Oldfield, High-resolution multi-proxy climate records from Chinese loess: Evidence for rapid climatic changes over the last 75 kyr, *Palaeogeogr. Palaeoclimatol. Palaeoecol.*, *130*, 323–335, 1997.

Chen, M. T., and C. Y. Huang, Ice-volume forcing of the winter monsoon climate in the South China Sea, *Paleoceanography*, *13*(6), 622–633, 1998.

Cortijo, E., L. Labeyrie, M. Elliot, E. Balbon, and N. Tisnerat, Rapid climatic variability of the North Atlantic Ocean and global climate: A focus of the IMAGES program, *Quat. Sci. Rev.*, *19*, 2000.

Damon, P. E., and J. L. Jirikowic, The sun as a low-frequency harmonic oscillator, *Radiocarbon*, *34*(2), 199–205, 1992.

Dannenmann, S., B. K. Linsley, D. W. Oppo, and R. D. Norris, Centennial resolution isotopic record from the Sulu Sea: 10 kyr to 60 kyr, *Eos Trans. AGU*, *79*(45), Fall Meet. Suppl., F454, 1998.

Dansgaard, W., S. J. Johnsen, H. B. Clausen, N. Dahl-Jensen, N. Gundestrup, and C. U. Hammer, North Atlantic climatic oscillations revealed by deep Greenland ice cores, in *Climate Processes and Climate Sensitivity, Geophys. Monogr. Ser.*, vol. 29, edited by J. E. Hansen and T. Takahashi, pp. 288–298, AGU, Washington, D. C., 1984.

Dansgaard, W., et al., Evidence for general instability of past climate from a 250 kyr ice-core record, *Nature*, *364*, 218–220, 1993.

Duplessy, J.-C., E. Bard, M. Arnold, N. J. Shackleton, J. Duprat, and L. Labeyrie, How fast did the ocean-atmosphere system run during the last deglaciation?, *Earth Planet. Sci. Lett.*, *103*, 27–40, 1991.

Fairbanks, R. G., A 17000 year glacio-eustatic sea-level record: Influence of glacial melting rates on the Younger Dryas event and deep-ocean circulation, *Nature*, *342*, 637–642, 1989.

Heinrich, H., Origin and consequences of cyclic ice rafting in the northeast Atlantic during the past 130 000 years, *Quat. Res.*, *29*, 142–152, 1988.

Imbrie, J., J. D. Hays, D. G. Martinson, A. McIntyre, A. C. Mix, J. J. Morley, N. G. Pisias, W. L. Prell, and N. J. Shackleton, The orbital theory of Pleistocene climate: Support from a revised chronology of the marine $\delta^{18}O$ record, in *Milankovitch and Climate*, edited by A. L. Berger et al., pp. 269–305, D. Reidel, Norwell, Mass., 1984.

Jouzel, J., Calibrating the isotopic paleothermometer, *Science*, *286*, 910–911, 1999.

Kudrass, H. R., H. Erlenkeuser, R. Vollbrecht, and W. Weiss, Global nature of the Younger Dryas cooling event inferred from oxygen isotope data from Sulu sea cores, *Nature*, *349*, 406–409, 1991.

Kuehl, S. A., T. G. Fuglseth, and R. C. Thunell, Sediment mixing and accumulation rates in the Sulu and the South China Seas: Implications for organic preservation in deep-sea sediments, *Mar. Geol.*, *111*, 15–35, 1993.

Kutzbach, J. E., P. J. Guetter, P. J. Behling, and R. Selin, Simulated climatic changes: Results of the COHMAP climate-model experiments, in *Global Climates Since the Last Glacial Maximum*, edited by H. E. Wright Jr. et al., pp. 24–93, Univ. of Minn. Press, Minneapolis, 1993.

Le Treut, H., and M. Ghil, Orbital forcing, climatic interactions and glaciations cycles, *J. Geophys. Res.*, *88*, 5167–5190, 1983.

Linsley, B. K., Oxygen-isotope record of sea-level and climate variations in the Sulu Sea over the past 150,000 years, *Nature*, *380*, 234–237, 1996.

Linsley, B. K., and R. C. Thunell, The record of deglaciation in the Sulu Sea: Evidence for the Younger Dryas event in the tropical western Pacific, *Paleoceanography*, *5*(6), 1025–1039, 1990.

Linsley, B. K., R. C. Thunell, C. Morgan, and D. Williams, Oxygen minimum expansion in the Sulu Sea, western equatorial Pacific, during the last glacial low stand of sea level, *Mar. Micropaleontol.*, *9*, 395–418, 1985.

Mayewski, P. A., L. D. Meeker, M. S. Twickler, S. Whitlow, Q. Yang, W. B. Lyons, and M. Prentice, Major features and forcing of high-latitude Northern Hemisphere atmospheric circulation using a 110,000-year long glaciogeochemical series, *J. Geophys. Res.*, *102*, 26,345–26,366, 1997.

McGregor, G. R., and S. Nieuwolt, *Tropical Climatology*, 339 pp., John Wiley, New York, 1998.

Miao, Q., R. Thunell, and D. M. Anderson, Glacial-Holocene carbonate dissolution and sea surface temperatures in the South China and Sulu Seas, *Paleoceanography*, *9*(2), 269–290, 1994.

Mix, A., Influence of productivity variations on long-term atmospheric CO_2, *Nature*, *337*, 541–544, 1989.

Molfino, B., and A. McIntyre, Precessional forcing of nutricline dynamics in the equatorial Atlantic, *Science*, *249*, 766–769, 1990.

Naidu, P. D., and B. A. Malgrem, A 2,200 years periodicity in the Asian monsoon system, *Geophys. Res. Lett.*, *22*(17), 2361–2364, 1995.

Nair, R. R., V. Ittekkot, S. J. Manganini, V. Ramaswamy, B. Haake, E. T. Degens, B. N. Desai, and S. Honjo, Increased particle flux to the deep ocean related to monsoons, *Nature*, *338*, 749–751, 1989.

Okada, H., and S. Honjo, The distribution of oceanic coccolithophorids in the Pacific, *Deep Sea Res.*, *20*, 355–374, 1973.

Oppo, D. W., B. K. Linsley, S. Dannenmann, and R. D. Norris, Centennial-to-millennial scale variability recorded in Holocene sediments from the Sulu and South China Seas, *Eos Trans. AGU*, *79*(45), Fall Meet. Suppl., F454, 1998.

Paillard, D., L. Labeyrie, and P. Yiou, Macintosh performs time-series analysis, *Eos Trans. AGU*, *77*(39), 379, 1996.

Patterson, R. T., and E. Fishbein, Re-examination of the statistical methods used to determine the number of point counts needed for micropaleontological quantitative research, *J. Paleontol.*, *63*(2), 245–248, 1989.

Pelejero, C., J. O. Grimalt, S. Heilig, M. Kienast, and L. Wang, High-resolution U_{37}^{k} temperature reconstructions in the South China Sea over the past 220 kyr, *Paleoceanography*, *14*(2), 224–231, 1999a.

Pelejero, C., J. O. Grimalt, M. Sarnthein, L. Wang, and J. A. Flores, Molecular biomarker record of sea-surface temperature and climatic change in the South China Sea during the last 140,000 years, *Mar. Geol.*, *156*, 109–121, 1999b.

Pelejero, C., M. Kienast, L. Wang, and J. O. Grimalt, The flooding of Sundaland during the last deglaciation: Imprints in hemipelagic sediments from the southern South China Sea, *Earth Planet. Sci. Lett.*, *171*, 661–671, 1999c.

Pestiaux, P., I. Van Der Mersch, A. Berger, and J.-C. Duplessy, Paleoclimatic variability at frequencies ranging from 1 cycle per 10,000 years to 1 cycle per 1000 years—Evidence for non-linear behaviour of the climate system, *Clim. Change*, *12*, 9–37, 1988.

Porter, S. C., and A. Zhisheng, Correlation between climate events in the North Atlantic and China during the last glaciation, *Nature*, *375*, 305–308, 1995.

Schulz, H., U. von Rad, and H. Erlenkeuser, Correlation between Arabian Sea and Greenland climate oscillations of the past 110,000 years, *Nature*, *393*, 54–57, 1998.

Schulz, M., W. H. Berger, M. Sarnthein, and P. M. Grootes, Amplitude variations of 1470-year climate oscillations during the last 100,000 years linked to fluctuations of continental ice mass, *Geophys. Res. Lett.*, *26*(22), 3385–3388, 1999.

Sirocko, F., D. Garbe-Schönberg, A. McIntyre, and B. Molfino, Teleconnections between the subtropical monsoons and high-latitude climates during the last deglaciation, *Science*, *272*, 526–529, 1996.

Stuiver, M., and T. F. Braziunas, Sun, ocean, climate and atmospheric $^{14}CO_2$: An evaluation of causal and spectral relationships, *Holocene*, *3*(4), 289–305, 1993.

Stuiver, M., and P. J. Reimer, Calib Rev. 3, *Radiocarbon*, *35*, 215–230, 1993.

Thompson, P. R., A. W. H. Bé, J.-C. Duplessy, and N. C. Shackleton, Disappearance of pink-pigmented *Globigerinoides ruber* at 120,000 yr BP in the Indian and Pacific Oceans, *Nature*, *280*, 554–558, 1979.

Thomson, D. J., Spectrum estimation and harmonic analysis, *IEEE Proc.*, *70*, 1055, 1982.

Thouveny, N., E. Moreno, D. Delanghe, L. Candon, Y. Lancelot, and N. J. Shackleton, Rock-magnetic detection of distal ice rafted debries: Clue for the identification of Heinrich layers on the Portuguese margin, *Earth Planet. Sci. Lett.*, *180*, 61–75, 2000.

Thunell, R. C., and Q. C. Miao, Sea-surface temperature of the western equatorial Pacific during the Younger Dryas, *Quat. Res.*, *46*, 72–77, 1996.

Vautard, R., and M. Ghil, Singular spectrum analysis in nonlinear dynamics, with applications to paleoclimatic time series, *Physica D*, *35*, 395–424, 1989.

Wang, L., M. Sarnthein, H. Erlenkeuser, J. Grimalt, P. Grootes, S. Heilig, E. Ivanova, M. Kienast, C. Pelejero, and U. Pflaumann, East Asian monsoon during the late Pleistocene: high-resolution sediment records from the South China Sea, *Mar. Geol.*, *156*, 245–284, 1999.

Wiesner, M. G., L. Zheng, H. K. Wong, Y. Wang, and W. Chen, Fluxes of particulate matter in the South China Sea, in *Particle Flux in the Ocean*, edited by J. Ittekkot et al., pp. 293–312, John Wiley, New York, 1996.

Xiao, J. L., Z. S. An, T. S. Liu, Y. Inouchi, H. Kumai, S. Yoshikawa, and Y. Kondo, East Asian monsoon variation during the last 130,000 years: Evidence from the Loess Plateau of central China and Lake Biwa of Japan, *Quat. Sci. Rev.*, *18*, 147–157, 1999.

Yan, X.-H., C.-R. Ho, Q. Zheng, and V. Klemas, Temperature and size variabilities of the Western Pacific Warm Pool, *Science*, *258*, 1643–1645, 1992.

Yiou, P., K. Fuhrer, L. D. Meeker, J. Jouzel, E. Jansen, and P. A. Mayewski, Paleoclimatic variability inferred from the spectral analysis of Greenland and Antartic ice-core data, *J. Geophys. Res.*, *102*, 26,441–26,454, 1997.

Zhang, Y., East Asian winter monsoon: Results from eight AMIP models, *Clim. Dyn.*, *13*(11), 797–820, 1997.

Chapitre 2 : Relargages massifs de clathrates de méthane pendant le dernier stade glaciaire :

Le méthane (CH_4) est un gaz à effet de serre dont l'effet radiatif est 23 fois supérieur à celui du CO_2 (Houghton et al., 2001). L'analyse des gaz emprisonnés dans les carottes de glace aux pôles, indique que les changements de concentration en méthane atmosphérique covarient avec les températures aux hautes latitudes lors des événements de Dansgaard-Oeschger (Chappellaz et al., 1993). L'effet radiatif associé aux variations de concentrations atmosphériques de méthane entre un stadiaire (froid) et un interstadiaire (chaud) correspond à un changement de température global compris entre 1 et 3°C (Raynaud et al., 1998). Les augmentations de concentration en méthane atmosphérique lors du passage d'un stadiaire à un interstadiaire ont un retard compris entre 0 et 30 ans sur les températures (Brook et al., 1999 ; Brook et al., 2000; Severinghaus and Brook, 1999). Ce retard implique que les concentrations en méthane, répondent à un forçage de la température, et n'agissent qu'en amplifiant des variations de température produites par d'autres mécanismes.

La principale source de méthane atmosphérique provient des terres humides (marécages) des basses latitudes (Dällenbach et al., 2000), et des changements majeurs de source de méthane ne sont pas suspectés au cours du dernier cycle climatique. Le scénario le plus couramment accepté explique que des températures relativement chaudes, correspondaient à une intensification du cycle hydrologique aux basses latitudes, et donc à une plus grande extension des marécages pendant les interstadiaires (Dällenbach et al., 2000). Cependant, ce schéma classique n'a pas fait l'objet de modélisations convaincantes, et celui-ci a été récemment remis en question. Par exemple, (de Noblet-Ducoudré et al., 2002) ont montré en utilisant un modèle hydrologique, que les périodes chaudes et humides correspondent à une régression des zones humides aux basses latitudes, et qu'inversement, les périodes froides et sèches sont marquées par une augmentation de la surface des terres humides. Ces auteurs interprètent cette relation surprenante par une baisse des niveaux lacustres pendant les périodes sèches, et qui correspond alors à une augmentation de la surface des marécages.

La relation de causalité entre les températures et les concentrations de méthane atmosphérique n'est donc pas encore clairement élucidée. En outre, cette interprétation repose exclusivement sur l'hypothèse que les sources principales de méthane atmosphériques proviennent des zones humides continentales.

Cependant, une source de méthane récemment découverte proviendrait de déstabilisations des gaz-hydrates, ou clathrates. Les gaz-hydrates sont des molécules de gaz (principalement du CH_4, mais également du CO_2, CH_3) piégées dans une structure cyclique de molécules d'eau (Kvenvolden, 1995) (figure 5.1). Ces gaz-hydrates sont stables à certaines conditions de pression-température sur les marges continentales (Dickens and Quinby-Hunt, 1994 ; Dickens and Quinby-Hunt, 1997; Paull et al., 1991 ; Zatsepina and Buffett, 1998). Ils ont été découverts sur la plupart des marges continentales

(figure 5.2). Une baisse de pression et/ou une augmentation de température peut permettre de rompre la structure cyclique et de dégazer abruptement de grandes quantités de méthane.

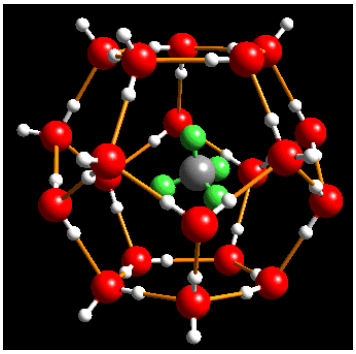

Figure 5.1 : agencement moléculaire d'un clathrate de méthane : au centre de la structure se trouve une molécule de CH4 entouré par les molécules d'eau (structure de type I – d'après (Kvenvolden, 1995)).

En raison du pouvoir radiatif du méthane, de tels relargages ont pu avoir un effet climatique important (Kvenvolden, 1988). Ainsi la rapidité de la déglaciation et les changements climatiques rapides du stade marin isotopique 3 sont expliqués par certains auteurs comme provenant de déstabilisations massives de clathrates de méthane(Kennett et al., 2000; Nisbet, 1992; Paull et al., 1991). Ces spéculations n'ont cependant pas encore été étayées par des observations convaincantes.

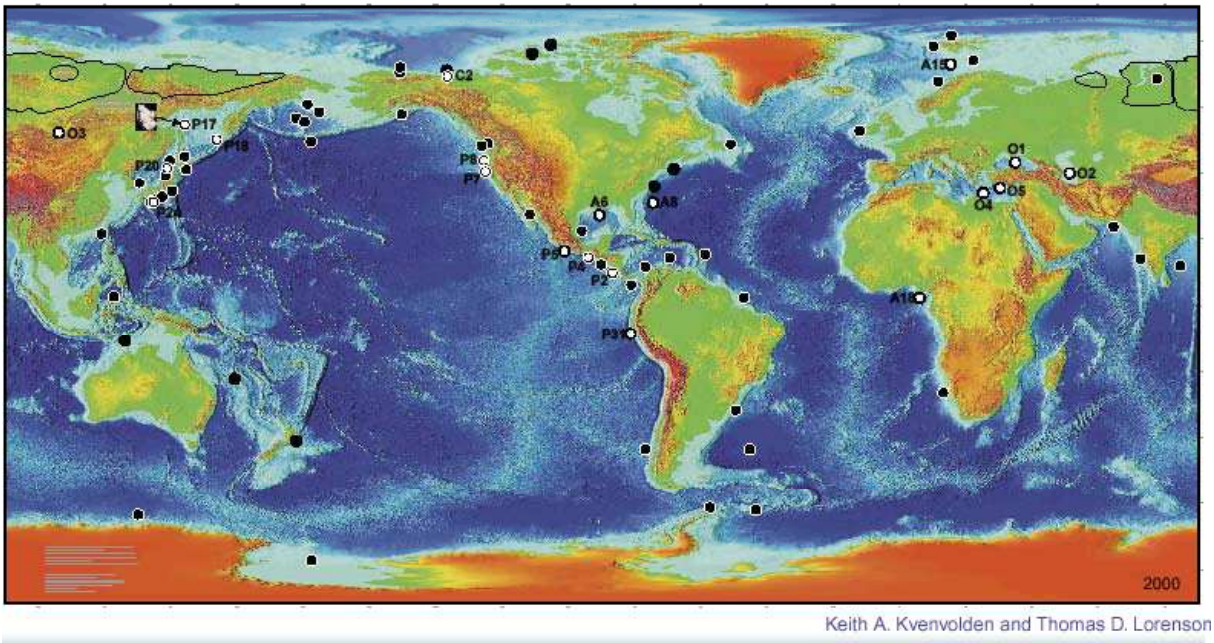

Figure 5.2 : carte de distribution des gaz-hydrates en 2001. Présence déduite soit des BottomsSimulating Reflectors (BSRs – cercles noirs pleins), soit observation in situ (cercles blancs)

Pendant la déglaciation, Nisbet propose que la remontée du niveau marin ainsi que la fonte des calottes polaires, réduit la pression et déstabilise les gaz-hydrates (Nisbet, 1992). En confirmation de cette hypothèse, Smith a pu observer que les marges Groenlandaises ont dégazés des clathrates lors de la terminaison I (Smith et al., 2001). Cependant, les événements reposrtés par ces auteurs sont situées aux extrémités des carottes, de sorte que le modèle d'âge ne peut être contraint. Une seconde hypothèse indique qu'une baisse du niveau marin liée à l'englacement des pôles, entrainerait une

déstabilisation de gaz-hydrates qui agiraient comme facteur limitant des basses températures dans les stades glaciaires (Paull et al., 1991). Cette théorie a été adaptée aux changements climatiques rapides de type Dansgaard-Oeschger par (Kennett et al., 2000). Ces auteurs suggèrent que les changements de concentration en méthane atmosphérique de type D.-O. sont liés à des relargages de clathrates. Ces auteurs observent dans les sédiments du bassin de Santa Barbara de « larges » allègements de la composition en $\delta^{13}C$ des tests de foraminifères benthiques et exceptionnellement de foraminifères planctoniques pendant les D.-O., qu'ils attribuent à des relargages de méthane lors des phases de réchauffement (figure 5.3). Des observations actuelles tendent à modérer leur argument qui est basé sur différentes espèces, et pouvant donc être fortement sujettes à des effets vitaux (Stott et al., 2002). Des évidences de relargages massifs affectant toute la colonne d'eau qui auraient pu ainsi dégazer de grandes quantités de méthane n'ont donc pas encore été mises en évidence.

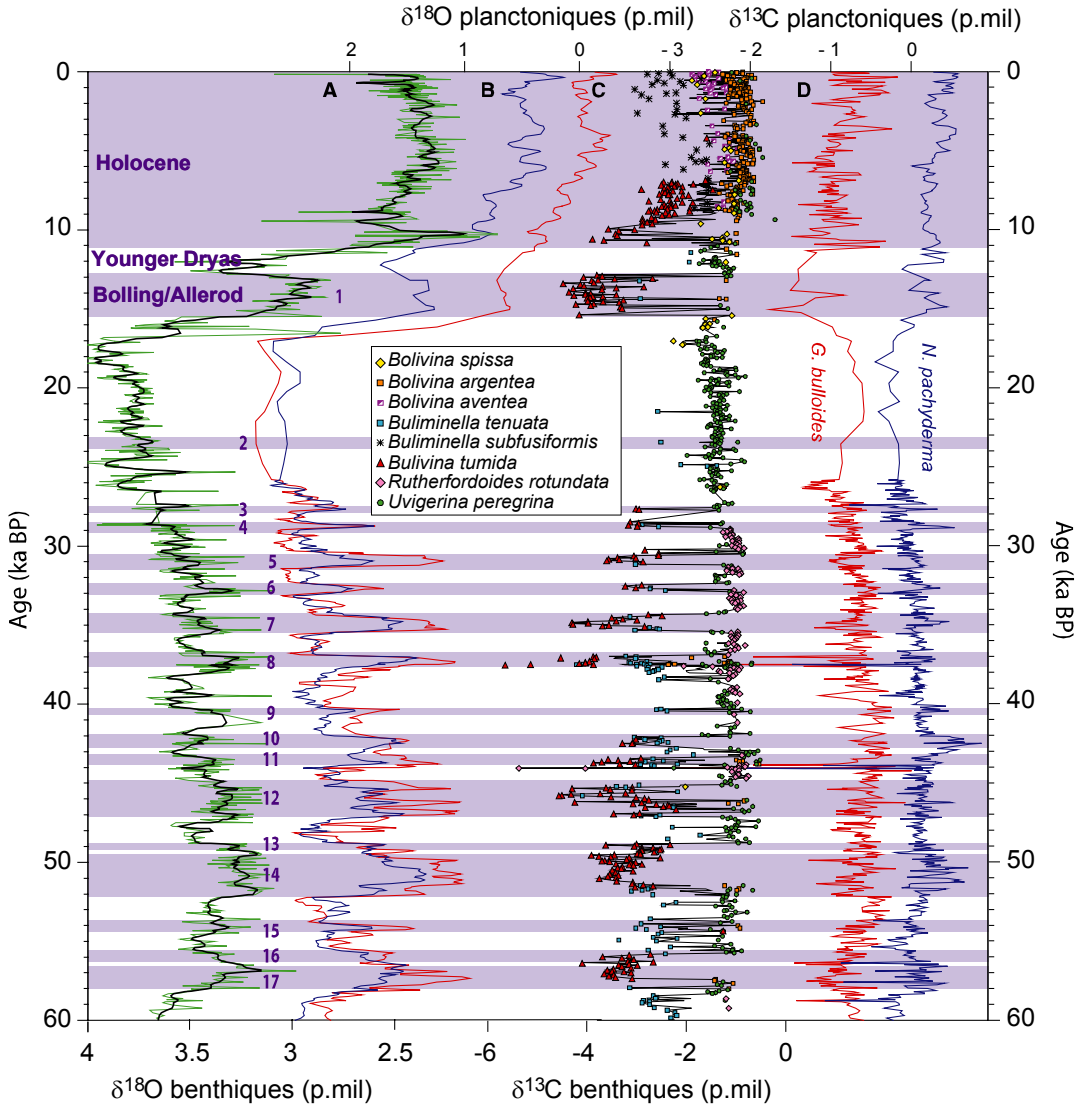

Figure 5.3 : enregistrements isotopiques des foraminifères planctoniques et benthiques du Bassin de Santa Barbara (d'après (Kennett et al., 2000)).

Méthode :

Isotopes stables :

Le test des foraminifères planctoniques est composé de carbonate de calcium ($CaCO_3$). La composition en isotopes de l'oxygène et du carbone de ce test permet de retracer les conditions environnementales lors de leur calcification. La composition isotopique d'un échantillon est exprimée par rapport à un standard international, pour les carbonates par exemple, le *Vienna Pee Dee Belemnite*.

Isotopes de l'Oxygène :

$$\delta^{18}O = \left\{ \frac{\left(\frac{^{18}O}{^{16}O}\right)_{échantillon} - \left(\frac{^{18}O}{^{16}O}\right)_{VPDB}}{\left(\frac{^{18}O}{^{16}O}\right)_{VPDB}} \right\} \times 1000$$

Le $\delta^{18}O$ des foraminifères planctoniques varie en fonction de la composition isotopique de l'eau de mer et de la température à laquelle le test a été cristallisé. Si l'effet de température est relativement constant au cours du temps pour une espèce donnée de foraminifères, la composition isotopique de l'eau de mer est plus variable. Elle va dépendre de facteurs locaux comme la salinité, mais également de changements globaux (le volume des glaces continentales).

Isotopes du Carbone :

$$\delta^{13}C = \left\{ \frac{\left(\frac{^{13}C}{^{12}C}\right)_{échantillon} - \left(\frac{^{13}C}{^{12}C}\right)_{VPDB}}{\left(\frac{^{13}C}{^{12}C}\right)_{VPDB}} \right\} \times 1000$$

Le $\delta^{13}C$ de l'eau de mer est compris entre – 2 et + 2 ‰ (Berger and Vincent, 1986). Le $\delta^{13}C$ du CO_2 atmosphérique est d'environ – 7 ‰ (Keeling, 1961). La décomposition de la matière organique par l'action biogénique ou thermogénique permet seule d'obtenir des valeurs de $\delta^{13}C$ inférieures à – 10 ‰. En particulier, la composition du $\delta^{13}C$ des gaz hydrates de méthane est estimée à environ - 65 ‰ (Kvenvolden, 1995). Les isotopes du carbone des foraminifères s'ils enregistrent des valeurs extrêmement appauvries, peuvent donc être des indicateurs de relargages de gaz hydrates de méthane.

Résumé de l'article :

Les changements de concentration atmosphériques en méthane sont enregistrés dans les carottes de glace pôlaires. Ces changements varient en phase avec les variations climatiques rapides du dernier stade glaciaire. La source principale de méthane atmosphérique provient des marécages des basses latitudes. Néanmoins, les déstabilisations de gaz hydrates peuvent aussi affecter le cycle global du carbone par des relargages catastrophiques de méthane. Nous décrivons dans ce travail, un enregistrement à très haute résolution des changements des isotopes stables du carbone dans le Golfe de Papouasie. Cet enregistrement montre deux excursions très négatives (atteignant – 9‰) à ~39 ka BP et ~55 ka BP qui affectent toute la colonne d'eau. La seule cause possible pour de telles appauvrissements du $\delta^{13}C$ est le relargage massif de gaz hydrates de méthane de la marge continentale. Ces larges quantités de méthane ont été dégazées par dissociation thermique des gaz hydrates pendant le bas niveau du stade marin isotopique 3 dans le Golfe de Papouasie. Si de tels relargages de méthane sont communs des marges continentales de basses latitudes pendant les phases chaudes des bas niveaux marins, les gaz hydrates de méthane ont été une composante majeur du cycle global du méthane.

Références :

Berger, W.H., and Vincent, E., 1986, Deep-sea carbonates: reading the carbon-isotope signal: Geologische Rundschau, v. 75, p. 249-269.

Brook, E.J., Harder, S., Severinghaus, J., and Bender, M., 1999, Atmospheric methane and millenial-scale climate change, Mechanisms of Global Climate change at millenial time scales, Volume Geophysical Monograph 112, AGU, p. 165-175.

Brook, E.J., Harder, S., Severinghaus, J., Steig, E.J., and Sucher, C.M., 2000, On the origin and timing of rapid changes in atmospheric methane during the last glacial period: Global Biogeochemical Cycles, v. 14, p. 559-572.

Chappellaz, J., Blunier, T., Raynaud, D., Barnola, J.-M., Schwander, J., and Stauffer, B., 1993, Synchronous changes in atmospheric methane and Greenland climate between 40 and 8 kyBP: Nature, v. 366, p. 443-445.

Dällenbach, A., Blunier, T., Flückiger, J., Stauffer, B., Chappellaz, J., and Raynaud, D., 2000, Changes in the atmospheric CH4 gradient between Greenland and Antarctica during the Last Glacial and the transition to the Holocene: Geophysical Research Letters, v. 27, p. 1005-1008.

de Noblet-Ducoudré, N., Poutou, E., Chappellaz, J., Coe, M., and Krinner, G., 2002, Indirect relationship between surface water budget and wetland extent: Geophysical Research Letters, v. 29, p. 1029-1033.

Dickens, G.R., and Quinby-Hunt, M.S., 1994, Methane hydrate stability in seawater: Geophysical Research Letters, v. 21, p. 2115-2118.

Dickens, G.R., and Quinby-Hunt, M.S., 1997, Methane hydrate stability in pore water: a simple theoretical approach for geophysical applications: Journal of Geophysical Research, v. 102, p. 773-783.

Houghton, J.T., Ding, Y., Griggs, D.J., Noguer, M., van der Linden, P.J., and Xiaosu, D., 2001, Climate Change, 2001 : The Scientific Basis - Contribution of Working Group I to the third assessment report of the Intergovernmental Panel on Climate Change (IPCC): Cambridge, Cambridge University Press, 944 p.

Keeling, C.D., 1961, The concentration and isotopic abundances of atmospheric carbon dioxide in rural air and marine air: Geochimica et Cosmochimica Acta, v. 24, p. 277-298.

Kennett, J.P., Cannariato, K.G., Hendy, I.L., and Behl, R.J., 2000, Carbon isotopic evidence for methane hydrate instability during quaternary interstadials: Science, v. 288, p. 128-133.

Kvenvolden, K.A., 1988, Methane hydrates and global climate: Global Biogeochemical Cycles, v. 2, p. 221-229.

Kvenvolden, K.A., 1995, A review of the geochemistry of methane in natural gas hydrate: Organic Geochemistry, v. 23, p. 997-1008.

Nisbet, E.G., 1992, Sources of atmospheric CH4 in early postglacial time: Journal of Geophysical Research, v. 97, p. 12,859-12,867.

Paull, C.K., Ussler III, W., and Dillon, W.P., 1991, Is the extent of glaciation limited by marine gas-hydrates ?: Geophysical Research Letters, v. 432-434, p. 3.

Raynaud, D., Chappellaz, J., and Blunier, T., 1998, Ice-core record of atmospheric methane changes: relevance to climatic changes and possible gas hydrate sources, *in* Henriet, J.-P., and Mienert, J., eds., Gas hydrates: relevance to world margin stability and climate change, Volume 137: Special Publications: London, Geological Society, p. 327-331.

Severinghaus, J.P., and Brook, E.J., 1999, Abrupt climate change at the end of the last glacial period inferred from trapped air in polar ice: Science, v. 286, p. 930-934.

Smith, L.M., Sachs, J.P., Jennings, A.E., Anderson, D.M., and deVernal, A., 2001, Light d13C events during deglaciation of the East Greenland continental shelf attributed to methane realease from gas hydrates: Geophysical Research Letters, v. 28, p. 2217-2220.

Stott, L.D., Bunn, T., Prokopenko, M., Mahn, C., Gieskes, J., and Bernhard, J.M., 2002, Does the oxidation of methane leave an isotopic fingerprint in the geologic record ?: Geochemistry, Geophysics, Geosystems, v. 3, p. 1-16.

Zatsepina, O.Y., and Buffett, B.A., 1998, Thermodynamic conditions for the stability of gas hydrate in the seafloor: Journal of Geophysical Research, v. 103, p. 24,127-24,139.

Large Gas Hydrate Methane Releases During the Last Glacial Stage

THIBAULT DE GARIDEL-THORON AND LUC BEAUFORT
CEREGE-CNRS AND UNIVERSITE D'AIX-MARSEILLE III
BP80
13545 AIX-EN-PROVENCE CEDEX 4, FRANCE

FRANCK BASSINOT
LSCE
DOMAINE DU CNRS
91198 GIF-SUR-YVETTE CEDEX, FRANCE

Past oscillations in atmospheric methane concentration are recorded in ice-cores and they appear to vary together with rapid major climatic changes during the last glacial stage (Brook et al., 2000; Chappellaz et al., 1993). The main estimated sources of methane are low-latitude wetlands (Dallenbach et al., 2000). However gas hydrates destabilizations are also suspected to strongly affect the global carbon cycle through catastrophic releases of methane (Dickens et al., 1995). Here we describe a very high resolution marine record of stable carbon isotopic changes from the Papua Gulf off New Guinea which exhibits two extremely large negative excursions. During these events, the shift in carbon isotopic composition of benthic and planktonic foraminifera reached -9‰. The only possible cause of such large depletions of $\delta^{13}C$ is abrupt and massive gas hydrates methane releases from the continental slope. The whole water column was affected by these releases occurring after a slight warming of the deep sea waters. It indicates that large amounts of methane have been outgassed by thermal dissociation of methane gas hydrates during low sea-level stand in the Papua Gulf. If such methane releases were a common feature of the low latitudes margins during the warm phases of the marine low stands, the methane gas hydrates would have been a major component of the global methane cycle.

During the last glacial stage, rapid climatic changes recorded in ice core-records are associated with variations in atmospheric methane concentration showing a maximum amplitude of ~400 ppbv (Chappellaz et al., 1993 ; Raynaud et al., 1998) (fig. 1). These changes in methane concentration are interpreted as resulting mainly from continental low-latitudes wetlands (Dallenbach et al., 2000). However, to our knowledge, none of the low-latitude records show evidence of hydrological changes strong enough to drive the methane variations as recorded in ice-cores. Moreover, low-latitude climatic changes could lead temperature changes in the Northern Hemisphere, at millennial time-scale (Broecker and Hemming, 2001). Additional sources of methane have, therefore, to be identified to explain the amplitude of Dansgaard/Oeschger methane oscillations (Severinghaus and Brook, 1999). Large gas hydrate destabilizations could have released a large amount of methane in the atmosphere (Kennett et al., 2000). Gas hydrate formation requires the conjunction of a range of pressure, temperature and high organic matter fluxes that lead to methanogenesis in the sediments (Kvenvolden, 1995). The methanogenesis could occur in the regions of high sedimentation rates close to the largest rivers. But the paucity of good quality cores spanning the time interval down to the isotopic stage 3 in areas satisfying these conditions limits the possibility of documenting past methane gas hydrates releases.

We studied the IMAGES MD97-2134 piston core located in the Papua Gulf (depth 760 m, lat. 9°54'S, lon. 144°39'E), 500 km off the Fly river delta (fig. 2). The terrigenous inputs from Papua New Guinea explain the high sedimentation rates of ~40 $cm.ka^{-1}$ during the last glacial stage (fig. 1). These high sedimentation rates are due to the unique morphology of the Papuan shelf which circumvents glacial sedimentation on the shelf, and carries most of the terrigenous sediments offshore (Harris et al., 1996). The core contains dark argillaceous muds with abundant coccoliths, foraminifera and pteropods which certify the pelagic sedimentation. This core was retrieved on a topographic high located within the continental slope, preventing the climatic record from turbidite perturbations. The chronostratigraphy was established by 13 AMS ^{14}C ages on the planktonic foraminifera *Globigerinoides ruber*. The Laschamp excursion (1050 cm – 40 kaBP) is well marked in the magnetic record, and gives a chronological constraint in the isotopic stage 3 (Gillot et al., 1979)(N. Thouveny, C. Blanchet, in prep.). The similarity of MD97-2134 paleointensity record and paleomagnetic reference stacks indicates that no hiatus interrupts the sedimentation during the last 60 ka BP (Guyodo and Valet, 1996; Laj et al., 2000). The marine stage 4/3 boundary in the oxygen isotope record at 1600 cm was also tuned to the SPECMAP reference curve (Imbrie et al., 1984). The associated uncertainty in age's accuracy is around 2-3 ka, preventing the direct comparison of our record with ice-core records which have also similar ages uncertainties during the marine isotopic stage 3.

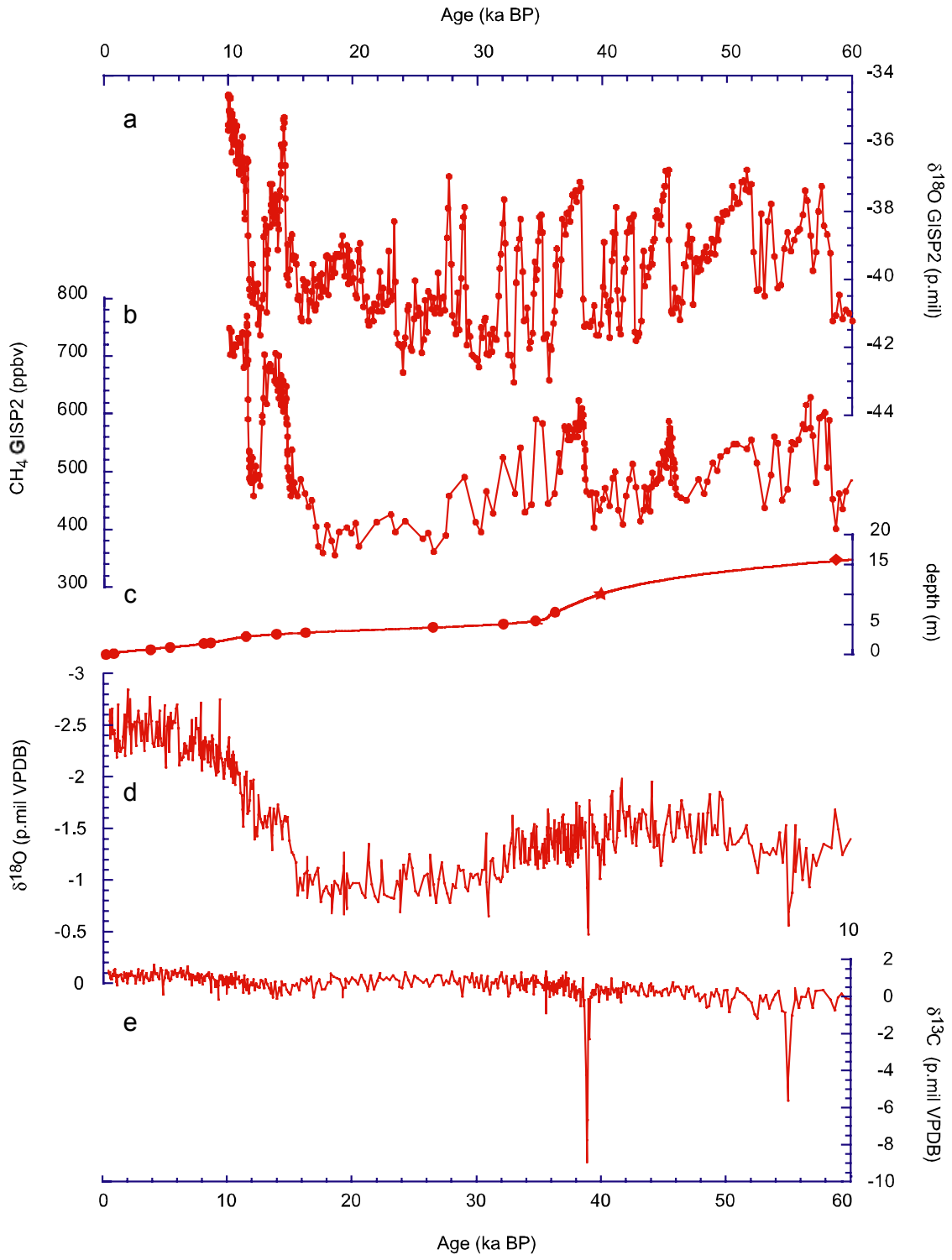

Figure 1 : (a) $\delta^{18}O$ record in Greenland ice-core GISP2, and (b) the atmospheric methane concentration in the same core that exhibits the same millennial-scale variability (Blunier and Brook, 2001). (c) points used to design the age model of the core with circles corresponding to the radiocarbon dates, the star to the Laschamp paleomagnetic excursion (N. Thouveny, C. Blanchet, in prep.), and the losange to the stage 4/3 boundary. The two bottom panels show the MD97-2134 oxygen (d) and carbon (e) isotope records of *Globigerinoides ruber* measured in the LSCE.

We document past changes in surface hydrology using stable isotopes measured in the planktonic foraminifera *G. ruber*,. species living in the upper oceanic layers (fig. 1). The $\delta^{18}O$ record displays global glacial/interglacial changes associated to the growth and decay of the polar ice-sheets. The $\delta^{13}C$ record of *G. ruber* exhibits two large excursions reaching –8.95‰ (Δ=-9‰ from the trend) and -5.62‰ (Δ=-5.7‰) at 39 and 55 ka BP, respectively (fig. 1). These values, extremely depleted, have no analogs in modern open ocean. Associated to the $\delta^{13}C$ negative excursions, the $\delta^{18}O$ of *G. ruber* shows strong positive anomalies reaching –0.45‰ (Δ=+1.05‰ from the trend) and –0.6‰ (Δ=+0.7‰ from the trend) at 39 and 55 kaBP, respectively. Due to the thickness of the 39 kaBP excursion (25 cm), bioturbation has a no significative dilution effect on its amplitude, but may induce a smoothing on the 55 kaBP event (10cm thick). To examine whether or not the entire water column was affected during these events, we analyzed stable isotopes in two other foraminifera species : *Globorotalia truncatulinoides*, a deep-dweller species (Mulitza et al., 1997), and an epibenthic foraminifera : *Uvigerina sp*. (fig. 3). The deep-dweller species shows as well $\delta^{13}C$ anomalies at 39 ka BP reaching –5.8‰ (Δ=-5.4 ‰), and at 55 kaBP reaching –3.12‰ (Δ=-2.6‰). In the benthic foraminifera, the $\delta^{13}C$ decreases to –9.4‰ (Δ=-8.5 ‰) at 39 kaBP, and to –6.22‰ (Δ=-5.2 ‰) at 55 kaBP. The species specific $\delta^{13}C$ and $\delta^{18}O$ values indicate that the record was not balanced by any diagenetic process. Moreover, in the contrary to diagenetized samples that exhibit strong positive correlation between $\delta^{18}O$ and $\delta^{13}C$ (Cornu et al., 1993), a negative correlation is found for the three species during the events (e.g. for the measurements with $\delta^{13}C_{G.ruber}$<-2‰ ; slope = -4.9 with r^2=0.65).

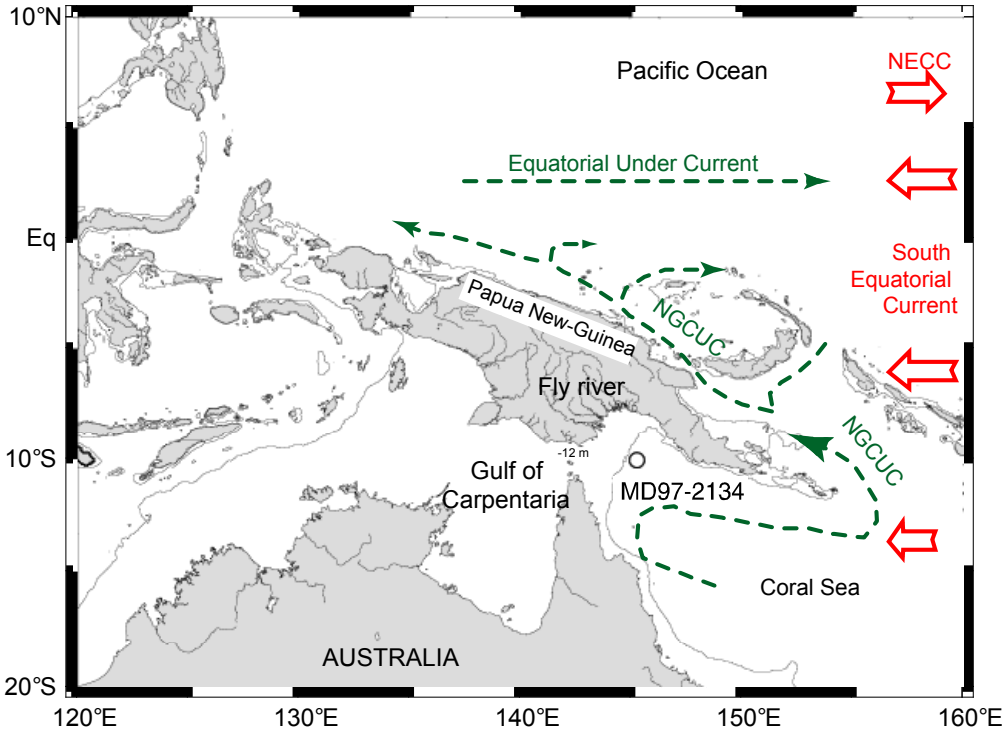

Figure 2 : Map location of the MD97-2134 core in the Papua Gulf: The MD97-2134 core is located off the Fly river mouth, at 700 m depth, and above the path of the New Guinea Coastal Undercurrent (NGCUC) that feeds the Equatorial Undercurrent.

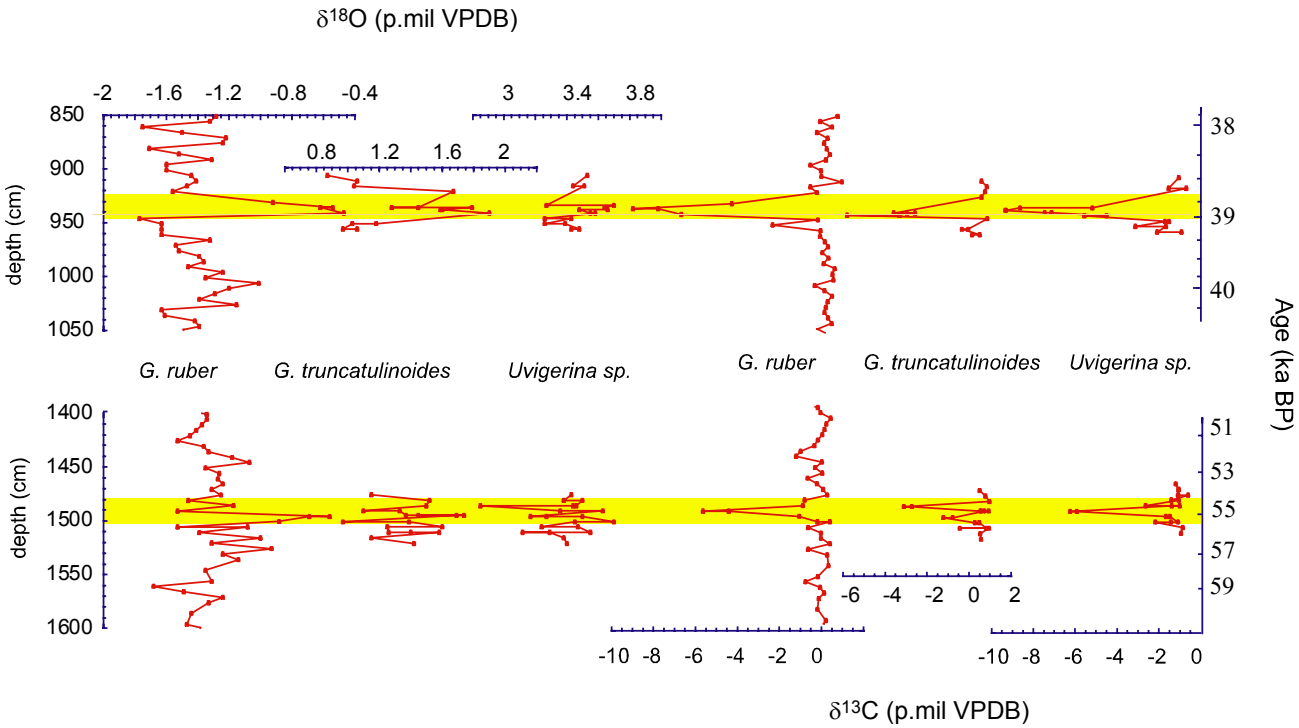

Figure 3 : Oxygen and carbon isotope records in the MD97-2134 for three foraminifera species: *G. ruber* (shallow-dwelling), *G. truncatulinoides* (deep-dwelling) and *Uvigerina sp*. (benthic).

The foraminifera $\delta^{13}C$ is a function of the $\delta^{13}C$ of Dissolved Inorganic Carbon (DIC), air-sea exchange rate and temperature(Spero et al., 1997). The last two factors have only minor influence on $\delta^{13}C$ (Lynch-Steiglitz et al., 1995). Three $\delta^{13}C$ depleted sources have been invoked to explain past excursions in the DIC isotopic composition. (A) Volcanic and hydrothermal activities release large amounts of CO_2 with $\delta^{13}C$ of ~ –5‰ (Wignall, 2001). This value is nevertheless to high to explain the 39 and 55 ka BP excursions of our record. (B) An alternate hypothesis could be the occurrence of exceptional flows from the Fly river with $\delta^{13}C_{DIC}$ of ~ -10‰. Three counter-arguments exclude this hypothesis : First, atmosphere-river CO_2 exchange tends to modify the DIC isotopic composition towards the equilibrium value of $\delta^{13}C_{DIC}$~1‰ (Yang et al., 1996). The "flow hypothesis" would also imply that the isotopic composition of the 700m thick water column reflects only the riverine pool, without any influence from the seawater pool. Moreover, the Fly river flow scenario does not agree with the positive ~0.8‰ peak occurring simultaneously in the planktonic $\delta^{18}O$ record. This shift corresponds to an approximate 2°C cooling, and/or an increase in local salinity. A catastrophic increase of riverine inputs from the Papua New Guinea should have corresponded to a decrease in salinity leading to a depleted $\delta^{18}O$ excursion, opposite to what is observed in our record. (C) Finally, large methane gas hydrate releases with an average $\delta^{13}C$ value of ~–65‰ can be invoked to explain the amplitude of the carbon excursion. They would correspond to large discharges correlated with

instabilities on the continental slope (Dickens et al., 1997). Bottom Simulating Reflectors which are associated with gas hydrates occurrences in deep sea sediments, have been described in the western Pacific marginal seas (McKirdy and Cook, 1980; Neben et al., 1998). They certify that conditions of gas hydrate storage and formation are assembled in this area.

A large degassing of methane, lasting less than 10,000 years, has been invoked to explain anomalously depleted $\delta^{13}C$ values during the Late Paleocene Maximum Temperature interval in the North Atlantic (Dickens et al., 1995). The source of methane, identified on seismic tracks, has been attributed to the Black Nose slump. Simple modeling studies show that a methane release of such an amplitude would lead to a warming of 5°C in the high latitudes and 1-2°C in the low latitudes, by enhancing the greenhouse effect (Schmidt and Shindell, submitted). Similarly, four isotopic excursions, associated with warm intervals in marine isotopic stage 3, were described in multi-species benthic foraminifera records from the Santa Barbara Basin (Kennett et al., 2000). The amplitude of those excursions is lower than the amplitude of anomalies recorded in our core MD97-2134 (~2.5‰ and 9‰, respectively). The authors attribute these events to large hydrate destabilizations occuring during the interstadials of isotopic stage 3 (Kennett et al., 2000). However, the isotopic anomalies in the planktonic fauna are only short events, restricted to two peaks at 39 and 44 ka BP (Dansgaard-Oeschger 8 and 11). Furthermore, Stott et al. (Stott et al., 2002) have recently underlined the strong $\delta^{13}C$ gradient existing in the sediment pore water. This microhabitat effect linked with carbon fluxes could explain part of the 2.5‰ excursion in benthic foraminifera. We avoid this type of problem by considering a single foraminifera species throughout the event. This strategy is possible because there are little oceanic changes in sea temperatures and nutrient conditions in the western Pacific warm pool during stage 3.

Stability of gas hydrates varies with temperature and pressure (Kvenvolden, 1988). During the stage 3, the sea-level was lowered by 80 m (Yokoyama et al., 2001), reducing the hydrostatic pressure and enhancing the probability of clathrate dissociations. The 39 kyr event, which shows the strongest anomaly, is marked by two successive steps : the $\delta^{18}O$ decrease of benthic foraminifera indicates a slight warming (~1°C) of deep-sea waters, this warming being interrupted by a sharp cooling, in phase with the carbon isotopic anomaly (Fig.3). The cooling phase affects more strongly shallow ($\Delta\delta^{18}O \approx +1‰$ i.e.~ –4°C) than deep-sea waters. We interpret this cooling as the mixing of the water column induced by the thermal dissociation of gas hydrates, as recorded by benthic foraminifera. The cooling of the deep-sea waters likely occurred due to the mixing with deeper, and thus cooler waters. The chronological succession is less clear for the 55 kyr BP excursion. The difference between the two events might be linked to a lower sedimentation rate at 55 kyr BP and thus a stronger effect of the bioturbation which altered its small scale details (Bard, 2001).

The methane released during these events was oxidized in the water column. The increase in ΣCO_2 in the water column due to methane oxidation; leaded to an increase of the deep-sea carbonate dissolution (Dickens, 2001). This increase in ΣCO_2 and carbonate dissolution is confirmed by the presence of automorphic gypsum in the sediments, as determined by X-ray diffraction. The crystallization of gypsum results from the availability of Ca^{2+} ions in the seawater due to the dissolution of carbonates. If the methane released was completely oxidized in the water column, we should expect a gradient in $\delta^{13}C_{DIC}$ from the bottom to the surface waters, with the more depleted values close to the sea-floor as established nowadays above modern gas hydrate vents (Suess et al., 1999). However, the $\Delta\delta^{13}C$ values recorded in the sea-surface waters are close to the deep waters ones during the two excursions (fig. 3). This implies that the process which released the gas hydrates was very short and massive. The methane in excess could have been degassed in the atmosphere, warming up the temperatures by its greenhouse effect (Nisbet, 1992). Sediment destabilization due to the thermal dissociation of clathrates is the most likely phenomenon which could degas these very large amounts of methane (Katz et al., 1999). The amount of methane released that can be estimated represents only the oxidized part of the gas hydrate, and cannot be refined due to the rather poor understanding of modern methane oxidation processes.

Using a C-isotope mass-balance equation, we estimated the amount of oxidized methane. Assuming that the anomaly recorded in the MD97-2134 core affected an oceanic volume of $1000km^3$, which is not unrealistic given the surface of the Papua Gulf and its location in the open Pacific, the volume of CH_4 degassed during the main event at ~39 ka BP is about $\sim 4.5\times10^{10}$ m^3 [1]. It corresponds to ~4 Tg of methane, which is 3 times higher than the estimates made for the Santa Barbara Basin by Kennett et al.(Kennett et al., 2000). The assumption made on the volume of the ocean affected by the event linearly controls this estimate (with a slope equal to 1). A single core does not allow a better constrain on that parameter. Given a gas hydrate density of $0.9g/cm^3$, and assuming that the slump affects a sediment depth of 20 meters in which 50% of the expected 20% porosity is filled by the gas-hydrate, Paull et al.(Paull et al., 1991) computed that $1.8.10^8$ gC are released by 1 km^2 of slump. Using our estimates of methane release, the corresponding size of the slump is $22km^2$; in comparison to the 5-10 km^2 slump associated to the Sissano, Papua New Guinea tsunami of 1998 (Tappin et al., 2001) and to the 34,000 km^2 width of the largest slump reported (Paull et al., 1991). If we assume that an equivalent quantity of methane oxidized in the water column is released in the atmosphere, the direct radiative effect of the 39 kaBP excursion reaches ~0.05 $W.m^{-2}$, and ~0.002 $W.m^{-2}$ if we account for methane reaction with OH in the troposphere (Houghton et al., 2001). This magnitude corresponds to a minimal estimate, and could easily be increased by one order of magnitude by changing the volume of

[1] For this estimation, we assume that the isotopic anomaly in the d13C *G. ruber* of -8.31‰ results from a linear mixing between the methane pole (9) (-65‰) and the sea-water pole (corresponding to the

water affected, the ratio of degassed/oxidized methane or by taking into account the methane trapped under the gas hydrates.

The amounts of methane released during these events have to been considered in models of the global methane cycle and of climate modelling. Because these events are short in duration, only very high sedimentation records can reveal them. Such records in low latitudes are extremely rare at the moment, and explain the uniqueness of our findings. However such events should have been extremely common in other low latitude margins because they are richer in Bottom Simulating Reflectors than the Papua Gulf. Therefore huge amounts of gas hydrates could have been released during warm parts of low sea-level stands on low latitudes margins. Confirmation of such releases will be adduced by retrieval of other high-resolution sedimentary records, in comparable environments. The thermal dissociation of clathrate should be synchronous on the margins where the gas hydrates are located, and thus act as a strong positive feedback of the global climate system at millenial time-scale. This amplification of a warming by thermal dissociation of methane gas hydrates could explain the 0-30 yrs time-lag between the temperatures and the methane concentration in the ice-cores records (Severinghaus and Brook, 1999), by the time needed to transfer the atmospheric heating to the marginal sediments.

Acknowledgements : The support of French MENRT, TAAF, CNRS/INSU and IFRTP to the Marion-Dufresne and the IMAGES Program was necessary to perform this work. Thanks to B. Lecoat for performing mass spectrometry measurements in the LSCE. We are grateful to L. Labeyrie, G. Ménot-Combes and K. Tachikawa for careful reviews of early versions of the manuscript.

background value of 0.31‰). The DIC concentration in the Western Pacific is 0.0022 mol.l-1 (Zhang and Quay, 1997).

References and notes :

Bard, E., 2001, Paleoceanographic implications of the difference in deep-sea sediment mixing between large and fine particles: Paleoceanography, v. 16, p. 235-239.

Blunier, T., and Brook, E.J., 2001, Timing of millenial-scale climate change in Antarctica and Greenland during the last glacial period: Science, v. 291, p. 109-112.

Broecker, W., and Hemming, S., 2001, Climate swings come into focus: Science, v. 294, p. 2308-2310.

Brook, E.J., Harder, S., Severinghaus, J., Steig, E.J., and Sucher, C.M., 2000, On the origin and timing of rapid changes in atmospheric methane during the last glacial period: Global Biogeochemical Cycles, v. 14, p. 559-572.

Chappellaz, J., Blunier, T., Raynaud, D., Barnola, J.-M., Schwander, J., and Stauffer, B., 1993, Synchronous changes in atmospheric methane and Greenland climate between 40 and 8 kyBP: Nature, v. 366, p. 443-445.

Cornu, S., Pätzold, J., Bard, E., Meco, J., and Cuerda-Barcelo, J., 1993, Paleotemperature of the last interglacial period based on d18O of Strombus bubonius from the western Mediterranean Sea: Palaeogeography Palaeoclimatology Palaeoecology, v. 103, p. 1-20.

Dallenbach, A., Blunier, T., Fluckiger, J., Stauffer, B., Chappellaz, J., and Raynaud, D., 2000, Changes in the atmospheric CH4 gradient between Greenland and Antarctica during the Last Glacial and the transition to the Holocene: Geophysical Research Letters, v. 27, p. 1005-1008.

Dickens, G., 2001, On the fate of past gas: what happens to methane released from a bacterially mediated gas hydrate capacitor?: Geochemistry, Geophysics, Geosystems, v. 2.

Dickens, G.R., Castillo, M.M., and Walker, J.C.G., 1997, A blast of gas in the latest Paleocene: simulating first-order effects of massive dissociation of oceanic methane hydrate: Geology, v. 25, p. 259-262.

Dickens, G.R., O'Neil, J., Rea, D.K., and Owen, R.M., 1995, Dissociation of oceanic methane hydrate as a cause of the carbon isotope excursion at the end of the Paleocene: Paleoceanography, v. 10, p. 965-971.

Gillot, P.Y., Labeyrie, J., Laj, C., Guérin, G., Poupeau, G., and Delibrias, G., 1979, Age of the Laschamp geomagnetic polarity excursion revisited: Earth and Planetary Science Letters, v. 42, p. 444-450.

Guyodo, Y., and Valet, J.-P., 1996, Relative variations in geomagnetic intensity from sedimentary records: the past 200,000 years: Earth and Planetary Science Letters, v. 93, p. 239-256.

Harris, P.T., Pattiaratchi, C.B., Kenne, J.B., Darlymple, R.W., Gardner, J.V., Baker, E.K., Cole, A.R., Mitchell, D., Gibbs, P., and Schroeder, W.W., 1996, Late quaternary deltaic and carbonate sedimentation in the Gulf of Papua foreland basin : response to sea-level change: Journal of Sedimentary Research, v. 66, p. 801-819.

Houghton, J.T., Ding, Y., Griggs, D.J., Noguer, M., van der Linden, P.J., and Xiaosu, D., 2001, Climate Change, 2001 : The Scientific Basis - Contribution of Working Group I to the third assessment report of the Intergovernmental Panel on Climate Change (IPCC): Cambridge, Cambridge University Press, 944 p.

Imbrie, J., Hays, J.D., Martinson, D.G., McIntyre, A., Mix, A.C., Morley, J.J., Pisias, N.G., Prell, W.L., and Shackleton, N.J., 1984, The orbital theory of pleistocene climate: support from a revised chronology of the marine $\delta^{18}O$ record, *in* A.L. Berger, e.a., ed., Milankovitch and climate, Volume I, D. Reidel Publishing Company, p. 269-305.

Katz, M.E., Pak, D.K., Dickens, G.R., and Miller, K.G., 1999, The source and fate of massive carbon input during the latest Paleocene thermal maximum: Science, v. 286, p. 1531-1533.

Kennett, J.P., Cannariato, K.G., Hendy, I.L., and Behl, R.J., 2000, Carbon isotopic evidence for methane hydrate instability during quaternary interstadials: Science, v. 288, p. 128-133.

Kvenvolden, K.A., 1988, Methane hydrates and global climate: Global Biogeochemical Cycles, v. 2, p. 221-229.

Kvenvolden, K.A., 1995, A review of the geochemistry of methane in natural gas hydrate: Organic Geochemistry, v. 23, p. 997-1008.

Laj, C., Kissel, C., Mazaud, A., Channell, J.E.T., and Beer, J., 2000, North Atlantic paleointensity stck since 75 ka BP (NAPIS-75) and the duration of the Laschamp event: Philosophical Transactions of the Royal Society London A, v. 1768, p. 1009-1025.

Lynch-Steiglitz, J., Stocker, T.F., Broecker, W.S., and Fairbanks, R.G., 1995, The influence of air-sea exchange on the isotopic composition of oceanic carbon: observations and modeling: Global Biogeochemical Cycles, v. 9, p. 653-665.

McKirdy, D.M., and Cook, P.J., 1980, Organic geochemistry of Pliocene-Pleistocene calcareous sediments, DSDP site 262, Timor trough: American Association Petroleum Geologists Bulletin, v. 64, p. 2118-2138.

Mulitza, S., Dürkoop, A., Hale, W., Wefer, G., and Niebler, H.S., 1997, Planktonic foraminifera as recorders of past surface-water stratification: Geology, v. 25, p. 335-338.

Neben, S., Hinz, K., and Beiersdorf, H., 1998, Reflection characteristics, depth and geographical distribution of bottom simulating reflectors within the accretionary wedge of Sulawesi, *in* Henriet, J.-P., and Mienert, J., eds., Gas hydrates- relevance to world margin stability and climatic change, Volume 137: Special Publication: London, The Geological Society, p. 255-265.

Nisbet, E.G., 1992, Sources of atmospheric CH4 in early postglacial time: Journal of Geophysical Research, v. 97, p. 12,859-12,867.

Paull, C.K., Ussler III, W., and Dillon, W.P., 1991, Is the extent of glaciation limited by marine gas-hydrates ?: Geophysical Research Letters, v. 432-434, p. 3.

Raynaud, D., Chappellaz, J., and Blunier, T., 1998, Ice-core record of atmospheric methane changes: relevance to climatic changes and possible gas hydrate sources, *in* Henriet, J.-P., and Mienert, J., eds., Gas hydrates: relevance to world margin stability and climate change, Volume 137: Special Publications: London, Geological Society, p. 327-331.

Schmidt, G.A., and Shindell, D.T., submitted, Atmospheric composition, radiative forcing and climate change as a consequence of a massive methane hydrate release: Paleoceanography.

Severinghaus, J.P., and Brook, E.J., 1999, Abrupt climate change at the end of the last glacial period inferred from trapped air in polar ice: Science, v. 286, p. 930-934.

Spero, H.J., Bijma, J., Lea, D.W., and Bemis, B.E., 1997, Effect of seawater carbonate concentration on foraminiferal carbon and oxygen isotopes: Nature, v. 390, p. 497-500.

Stott, L.D., Bunn, T., Prokopenko, M., Mahn, C., Gieskes, J., and Bernhard, J.M., 2002, Does the oxidation of methane leave an isotopic fingerprint in the geologic record ?: Geochemistry, Geophysics, Geosystems, v. 3, p. 1-16.

Suess, E., Torres, M.E., Bohrmann, G., Collier, R.W., Greinert, J., Linke, P., Rehder, G., Trehu, A., Wallmann, K., Winckler, G., and Zuleger, E., 1999, Gas hydrate destabilization: enhanced dewatering, benthic material turnover and large methane plumes at the Cascadia convergent margin: Earth and Planetary Science Letters, v. 170, p. 1-15.

Tappin, D.R., Watts, W., McMurtry, G.M., Lafoy, Y., and Matsumoto, T., 2001, The Sissano, Papua New Guinea tsunami of July 1998 - offshore evidence of source mechanism: Marine Geology, v. 175, p. 1-23.

Wignall, P.B., 2001, Large igneous provinces and mass extinctions: Earth Science Reviews, v. 53, p. 1-33.

Yang, C., Telmer, K., and Veizer, J., 1996, Chemical dynamics of the "St. Lawrence" riverine system: dD H2O, d18O H2O, d13C DIC, d34S sulfate, and dissolved 87Sr/86Sr: Geochimica et Cosmochimica Acta, v. 60, p. 851-866.

Yokoyama, Y., Esat, T.M., and Lambeck, K., 2001, Coupled climate and sea-level changes deduced from Huon peninsula coral terraces of the last Ice age: Earth and Planetary Science Letters, v. 193, p. 579-587.

Zhang, J., and Quay, P.D., 1997, The total organic carbon export rate based on 13C and 12C of DIC budgets in the equatorial Pacific region: Deep-Sea Research II, v. 44, p. 2163-2190.

Partie II

-

Dynamique Glaciaire-Interglaciaire

Chapitre 3 : Températures glaciaires-interglaciaires des eaux de surface de l'océan Pacifique équatorial :

La température des eaux de surface de l'océan Pacifique ouest équatorial est critique dans la circulation atmosphérique globale. Actuellement avec des températures annuelles supérieures à 28°C (Yan et al., 1992), la convection nuageuse à grande échelle existe toute l'année dans cette zone, formant la branche ascendante des cellules de Walker, de mousson transverse, et de mousson latérale (cf. introduction). En dessous du seuil de 27.5°C, cette convection dite « profonde » (« deep convection »), cesse de fonctionner, et le fonctionnement des trois cellules atmosphériques est modifié (Waliser and Graham, 1993). En dessus de 29.5°C, la convection nuageuse caractéristique du Pacifique ouest, est également arrêté (Waliser and Graham, 1993). Les variations de température au cours du temps dans la zone d'eaux chaudes du Pacifique ouest sont donc critiques pour la compréhension de la dynamique atmosphérique globale.

Les températures au dernier maximum glaciaire ont fait l'objet d'un grand débat depuis les estimations du groupe CLIMAP (CLIMAP, 1976). Ce groupe indiquait un refroidissement d'environ 1°C dans le cœur du réservoir d'eaux chaudes du Pacifique occidental. En contraste, les données continentales semblent indiquer un refroidissement plus marqué, d'environ 4°C, d'après la présence de glacier sur la Papouasie Nouvelle Guinée, et les données polliniques (Farrera et al., 1999). La compilation récente de toutes les données environnementales disponibles pointe vers des températures 2.5°C plus froides au dernier maximum glaciaire (Crowley, 2000).

La différence entre les estimations issues des données continentales et celles fournies par les marqueurs marins a fait l'objet de nombreuses interprétations. Pour le domaine océanique, un biais pourrait provenir de la dissolution des carbonates qui modifierait la composition des assemblages de foraminifères planctoniques utilisé dans les reconstructions des tempéraures des eaux de surface (Thompson, 1981). Une seconde hypothèse implique les faibles taux de sédimentation des carottes étudiées dans cette zone : les assemblages glaciaires et holocènes seraient affectés par la bioturbation qui atténuerait l'amplitude glaciaire-interglaciaire (Anderson et al., 1989). La dernière objection repose sur l'absence de carottes convenablement datées du dernier maximum glaciaire, même dans le travail de CLIMAP.

Dans ce chapitre, nous avons étudié la variabilité des températures des eaux de surface dans la carotte MD97-2138, située dans le cœur de la zone d'eaux chaudes du Pacifique ouest. Cette carotte possède un taux de sédimentation important, est peu affectée par la dissolution des carbonates et a été bien datée. Nous avons utilisé pour établir les paléotempératures des eaux de surface, deux marqueurs : l'insaturation des alkénones, lipides produits par les prymnesiophycées (coccolithophoridés) dont le degré d'insaturation est une fonction de la température de croissance, et les fonctions de transfert des assemblages de foraminifères planctoniques.

Principe des fonctions de transfert :

La composition spécifique des assemblages de foraminifères planctoniques est contrôlée par différents facteurs environnementaux (biotiques et abiotiques) dans lequel vivaient les organismes. Les processus sédimentaires peuvent également modifier les assemblages. Les fonctions de transfert sont des méthodes statistiques qui permettent de quantifier la relation existant entre les assemblages de foraminifères planctoniques et ces paramètres environnementaux. La température des eaux de surface océaniques a depuis plus de 30 ans fait l'objet de reconstructions par des fonctions de transfert sur les foraminifères planctoniques. Depuis, les facteurs qui ont été considérés comme critiques pour la composition spécifique outre la température des eaux de surface sont la production primaire et la profondeur de la thermocline/ profondeur de la couche de mélange. Plus récemment, la modification induite par la dissolution préférentielle de certaines espèces a été utilisée pour reconstruire le pH des environnements sédimentaires (Anderson and Archer, 2002).

L'hypothèse fondamentale de ces méthodes est celle de l'actualisme : c'est à dire que les relations existantes entre les assemblages et les paramètres biotiques et abiotiques sont supposées ne pas avoir changé au cours du temps. Cette hypothèse est particulièrement problématique dans le cas d'assemblages fossiles n'ayant pas d'analogues actuels. Cette hypothèse peut également être problématique dans le cas d'assemblages modernes similaires mais liés à des conditions environnementales différentes.

Trois principales méthodes statistiques ont été utilisées pour les reconstitutions environnementales à partir des foraminifères planctoniques :

1 – Les fonctions de transfert d'Imbrie et Kipp (1971) :

Ces méthodes désormais classiques en paléoclimatologie, se basent sur la diagonalisation de la matrice espèces-abondances relatives des échantillons de sédiment de surface. Le poids relatif des différentes espèces pour chaque facteur issu de la diagonalisation, fait alors l'objet d'une régression multiple avec le paramètre choisi, en l'occurrence, dans le travail original d'(Imbrie and Kipp, 1971), la température des eaux de surface. Cette régression multiple permet d'obtenir une équation reliant le paramètre voulu à l'assemblage fossile.

2 – La méthode des analogues :

Cette méthode calcule une distance algébrique, appelée coefficient de dissimilarité, entre deux assemblages (Hutson, 1980; Prell, 1985). Chaque assemblage fossile est comparé avec une base de données d'assemblages modernes, pour trouver les n plus proches analogues en fonction du coefficient de dissimilarité (en moyenne 5 à 10). Les valeurs environnementales des analogues seront alors pondérées par ce coefficient pour reconstruire les paléo-environnements. Une révision de cette

méthode permet de choisir dynamiquement le nombre d'analogues le plus approprié à chaque assemblage fossile (Waelbroeck et al., 1998).

3 – Les réseaux neuronaux :

Cette méthode utilise les réseaux de neurones qui font l'apprentissage des assemblages en fonction du paramètre choisi pour prédire en fonction de cet assemblage les paléo-paramètres (Malmgren and Healy-Williams, 1978). Chaque neurone est une fonction non-linéaire. Cette méthode permet d'obtenir de très bons résultats sur les bases de données modernes. Cependant, la justesse des résultats obtenus ne peut pas être quantifiée.

Jusqu'à présent, la principale limitation des fonctions de transfert était l'absence d'analogues modernes pour des assemblages fossiles. Cet écueil a été résolu en diagonalisant non plus les sédiments modernes, mais les sédiments de carotte qui permettent de prendre en compte la variabilité temporelle (Cayre et al., 1999; Mix et al., 1999). L'autre problème des fonctions de transfert peut être la présence d'analogues modernes non pertinents, dans lesquels la composition des assemblages est influencée par un autre paramètre que celui reconstruit. Dans ce chapitre nous mettons en évidence que la suppression de la base de données de tels échantillons, en l'occurence non pas influencés par les températures mais par la structure trophique, permet de proposer une solution au paradoxe des températures du Pacifique Ouest pendant le dernier stade glaciaire.

Résumé de l'article en anglais (soumis le 13 mars 2002 à *Paleoceanography*)

Les températures des eaux de surface du Pacifique Ouest équatorial ont été reconstruites pour les 180 000 dernières années en utilisant deux méthodes indépendantes : les alkénones et les fonctions de transfert basées sur les foraminifères planctoniques dans la carotte IMAGES MD97-2138 située au Nord de la Papouasie Nouvelle Guinée. Pour la fonction de transfert basée sur les foraminifères planctoniques, pour éviter les biais liés à la dissolution et à la structure de la colonne d'eau, nous avons développé une nouvelle fonction de transfert régionale (TROP-2), que nous avons calibré avec des sédiments de sommets de carotte excluant la zone Est Pacifique où les abondances de *Neogloboquadrina dutertrei.* Cette anomalie résulterait plus probablement de l'écosystème particulier riche en nitrate et pauvre en chlorophylle (zone HNLC) que de la température ou de la profondeur de la thermocline. En utilisant cette nouvelle fonction de transfert, la différence de température des eaux de surface entre le dernier maximum glaciaire et le sommet de carotte est comprise entre 0.1-1.3°C en accord avec les estimations de CLIMAP. Toutefois, l'amplitude dernier stade glaciaire/Holocène atteint des valeurs plus grandes de 2.2°C, pour les deux méthodes. Pendant les 30 derniers ka, les températures les plus froides régnaient il y a environ 18 cal. Ka BP, postérieurement au dernier maximum glaciaire s.s. ; l'intervalle le plus chaud a eu lieu entre 9 et 5 cal. Ka BP, dans l'Holocène récent. La différence de température entre le stade 6 et le stade 5 est d'environ 2°C en utilisant les

foraminifères planctoniques, et de 0.9°C avec la méthode des alkénones. Nous concluons que dans le Pacifique ouest équatorial, une stratégie de calibration des fonctions de transfert prenant en compte la structure des écosystèmes donne de meilleures estimations des températures des eaux de surface. En utilisant cette méthode les intervalles les plus chauds et les plus froids ne sont pas synchrones, respectivement, des périodes modernes et du dernier maximum glaciaire. L'amplitude totale de variations des températures des eaux de surface dans le Pacifique équatorial est d'environ 2-3°C au cours du Pléistocène récent.

Références :

Anderson, D.A., and Archer, D., 2002, Glacial-interglacial stability of ocean pH inferred from foraminifer dissolution rates: Nature, v. 416, p. 70-73.

Anderson, D.M., Prell, W.L., and Barratt, N.J., 1989, Estimates of sea-surface temperatures in the Coral Sea at the last Glacial Maximum: Paleoceanography, v. 4, p. 615-627.

Cayre, O., Beaufort, L., and Vincent, E., 1999, Paleoproductivity in the Equatorial Indian Ocean for the last 260,000 yr : A transfer function based on planktonic foraminifera: Quaternary Science Reviews, v. 18, p. 839-857.

CLIMAP, P.M., 1976, The surface of the ice-age earth: Science, v. 191, p. 1131-1137.

Crowley, T.J., 2000, CLIMAP SSTs revisited: Climate Dynamics, v. 16, p. 241-255.

Farrera, I., Harrison, S.P., Prentice, I.C., Ramstein, G., Guiot, J., Bartlein, P.J., Bonnefille, R., Bush, M., Cramer, W., von Grafenstein, U., Holmgren, K., Hooghiemstra, H., Hope, G., Jolly, D., Lauritzen, S.-E., Ono, Y., Pinot, S., Stute, M., and Yu, G., 1999, Tropical climates at the Last Glacial Maximum: a new synthesis of terrestrial palaeoclimate data. I. Vegetation, lake-levels and geochemistry: Climate Dynamics, v. 15, p. 823-856.

Hutson, W., 1980, The Agulhas Current during the Late Pleistocene: Analysis of modern faunal analogs: Science, v. 207, p. 64-66.

Imbrie, J., and Kipp, N.G., 1971, A new micropaleontological method for quantitative paleoclimatology : application to a late Pleistocene Caribbean core, *in* Turekian, K.K., ed., The late Cenozoic Glacial Ages: New Haven, Conn., Yale University Press, p. 71-181.

Malmgren, B., and Healy-Williams, N., 1978, Variation in test diameter of Orbulina universa in the paleoclimatology of the late Quaternary of the Gulf of Mexico: Palaeogeography Palaeoclimatology Palaeoecology, v. 25, p. 235-240.

Mix, A.C., Morey, A.E., and Pisias, N.G., 1999, Foraminiferal faunal estimate of paleotemperature: circumventing the no-analog problem yields cool ice age tropics: Paleoceanography, v. 14, p. 350-359.

Prell, W.L., 1985, The stability of low-latitude sea-surface temperatures: an evaluation of the CLIMAP reconstruction with emphasis on the positive SST anomalies: Providence, Brown University, p. 60.

Thompson, P.R., 1981, Planktonic foraminifera in the western North Pacific during the past 150 000 years: comparison of modern and fossil assemblages: Palaeogeography, Palaeoclimatology, Palaeoecology, v. 35, p. 241-279.

Waelbroeck, C., Labeyrie, L., Duplessy, J.-C., Guiot, J., Labracherie, M., Leclaire, H., and Duprat, J., 1998, Improving past sea surface temperature estimates based on planktonic fossil faunas: Paleoceanography, v. 13, p. 272-283.

Waliser, D.E., and Graham, N.E., 1993, Convective cloud systems and warm pool SSTs: coupled interactions and self-regulation: Journal of Geophysical Research, v. 98, p. 12881-12893.

Yan, X.-H., Ho, C.-R., Zheng, Q., and Klemas, V., 1992, Temperature and size variabilities of the Western Pacific Warm Pool: Science, v. 258, p. 1643-1645.

Glacial-Interglacial Sea Surface Temperatures in the equatorial Western Pacific using planktonic foraminifera and alkenones.

Thibault de Garidel-Thoron*, Luc Beaufort, Edouard Bard, Corinne Sonzogni
CEREGE/Université d'Aix-Marseille III – Europôle Méditerranéen de l'Arbois
13545 Aix-en Provence CEDEX4
France

Alan C. Mix
College of Oceanography and Atmospheric Sciences, Oregon StateUniversity, Corvallis, OR97331, USA

Submitted to Paleoceanography 13 march 2002-03-13
MS #2002PA000785

Abstract :

We investigated past changes in Sea Surface Temperatures of the Western Pacific Warm Pool during the last 180,000 years, by applying two independent methods: alkenones and transfer functions based on planktonic foraminifera in core MD97-2138, located north of Papua New Guinea. For the latter, to circumvent dissolution and biases linked to hydrological structure we developed a new regional transfer function (TROP-2), which we calibrated with intertropical core-tops excluding the Eastern Pacific area where anomalous high abundances of *Neogloboquadrina dutertrei* may result more from the High Nitrate Low Chlorophyll ecosystem than from temperature or thermocline depth gradients. Using this new transfer function, the core-top-LGM SST difference is about 0.1-1.3^{o}C, consistent with CLIMAP estimates. However, the total Late Glacial-to-Holocene SST range here, based on both proxies, is substantially greater, about 2.2°C. Within the past ~30 ka, the coldest conditions occurred near 18 cal. ka BP, younger from the L.G.M. *s.s,* and the warmest interval occurred between 5-9 ka, in the early Holocene. The stage 6 - stage 5 difference is about 2°C using TROP-2 and only 0.9°C using the alkenones method, and overall the time series from the two different proxies are different. Nevertheless, we conclude that in the WPWP, a strategy of calibrating regional, ecosystem-relevant transfer functions yields better estimates of SST change, and based on this proxy, peak warm and cold conditions here were not coincident with modern and LGM time intervals. The total range of SST variability in the region is 2-3^{o}C in late Pleistocene time.

1 Introduction :

The Western Pacific Warm Pool (WPWP), with the warmest waters of the global ocean (Fig.1), is a key area to understand past changes in latitudinal and longitudinal climatic gradients. For example, the modern WPWP is involved in the strength of the East Asian monsoon, plays a role in the Walker atmospheric circulation processes that are at the origin of the El Niño Southern Oscillation (ENSO) phenomenon, and may help to control the water vapor content of the troposphere [*Pierrehumbert*, 2000]. The stability of the WPWP during the glacial times is critical for the past atmospheric dynamics reconstructed by General Circulation Models (e.g [*Yin and Battisti*, 2001]).

The first global SST reconstruction [*CLIMAP*, 1976] indicated that SSTs in the WPWP were 1.1°C colder than at present during the Last Glacial Maximum (LGM). In the WPWP, alkenones reconstructions have shown a cooling of the same order during the LGM [*Ohkouchi et al.*, 1994]. However, other proxies have shown that tropical SSTs in this region may have been cooler during the LGM (e.g.[*Bard*, 1999]). Pollen data from Papua New Guinea indicate continental temperatures lowered by 4°C during the LGM [*Hope and Tulip*, 1994]. Glacier advances, broadly associated with the glacial maximum but not well dated, suggest WPWP cooling of about 3^{o}C relative to modern conditions [*Hostetler and Clark*, 2000]. In agreement, taking into account glacial sea-level lowering, Mg/Ca in planktonic foraminifera show glacial SSTs cooled by 2.6°C in the WPWP [*Lea et al.*, 2000]. By contrast, coral records Sr/Ca paleothermometry from the Papua New Guinea indicate that late glacial SSTs were 5-6°C cooler [*Beck et al.*, 1997; *Gagan et al.*, 2000].

In this study, we designed a SST transfer function that is not biased by other parameters like depth of the thermocline or the trophic structure in the water column. Planktonic foraminifera assemblages in core MD97-2138 (1°25'S, 146°24'E, 1900 m deep) taken in the WPWP during the IMAGES III cruise were investigated to document past changes in SSTs during the last 180,000 years in the WPWP. We will compare the results from estimates of the planktonic foraminifera transfer function with those obtained by the alkenones method.

2 – Methods

2.1 – Imbrie-Kipp transfer functions :

The classical Imbrie-Kipp transfer functions [*Imbrie and Kipp*, 1971] are based on a principal component analysis of the modern countings which results are regressed with the oceanic parameters. One limitation of this method is the assumption that glacial assemblages are represented in the modern core-tops data-set. If this is not the case, the method can result in an unstable extrapolation of the faunal space. To test this assumption , the communality, a measure of the similarity of the modern and fossil fauna, is computed. Low communalities imply so-called "no-analog" conditions. An approach to circumvent the no-analog problem consists in a downcore matrix diagonalization of the assemblages

to include in the factor matrix both the glacial and interglacial assemblages [*Cayre et al.*, 1999; *Mix et al.*, 1999]. In this method, core-top assemblages are expressed using the factor scores computed downcore, and core-tops which are included in the same range of factor loadings are regressed against modern oceanic parameters. This method is particularly useful for oceanic regions that have acute problems of glacial analogs and gives the useful advantage to be able to check the way it derives predictors from training data.

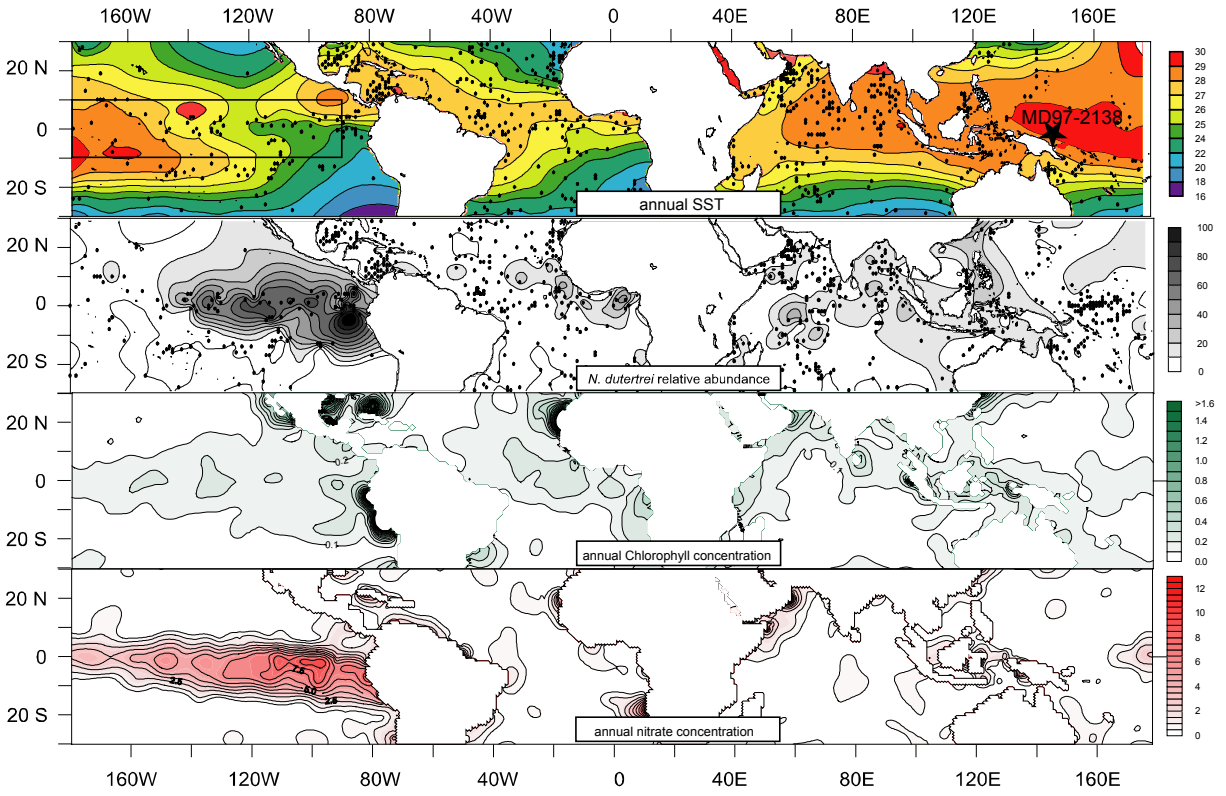

Figure 1 – (A) - Tropical Sea Surface Temperatures in the intertropical belt. The rectangular delimit the area of core-tops exclusion from the data-set for transfer function TROP2. Dots indicate the location of the core-tops from CLIMAP and from Martinez et al, 1998. The location of the core MD97-2138 is reported by a star. (B)- Relative abundance of *Neogloboquadrina dutertrei* from CLIMAP and Martinez et al, 1997 countings. (C) – annual sea surface chlorophyll concentration. (D) annual sea surface nitrate concentration.

2.2 - Modern Analog Technique (MAT)

The modern analog method of [*Hutson*, 1980] further tested by [*Prell*, 1985] and [*Pflaumann et al.*, 1996], computes the statistical similarity between fossil and modern assemblages. Modern oceanographic conditions associated with a selection of core-top samples that are most similar to the fossil sample are then averaged to yield paleoenvironmental estimates. The main advantage of this method is that it does not extrapolate with an a priori relationship between one parameter and one assemblage. A possible limit of this technique is its inability to reconstruct no-analog conditions that

have not been sampled adequately in the core-top calibration dataset, or that do not exist in the modern ocean. A derived method is the *Revised Analog Method* (RAM) [*Waelbroeck et al.*, 1998], which chooses dynamically the closest analogs, slightly differentiating from the MAT with an arbitrary number of analogs have to be fixed, and by smoothing the calibration data set by interpolating samples within a chosed environmental parameter space. Both the objective choice of analogs and the smoothing of the modern data set in the RAM method result in apparently improved precision of estimates, although the accuracy of estimates remains difficult to assess.

2.3 - A regional transfer function for the Western Pacific:

All transfer functions may be affected by biases resulting from partial dissolution of the fossil assemblages, bioturbation mixing, and error in identifying SST as responsible for faunal variations when it results either wholly or partially from an other parameter [*Ortiz and Mix*, 1997]. Dissolution bias can be diminished by excluding taxa sensitive to dissolution, and by making sure that dissolution effects within the calibration data set are uncorrelated with the primary effects to be estimated, such as SST [*Mix et al.*, 1999]. Bioturbation tends to obscure signals by mixing together fossil assemblages that lived under different environmental conditions, but this effect can be minimized by selecting cores with high enough sedimentation rates. Systematic bias in the transfer function within the calibration data set can be estimated by the slope and intercept of the regression line between observed and estimated values. Random errors can be estimated in the same way, by the root mean square of the residuals of the estimated vs. observed values.

When calibrating transfer functions, it is important to include samples that span a broad range of environments that may have occurred within the area of interest, but equally important to exclude samples from regions that are oceanographically or climatically irrelevant. We expect this is the case in past transfer-function estimates of SST in the WPWP. Several authors have proposed that SSTs are not the only parameter affecting the ecology of foraminifera. Among others, Primary Production [*Cayre et al.*, 1999; *Mix*, 1989], depth of the thermocline[*Andreasen and Ravelo*, 1997; *Chen and Prell*, 1998], and nutrient concentration [*Crowley*, 2000] have been proposed as sensitive factors for foraminifera distribution. Based on living assemblages in the equatorial Pacific Ocean, [*Watkins and Mix*, 1998] have shown that Primary Production might bias temperature predictions. Such effects may be especially problematic for paleoceanographic estimates in the WPWP based on transfer functions, because such a broad range of productivities and nutrient concentrations are found, from very high in the East, to moderate production and high nutrient concentration in the equatorial Eastern Pacific, to relatively low production and nutrient abundance in the West. Inclusion of samples from the eastern equatorial Pacific when calibrating transfer functions for the WPWP may thus induce ecological biases and poor temperature estimates.

2.3.1 Core-top data set :

To design a new regional transfer function for the WPWP, core-tops data were extracted from the Brown University Foraminiferal Database [*Prell et al.*, 1999] and additional Eastern Indian oceans samples were added from [*Martinez et al.*, 1998]. We limit the data-set to the latitudinal band 30°N-30°S . Within this latitude band,SSTs range from 20 to 30°C, much larger than the glacial inferred temperatures inferred from other proxies. Further, the depth water structure is typical in the intertropical zone, with, for example, sharp and deep thermocline/pycnoclines in the Western basins.

We retained 26 taxa following the choice by [*Mix et al.*, 1999] who exclude *Globorotalia tumida*, *Globorotalia menardii*, and *Globorotalia menardii flexuosa* in order to limit potential biases linked with selective preservation of these taxa. The *Neogloquadrina pachyderma–Neogloboquadrina dutertrei* (P-D) intergrade was grouped with the *N. dutertrei* taxa. Unlike Mix et al, [1999] our analysis was not log-transformed to avoid the amplification of the errors linked due to rare species counts.

2.3.2. Oceanic parameters :

SSTs, Sea-Surface Salinities (SSS) and Sea-Surface Nitrates (SSN) concentrations data were extracted from the World Ocean Atlas 1998 [*Conkright et al.*, 1998]. The thermocline depth was computed both as (1) the 18°C isotherm following [*Andreasen and Ravelo*, 1997] and as (2) the minimum of the first derivative of the polynomial fit of the depth/temperature profile. The density was computed using the equation of state [*Fofonoff and Millard*, 1983]. The pycnocline depth was determined as the maxima in the second derivative of the density/depth profile. The Primary Production (PP) estimates were derived using a model of column-integrated oceanic primary production deduced from the chlorophyll concentration as derived by satellite imagery [*Antoine et al.*, 1995].

2.4. Downcore analysis : foraminifera and stratigraphy

The foraminifera were picked in the fraction above 150 μm. Stable isotopes measurements were carried out on the surface-dweller species *Globigerinoides ruber* (white). Measurements were performed at the Oregon State University facility. Radiocarbon ages were determined also on *G. ruber* (white). ^{14}C dating was performed at the Tandetron in Gif/Yvette facility (table 1). ^{14}C ages were converted to calendar ages using the INTCAL98 calibration (1998) for the last 18,000 years and the polynomial fit of [*Bard*, 1998] for the age before the calibration range studied by INTCAL98. The $\delta^{18}O$ record was tuned to the SPECMAP stack (Fig. 2). The disappearance of *G. rube*r pink fits the termination II, validating the age model [*Thompson et al.*, 1979].

Table 1 : Age Model of MD97-2138 Core

Radiocarbon Ages and Tie-points from the SPECMAP stack used in MD97-2138 chronology

Depth in Core, cm	AMS 14C Age	Error	Calendar Age, years		Accession Number
1	3 350	60	3208	*G. ruber (white)*	GifA-101001
65	9 210	90	9830	*G. ruber (white)*	GifA-101002
101	11 790	110	13177	*G. ruber (white)*	GifA-101003
165	15 630	140	18090	*G. ruber (white)*	GifA-101004
220	19 420	150	22451	*G. ruber (white)*	GifA-101005
280	25 030	230	28930	*G. ruber (white)*	GifA-101006
501			60000	SPECMAP	
561			69000	SPECMAP	
646			83000	SPECMAP	
745			113000	SPECMAP	
826			128000	SPECMAP	
991			180000	SPECMAP	

Figure 2 – Oxygen isotopes of the planktonic foraminifera G.ruber in the MD97-2138 core. 14C ages position are indicated together with the Late Appearance datum of Globigerinoides ruber (pink) at the termination II.

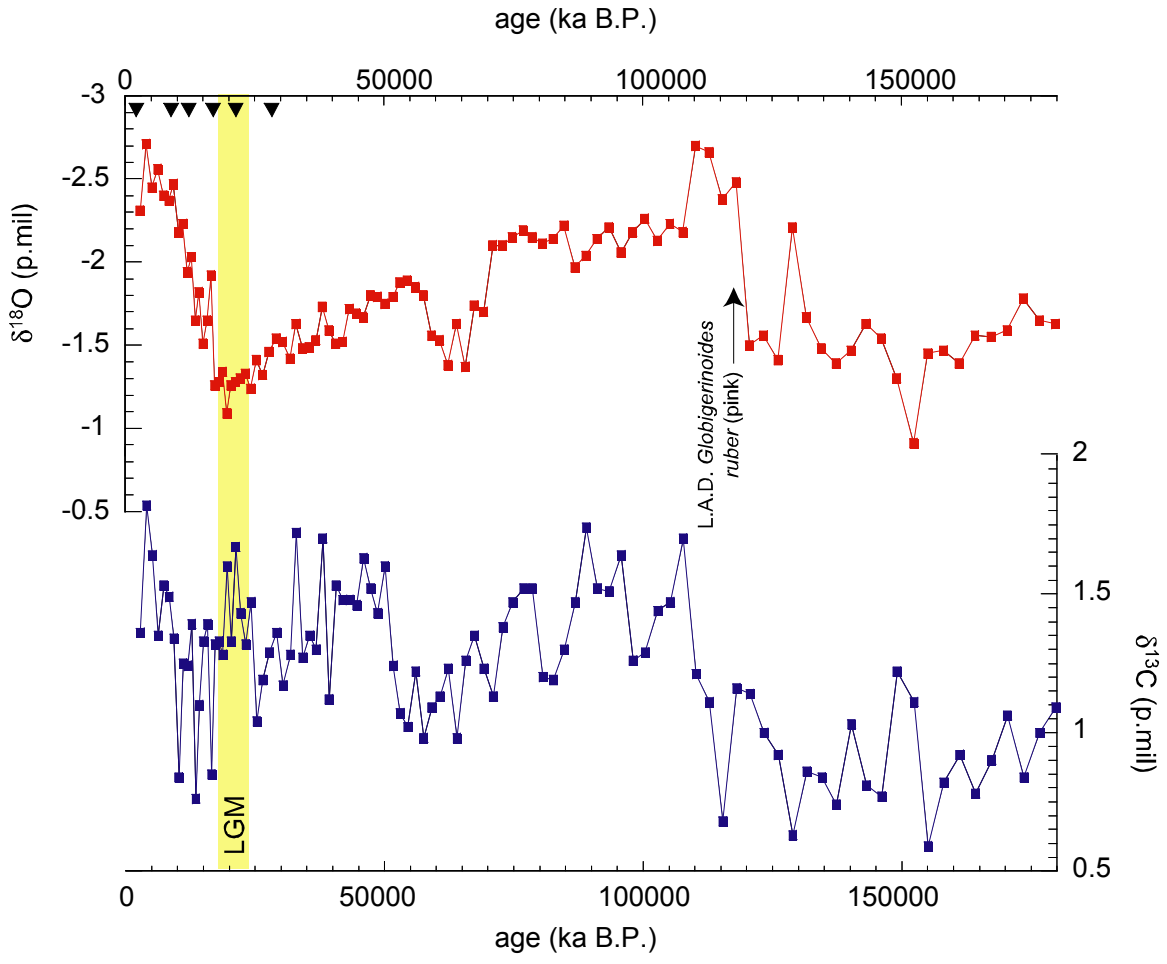

2.5 Alkenone measurements :

Alkenones were analysed by gas-chromatography following the method described by [*Sonzogni et al.*, 1997] except that an automated Dionex Accelerated Solvent Extractor (ASE-200) was used to perform lipid extraction. Proper identification and quantification of alkenones was verified by gas-chromatography mass spectrometry. The concentration of C37 alkenone is expressed as ng/g of dry sediment as calculated with a C32 ester internal standard added in the ASE-cell before the extraction. The analytical precision based on repeated extraction of internal laboratory sediment standard during the whole procedure is about 15% for C37 alkenone concentrations and 0.01 units (roughly equivalent to 0.3°C). The accuracy of our procedure has been checked within the framework of the international alkenone intercomparison [*Rosell-Mélé et al.*, 2001].

3 . Results :

3.1 : Eastern equatorial Pacific an anomalous area ? - modification of the core-top data-set

[*Andreasen and Ravelo*, 1997] showed that the Pacific foraminifera fauna can be correlated to the depth of the thermocline. *Neogloboquadrina dutertrei* (including P.-D. intergrade) in the core-tops from the intertropical area, is highly abundant in the Eastern Pacific (between 80 and 140°W) (~95% , Fig. 1). This anomaly is restricted to the Eastern Pacific and does not reach the same amplitude in the Eastern Atlantic (42.8% at the maximum) or in the Indian Ocean (28.4 % at maximum) in spite of similar SST conditions. Clearly, SST is not uniquely responsible for the geographical distribution of *N. dutertrei on a global basis*. [*Andreasen and Ravelo*, 1997] have noticed that in the Pacific, their factor with high loadings of *N. dutertrei* is correlated to thermocline depth. This is the case for relative abundance above 20%, but not for abundances below 20% which are common in the rest of the intertropical ocean (Fig. 3 and Tab. 2).

Table 2 : Neogloboquadrina dutertrei relative abundance correlation coefficients against the thermocline depth.

Core-top data-set and correlation coefficients between thermocline depth and N. dutertrei abundance

Core-top dataset	R2	Number of core-tops
Intertropical	0.19	888
Atlantic	0.12	286
Indian	0.07	323
Pacific	0.57	279
HNLC box	0.61	52
Pacific w/o HNLC	0.48	227

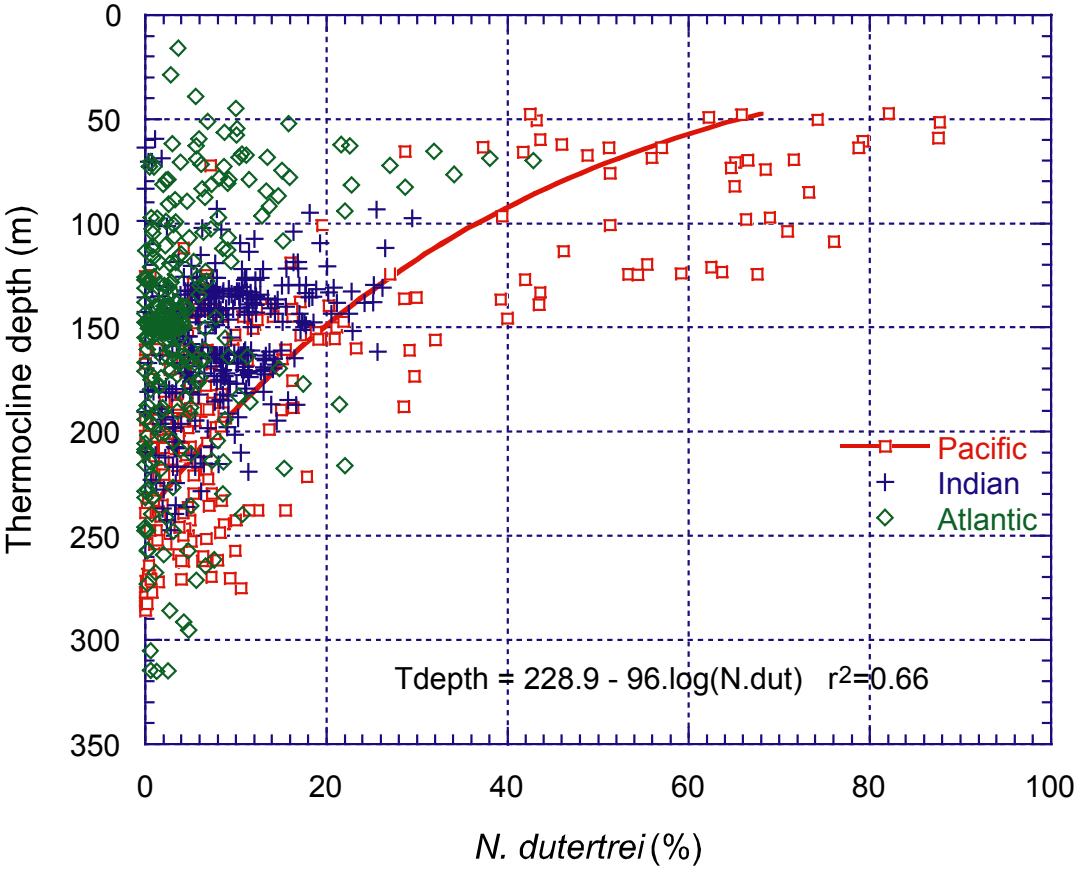

Figure 3 – Relative abundance of *N. dutertrei* vs. the depth of thermocline (here isotherm 18°C). The abundances above 20% occur prominently in the Eastern Pacific.

The Eastern equatorial Pacific is special in the tropics because the nutrients are abundant in the upper surface, but the PP is moderate and nutrients are not consumed to zero in surface waters (Fig. 1). This state is called the High-Nitrate Low-Chlorophyll (HNLC) paradox. The hypothesis of productivity limited by low iron concentration [*Martin*, 1990] has been validated by laboratory and in-situ experiments in the Eastern Pacific and in the Southern Pacific (e.g. [*Coale et al.*, 1996]). Such areas appear to result in unique ecosystems. We suggest that this feature of the eastern equatorial Pacific could be responsible of the high abundances of *N. dutertrei* limited to that area. [*Andreasen and Ravelo*, 1997] use the relationship between *N. dutertrei* and the depth of the thermocline to reconstruct past thermocline depths changes. This relationship is very strong in the Eastern Pacific but weak anywhere else. Because we observe that this relation is regional, we choose to exclude the Eastern Pacific from our core-top database by excluding the 180°W-90°W/10°N-10°S core-tops for our new (TROP-2) transfer function to reconstruct past SSTs changes in the Western Pacific. This area is slightly larger than the *N. dutertrei* anomalous area, but accounts for the HNLC area defined by other proxies [*Longhurst*, 2001]. For comparison, we will show also the result of a transfer function (TROP-1) which is calibrated using all core-tops of the tropics including those from the HNLC area. We speculate that the regional anomaly in *N. dutertrei* could be the result of a cryptic speciation of

this planktonic phenotype, as already shown for other foraminifera species which also show different environmental preferences [*Darling et al.*, 1997; *de Vargas et al.*, 1999].

Using this dataset, we tried to test empirically which oceanic parameter gives the best correlation with foraminifera fauna using a Imbrie-Kipp approach (Table 3). We establish that the correlation coefficient between predicted and observed SSTs for the transfer function TROP-2 is the best, and its Residual Mean Square (RMS) error is ~1.2°C. The PP could also be estimated using an Imbrie-Kipp transfer function. However, its RMS error (± 48 $g.C.m^{-2}.a^{-1}$) is as large as the PP variability observed in the Western Pacific. The stratification of the upper water column are not adequately predicted by these transfer functions. Therefore SST is the parameter that can be estimated from foraminiferal assemblages with the best precision in the WPWP.

Table 3 : Imbrie-Kipp transfer functions properties for different oceanic parameters.

parameter	R^2	RMS	# of Factors	# of Core-Tops
SST	0.78	1.14	8	860
PP	0.76	47.70	8	882
SSNitrate	0.61	0.72	8	859
Sea-surface salinity	0.53	0.67	8	860
pycnocline depth	0.52	26.46	8	837
thermocline depth	0.49	36.59	8	836
TDOT	0.44	1.76	8	837

3.2 : Faunal factors

The factor loadings of the transfer function TROP-2 were mapped in figure 4. The distribution of the different faunal factors is very similar to transfer functions produced in other studies (e.g. [*Mix et al.*, 1999; *Thompson*, 1981]). However, the weightings differ with lower influence of *N. dutertrei* than in [*Andreasen and Ravelo*, 1997] and [*Mix et al.*, 1999].

In our TROP-2 analysis, Factor 1 has high loadings in the oligotrophic subtropical areas. It is dominated by *G. ruber* and *G. sacculifer*, two near-surface dwellers that live in relatively warm conditions (Tab.4). Factor 2 is dominated by *G. bulloides* and *G. glutinata, species common* in upwelling regions of the Arabian Sea and off South America, and to a lesser extent off California (Tab.4). Factor 3 corresponds to *Neogloboquadrina dutertrei,* and its loadings are highest in the Eastern Pacific, in the Eastern Atlantic and in the Eastern Indian oceans. Factor 4 have high weights in the upwelling of Benguela and off Mauritania. These areas are dominated by *Neogloboquadrina*

pachyderma right and by *G. inflata* (Tab.4). The distribution of Factor 5seems to be linked with the western equatorial currents where *Pulleniatina obliquiloculata* is the main contributor (Tab.4).

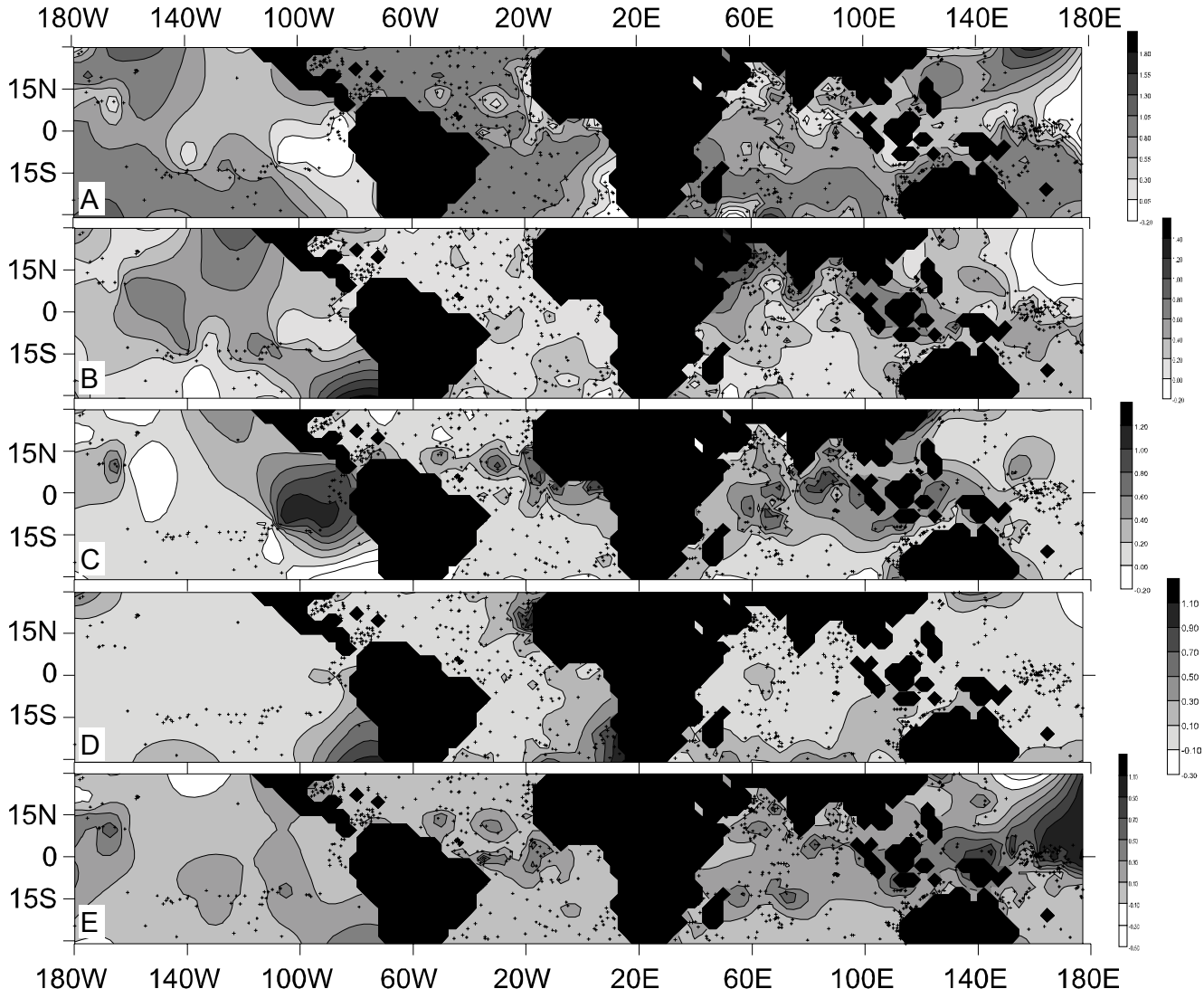

4 - Factor distribution of the transfer function TROP-2. A : First factor. B: second factor. C : Third factor. D : fourth factor. E : fifth factor.

3.3 : Evaluating transfer function bias

The residuals of the estimated vs. observed SSTs were plotted in function of several parameters to test for eventual systematic biases in the transfer function that should modify the cluster distribution of this plot (Fig. 5). This test together with the empirical method of testing the possibility to develop a robust transfer function (Tab. 3), indicate potential biases of the transfer functions. The SST residuals appear not to be influenced by the water depth, which is assumed to be correlated with dissolution intensity. The withdrawal of the menardiids from the database has thus minimized

dissolution biases. The thermocline depth and the pycnocline depth do not affect SST residuals, indicating that the estimation of SSTs is not linked with the stratification of the upper layers. Similarly, Primary Production does not bias systematically the SST residuals. In conclusion, it appears that the residuals of the TROP-2 estimated vs. observed SSTs do not seem to be influenced by other parameters currently argued to influence transfer functions.

Table 4 : Varimax loading scores of the transfer function TROP-2 (abbreviations follow the CLIMAP acronyms[*CLIMAP*, 1976]).
Varimax factor scores matrix TF TROP2

	FACTOR 1	FACTOR 2	FACTOR 3	FACTOR 4	FACTOR 5	FACTOR 6	FACTOR 7	FACTOR 8
univ----	0.02	-0.01	0.02	0.03	0.01	0.02	0.01	0.04
cglo----	0.04	-0.01	0.05	-0.02	0.04	0.03	0.02	0.02
rubt----	0.95	0.05	0.01	0.03	-0.01	-0.25	-0.13	0.00
tene----	0.03	0.03	-0.01	0.02	-0.01	-0.04	0.02	0.02
sact----	0.25	-0.06	0.13	0.02	0.06	0.93	0.00	-0.02
dehi----	0.00	-0.01	0.06	-0.01	0.05	-0.01	0.01	0.00
aequ----	0.08	0.01	0.05	-0.01	0.11	0.17	0.06	0.02
cali----	0.04	0.02	0.01	0.02	0.01	0.01	-0.02	0.03
bull----	-0.11	0.71	-0.04	0.09	0.01	0.09	-0.65	-0.02
falc----	0.00	0.13	-0.04	0.04	0.00	0.00	-0.12	0.20
digi----	0.00	0.00	0.05	-0.01	0.00	0.01	0.02	0.04
rubs----	0.02	0.02	-0.01	0.01	0.00	-0.03	0.02	0.00
quin----	0.00	0.00	0.00	0.02	0.00	0.00	0.00	0.00
pacl----	0.00	0.00	0.00	0.03	0.01	0.00	0.00	-0.01
pacr----	-0.02	-0.03	0.02	0.94	0.01	-0.03	0.10	-0.32
pdtr----	-0.05	0.09	0.98	-0.01	-0.08	-0.13	0.01	0.02
cglm----	0.00	0.01	0.06	-0.03	0.01	0.07	0.02	0.00
hexa----	0.00	0.02	0.02	-0.01	-0.01	0.01	0.01	-0.01
obli----	-0.02	0.01	0.06	-0.02	0.99	-0.09	0.00	0.00
infl----	-0.02	-0.04	-0.01	0.32	0.00	0.02	0.03	0.90
trul----	0.01	-0.01	-0.01	0.01	0.00	-0.02	-0.01	0.12
trur----	0.03	-0.02	-0.01	0.01	0.02	-0.06	-0.04	0.15
cras----	0.01	-0.01	0.03	0.00	0.01	0.00	-0.01	0.04
hirs----	0.00	0.00	0.00	0.01	0.00	-0.01	-0.01	0.06
scit----	0.01	0.00	0.00	0.01	0.00	0.00	0.00	0.04
glut----	0.07	0.68	-0.07	-0.04	0.00	0.02	0.73	0.02
VARIANCE	51.17	18.66	10.32	3.29	6.67	3.22	2.17	2.27
CUM. VAR	51.17	69.82	80.15	83.44	90.11	93.34	95.51	97.78

3.4 : Application to the Western Pacific core MD 97-2138

We apply the transfer function TROP-2 to faunal counts in the MD97-2138 core (Fig. 6). The SSTs inferred from a whole intertropical data-set of core-tops (integrating the Eastern equatorial Pacific core-tops) are also plotted (transfer function TROP-1). The TROP-1 estimate of 27.5°C from

core-top SST is cooler than modern temperatures, which are 29.4°C, with a low seasonal range of 0.4°C, WOA98[*Conkright et al.*, 1998]. Using TROP-2, SST estimates closest to the core top are slightly warmer than TROP-1, about 27.8°C, and the Holocene mean value resulting from TROP-2 is about 28°C. This is slightly lower than modern values, and equivalent to temperatures at ~100 m depth, roughly the base of the euphotic zone. An early Holocene temperature optimum, with TROP-2 estimates above 29°C appears between 5 and 9 cal ka BP. TROP-1 estimates from the early Holocene (~28.6°C) are also warmer than late-Holocene values, but not as warm at TROP-2 estimates. At greater ages, TROP-1 and TROP-2 estimates diverge and in some cases (such as MIS-6) are essentially uncorrelated.

The coldest SSTs during the marine isotopic stage 2 computed with TROP-2 are around 26.7°C (i.e. 2.3°C colder than the early Holocene warm SSTs). The SST difference between modern (core-top) and LGM (18-24 calendar ka BP as defined by EPILOG, [*Mix et al.*, 2001]) only 0.6°C using the TROP2 transfer function. The TROP-1 transfer function estimates SSTs during the LGM the same or wamer than for the core-top. Down-core, SSTs computed with TROP2 indicate warmer SSTs during the stages 5.1; 5.3 and 5.5 at about 28.5°C. The SSTs computed with TROP-1 for these interglacials stages are not significantly warmer than those of the glacial stages. Stage 5.5 SSTs inferred from TROP2 transfer function are slightly warmer than the coretop SSTs, but cooler than the early Holocene warmth, and have similar values in stages 5.1 and 5.3. Stage 6 SSTs are estimated around 26.5°C with TROP-2 and 27.5°C with TROP-1. In summary, it appears that transfer function TROP-2 yields glacial SSTs ~2°C cooler than typical interglacial SSTs. Coolest temperatures, between 15 and 18 ka BPpostdate the LGM, and warmest temperatures occurred in the early Holocene.

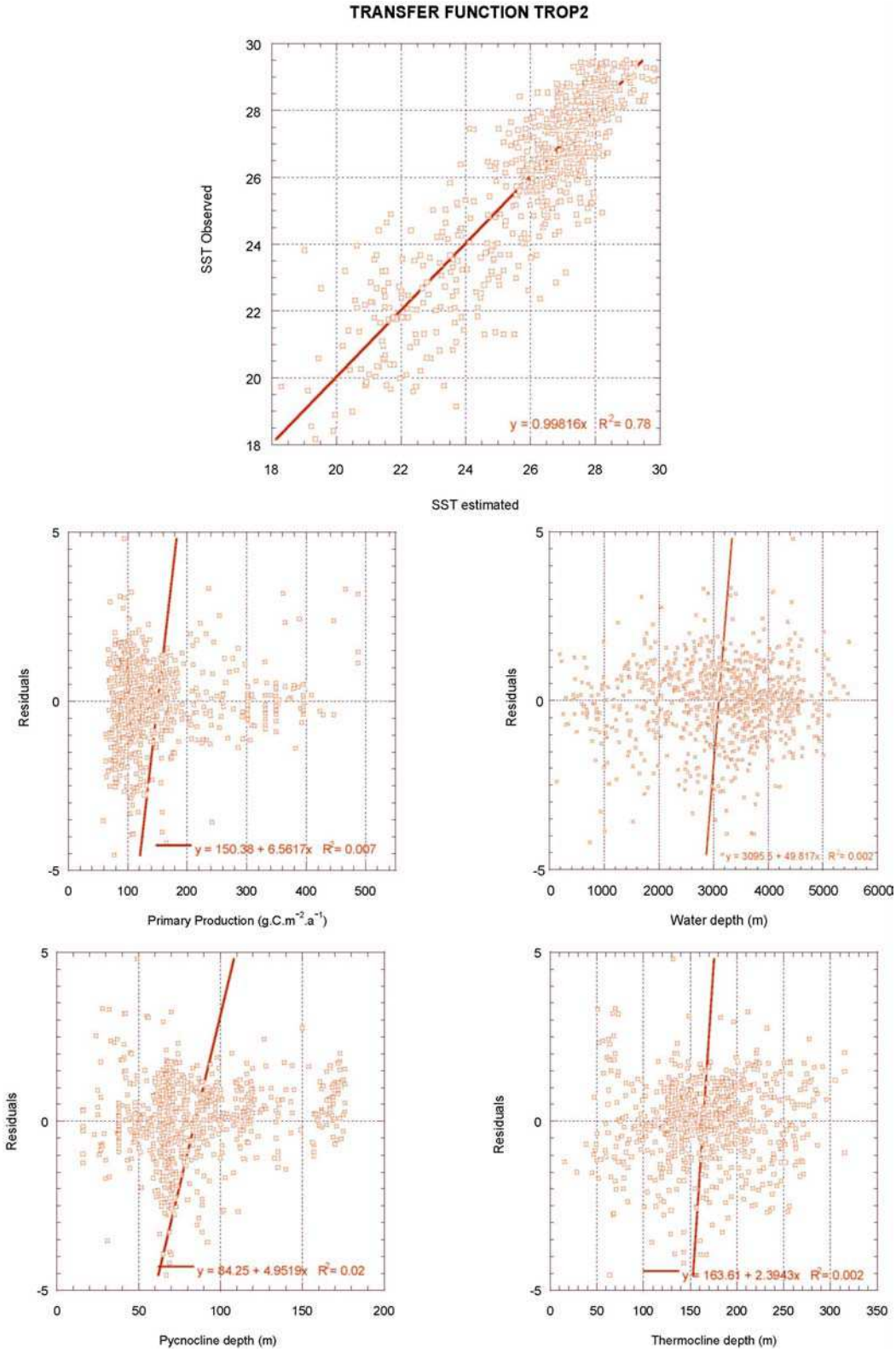

5 – Test of the transfer function TROP-2 : A - observed vs. estimated temperatures of TROP-2. (B) Primary Production (C) pycnocline depth (D) water depth and (E) Sea-surface salinities do not show any correlation with the residuals of the predicted SSTs by TROP-2 indicating that the transfer function is not biased the PP, the hydrologic structure of the upper water column, and by dissolution affecting the planktonic foraminifera.

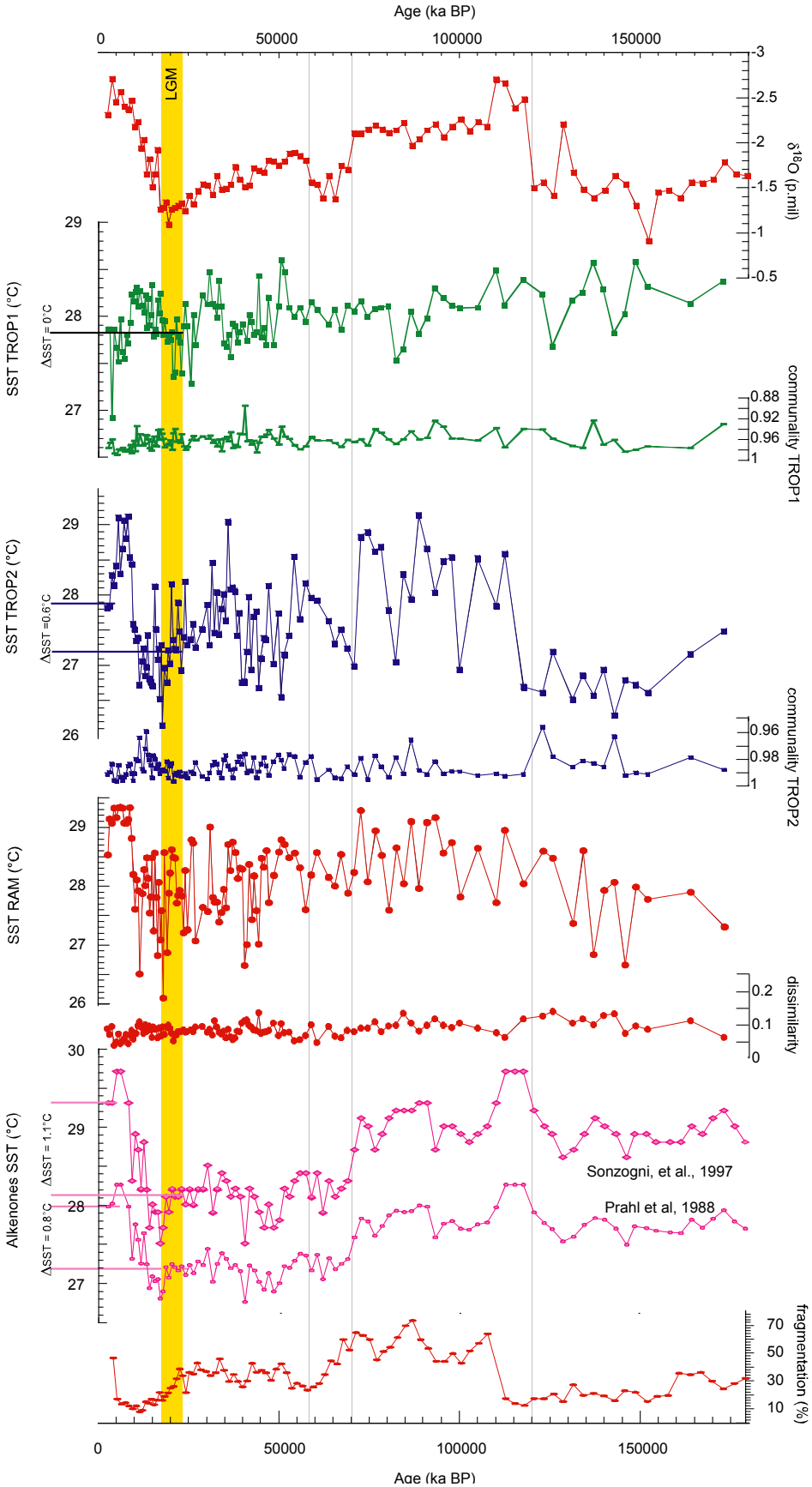

Figure 6 – Sea surface temperatures inferred from planktonic foraminifera transfer functions and alkenones. (A) TROP-2 , the transfer function which does not include Eastern Pacific core-tops (B) TROP-1, computed with Eastern Pacific core-tops (C) RAM transfer functions using a core-top database which includes the Eastern Pacific.

We infer that TROP-2 SST estimates are not biased by dissolution, based on the absence of correlation between the SSTs and the fragmentation index of planktonic foraminifera (Fig. 6). However, during the stage 5, the fragmentation index is very high so that foraminifera SSTs should be used with caution during this time period. The lack of any clear trend in the TROP-1 transfer function SSTs estimates is indicative of the bias introduced by Eastern Pacific samples. In TROP-1, the inclusion of core-top samples with very large abundances of N. dutertrei in cool waters of the eastern equatorial Pacfic has desensitised the transfer function to changes that do not involve that species. That implies that previous transfer function estimates of the WPWP that included eastern Pacific samples may had been biased by ecological problems and therefore should be discounted.

3.5 : Alkenones SSTs :

Uk'_{37} SSTs were also derived from two different calibration equations: (1) the [*Prahl et al.*, 1988] equation is based on culture experiments of *Emiliania huxleyii* (2) the [*Sonzogni et al.*, 1997] equation is derived from low latitude core-tops. The two equations have their own pitfalls, because that of Prahl does not take into account the effect of gephyrocapsiids on alkenone unsaturation index, and that of Sonzogni has not been yet validated in the equatorial Pacific. The core-top SSTs estimates are respectively 29.3°C using Sonzogni and 28°C with the Prahl equation, both close to the saturation of the alkenone paleothermometer. The estimates of Sonzogni are about 1^oC higher than those of Prahl. In the core top, the Sonzogni estimates approximate modern atlas temperatures(29.4^oC), while those of Prahl are consistent with temperatures at the base of the euphotic zone.

The coldest SSTs estimates based on alkenones during the isotopic stage 2 occur around 18 cal. Ka BP, roughly coincident with coolest SSTs estimated by TROP-2, but the Sonzogni alkenone estimates are warmer, ~27.5°C, whereas the Prahl alkenone estimates of 26.8°C are approximately the same ast the TROP-2 values. The SST difference between modern and L.G.M. *s.s*. are respectively 1.1°C and 0.8°C using the Sonzogni and Prahl estimates. The total glacial-interglacial SST range is around 2.2°C for termination I using Sonzogni calibration. The glacial substages of marine isotopic stage 5 are associated with a change in SST weaker than 0.4°C. The stage 5.5 alkenones SSTs reach the same temperatures as the early Holocene SSTs. Stage 6 alkenones SST estimates are only 1°C cooler than the stage 5.5 estimates using the same equations, and both are substantially warmer than the transfer function estimates made with TROP-2.

4. Discussion :The glacial SSTs in the Western Pacific

4.1 : The Last Glacial Maximum:

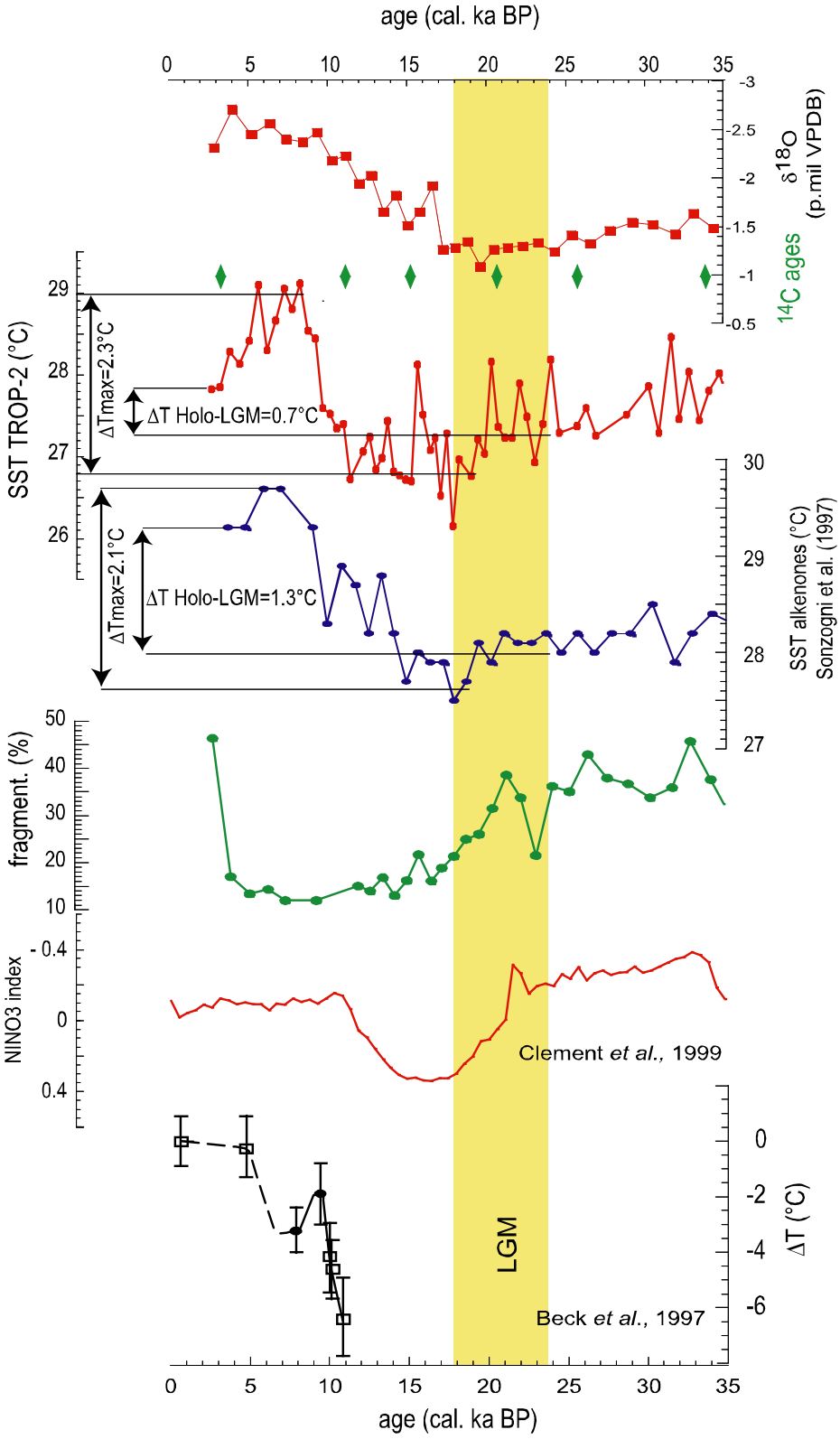

Figure 7 – Sequence of the deglaciation inferred from planktonic foraminifera transfer function TROP-2 ; alkenones SSTs. Coral SST record from the Vanuatu island shows the same abrupt warming at about 10 cal. ka BP.

Estimating glacial SSTs in the WPWP is important because even relatively small changes in the warm pool are important to global climate processes [*Crowley*, 2000]. Previous foraminiferal transfer functions showed LGM SSTs that were 0.5°C-1°C cooler than the modern SSTs [*Anderson et al.*, 1989; *Thompson*, 1981]. Our total deglacial temperature range of ~2.2oC is significantly larger than these estimates, but our difference between core-top and LGM values of ~1°C is within the range of these previous estimates.

Compared to the CLIMAP LGM temperatures estimates, our LGMs SSTs are in the same range (1°C cooler). However, in the CLIMAP study, none of the 10 cores located in the equatorial Western Pacific have been radiocarbon dated [*Moore et al.*, 1980]. Half of the 10 cores located in this area were dated using the oxygen isotope, and the five other ones were dated using faunal assemblages and lithologic evidences. In the MD97-2138 core, using the oxygen isotope record the LGM cannot be distinguished from the coldest maximum around 17 cal.ka BP. The paleotemperature WPWP CLIMAP reconstruction for the LGM *s.s.* should be used with caution due to chronological uncertainties.

Elsewhere, using the transfer function FP12-E, [*Lee and Slowey*, 1999] find glacial SSTs 2°C colder than at present in the central subtropical. However, this core is close to the coast (6km from Oahu, Hawaï), so that island effect on the glacial SSTs could have amplified LGM cooling coastal mixing associated with stronger winds. Note that we suggest that the CLIMAP transfer function FP12-E is not suitable in the WPWP due to the bias linked to the Eastern Pacific core-tops. Mg/Ca SSTs from planktonic foraminifera in the WPWP indicate a glacial-interglacial range of about 2.8°C [*Lea et al.*, 2000] in approximate agreement with our results. Using the alkenone method, the LGM was 1°C cooler in the WPWP [*Ohkouchi et al.*, 1994], however this result was from a core with a very low sedimentation rate and bioturbation could have mixed glacial and interglacial sediments. Our observed range of alkenone temperatures is larger, near 2.1°C, however our glacial-coretop difference is quite similar to that of Ohkouchi et al., [1994], suggesting that bioturbation has not destroyed the basic signal.

Continental records exhibit larger glacial/interglacial temperature amplitude. The ~ 130 m sea-level lowering during the L.G.M [*Clark et al.*, 2001], implies a ~1°C amplification of the sea-continent temperature differences. The Equilibrium Lines Altitudes (ELA-snowlines) show that the Western Pacific surrounding ELAs were depressed by more than 900 m (±135 m) in the New Guinea island, corresponding to a cooling of about 6°C to 3.5°C (5°C to 2°5C sea-level corrected) as reviewed by [*Porter*, 2001]. Modeling studies indicate that this ΔELA corresponds with a SST cooling in the WPWP of about 2.5-3°C cooler than modern SSTs [*Crowley*, 2000; *Hostetler and Mix*, 1999]. We suggest that the difference between the continental reconstructions and our marine record could be due to the uncertainties in the temporal framework of the continental glaciers. The maximum glacial advance could postdate the LGM *s.s*. and thus be synchronous with the coldest maximum in the

MD87-2138 core. At our knowledge, there is no coral SST record spanning the LGM in the Western Pacific.

4.2. : Precession and ENSO dynamics in the Western Equatorial Pacific :

The MD97-2138 SST record is unusual for termination I (Fig. 7). At theLGM *s.s.* [*Mix et al.*, 2001] SSTs are 1°C warmer than the coolest SSTs at about 19 ka BP. Between 19 ka BP and 11 ka BP, cooler conditions prevailed before the SSTs increase abruptly to reach their maxima in the early Holocene (around 5-9 cal ka BP). The cooling between 18 and 10 ka BP corresponds to a higher productivity as recorded by coccolithophorids [*Beaufort et al.*, 2001] , which may be linked to paleo-ENSO variability; stronger ENSO events tend to lift the thermocline (and with it the nutricline) in the WPWP. The relative cooling before 10 ka BP could be linked to a regional process that affects the whole Western Pacific including also the Vanuatu area [*Beck et al.*, 1997].

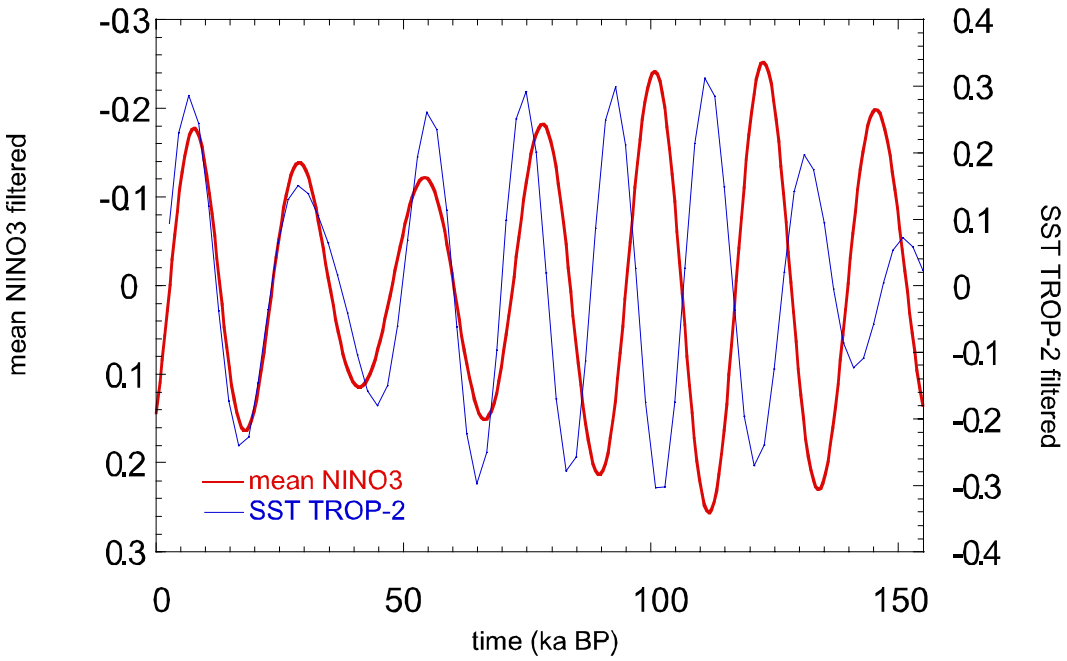

Figure 8 - Comparison of TROP-2 SSTs estimates (thin line) and mean NINO3 index (bold line) from [*Clement et al.*, 1999] : raw data (A) and filtered data in the precession band (B). A positive NINO3 index indicates warm SSTs in the Eastern Pacific which correspond with El Niño-like state of equatorial Pacific circulation.

Precessional forcing of the ENSO at that time is predicted by a simple coupled ocean-atmosphere model forced by orbital parameters [*Clement et al.*, 1999]. During an El Niño, the trade winds are weaker, the Western Pacific SSTs cool and the thermocline depth shallows in the Western Pacific. This precessional forcing on western equatorial Pacific SSTs is very strong during the last 85 ka BP (Fig. 8). Before this period, our SST records and the paleo-ENSO outputs from the Clement et

al. model become out of phase. This could indicate that SSTs in the WPWP are not purely dependant of ENSO conditions or that the two dissolution peaks in stage 5 may have altered the SST record inferred from foraminifera.

4.3 The marine isotope stage 6 :

The alkenones average between the two calibrations and the TROP-2 SSTs are roughly well correlated (Fig. 9). The mean difference during the last 120,000 years is close to 0°C with a correlation coefficient r=0.68, over narrow range smaller than 3°C (with 67 samples taken at the exact same depth). The correlation between alkenone estimates and TROP-2 estimates supports the hypothesis of excluding core-tops from the Eastern Pacific.

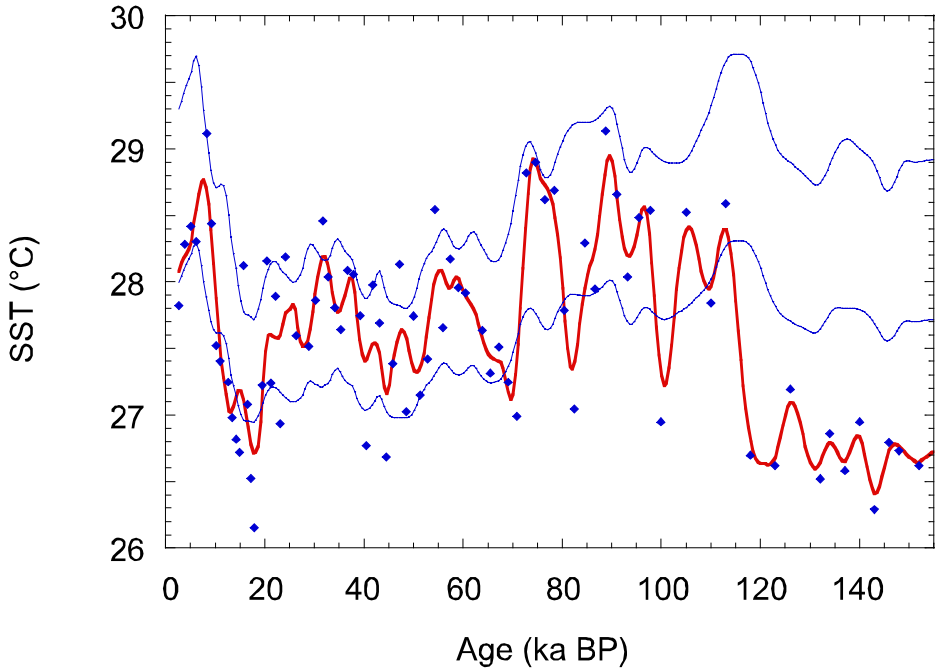

Figure 9 - Comparison of SST derived from foraminifera transfer function TROP-2 (filled diamonds) with alkenones SSTs derived using [*Prahl et al.*, 1988] equation (thin line down) and the [*Sonzogni et al.*, 1997] equation (thin line down) in the MD97-2138 core. The data were smoothed using a moving average of 2000 years after a resampling with a 500 years steps, to account for different sampling steps between these two proxies.

The alkenone SST estimates are about 1°C warmer than the planktonic foraminifera estimates arises before 120,000 years (isotopic stage 6). The difference between the two proxies reaches 1.6°C between 160 and 120 ka BP. The Mg/Ca SST record from the Ontong-Java plateau indicates SSTs cooler by 1.8°C in the stage 6 [*Lea et al.*, 2000], in agreement with the TROP-2 transfer function estimates. Coral Sr/Ca SSTs estimates from Huon peninsula indicateand even greater cooling of 6°C prior to termination II [*McCulloch et al.*, 1999].

These warm stage 6 alkenones estimates are not restricted to the Western Pacific ones : [*Rostek et al.*, 1993] in the Indian ocean also observe such warm glacial alkenones SSTs ; [*Schneider*

et al., 1999] reviews a set of Atlantic low latitude cores that exhibits this pattern ; [*Calvo et al.*, 2001] in the subtropical eastern Pacific observed warmer SSTs in the stage 6 by 0.6-1.3°C compared to stages 2-4 . The alkenones are, at our knowledge, the only proxy that shows such anomalously warm SSTs

Two hypotheses might account for anomalously warm alkenone SSTs in stage 6. First, Schneider et al., [1999] suggests a direct response of low-latitude sea-surface waters to insolation forcing. For these authors, the modulation of the orbital precessional forcing on the low latitudes by the high eccentricity during the stage 6 is sufficient to warm up the SSTs during te stage 6. But that hypothesis cannot explain the cool temperatures in stage 6 estimated by the other proxies.

Alternatively, a change in coccolith flora with a different Uk'37-temperature calibration could have yielded anomalously warm SSTs in stage 6. However [*Müller et al.*, 1997] have shown that alkenone estimates gave reasonable paleo-SST estimates during the late Quaternary event with floral changes.

Differences in PP inferred from coccoliths between Stage 2 and Stage 6, [*Beaufort et al.*, 2001]does not show any strong difference that could help to explain the apparent offset between alkenone and foraminiferal temperature estimates. We have no convincing explanation for the apparent mismatch between alkenone and foraminiferal temperatures through time, but hope that future coupled alkenones/coccoliths studies will help to resolve this discrepancy between alkenones and other proxies estimates.

5 - Conclusions :

We apply the Imbrie/Kipp transfer function method to a geographically restricted data-set that permits SST reconstructions using planktonic foraminifera suitable for the Western tropical Pacific (the TROP-2 equation). Core-tops from the Eastern Central Pacific ocean have been excluded because they produce spurious SSTs estimates. We suggest that anomalous trophic structure in the Eastern Pacific could de-sensitize transfer functions to true changes that occurred in the WPWP. The anomalous high relative abundance of *N. dutertrei* in the Eastern Pacific, an unique feature in the global ocean, could be linked with the High Nutrient-Low Chlorophyll area. We speculate that the *N. dutertrei* that live in the Eastern equatorial Pacific have probably different genotypes than the *N. dutertrei* that live in the other parts of the intertropical ocean.

This transfer function was applied to new counts in the Western Pacific core MD97-2138. Glacial SSTs are 2.2°C cooler than the warmest early-Holocene SSTs; however, the differences between core-top and LGM (*sensu* EPILOG) intervals is about 1°C, roughly similar to the original estimates of CLIMAP. For the deglacial interval, our primary finding is that coolest SST's postdate the global LGM, and warmest SST's occurred in early Holocene time. Similar Glacial/Interglacial differences in planktonic foraminifera SSTs of about 2-3°C are observed from the stage 6 to stage 5, and from stage 2 to the Holocene. In contrast, alkenone-based estimates of SST vary by about 1-2°C since the LGM, but change by only about 0.5-1.0°C from Stage 6 to Stage 5. We have no good explanation for the mismatch between the alkenone and foraminiferal proxies, but prefer the foraminiferal estimates because they yield roughly similar ranges throughout the time span we studied. 4 - Foraminiferal SST estimates are consistent with precessional forcing of SSTs in the Western equatorial Pacific. In modern interannual variability, cool SSTs in the Western Pacific are associated with El Niño-like state mainly driven by precessional forcing. However, the correlation between our MD97-2138 SST estimates and the modelled response of ENSO to orbital forcing implies a complex response of the WPWP SSTs to orbital forcing in terms of amplitude and of timing.

Acknowledgements :
We are thankful to Edith Vincent for her help with foraminifera taxonomy and ecology. The support of French MENRT, TAAF, CNRS/INSU and IFRTP to the Marion-Dufresne and the IMAGES Program was necessary to perform this work. Financial support from INSU grant and ECLIPSE is acknowledged.

References :

Anderson, D.M., W.L. Prell, and N.J. Barratt, Estimates of sea-surface temperatures in the Coral Sea at the last Glacial Maximum, *Paleoceanography*, *4* (6), 615-627, 1989.

Andreasen, D.J., and A.C. Ravelo, Tropical Pacific Ocean thermocline depth reconstructions for the last glacial maximum, *Paleoceanography*, *12* (3), 395-413, 1997.

Antoine, D., J.-M. André, and A. Morel, Oceanic primary production 2. Estimation at global scale from satellite (coastal zone color scanner) chlorophyll, *Global Biogeochemical Cycles*, *10*, 57, 1995.

Bard, E., Geochemical and geophysical implications of the radiocarbon calibration, *Geochemica et Cosmochimica Acta*, *62* (12), 2025-2038, 1998.

Bard, E., Ice age temperatures and geochemistry, *Science*, *284*, 1133-1134, 1999.

Beaufort, L., T. de Garidel-Thoron, A.C. Mix, and N.G. Pisias, ENSO-like forcing on oceanic primary production during the late Pleistocene, *Science*, *293*, 2440-2444, 2001.

Beck, J.W., J. Recy, F. Taylor, R.L. Edwards, and G. Cabioch, Abrupt changes in early Holocene tropical sea surface temperature derived from coral records, *Nature*, *385* (6618), 705-707, 1997.

Calvo, E., C. Pelejero, J.C. Herguera, A. Palanques, and J.O. Grimalt, Insolation dependance of the Southeastern subtropical Pacific sea surface temperature over the last 400 kyrs, *Geophysical Research Letters*, *28* (12), 2481-2484, 2001.

Cayre, O., L. Beaufort, and E. Vincent, Paleoproductivity in the Equatorial Indian Ocean for the last 260,000 yr : A transfer function based on planktonic foraminifera, *Quaternary Science Reviews*, *18*, 839-857, 1999.

Chen, M.-T., and W.L. Prell, Faunal distribution patterns of planktonic foraminifers in surface sediments of the low-latitude Pacific, *Paleogeography, Palaeoclimatology, Palaeoecology*, *137*, 55-77, 1998.

Clark, P.U., A.C. Mix, and E. Bard, Ice sheets and sea level of the Last Glacial Maximum, *EOS trans., American Geophysical Union*, *82* (22), 241, 246-247, 2001.

Clement, A.C., R. Seager, and M.A. Cane, Orbital controls on the El Nino/Southern Oscillation and the tropical climate, *Paleoceanography*, *14* (4), 441-456, 1999.

CLIMAP, P.M., The surface of the ice-age earth, *Science*, *191*, 1131-1137, 1976.

Coale, K.H., K.S. Johnson, S.E. Fitzwater, R.M. Gordon, S. Tanner, F.P. Chavez, L. Ferioli, C. Sakamoto, P. Rogers, F. Millero, P. Steinberg, P. Nightingale, D. Cooper, W.P. Cochlan, M.R. Landry, J. Constantinou, G. Rollwagen, A. Trasvina, and R. Kudela, A massive phytoplankton bloom induced by an ecosystem-scale fertilization experiment in the equatorial Pacific Ocean, *Nature*, *383*, 495-501, 1996.

Conkright, M., S. Levitus, T. O'Brien, T. Boyer, J. Anotonov, and C. Stephens, World Ocean Atlas 1998 CD-ROM Data set documentation, pp. 16, NODC, Silver Spring, MD, 1998.

Crowley, T.J., CLIMAP SSTs revisited, *Climate Dynamics*, *16*, 241-255, 2000.

Darling, K.F., C.M. Wade, D. Kroon, and A.J. Leigh Brown, Planktic foraminiferal molecular evolution and their polyphyletic origins from benthic taxa, *Marine Micropaleontology*, *30*, 251-266, 1997.

de Vargas, C., R. Norris, L. Zaninetti, S.W. Gibb, and J. Pawlowski, Molecular evidence of cryptic speciation in planktonic foraminifers and their relation to oceanic provinces, *Proceeding of the National Academy of Sciences*, *96*, 2864-2868, 1999.

Fofonoff, R., and R. Millard, Algorithms for computations of fundamentals properties of seawater, *Unesco Technical Papers in Marine Sciences*, *44*, 1-53, 1983.

Gagan, M.K., L.K. Ayliffe, J.W. Beck, J.E. Cole, E.R.M. Druffel, R.B. Dunbar, and D.P. Schrag, New views of tropical paleoclimates from corals, *Quaternary Science Reviews*, *19*, 45-64, 2000.

Hope, G., and J. Tulip, A long vegetation history from lowland Irian Jaya, Indonesia, *Palaeogeography, Palaeoclimatology, Palaeoecology*, *109*, 385-398, 1994.

Hostetler, S.W., and P.U. Clark, Tropical climate at the Last Glacial Maximum inferred from glacier mass-balance modeling, *Science*, *290*, 1747-1750, 2000.

Hostetler, S.W., and A.C. Mix, Reassesment of ice-age cooling of the tropical ocean and atmosphere, *Nature*, *399*, 673-676, 1999.

Hutson, W., The Agulhas Current during the Late Pleistocene: Analysis of modern faunal analogs, *Science*, *207*, 64-66, 1980.

Imbrie, J., and N.G. Kipp, A new micropaleontological method for quantitative paleoclimatology : application to a late Pleistocene Caribbean core, in *The late Cenozoic Glacial Ages*, edited by K.K. Turekian, pp. 71-181, Yale University Press, New Haven, Conn., 1971.

Lea, D.W., D.K. Pak, and H.J. Spero, Climate impact of late quaternary equatorial Pacific sea surface temperature variations, *Science*, *289*, 1719-1724, 2000.

Lee, K.E., and N.C. Slowey, Cool surface waters of the subtropical North Pacific Ocean during the last glacial, *Nature*, *397*, 512-514, 1999.

Longhurst, A., *Ecological geography of the sea*, Academic Press, San Diego, 2001.

Martin, J.H., Glacial-interglacial CO2 change: the iron hypothesis, *Paleoceanography*, *5* (1), 1-13, 1990.

Martinez, J.I., L. Taylor, P. De Deckker, and T. Barrows, Planktonic foraminifera from the eastern Indian Ocean: distribution and ecology in relation to the Western Pacific Warm Pool (WPWP), *Marine Micropaleontology*, *34*, 121-151, 1998.

McCulloch, M.T., A.W. Tudhope, T.M. Esat, G.E. Mortimer, J. Chappell, B. Pillans, A.R. Chivas, and A. Omura, Coral record of equatorial sea-surface temperatures during the penultimate deglaciation at Huon peninsula, *Science*, *283*, 202-204, 1999.

Mix, A., Influence of productivity variations on long-term atmospheric CO2, *Nature*, *337*, 541-544, 1989.

Mix, A.C., E. Bard, and R. Schneider, Environmental processes of the ice age: land, ocean, glaciers (EPILOG), *Quaternary Science Reviews*, *20*, 627-657, 2001.

Mix, A.C., A.E. Morey, and N.G. Pisias, Foraminiferal faunal estimate of paleotemperature: circumventing the no-analog problem yields cool ice age tropics, *Paleoceanography*, *14* (3), 350-359, 1999.

Moore, T.C.J., L.H. Burckle, K. Geitznauer, B. Luz, A. Molina-Cruz, J.H. Robertson, H. Sachs, C. Sancetta, J. Thiede, P. Thompson, and C. Wenkam, The reconstruction of sea surface temperatures in the Pacific Ocean of 18, 000 B.P., *Marine Micropaleontology*, *5*, 215-247, 1980.

Müller, P.J., M. Cepek, G. Ruhland, and R.R. Schneider, Alkenone and coccolithophorid species changes in late Quaternary sediments from the Walvis ridge : implications for the alkenone paleotemperature method, *Palaeogeography Palaeoclimatology Palaeoecology*, *135*, 71-96, 1997.

Ohkouchi, N., K. Kawamura, T. Nakamura, and A. Taira, Small changes in the sea surface temperature during the last 20,000 years: Evidence from the western tropical Pacific, *Geophysical Research Letters*, *21* (20), 2207-2210, 1994.

Ortiz, J.D., and A.C. Mix, Comparison of Imbrie-Kipp transfer function and modern analog temperature estimates using sediment trap and core top foraminiferal faunas, *Paleoceanography*, *12* (2), 175-190, 1997.

Pflaumann, U., J. Duprat, C. Pujol, and L.D. Labeyrie, SIMMAX, a modern analog technique to deduce Atlantic sea surface temperatures from planktonic foraminifera in deep-sea sediments, *Paleoceanography*, *11* (1), 15-35, 1996.

Pierrehumbert, R.T., Climate change and the tropical Pacific : the sleeping dragon wakes, *Proceedings of the National Academy of Sciences*, *97* (4), 1355-1358, 2000.

Porter, S., Snowline depression in the tropics during the Last Glaciation, *Quaternary Science Reviews*, *20*, 1067-1091, 2001.

Prahl, F.G., L.A. Melhausen, and D.L. Zahnle, Further evaluation of long-chain alkenones as indicators of paleoceanographic conditions, *Geochimica et Cosmochimica Acta*, *52*, 2303-2310, 1988.

Prell, W., A. Martin, J. Cullen, and M. Trend, The Brown University Foraminiferal Data Base, NOAA/NGDC Paleoclimatology Data Center for Paleoclimatology, Boulder CO, USA., 1999.

Prell, W.L., The stability of low-latitude sea-surface temperatures: an evaluation of the CLIMAP reconstruction with emphasis on the positive SST anomalies, pp. 60, Brown University, Providence, 1985.

Rosell-Mélé, A., E. Bard, K.-C. Emeis, J.O. Grimalt, P. Müller, R.R. Schneideir, T. Blanz, I. Bouloubassi, B. Epstein, K. Fahl, A. Fluegge, K. Freeman, M. Goni, U. Güntner, D. Hartz, S. Hellebust, T. Herbert, M. Ikehara, R. Ishiwatari, K. Kawamura, F. Kenig, J. de Leeuw, S. Lehman, L. Mejanelle, N. Okhouchi, R.D. Pancost, C. Pelejero, F. Prahl, J. Quinn, J.-F. Rontani, F. Rostek, J. Rüllkotter, J. Sachs, K. Sawada, D. Schulz-Bull, E. Sikes, C. Sonzogni, Y. Ternois, G. Versteegh, J. Volkman, and S. Wakeham, Precision of the current methods to measure the alkenone proxy UK37' and absolute abundance in sediments : results of an interlaboratory comparison study, *Geochemistry, Geophysics, Geosystems*, *2* (#141), 1-28, 2001.

Rostek, F., G. Ruhland, F. Bassinot, P.J. Muller, L. Labeyrie, Y. Lancelot, and E. Bard, Reconstructing sea-surface temperature and salinity using ð^{18}O and alkenones record, *Nature*, *364*, 319-321, 1993.

Schneider, R.R., P.J. Müller, and R. Acheson, Atlantic alkenone sea-surface temperature records : low latitude versus mid latitudes and differences between hemispheres, in *Reconstructing ocean history: a window into the future*, edited by F. Abrantes, and A. Mix, pp. 33-55, Kluwer academics/Plenum publishers, New York, 1999.

Sonzogni, C., E. Bard, F. Rostek, R. Lafont, A. Rosell-Mele, and G. Eglinton, Core-top calibration of the alkenone index vs sea surface temperature in the Indian Ocean, *Deep-Sea Research II*, *44* (6-7), 1445-1460, 1997.

Thompson, P.R., Planktonic foraminifera in the western North Pacific during the past 150 000 years: comparison of modern and fossil assemblages, *Palaeogeography, Palaeoclimatology, Palaeoecology*, *35*, 241-279, 1981.

Thompson, P.R., A.W.H. Bé, J.-C. Duplessy, and N.C. Shackleton, Disappearance of pink-pigmented Globigerinoides ruber at 120,000 yr BP in the Indian and Pacific Oceans, *Nature*, *280*, 554-558, 1979.

Waelbroeck, C., L. Labeyrie, J.-C. Duplessy, J. Guiot, M. Labracherie, H. Leclaire, and J. Duprat, Improving past sea surface temperature estimates based on planktonic fossil faunas, *Paleoceanography*, *13*, 272-283, 1998.

Watkins, J.M., and A.C. Mix, Testing the effects of tropical temperature, productivity and mixed-layer depth on foraminiferal transfer functions, *Paleoceanography*, *13* (1), 96-105, 1998.

Yin, J.H., and D.S. Battisti, The importance of tropical sea surface temperature patterns in simulations of Last Glacial Maximum climate, *Journal of Climate*, *14*, 565-581, 2001.

Chapitre 4 : Forçage de type ENSO de la production primaire océanique dans l'océan Indo-Pacifique équatorial au cours du Pléistocène récent.

La convection atmosphérique « profonde » au-dessus de la zone chaude du Pacifique ouest équatorial a fonctionné au cours des derniers 185 000 ans (chapitre précédent). Cette zone de convection correspond à la branche ascendante de la cellule atmosphérique de Walker dans le Pacifique (figure 4.1). La circulation de Walker est également présente dans l'océan Indien. La profondeur de la thermocline est liée aux températures de surface, ainsi la profondeur de la thermocline baisse le long de l'équateur du Pacifique Est vers l'Ouest et remonte le long de la côte Ouest Africaine. Périodiquement, pendant les années El Niño, une baisse de l'intensité des alizés et des vents d'ouest plus violents provoquent un déplacement de la zone d'eaux chaudes vers l'Est, entrainant la branche ascendante de la cellule zonale, qui se divise pour former deux cellules dans le Pacifique, et une cellule dans l'océan Indien. Le gradient de profondeur de la thermocline est relaxé dans le Pacifique.

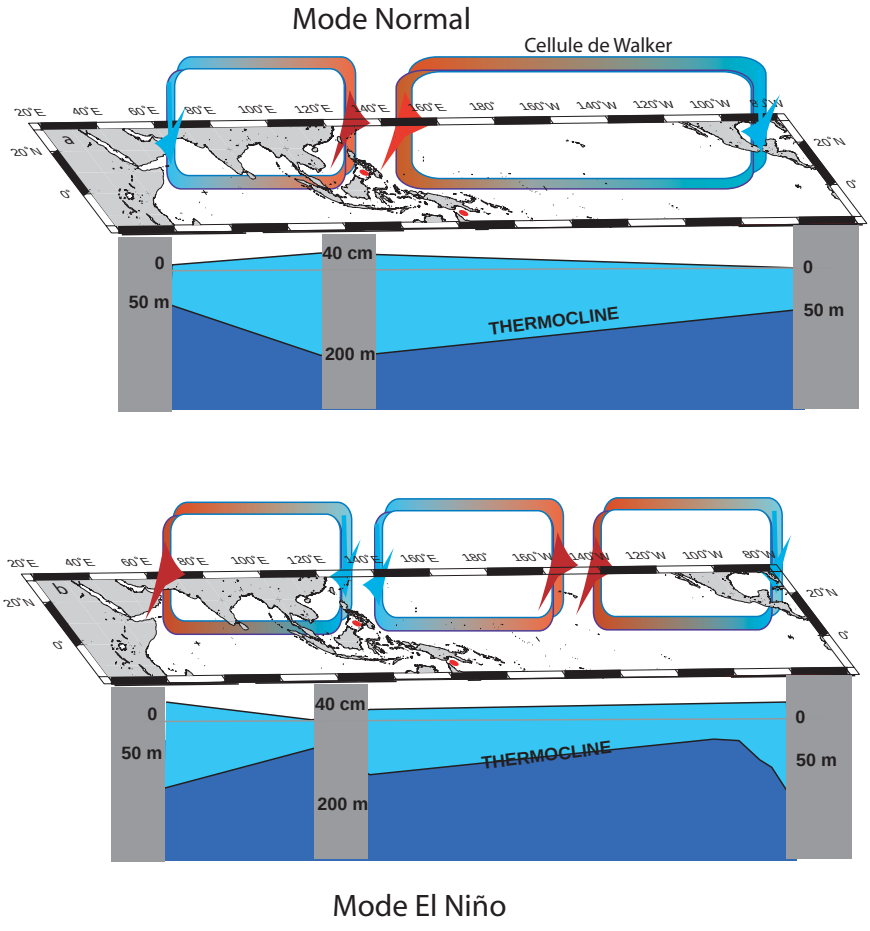

figure 4.1 : lien entre profondeur de la thermocline le long de l'équateur dans les océans Indo-Pacifique et la circulation atmosphérique zonale pendant les annéees normales (en haut) et les années El Niño (en bas) – d'après Beaufort (comm.pers.).

Beaufort et al. (1997) ont montré que la production primaire dans l'Océan Indien équatorial au cours du Pléistocène récent était indépendante du forçage des hautes latitudes, et suggéraient que la dynamique de la production primaire était liée à l'ENSO. Ce travail teste l'hypothèse d'un mécanisme ressemblant à l'ENSO mais à une échelle de temps beaucoup plus longue. Ce travail utilise le rapport *Florisphaera profunda*/autres espèces de coccolithes, proxy présenté dans le chapitre 1.

Résumé de l'article en anglais :

L'analyse quantitative des changements de nannoflores dans des carottes sédimentaires de l'océan Indo-Pacifique enregistrent les variations de production primaires au Pléistocène récent. Les variations de production primaire sont causées en premier lieu (1) par la variabilité glaciaire-interglaciaire, suivant les cycles de l'excentricité et de l'obliquité, et en second lieu (2) par les changements liés aux cycles de précession. (1) La variabilité glaciaire-interglaciaire globale (« mean state ») influence l'ENSO et donc la profondeur de la thermocline via les changements de température de surface de l'océan global (Fedorov and Philander, 2000). (2) Les cycles de précession contrôlent le basculement est-ouest de la profondeur de la thermocline. Ce mode oppose la profondeur de la thermocline de l'océan Pacifique ouest équatorial des autres enregistrements. Ces changements liés à la précession sont liés à des processus similaires à l'Oscillation Australe, et ils précèdent de 2-3 ka le $\delta^{18}O$, indiquant qu'ils ne sont pas liés aux variations des calottes glaciaires. L'existence d'une réponse de l'ENSO aux cycles de précession a été démontré par la modélisation (Clément, et al. 1999). Un pic de 30 ka dans l'analyse spectrale des enregistrements de productiviyé primaire Indo-Pacifique est également présent dans les enregistrements de concentration atmosphérique en CO_2 d'Antarctique, suggérant un rôle important de la production biologique équatoriale dans les modifications du CO_2.

ENSO-like Forcing on Oceanic Primary Production During the Late Pleistocene

Luc Beaufort,[1] Thibault de Garidel-Thoron,[1] Alan C. Mix,[2] Nicklas G. Pisias[2]

[1] : CEREGE, Aix-en-Provence, France

[2] : COAS – Oregon State University, Corvallis, OR, USA

Abstract : Late Pleistocene changes in oceanic primary productivity along the equator in the Indian and Pacific oceans are revealed by quantitative changes in nanoplankton communities preserved in nine deep-sea cores. We show that variations in equatorial productivity are primarily caused by glacial-interglacial variability and by precession-controlled changes in the east-west thermocline slope of the Indo-Pacific. The precession-controlled variations in productivity are linked to processes similar to the Southern Oscillation phenomenon, and they precede changes in the oxygen isotopic ratio, which indicates that they are not the result of ice sheet fluctuations. The 30,000-year spectral peak in the tropical Indo-Pacific Ocean productivity records is also present in the Antarctica atmospheric CO_2 record, suggesting an important role for equatorial biological productivity in modifying atmospheric CO_2.

Interannual variability of the thermocline depth is a characteristic feature of the equatorial Pacific Ocean that has a strong influence on oceanic primary production (1). Most of the time, the tropical trade winds transport surface waters westward. This lifts the thermocline along the equator in the central and eastern Pacific but deepens the thermocline in the western Pacific, where warm surface waters pile up against the Australian and Asian continents. In the Indian Ocean, an analogous pattern exists but with a shallow thermocline in the west (the Somalian upwelling) and a deep thermocline in the east (2). When trade winds relax, the slope of this basin-wide thermocline changes intensely. The thermocline rises in the western Pacific and in the eastern Indian Ocean, whereas it deepens on the other sides of these two basins [i.e., causing a typical El Niño-Southern Oscillation (ENSO) event in the Pacific]. Although the two oceans appear to be climatically independent of each other (2, 3), a synchronism of equatorial wind intensity has been observed between the Pacific and Indian oceans on decadal scales (4, 5). A shoaling of thermocline produces an increase in primary production. Thus, the ENSO-related thermocline slope variability has been recognized as responsible for the "largest known natural perturbation of the global carbon cycle" on decadal scales (1). Here, we document long-term variations in the slope of the equatorial thermocline on the basis of patterns of changing primary productivity during the last two glacial cycles and its relation to global climate and orbital forcing.

We analyzed the coccolithophore community preserved in nine deep-sea cores taken from the tropical Indian and Pacific oceans (Fig. 1) (6). A precise chronology was obtained by tuning oxygen isotope

records from foraminifera in most of the cores to the SPECMAP stacked record (7) so that our sampling achieves a temporal resolution of 0.7 to 3 thousand years (ky). Six records span at least the last 240 ky, two shorter cores (M38 and M40) the last 180 ky, and one (M74) the last 150 ky. Most of the coccolithophore species live in near-surface waters where light for photosynthesis is abundant. Phytoplankton also requires nutrients, and thus thrives where a shallow thermocline brings subsurface nutrients into the upper euphotic zone. In contrast, the coccolithophore *Florisphaera profunda* lives in the deep-photic zone, where nutrients are relatively abundant but light is rare (8). Where the thermocline is deep, total primary productivity is low, and the dominant coccolith species in fossil assemblages is *F. profunda* (9). As productivity increases, the relative abundance of *F. profunda* decreases. Thus, estimates of primary productivity (ePPs) are made from counts of the relative abundance of *F. profunda* (%Fp) (6, 10). The data are given as productivity estimates because, within tropical systems, productivity is highly correlated with the depths of the nutricline and the thermocline (1, 11, 12).

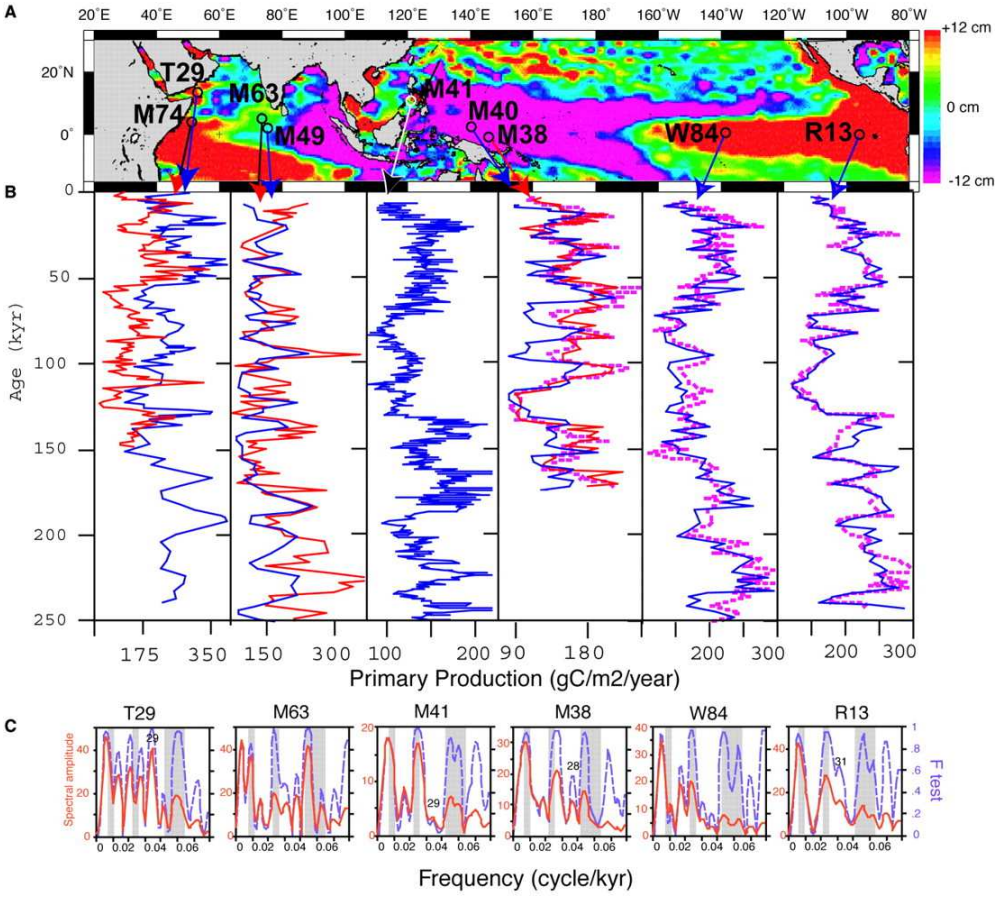

Fig. 1. (**A**) Map showing core locations and sea level anomalies relative to a 3-year mean recorded by Topex-Posidon during El Niño 1997 (cycle 193); scale is on the right. (**B**) Record of primary production from each core estimated on the basis of human (blue or red curves) and automated (neural network) counts (36)(dashed lines) of coccoliths. (**C**) Spectral analysis (multitaper method) of ePP records. Amplitude spectra are in orange; the significance values of the peaks (*F* test) are in blue. Shaded areas indicate the orbital periods of 100, 41, and 23 to 19 ky. Significant peaks with a period of about 30 ky are also indicated

The ePP records (Fig. 1) show large amplitude variability with regional similarities and contrasts that are explored using empirical orthogonal functions (EOFs). EOFs reduce the set of observations to a small number of spatiotemporal patterns (an EOF series) that can adequately describe the data (13, 14). It also provides statistics (loading) on how each original record contributes to the EOF series. Two significant EOF series (EOF-1 and EOF-2) have been extracted for the last 180 ky from the eight cores (Figs. 2, 3; the maximum duration represented by cores M38 and M40 is 180 ky). They describe 60% of the total variance in all eight cores. EOF-2 reflects a straightforward mechanism and is discussed first.

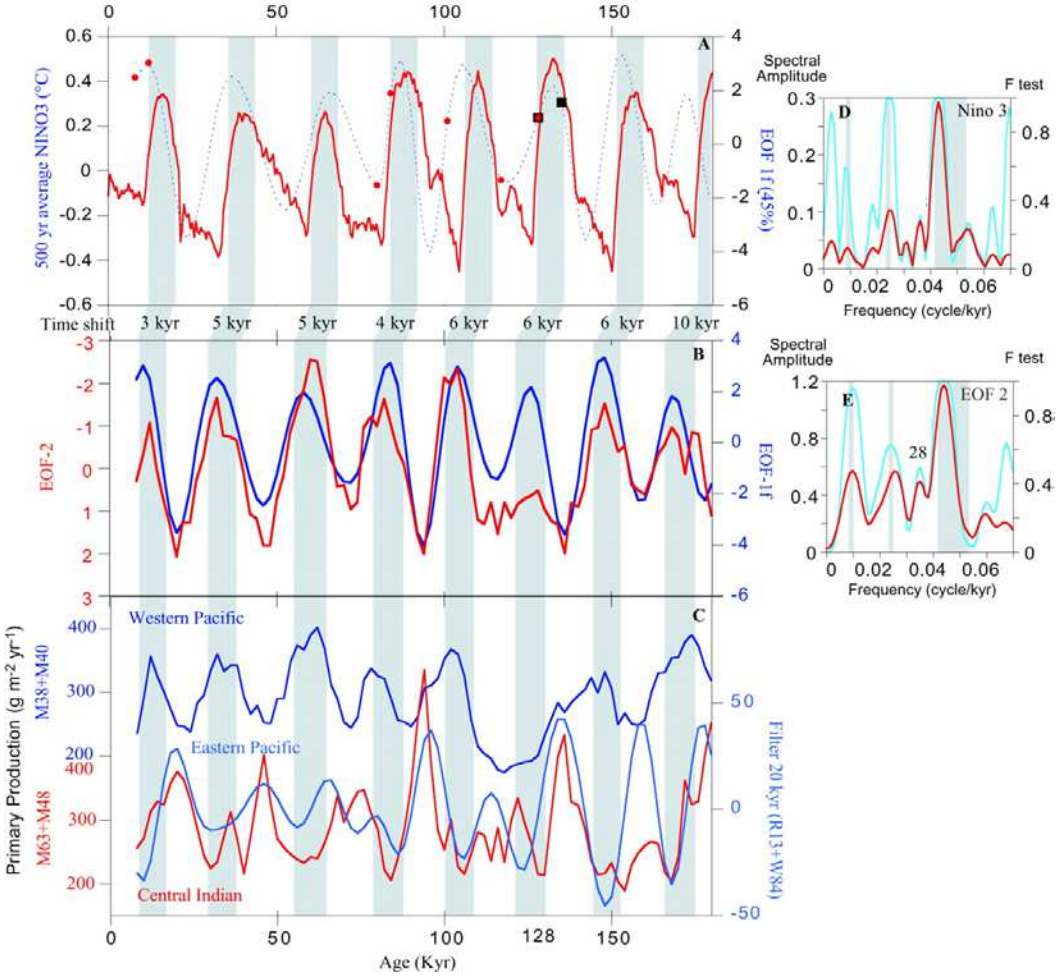

Fig. 2. (**A**) The 500-year average NINO3 index from Zebiak-Cane model forced with Milankovitch solar variations (16) (solid red line). EOF-1 from the 20-ky bandpass-filtered ePP series (dashed blue line) with chronology based on U-Th date from Gallup *et al*. (19) (red dots) and Henderson and Slowey (20) (black squares). The data in (A) are shifted by 5 ky to match visual thermocline dynamics expressed in (B) and (C) (shaded areas correspond to high EOF-1f values). (**B**) EOF-2 from eight raw ePP records on reverted scale (red) and EOF-1 (EOF-1f) from the 20-ky bandpass-filtered ePP series (blue). (**C**) Productivity records added by pairs of cores: western Pacific (M38 added to M40 in dark blue), central Indian Ocean (M63 added to M48 in red), and eastern Pacific (20-ky filters of W84 added to 20-ky filter of core R13 in light blue). (**D** and **E**) Spectral analysis (multitaper method) of ENSO model (D) and EOF-2 (E). Amplitude spectra are in red; the significance values of the peaks (*F* test) are in light blue. Shaded areas indicate the orbital periods of 100, 41, and 23 to 19 ky.

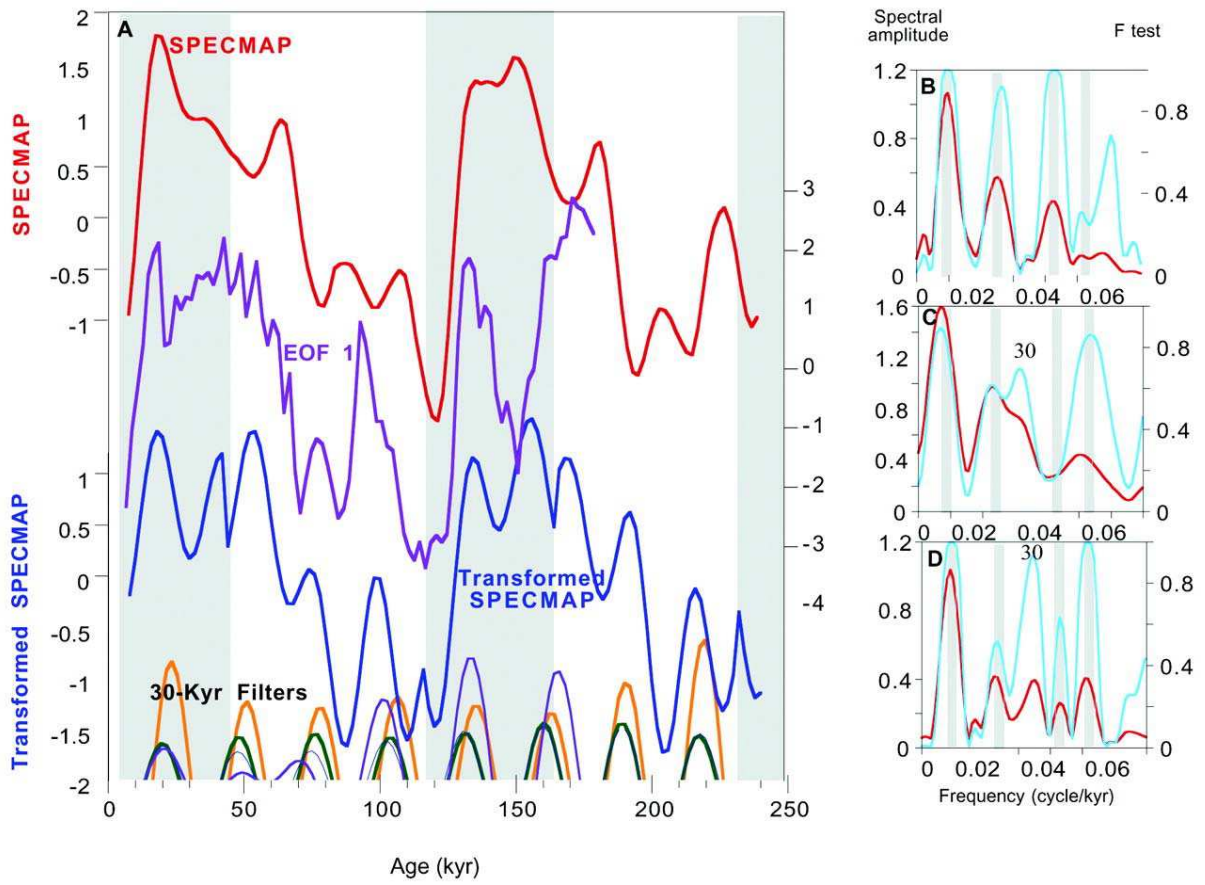

Fig. 3. (**A**) Purple line, first component of the EOF; red line, SPECMAP stack; blue line, SPECMAP stack transformed in the following manner: the stack was filtered at 100, 41, and 20 ky. The 20-ky filter was inverted for interglacial periods (unshaded areas) and kept as initial in glacials and during terminations (shaded area). The three filtered series were then added together. At the bottom positive part of 30-ky Gaussian filters (37) (centered on 0.034 ky^{1} with a band width of 0.004 with cutting at period of 26.6 and 34.3 ky) of EOF (purple), transformed SPECMAP (blue), 23-ky sine-wave frequency modulated by 100- and 40-ky cycle from SPECMAP (green) (38), and -CO_2 from Vostok (orange) (30). (**B** to **D**) Spectral analysis (37) (multitaper method) of SPECMAP (B), EOF-1 (C), and transformed SPECMAP (D). Amplitude spectra are in red; the significance values of the peaks (*F* test) are in light blue. Shaded areas indicate the orbital periods of 100, 41, and 23 to 19 ky. The extra 30-ky period is also indicated.

EOF-2 accounts for 19% of the total variance and opposes essentially the western Pacific with the central Indian Ocean (6), and it clearly fluctuates with the 23-ky cycle of Earth's precession (Fig. 2E). However, the eastern Pacific ePP records show weak precession cycles in comparison with the 41- and 100-ky cycles, and consequently they do not contribute significantly to EOF-2. We repeated the EOF analyses on 23-ky bandpass-filtered ePP records. This filtering technique suppresses the influence of the large glacial-interglacial variability on the eastern Pacific productivity records. The first component of this new test (EOF-1f) approximates that of EOF-2, although it gives a much clearer picture of the opposition in dynamic between the western and eastern Pacific ePPs (Fig. 2) (6). This cyclic opposition can also be seen when comparing basin average regional records (Fig. 2C). Contemporary interannual variability in ENSO shows a similar spatial opposition in the altimetric anomaly (Fig. 1),

thermocline depth, and hence productivity fluctuations in the equatorial Pacific (1) and equatorial Indian oceans (2). Thus, the opposition we found is likely to reflect similar variations in equatorial thermocline slope, although on a much longer time scale (15).

Interestingly, in every core analyzed, ePP records lead by about 2 ky the ^{18}O records in the precession band (6). This lead indicates that insolation is the direct cause of ePP fluctuations, and that polar ice volume variations (^{18}O) do not significantly affect the low-latitude climate dynamics in that time scale. An ENSO modeling experiment over the past glacial-interglacial cycles has shown that changes in low-latitude insolation induce variations in the frequency and intensity of ENSO events (16). A very good agreement is found between the predictive ENSO model and EOF-2-1f time series, although an almost constant shift of about 5 ky occurs between the model and the EOFs (Fig. 2). This offset may partly be explained by the use of the SPECMAP chronology for our age model (7), because new radioisotope dates point to significantly older ages for most of the isotopic record than previously estimated [compare (17-20) with (7)]. Calibrating the ^{18}O chronology based solely on the recent U/Th dates, the EOFs offer a better synchronism with the ENSO model (Fig. 2A). Although chronology is beyond the objective of this work, it appears that older ages in the SPECMAP chronology would reconcile model predictions and observed/measured data. Hence, the observed long-term variations of the equatorial thermocline slope would seem to be related to variations in the intensity of ENSO events driven by precession-related insolation changes.

EOF-1 accounts for 40% of the total variance. It characterizes productivity variations common to all sites (Fig. 3) (6). Because it contains significant periods close to the 100-ky (eccentricity) and 41-ky (obliquity) bands, and because EOF-1 broadly covaries with the SPECMAP stacked oxygen isotope record (Fig. 3), EOF-1 expresses the dominant influence of glacial variability on equatorial productivity. High EOF-1 values (i.e., high-productivity conditions) occur during maximum glacial conditions, low EOF-1 values (i.e., low-productivity conditions) during interglacial times. EOF-1 varies in phase with ^{18}O in the eccentricity band and lags it in the obliquity band, indicative of a significant response of low-latitude productivity dynamics to glacial-interglacial variability. These spectral characteristics are shown by each ePP series (6), except the central Indian Ocean one (10). The process that increases primary production during glacial in the equatorial Indo-Pacific remains uncertain. It cannot correspond to an increase in the strength of zonal winds, because that would produce an increase of the slope of thermocline in the Pacific, a fact that is not observed for EOF-1 (6). Such a general rise of nutrient in the equatorial upper photic zone could be related to a global increase of nutrient concentration in the intermediate waters that upwell into the photic zone. More likely it results from a weakened and/or shoaled stratification that permits an increased flux of new nutrients. A decrease of equatorial sea surface temperatures (14, 21, 22) relative to the intermediate water temperatures during glacial periods would weaken the stratification, and the thermocline would shoal (23). Dry weather conditions in the western Pacific (24) would further reduce stratification because a

reduction of heavy rains would reduce fresh surface water inputs and its strong specific halocline. It has been shown that the global climate variability modulates the ENSO (23) by altering the background state and in particular the depth of the thermocline: Warmer climate increases the frequency and strength of the El Niño. The general fluctuations of the thermocline depth as recorded by EOF-1 are in complete agreement with those of the influence of the global climate on low-latitude oceanography.

Finally, the spectra of EOF-1, and to a lesser degree of EOF-2, reveal significant peaks at 30 and 19 ky (Figs. 2 and 3). These spectral peaks are interpreted as reflecting the phase modulation of precession in ePP: The time series of EOF-1 seems to be in phase with those of SPECMAP during maximum glacial and deglaciation (stripped in gray in Fig. 3A) conditions, but in anti-phase during interglacial periods. To illustrate this, we inverted the precession signal of the SPECMAP record for each interglacial period. The spectral signature of this new series (transformed SPECMAP, Fig. 3A) shows a distinct 30-ky period and a shift of the precession period from 23 ky to 19 ky (Fig. 3D). These spectral signatures are those of EOF-1. Therefore, the 30-ky component that occurs in EOF-1 as well as in most of the ePP series (Fig. 1) corresponds to a cyclic phase shift of the precession parameter. Two forcings are acting in phase opposition at a 20-ky time scale and in amplitude opposition at a 100-ky time scale. The mechanism involved is uncertain, but could be linked to the boreal summer monsoon (BSM) dynamics. Present climate studies show that the strengths of BSM and ENSO are often correlated with stronger BSMs during La Niña events [for example, (25)]. But on Milankovitch time scales, this is not the case: BSMs intensify during interglacial periods (26), whereas we have shown that ePPs (La Niña equivalent) increase during glacial periods. It is therefore plausible that during interglacials, intense BSMs somehow altered the path of the thermocline depth dynamics described above and were responsible for that 30-ky period.

A 30-ky period has been found in series from the tropical Pacific [see discussion in (14)] and tropical Indian (27-29) oceans, but so far not from the tropical Atlantic. We speculate that the 30-ky cycle is restricted to the tropical Indo-Pacific Ocean (14), because the ENSO is characteristic of that area. However, the CO_2 record from the Vostok ice core also reveals a 30-ky cycle (30). Cross-spectral analyses indicate that the productivity series are highly coherent with the CO_2 record at the 30- and 23-ky periods, and that low CO_2 values are associated with high productivity (Fig. 3) (6). It is therefore possible that, with primary production acting as a significant sink in the carbon cycle, the 30-ky record in global CO_2 is the signature of ENSO-like control of biological production in the equatorial Indo-Pacific. This is consistent with a significant role of the low-latitude biological pump in controlling atmospheric CO_2 concentrations (31).

We have identified two independent forcings responsible for 60% of the long-term equatorial Indo-Pacific productivity dynamics. The first forcing concerns the response of the depth of the equatorial

thermocline to global climatic variations. The second forcing is related to changes in the equatorial east-west thermocline tilt and is linked to the 23-ky period of Earth's precession. This precession-related variability could reflect the influence of low-latitude insolation on ENSO, as a predictive ENSO model stipulates (16). A similar dual "precession-glacial" forcing has been described recently on New Guinea corals (32). The 23-ky signal precedes ice volume variations by about 2 ky. Thus, long-term ENSO dynamics provide a possible causality for the growing body of evidence that low-latitude climates are early responders to orbital forcing (9, 10, 22, 33-35). Although minor, a 30-ky period is also evidenced. It is characteristic of the equatorial Indo-Pacific coherent with a similar period found in Vostok CO_2 record. That coherency attests to the importance of biological carbon fixation in the equatorial Indo-Pacific in controlling variations of atmospheric CO_2. Therefore, because of its early response and its possible effect on the carbon cycle, the 23-ky ENSO-like cycle is likely to have played a significant role in global climate dynamics.

REFERENCES AND NOTES

1. D. Turk, M. J. McPhaden, A. J. Busalacchi, M. R. Lewis, *Science* **293**, 471 (2001)
2. P. J. Webster, A. M. Moore, J. P. Loschnigg, R. R. Leben, *Nature* **401**, 356 (1999)
3. N. H. Saji, B. N. Goswami, P. N. Vinayachandran, T. Yamagata, *Nature* **401**, 360 (1999) .
4. C. D. Charles, D. E. Hunter, R. G. Fairbanks, *Science* **277**, 925 (1997).
5. J. E. Cole, R. B. Dunbar, T. R. McClanahan, N. A. Muthiga, *Science* **287**, 617 (2000).
6. Supplemental material is available at *Science* Online at www.sciencemag.org/cgi/content/full/293/5539/2440/DC1.
7. J. Imbrie *et al.*, in *Milankovitch and Climate, Part 1,* A. L. Berger, J. Imbrie, J. D. Hays, G. Kulka, B. Saltzman, Eds. (Reidel, Dordrecht, Netherlands, 1984), vol. 1, pp. 269-305.
8. H. Okada and S. Honjo, *Deep Sea Res.* **20**, 355 (1973).
9. B. Molfino and A. McIntyre, *Science* **249**, 766 (1990)
10. L. Beaufort *et al.*, *Science* **278**, 1451 (1997).
11. M. R. Lewis, W. G. Harrison, N. S. Oakey, D. Herbert, T. Platt, *Science* **234**, 870 (1986).
12. We recognize that in some special cases (e.g., eastern Pacific), a shallow nutricline is a necessary but not a sufficient condition for high primary production. But this does not alter the broad picture that we describe in that paper.
13. A. C. Mix, W. F. Ruddiman, A. McIntyre, *Paleoceanography* **1**, 43 (1986) .
14. N. G. Pisias and A. C. Mix, *Paleoceanography* **12**, 381 (1997).
15. The productivity record of Core M41 mimics those from the central and eastern Pacific. The effect of basin-wide thermocline tilt on productivity fluctuations in the Pacific has probably not been recorded in the Sulu Sea, because it is protected by the Philippine Islands and also because the PP dynamics is related to the winter monsoon.
16. A. C. Clement, R. Seager, M. A. Cane, *Paleoceanography* **14**, 441 (1999)
17. R. L. Edwards, J. H. Chen, T. L. Ku, G. J. Wasserburg, *Science* **236**, 1547 (1987)
18. E. Bard, B. Hamelin, R. G. Fairbanks, *Nature* **385**, 707 (1990) .

19. C. D. Gallup, R. L. Edwards, R. G. Johnson, *Science* **263**, 796 (1994).
20. G. M. Henderson and N. C. Slowey, *Nature* **404**, 61 (2000).
21. A. C. Mix, A. E. Morley, N. G. Pisias, S. W. Hostetler, *Paleoceanography* **14**, 350 (1999).
22. D. W. Lea, D. K. Pak, H. J. Spero, *Science* **289**, 1719 (2000).
23. A. V. Fedorov and S. G. Philander, *Science* **288**, 1997 (2000).
24. J. R. Flenley, *Clim. Change* **39**, 177 (1998).
25. G. A. Meehl, *J. Clim.* **6**, 31 (1993).
26. W. L. Prell, in *Milankovitch and Climate, Part 1,* A. L. Berger, J. Imbrie, J. D. Hays, G. Kukla, B. Saltzman, Eds. (Reidel, Dordrecht, Netherlands, 1984), vol. 1, pp. 349-366.
27. S. Clemens, W. L. Prell, D. Murray, G. Shimmield, G. Weedon, *Nature* **353**, 720 (1991).
28. F. C. Bassinot *et al.*, *Earth Planet. Sci. Lett.* **126**, 91 (1994).
29. G. J. Reichart, L. J. Lourens, W. J. Zachariasse, *Paleoceanography* **13**, 607 (1998).
30. J. R. Petit *et al.*, *Nature* **399**, 429 (1999).
31. J. J. Rich, D. Hollander, G. E. Birchfield, *Global Biogeochem. Cycles* **13**, 531 (1999).
32. A. W. Tudhope *et al.*, *Science* **291**, 1511 (2001).
33. E. M. Pokras and A. Mix, *Nature* **326**, 486 (1987).
34. J. Villanueva *et al.*, *Paleoceanography* **13**, 561 (1998).
35. S. E. Harris and A. C. Mix, *Quat. Res.* **51**, 14 (1999).
36. D. Dollfus and L. Beaufort, *Neural Networks* **12**, 553 (1999).
37. D. Paillard, L. Labeyrie, P. Yiou, *Eos* **77**, 379 (1996) .
38. The frequency modulation of precession by ice volume may be computed as $x_t = \cos(2t/23.4) + g_t/2$, where t is time and g_t is the modulating ice volume component (100 and 40 ky of SPECMAP varying between 0 and 1).
39. We thank IFRTP for financial and technical support for the Marion-Dufresne coring during IMAGES III cruise, Lamont-Doherty laboratory core repository for the samples from Core RC13-110, G. Ganssen for providing samples and stratigraphy from Core TY93-929, and M.-P. Aubry, L. Lourens, and two anonymous reviewers for reviewing an earlier version of the manuscript. Supported by NATO (L.B.) and by INSU ad'hoc ocean and CNRS ECLIPSE grant (L.B.).

Counting methods

Two counting methods were used: (i) Classical counts of at least 350 coccoliths per sample under a light microscope in all the cores; (ii) In three cores (R13, W84 and M38) we also applied an automatic counting device (SYRACO) using a Fat Artificial Neural Network (*1*) which has been trained with a database composed of 2300 digital images including coccoliths and non-coccoliths. SYRACO recognises the 12 most abundant species found in tropical recent deep-sea sediments. An automatic microscope LEICA DMRBE scanned microscopic slides and 50 view-fields were analysed by SYRACO. The digital images of coccoliths counted by SYRACO were stored in files that were checked and corrected by a nannoplankton specialist (LB) in order to obtain counts cleared from errors.

The percentages of *F. profunda* (%Fp) corresponds to %Fp = 100 × Fp/Tot where Fp and Tot are, respectively, the number of *F. profunda* and the total number of coccoliths counted in a slide using either of the two counting methods. %Fp produced by the two counting methods are in relatively good agreement (r > .89). The 95% confidence interval varies between ~5% in the case of a human count (Tot > 350) and ~3% in the case of an artificial count (Tot >1000).

Estimates of primary productivity (PP) were derived from %Fp by PP = 316 × log (%Fp + 3) (*2*), an equation derived to fit Indian Ocean core-top data with modern productivity based on satellite chlorophyll (*3*). The correlation between the estimated and observed productivity in the calibration data set is r = 0.94 and the standard deviation of the residuals is ±26 gC m^{-2} $year^{-1}$. This transfer function has been shown to be reliable in Equatorial Atlantic (*4*) and Pacific Ocean (*5*). In samples external to the calibration set, results based on %Fp agree qualitatively with several other primary productivity estimators: productivity estimates match well semi-quantitative productivity estimators such as radiolarian counts in Core M74 [compare with URI in (*6*), Corg or alkenone concentration in cores T29, M63 (*7*) organic carbon concentration in core W84 (*8*) or quantitative: foraminifer (*9*) and % Gephyrocapsa (Core M63) (*10*)]. However our ePP estimates disagree with estimates of export productivity based on benthic foraminifera in RC13 (*11*).

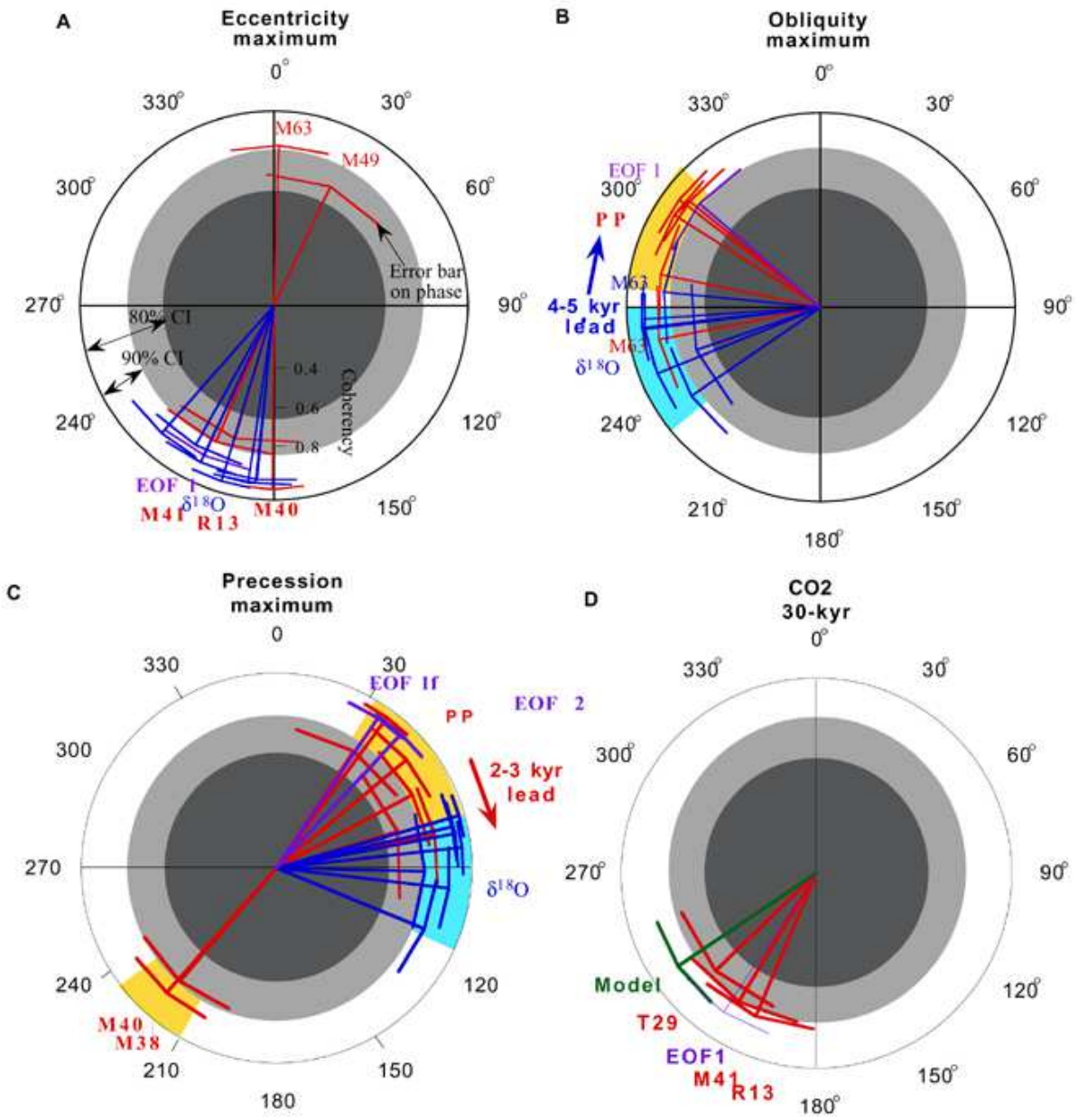

Supplemental Figure 1. Phase wheels for the eccentricity (**A**), obliquity (**B**), precession (**C**) and the 30-kyr filtered CO_2 from Vostok as reference series (**D**). The length of the "arrows" expresses the coherency between two series, and their width corresponds to the phase band width (80%). Dark (light) gray areas are below the confidence level of 80% (90%) (only series having a coherency above the 80% confidence level are shown). Blue arrows are for ^{18}O, red for PP and purple for EOFs. Orange areas correspond to phase area of PP and light blue for ^{18}O.

Supplemental Table 1. For each core, we give label, core acronym used in the text, longitude, latitude, depth, chronological resolution reached in productivity analysis, loading values for the EOF-1 and -2 on raw data, EOF-1 on filtered data, mean for establishing stratigraphy, and reference where stratigraphy is described.

Core	Acron.	Lat. N	Long.	Depth (m)	Resol. (ky)	EOF-1	EOF-2	EOF-1f	Strati.	Ref.
TY93-929	T29	13°42	53°15E	2490	1.7	-0.56	0.15	-0.28	*N. dut.*	(*7*)
MD85674	M74	3°11	50°26E	4875	1.1				^{18}O bulk	(*12*)
MD90949	M49	2°05	76°07E	3700	2.8	-0.44	0.64	-0.81	*G. ruber*	(10)
MD90963	M63	5°O3	73°53E	2446	2.0	-0.22	0.67	-0.85	*G. ruber*	(*13*)
MD972141	M41	8°47	121°17E	3633	0.3	-0.82	-0.07	-0.71	*G. ruber*	(*14*)
MD971240	M40	2°2	141°0E	2347	1.9	-0.59	-0.52	0.44	Color	This study
MD972138	M38	-1°25	146°14E	1912	1.7	-0.35	-0.62	0.71	*G. ruber*	This study
W84-14GC	W84	0°57	138°57W	4287	2.5	-0.86	0.09	-0.86	Benthic	(*8*)
RC13-110	R13	0°06	95°65W	3621	2.4	-0.85	-0.02	-0.66	Benthic	(*15*)

References

1. D. Dollfus, L. Beaufort, *Neural Networks* **12**, 553 (1999).
2. L. Beaufort *et al*., *Science* **278**, 1451 (1997).
3. D. Antoine, J.-M. André, A. Morel, *Global Biogeochem. Cycles* **10**, 57 (1996).
4. A. S. Henriksson, *Palaeogeogr. Palaeoclimatol. Palaeoecol.* **156**, 161 (2000).
5. L. Beaufort, unpublished data.
6. J.-P. Caulet, M.-T. Vénec-Peyré, C. Vergnaud-Grazzini, C. Nigrini, in *Upwelling Systems: Evolution Since the Early Miocene,* C. P. Summerhayes, W. L. Prell, K. C. Emeis, Eds., *Geol. Soc. Spec. Pub.* **64**, 379 (1992).
7. F. Rostek, E. Bard, L. Beaufort, C. Sonzogni, G. Ganssen, *Deep Sea Res. II* **44**, 1461 (1997).
8. J. P. Jasper, J. M. Hayes, A. C. Mix, F. G. Prahl, *Paleoceanography* **9**, 781 (1994).
9. O. Cayre, L. Beaufort, E. Vincent, *Quat. Sci. Rev.* **18**, 839 (1999).
10. L. Beaufort, F. C. Bassinot, E. Vincent, in *Reconstructing Ocean History: A Window into the Future,* F. Abrantes, A. C. Mix, Eds. (Kluwer Academic/Plenum, New York, 1999), pp. 245-272.
11. P. Loubere, *Nature* **406**, 497 (2000).
12. M.-T. Vénec-Peyré, J.-P. Caulet, C. Vergnaud Grazzini, *Paleoceanography* **10**, 473 (1995).
13. F. C. Bassinot *et al*., *Earth Planet. Sci. Lett.* **126**, 91 (1994).
14. T. de Garidel-Thoron, L. Beaufort, B. K. Linsley, S. Dannenmann, *Paleoceanography,* in press.
15. N. G. Pisias, A. C. Mix, *Paleoceanography* **12**, 381 (1997).

Chapitre 5 : *Orbulina universa* : morphométrie et paramètres environnementaux dans le Pacifique Ouest

Les reconstructions paléoclimatiques utilisant les microfossiles, les fonctions de transfert et la composition isotopique des tests de foraminifères par exemple, sont basées sur la reconnaissance d'espèces. L'espèce, en paléontologie, est définie en fonction de descripteurs morphologiques qui sont rarement quantifiés. Chaque espèce est supposée posséder des préférences écologiques spécifiques qui serviront pour l'établissement des fonctions de transfert ou pour l'utilisation des isotopes stables de ce microfossile. Or nous avons précédemment vu que pour le foraminifère planctonique *Neogloboquadrina dutertrei* (cf. chapitre 3) par exemple, ses affinités écologiques ne semblaient pas stables dans l'espace. Une hypothèse permettant de résoudre cette diversité d'affinités écologiques serait que le morphotype de cette espèce pourrait englober plusieurs espèces au sens génétique. Chaque espèce génétique posséderait ainsi différentes préférences environnementales.

Cette hypothèse a été testée depuis quelques années, par l'analyse du génotype de foraminifères planctoniques vivants. Ces études ont toutes révélé une diversité cryptique insoupconnée auparavant. Pour l'espèce *Orbulina universa* par exemple, deux ou trois espèces génétiques possèderaient la même morphologie pour un micropaléontologiste (de Vargas et al., 1999). Cependant, si cette diversité cryptique est détectable sur des organismes vivants, l'absence d'ADN chez les microfossiles carbonatés empêche de reconnaître celle-ci dans le passé. Nous avons donc essayé de tester l'existence possible de différents morphotypes qui pourraient correspondre à différents génotypes, par l'utilisation de descripteurs simples, en l'occurence la porosité et la taille des tests.

Orbulina universa (d'Orbigny) est un foraminifère planctonique vivant dans les eaux de surface de l'océan. Cette espèce est caractérisée par une chambre terminale sphérique aisément reconnaissable. Cette espèce est cosmopolite avec une préférence pour les latitudes moyennes. Son abondance relative, la simplicité de son test, et la reconnaissance d'une diversité cryptique par l'analyse d'ADN en font une espèce clé sur laquelle tester la diversité cryptique. De plus, de nombreux auteurs ont utilisé la taille de cette organisme comme marqueur paléo-environnemental.

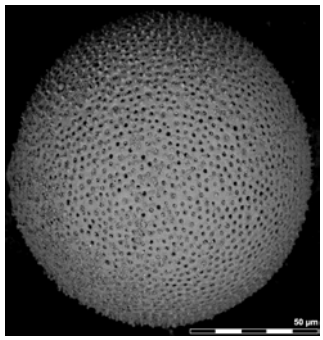

Figure 5.1 : photo d'*Orbulina universa* vue au MEB (la barre d'échelle représente 250 µm au total). Ce spécimen provient de sédiments de surface de l'océan Pacifique Ouest

Ainsi, (Bé et al., 1973) ont montré que la taille des Orbulines était actuellement corrélée aux paramètres hydrologiques de surface de température et de densité. Cette relation est également

montrée par De Deckker (pers. comm.) sur des sédiments de surface de l'océan Pacifique ouest. Des cultures en laboratoire ont mis en évidence un effet de la température des eaux sur la taille d'*O. universa*, mais également des apports en nutriments. La densité est un critère qui n'a pas été testé dans les cultures en laboratoire.

A partir de sédiments de surface du Pacifique ouest, nous essaierons de vérifier si les critères morphométriques de taille et de porosité permettent de discriminer des morphotypes différents chez cette espèce. Nous déterminerons quel sont les paramètres les plus critiques pour la porosité et la taille des Orbulines. Pour tester leur potentielle application dans des enregistrements sédimentaires, nous avons étudié deux carottes du Pacifique Ouest, la première recouvrant le dernier cycle climatique (carotte MD97-2138) et la seconde enregistrant les derniers 40 000 années en mer de Corail (carotte MD97-2134). Le but initial de cette étude était d'essayer de reconstruire les paléo-densités des eaux de surface du Pacifique ouest à partir du diamètre moyen des Orbulines, mais la calibration a malheureusement invalidé cette hypothèse.

Résumé du chapitre en anglais (article en préparation) :

Orbulina universa (d'Orbigny) est une espèce de foraminifère planctonique cosmopolite, caractérisée par une chambre finale circulaire typique. La porosité et le diamètre moyen ont été mesuré dans des échantillons de sommets de carottes du Pacifique ouest et dans deux carottes sédimentaires du Pacifique ouest equatorial. Tous les spécimens modernes d'*O. universa* sont caractérisés par deux classes de porosité interne, une plus petite que 8 µm et une plus grande comprise entre 10 et 15 µm. Deux morphotypes différents d'*O. universa* peuvent être séparés en fonction du mode de la plus petite porosité. Le premier type a un mode d'environ 3.3 µm et le second d'environ 6µm. Ces deux types ne peuvent pas être distingués par l'analyse de la porosité externe, et ne sont pas liés au diamètre moyen. Nous suggérons que cette diversité morphologique pourrait être liée à la diversité cryptique d'*O. universa*, en accord avec les études récentes du génotype de cette espèce. Le pourcentage de porosité des *O.universa* est significativement corrélé à la densité des eaux de surface. Cette correlations a été appliquée à la carotte MD97-2138 prélevée dans la zone d'eaux chaudes du Pacifique ouest equatorial. Néanmoins, un effet de la dissolution semble affecter la porosité, et pourrait empêcher son application dans des carottes sédimentaires. Nous avons compilé les précédentes mesures de la taille moyenne d'*O. universa* avec nos nouveaux résultats, pour fournir une nouvelle calibration en fonction de la température des eaux de surface. Cette nouvelle calibration a été appliquée à la carotte MD97-2138. L'amplitude des variations de température est en accord avec les résultats obtenus dans la même carotte par la fonction de transfert TROP-2. Cependant, en terme dynamique, les températures de surface obtenues par la taille moyenne d'*O. universa* sont affectées par un biais lié à la production primaire, et empêchent donc ce proxy d'être utilisable dans le Pacifique ouest equatorial.

Morphometry of the planktonic foraminifera *Orbulina universa* in the Western Pacific

In preparation (to be submitted to ***Marine Micropaleontology)***

Thibault de Garidel-Thoron[1]
CEREGE and Université Aix-Marseille III
Europôle Méditerranéen de l'Arbois, BP80
13545 Aix-en-Provence Cedex 4
France

Patrick De Deckker [2]
Dept of Geology, The Australian National University
Canberra ACT 0200.
Australia

Abstract :
Orbulina universa (d'Orbigny) is a cosmopolitan planktonic foraminifera characterized by a typical final circular chamber. Porosity and mean diameter of *O. universa* were measured in core-tops samples from the Western Pacific, and in two sediment cores from the equatorial Western Pacific. All the modern *O. universa* are characterized by two different inner porosities, one smaller than 8 µm and a 10 and 15 µm larger one. Two different morphotypes of *O. universa* can be separated following the mode of the smaller inner porosity. First type porosity has a mode around 3.3 µm and the second one has a mode of 6 µm. These two modes cannot be separated using the external porosity and have no relations with the mean diameter. We suggest that this morphologic diversity could be linked with a cryptic speciation in *O. universa*, in agreement with modern genotypes studies. The porosity % of modern *O. universa* is significantly correlated to the sea-surface density, and this proxy was succesfully applied to the MD97-2138 sediment core from the Western Pacific warm pool. However, the dissolution seems to be critical to downcore porosity studies. We compiled existing measurements of the mean diameter of *O. universa* with our results, and compute a new SST equation. This equation was applied to the MD97-2138 sediment core. The SST amplitude given by this proxy is in agreement with transfer function results. However, in the equatorial western Pacific, a secondary effect of the primary production prevents to use the mean *O. universa* diameter as a suitable paleoclimatic proxy of SST.

[1] Corresponding author - Fax : +33 442 97 15 95 / garidel@cerege.fr
[2] Fax: +61-2 6125 5544 / patrick.dedeckker@anu.edu.au

Introduction :

The concept of species is fundamental in paleontology, and obviously for all the disciplines which use fossils. The paleoenvironmental studies postulate that each species has its own stable ecological preferences. However, if in one same species defined by the paleontologist using the shape of the fossil, coexist different genetic species, which could have different ecological clines, it could induce strong biases in the interpretation of the paleoenvironmental reconstructions. The main argument of this hypothesis of cryptic genetic diversity was given by DNA analysis of living microzooplankton which showed that the number of foraminifera species could be increased by a two or three fold factor (Darling et al., 1997; de Vargas, 2000; de Vargas et al., 1999; de Vargas et al., 2001). The main group which was studied to test this cryptic genetic diversity is the planktonic foraminifera, which secrete a carbonate test widely used in paleoreconstructions. Among this group, the species *Orbulina universa* has been extensively studied, both in living conditions, and also in the Pleistocene sediment cores.

Orbulina universa is a cosmopolitan planktic foraminifera (zooplankton). This species is characterized by a final circular chamber built by the foraminifera when it reaches maturity, after a trochospiral stage. The question whether the final circular chamber is formed by different species or not, is an old question in micropaleontology. Since Rhumbler (1895 quoted in (Bé et al., 1973)), many authors have shown that different trochospiral morphologies are find in juveniles *O. universa*. (e.g. (Le Calvez, 1936)). (Bé et al., 1973), interpreted that the co-occurence of two types of porosity (small and large pores) in the final circular chamber of all the Indian ocean foraminifera they examined, could not be likely related to different species. Their data were reanalysed using cluster analysis by (Hecht et al., 1976) who demonstrated that the porosity abruptly changed around 10°S in the Indian ocean. This position corresponds to an oceanic front, so these authors argue that porosity studies of *O. universa* could be a useful paleoclimatic index. For (Hecht et al., 1976) the morphometric diversity of *O. universa* is mainly ecophenotypic. This question of mono- or multispecies origin was recently resolved by DNA studies of living foraminifera from plankton tows. (Darling et al., 1997) showed in tropical samples that the morphotype spherical chamber could be linked with two different genetic clusters. (de Vargas et al., 1999) analysing the DNA of Atlantic *O. universa*, distinguished three different genetic groups of *O. universa*, and argued that these genetic differences could correspond with different morphological characters : the test diameter and the porosity. Unfortunately, these authors were not able to quantify the differences in the morphology of the final chamber. These authors also argued that the spatial distribution of the different cryptic species could be associated to different oceanic productivity provinces.

In parallel to the cryptic speciation in *O. universa*, a few studies tried to quantify the relationship between the morphology of this final chamber, and the environmental parameters. The pioneering work of Stone (1956) demonstrated that the size of *O. universa* in core-tops samples, increases latitudinally towards a maximum at the equator in the Atlantic ocean. The Indian ocean *O. universa*, also show the same distribution pattern in latitudinal belts (Bé et al., 1973). These authors also successfully calibrated the porosity to the sea-surface density. Using, the mean size of *O. universa* in a set of cores from the Indian ocean, (Bé and Duplessy, 1976) reconstructed the shifts of the subtropical convergence zone during the late Pleistocene. As this species is relatively easy to grow in laboratory cultures, two studies tried to check for the relationship between mean size and growth culture conditions. First one gave strong evidences for the temperature effect on the mean size of *O. universa*, but also have seen that the positive slope of the linear relationship between size and temperature can be reversed in very high temperatures domain (Caron et al., 1987). A second study underscored the role of the nutrient availability in monitoring the mean size of the *O. universa*.(Bijma et al., 1992).
Here, using sediment samples from the Western Pacific area, and compiling previous studies, we document modern porosity and of mean size of *O. universa*, to distinguish (1) potential different morphotypes in the circular chamber of this species and (2) correlate the morphology of the final chamber of *O. universa* to the oceanic parameters. Finally we will test the *O. universa* morphometry as a paleoclimatic tool on downcore samples from the western Pacific, to compare with other proxies studies.

Methodology :

Optic microscopy :

The *O. universa* were picked in microsplitted samples of the above 150 µm granulometric fraction. Foraminifera were photographed with a standard 756 X 582 digitized camera on a black support. The *O. universa* mean size was extracted using a standard software of image processing, which was calibrated with a micrometer. We express the mean size as the mean diameter in microns of all the foraminifera measured in one sample, in order to compare with previous studies (Bé et al., 1973; De Deckker, unpublished). We measured in average 70 *O. universa* in the 151 samples to assess the size distribution in each sample. *O. universa* test diameter was measured on a total of 1189 specimens in the 12 surface sediments samples for the calibration and on 8720 specimens in 139 downcore samples.

S.E.M. images : test of the porosity

The hand-picked *O. universa* were prealably washed in an ultrasonic bath to remove coccoliths and clays from the test. High resolution pictures were done with Philips environmental scanning electronic microscope (SEM). External pictures of randomly choosed *O. universa* were saved at two

magnifications levels (1) at x120 for the whole *O. universa* picture to measure the diameter. (2) The same *O. universa* were then gently crashed and the inside porosity was photographed at x500. The number of pores and their relative surface were computed using a standard image software.

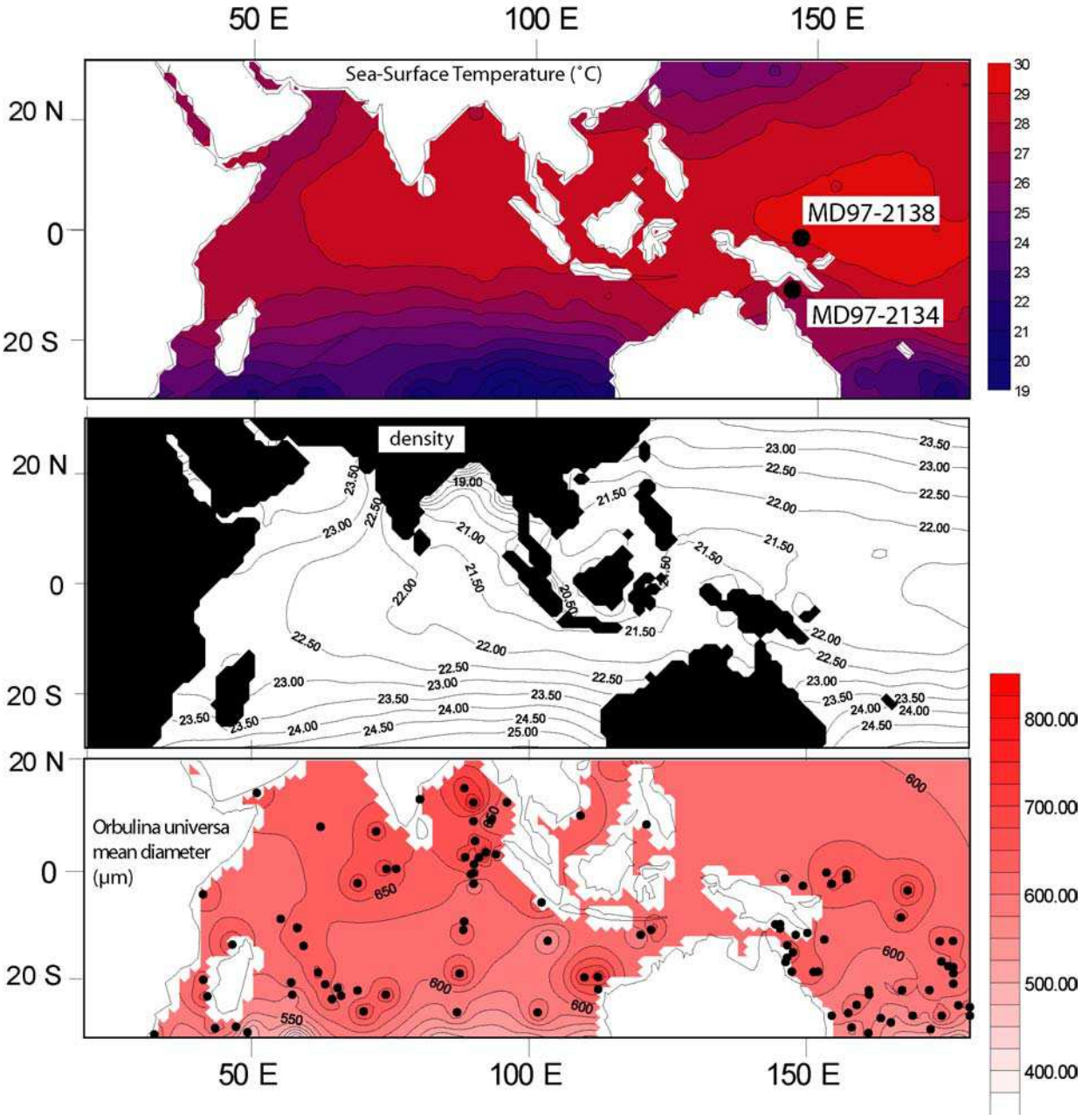

Figure 1 : (A)Sea–surface temperatures (°C) in the Indo-Pacific oceans. The position of the two cores is plotted. (B) Sea surface density. (C) *Orbulina universa* mean diameter (µm) compilation in the Indo-Pacific ocean from (Bé et al., 1973); (De Deckker, unpublished) and this study.

Sediment samples :

The sediments were retrieved during the IMAGES III - IPHIS cruise in 1997 on the R/V Marion-Dufresne, with the Giant Calypso corer. The twelve core-tops range from 30°S to 20°N (table 1). Two cores were studied in the low latitude Western Pacific area : the core MD97-2134 hereafter referred as

MD34 (depth 760 m, lat. 9°54'S, long. 144°39'E) and the core MD97-2138 –shortly MD38 (depth 1912 m, lat. 1.25 N , long. 146.14 E - fig 1.). The core MD34 is located in the Gulf of Papua South East off Papua New Guinea. We focused in this core on high frequency oscillations in the diameter of *O. universa*. The second core (MD38) is located in the core of the WPWP and spans the last 150kaBP. The chronological framework of the two cores has been previously described elsewhere (de Garidel-Thoron et al., submitted-a; de Garidel-Thoron et al., submitted-b). It is based on ^{14}C AMS ages on the planktonic foraminifera *Globigerinoides ruber*, which were calibrated according to INTCAL98 (Stuiver et al., 1998), and on planktonic foraminifera oxygen isotope stratigraphy tuned to the SPECMAP reference curve (Imbrie et al., 1984).

Sample name	latitude	Longitude	water depth (m)	mean diameter (μm)	standard deviation (μm)	standard deviation (%)	Number of Orbulina
MD97-2123	32.02 S	165.47 E	3202	492	115	10.84	112
MD97-2124	26.76 S	163.63 E	1493	590	162	12.16	177
MD97-2125	22.34 S	161.44 E	1684	633	138	9.82	197
MD97-2126	21.74 S	161.36 E	1454	554	150	19.08	62
MD97-2127	18.11 S	152.1 E	1630	618	144	16.52	76
MD97-2134	9.91 S	144.66 E	760	622	117	18.25	41
MD97-2137	2.99 S	149.59 E	2240	622	97	9.32	109
MD97-2138	1.25 N	146.14 E	1912	590	139	46.36	9
MD97-2141	8.79 N	121.3 E	3633	616	112	13.58	68
MD97-2145	21.03 N	120.59 E	1408	559	119	8.10	216
MD97-2147	20.53 N	118.25 E	2434	672	109	21.73	25
MD97-2150	8.73 N	109.87 E	292	650	115	11.70	97

Table 1 : Surface sediment samples used in this study

Oceanic parameters :

Oceanic parameters were extracted from the World Ocean Atlas 1998 (Conkright et al., 1998). Due to the interhemispheric distribution of the core-tops, and to the lack of evidence for an optimal seasonal growth of the *O. universa*, we choose to extract the annual values in surface where this species lives. The density was computed using the UNESCO equation state (Fofonoff and Millard, 1983). Primary production estimates were computed from the (Antoine et al., 1995) data sets. This algorithm links the ocean color measured from Coastal Zone Colour Satellites with the integrated primary production in the water column. We also computed cline parameters to assess for potential effects of the intermediate waters / sea-surface exchanges: the thermocline depth was computed as the minimal in the first derivative of the sea temperature vs. depth. The halocline was visually checked and corresponds to the maximal in the second derivative of the salinity profile through the water column.

Oceanic and Climatological setting :

The Western Pacific warm pool is characterized by the warmer global ocean waters (Yan et al., 1992) (figure 1), which are separated from intermediate waters by a strong pycnocline (Lindstrom et al., 1987). This pycnocline limits the exchanges between the deep ocean rich in nutrients, and the upper waters which are nutrient-depleted by the primary producers. This pycnocline is maintained by the strong precipitations that occur in the western Pacific where the ascending branch of the zonal atmospheric Walker circulation is located (Delcroix et al., 1996). The Walker circulation is periodically modified during the El Niño events, when the warm and fresh waters are moving towards the eastern Pacific. The location of the MD38 in this area, by reconstructing paleo-densities in the Western Pacific could indicate past changes in the ENSO, and could be compared with SSTs and productivity records inferred from other proxies (de Garidel-Thoron et al., submitted-a). The second core (MD34) is located at the mouth of the Fly river, one of the largest contributary to the tropical ocean. This core could give a record of the paleo-density changes linked with the Fly river runoff with a very resolution due to the large sedimentation rates. It is particularly important given the high terrestrial charge of the Fly river, and that the PNG rivers oceanic input strongly impacts the nutrient availability in the Pacific equatorial under current (Sholkovitz et al., 1999; Wells et al., 1999).

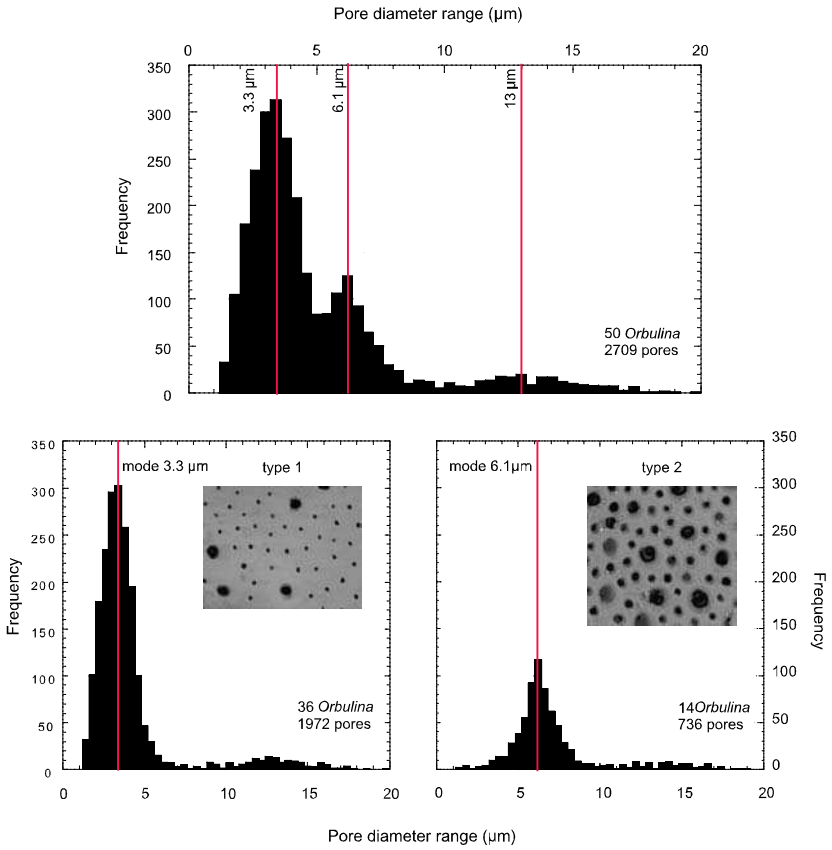

Figure 2 : (A) Size frequency distribution of the inner porosity diameter in all the core-tops *O. universa* studied. (B) Type 1 *O. universa* type defined from the inner porosity with a mode at 3.3 µm and a second one around 13 µm. (C) Type 2 *O. universa* defined from the inner porosity with a mode at 6.1 µm and a second one around 13 µm. Inserted in these two panels, a picture at the same scale of the two types of porosity.

Results

Modern calibration : porosity and test diameter :

Size distribution of inner porosity

We measured the diameter of the inner porosity of the core-tops samples. A cumulative histogram indicates that three modes of porosity can be found in the 50 *O. universa* (figure 2). First, the most abundant pores are found around 3.3 µm, the second mode being at around 6.1 µm and the weakest mode for the largest pores at about 13 µm. The *O. universa* porosity clusters in two different groups : the type 1 has a porosity mode between 2 and 5 µm ; and the type 2 has a mode above 5.5 µm (figure 2). The cumulative histograms of the two types of distribution are bimodal : the large pores around 13µm can be find in the two types of *O. universa*. This implies that the mean value of the porosity will reflect mainly the changes in the lowest mode (3.3 or 6.1 µm) (figure 3).

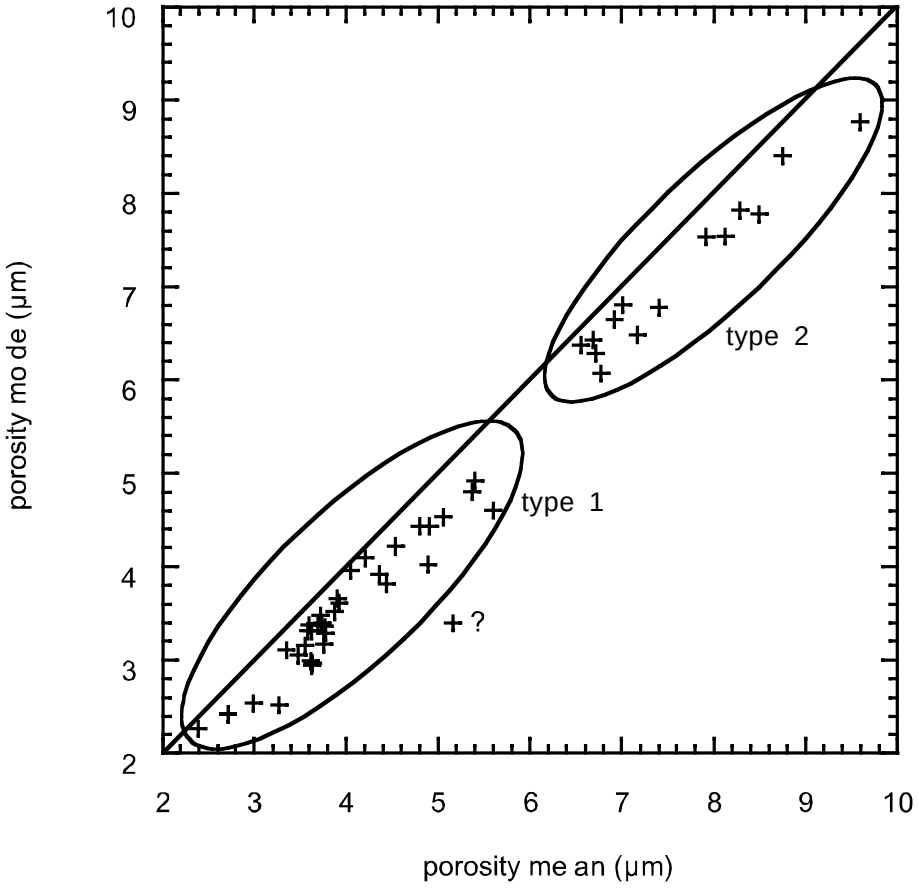

Figure 3 :Scatter plot of the mean inner porosity vs. the mode inner porosity in the core-top studied. One specimen have an anomalous mode, which is due to the remaining presence of coccoliths in some small pores, which have underestimated the mode versus the mean.

Size distribution of external porosity

In order to check if this clear cutoff between these two types was also a feature of the external porosity we compiled two size frequency distribution histograms (figure 4). The type 1 porosity shells appear to have an external porosity where the smaller pores are more abundants, but with a considerable scatter between 2 and 6-7 µm. The type 2 external porosity is bimodal, with a smaller than 5µm porosity and a larger than 7 µm. Looking at the SEM images, the two subtypes labelled "b" on figure 4 appear not distinguishable using the external porosity which is more regular than for the subtypes "a". This kind of texture on O. universa is typical of gametogenetic calcite crust (Bé et al., 1973). So the presence of gametogenetic calcite crust prevents the use of the external porosity as a valuable tool.

Modern calibration of the inner porosity :

The porosity % of *O. universa* in the Western Pacific core-tops have values between 7 to 22%, in the same range than Indian ocean measurements (Bé et al., 1973; Frerichs et al., 1972). We compare our results with the (Bé et al., 1973) measurements in the Indian ocean from surface sediments samples (figure 5.). The porosity index exhibits a robust correlation with the sea-surface salinity (r^2= ~0.5) for the Indian ocean measurements. In our data-set, such a correlation is not detectable. The correlation coefficient between the porosity index and the sea-surface density is better than for the sea surface salinity, and is mostly explained by the sea surface temperature field. Because, the slope is weaker for the density than for the temperature, the more robust parameter that could be estimated by the porosity index is the sea surface density.

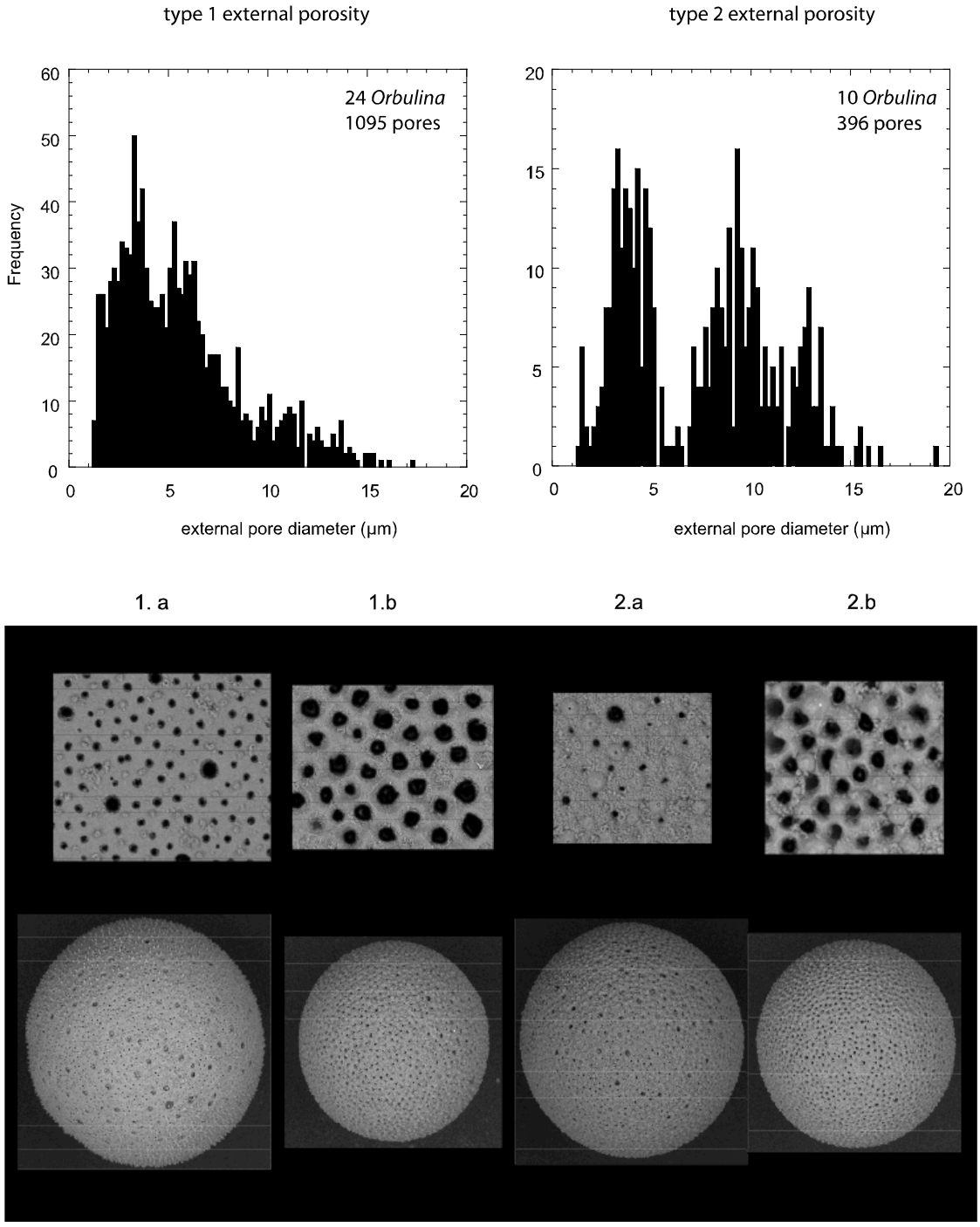

Figure 4 :Size frequency distribution of the external porosity in the two different types of *O. universa* defined from inner porosity mode. (A) Size frequency distribution of the external porosity of the *O. universa* type 1. (B) Size frequency distribution of the external porosity of the *O. universa* type 2. Below, at the same scale, close-up of the *O. universa* external porosity (x500), and general shape (x120), for the 4 sub-types.

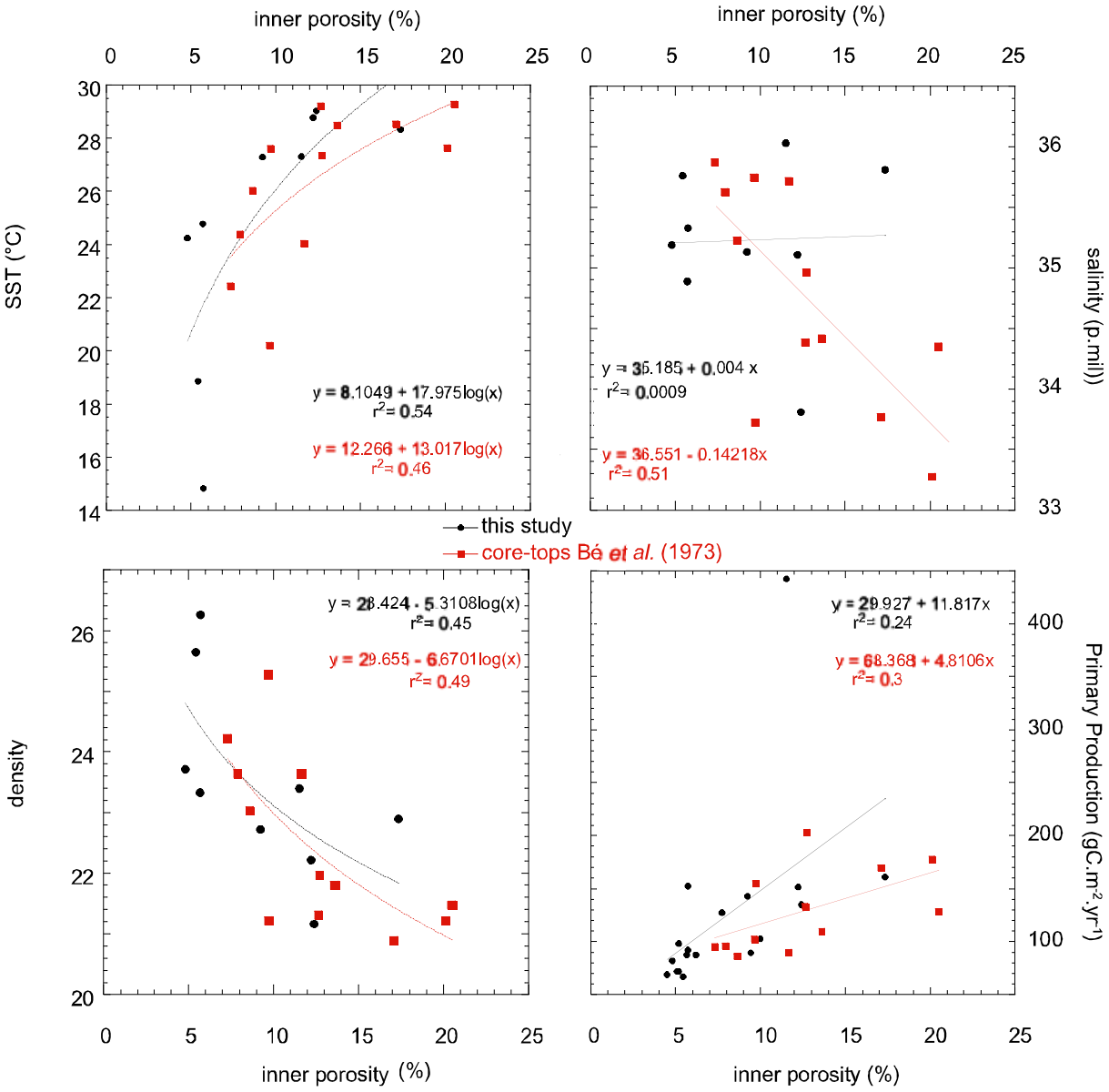

Figure 5 : Inner porosity index measured in core-tops samples vs. hydrographic parameters : (A) Sea-surface temperatures (B) sea surface salinity (C) sea surface density and (D) primary production. The regression lines and coefficient correlations are computed from single data-sets.

Porosity and mean diameter :

Bé et al.(1973) showed that the porosity (in %) is in linear relation with the diameter of the shell. However, in our samples, this relationship is not significant (fig. 5, r^2=0.01). This relationship neither exist between each *O. universa* type and the porosity percentage (fig. 5). The porosity and the mean diameter are thus independent from each other. So, the mean diameter will not be influenced by the relative abundance of the different types of *O. universa*.

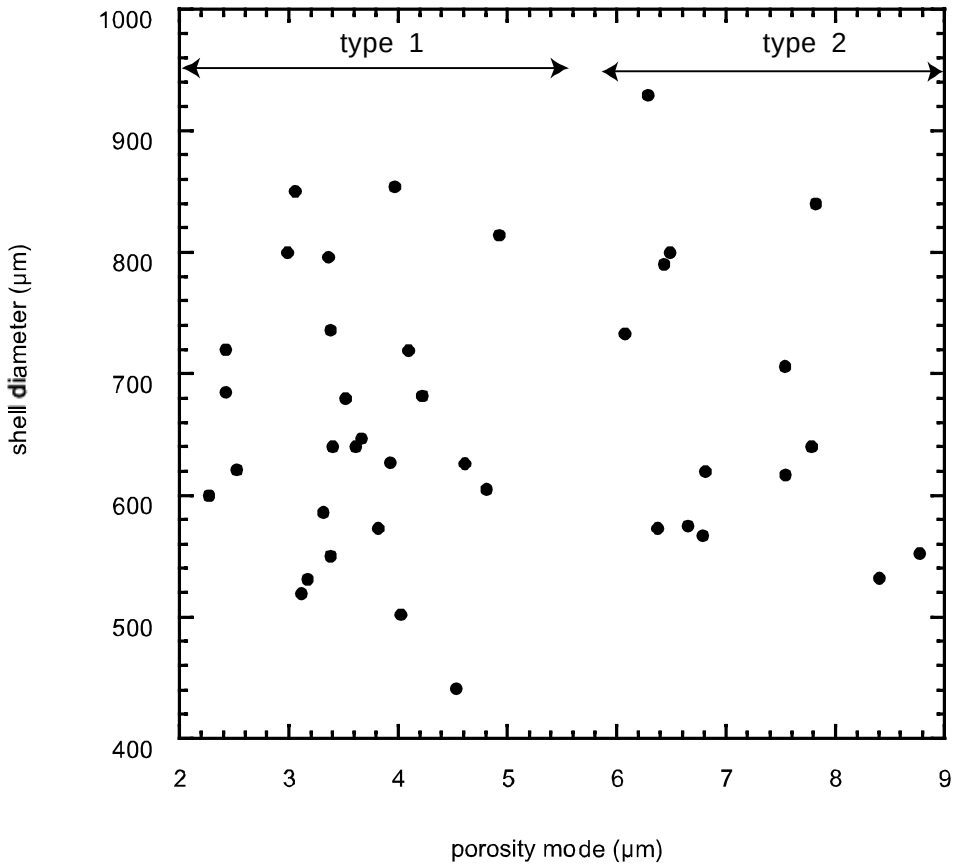

Figure 6 : Scatter plot of the porosity mode vs. the shell diameter.

Modern calibration of the mean test size

We check empirically the relationship between the oceanic parameters and the *O. universa* size compiling the Indian ocean data-set from (Bé et al., 1973), and Pacific measurements from (De Deckker, unpublished) and our data-set (figure 7). Using a linear regression, the sea surface temperature explains most of the variance of the *O. universa* diameter (r^2=0.74). Linked with the SST, the sea surface density explains a comparable variance (r^2=0.71). However, the error bar linked with the SST variability reaches ± 3°C. The *O. universa* diameter can be applied to paleo-SST reconstructions, but should be used with caution due to this large error in predictions. However, the error linked with the density of the seawater is ± 1 unit. A cluster around 600 µm and low densities (around 21-22) appears to worsen the correlation coefficient, which could be problematic for the low latitudes analyses. We also tested the possible relation between the *O. universa* diameter with other parameters (table 2). None of the other oceanic parameters display an as strong correlation coefficient than the the SST. However the relation between the mean size and the trophic associated parameters is not unsignificant, and could maybe explain part of the variance in the mean *O. universa* diameter.

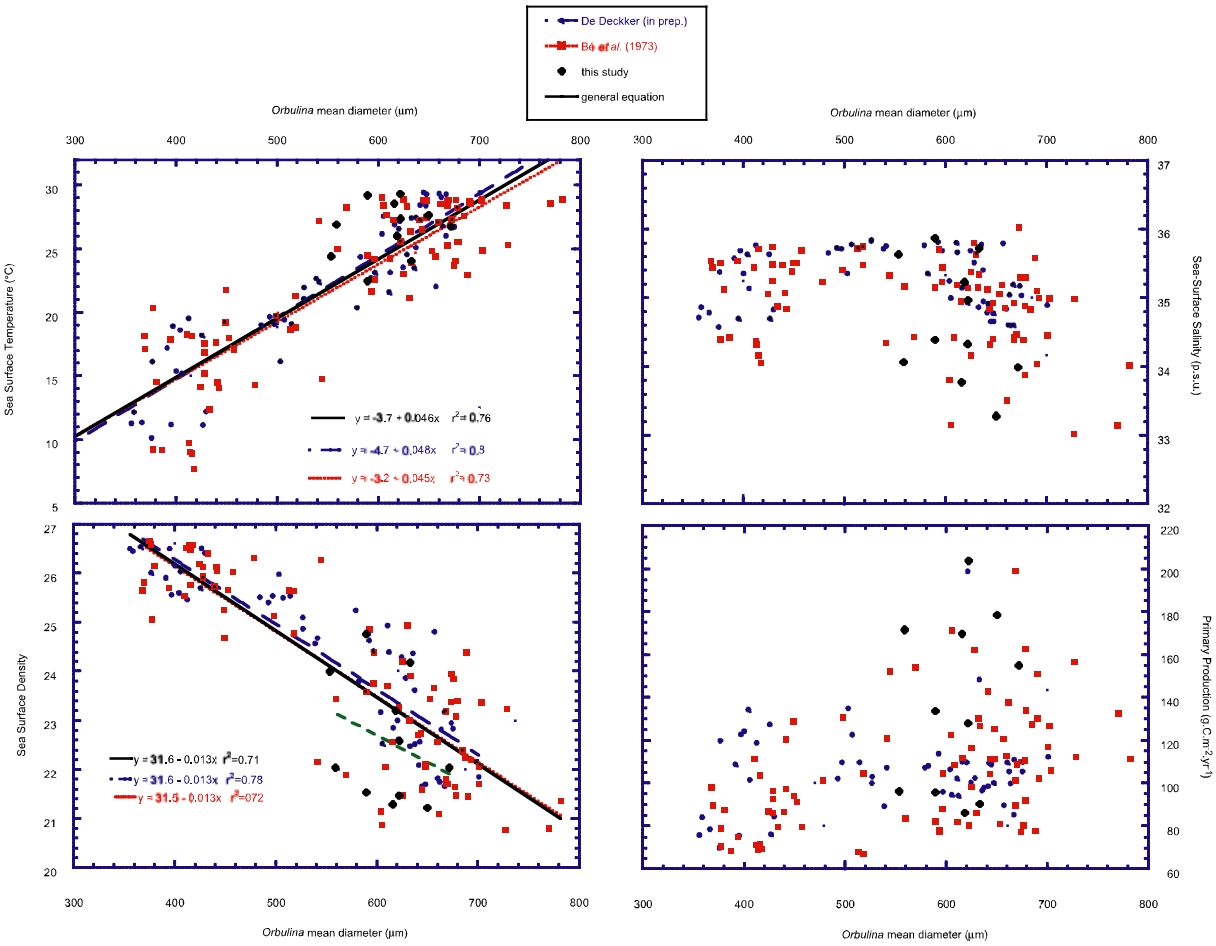

Figure 7 : Mean *O. universa* diameter vs. hydrographic parameters : (A) sea-surface temperatures (B) sea surface salinity (C) sea surface density and (D) primary production. Data from (Bé et al., 1973); (De Deckker, unpublished) and this study.

parameter	r^2	number of core-tops
SST (°C)	0.76	151
Sea Surface Density	0.71	149
Temperature at thermocline depth (°C)	0.49	61
chlorophyll (µmol.l^{-1})	0.31	151
nitrate (µmol.l^{-1})	0.29	151
Thermocline depth (m)	0.25	60
PP (gC.m^{-2}.a^{-1})	0.13	155
SSS (p.s.u.)	0.07	151
Halocline depth (m)	0.03	64

Table 2 : Correlation coefficient of mean diameter of *O. universa* measured in core-tops samples vs. sea-surface hydrology.

Downcore application

Inner porosity

The inner porosity of *O. universa* was examined in six samples in the MD97-2138, in each marine isotopic stage from stage 6 to 1 (table 3). The size frequency distribution of the downcore samples does not diverge from the core-top size frequency ditribution (figure 8). The two different types of *O. universa* can be seen in the stage 1, and stage 6 levels ; whereas the type 1 is dominating the others levels (stages 2 ; 3 ; 4 and 5) (figure 9). This indicates that the two types of *O. universa* can be find in glacial and interglacial stages. The predominance of each type is not linked with the dissolution of carbonates, as indicated by the lack of correlation between the inner mean pore diameter and the fragmentation percentage of planktonic foraminifera, a proxy of carbonate dissolution (r^2 = 0.06 for six samples).

depth (cm)	Age (cal. Ka)	number of Orbulina studied	% Orbulina type1	average nb pores/10000 µm^2	%porosity	density inferred from porosity index
0	3.29	4	75.0	44.98	9.63	22.61
185	19.4	8	75.0	46.19	7.29	23.36
485	56	4	75.0	44.18	9.23	22.73
535	64	9	55.6	40.13	8.00	23.11
735	106	8	75.0	48.50	7.05	23.45
885	146	7	71.4	45.62	7.04	23.46

Table 3 : MD97-2138 porosity measurements

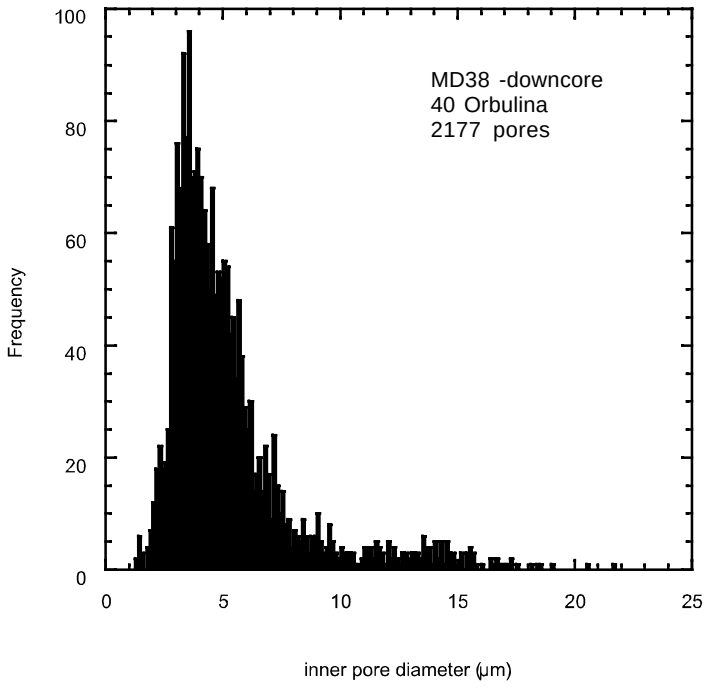

Figure 8 : MD97-2138 downcore inner pore diameter distribution spectrum.

The $\delta^{18}O$ composition of foraminifera is a function of the sea surface temperature and of seawater $\delta^{18}O$ composition, which is in turn correlated to the salinity through the Evaporation-Precipitation local bilan. If the porosity/sea surface density relationship established on the core-tops is a robust feature, we should expect a correlation between the porosity and the $\delta^{18}O$ on the downcore samples. The relationship between the $\delta^{18}O$ and the porosity is not statistically significant (r^2=0.3 for 6 samples). This relationship can be greatly improved by removing the stage 5 measurement (r^2 = 0.95 for 5 samples). At this level, the fragmentation is very high (>60%), indicating a strong dissolution of the planktonic foraminifera. This anomaly could be the result of preferential dissolution of the highly porous foraminifera, or an increase of the fragility of the *O. universa* that prevents its analysis in SEM.

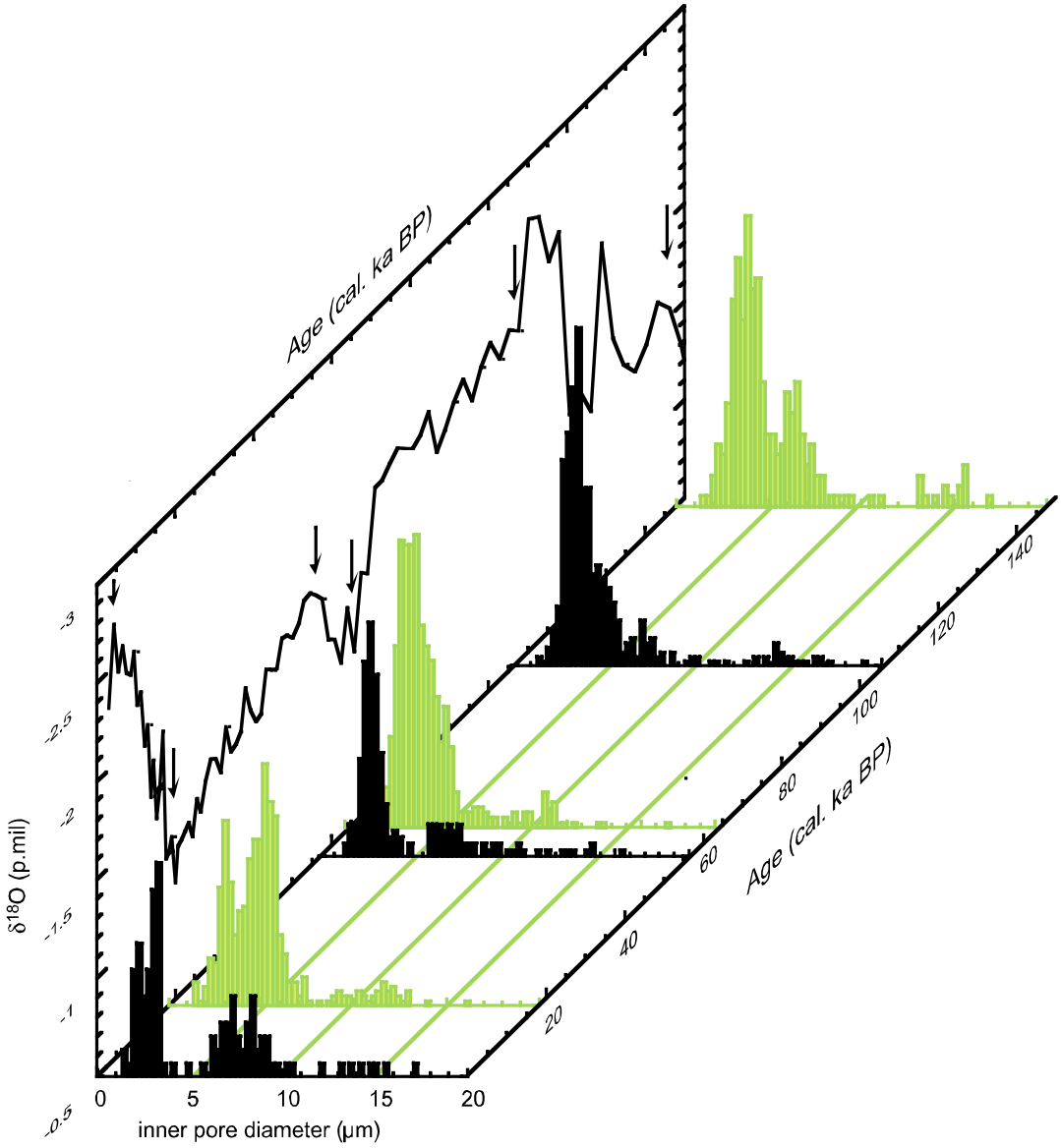

Figure 9 : MD97-2138 inner porosity distribution during the 6 last stages.

Diameter

Orbital scale oscillations : application to the MD97-2138 core

The *O. universa* diameter in the last 130 ka oscillates between 531 and 706µm with a mean value of 618µm, close to the core-top value of 615µm (figure 10). The record exhibits a semi-precessional signal during the last 60 ka. Before 60 ka BP, the size of *O. universa* shows little variability. Comparing to the other records of SST inferred from planktonic foraminifera transfer function and the Primary Production (PP), there is a broad fair agreement. The size of *O. universa* does not show any covariance with the fragmentation index (percentage of broken planktonic foraminifera) confirming the lack of any dissolution bias on this proxy.

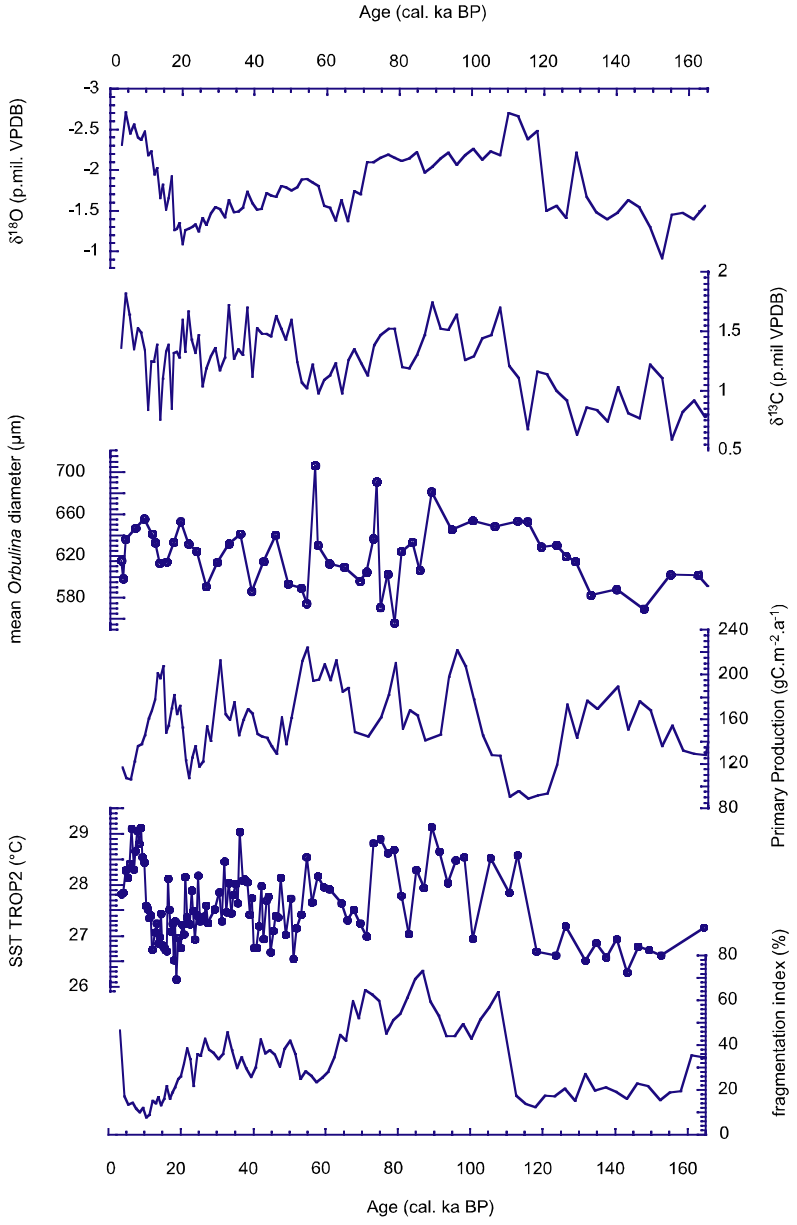

Figure 10 MD97-2138 $\delta^{18}O$, $\delta^{13}C$, *Orbulina universa* mean diameter, Primary Production, SST from planktonic foraminifera transfer function TROP-2 and foraminiferal fragmentation index.

To address the potential use the *O. universa* diameter as a paleothermometer, we compared the SST inferred from *O. universa* to the SSTs deduced from planktonic foraminiferal transfer function (figure 11). The temporal slope is understood in the range of the modern spatial slope scatter. However, the temporal slope have a constant and a slope different from the modern slope spatial slope, so that a supplemental factor could influence the growth of the *O. universa.*

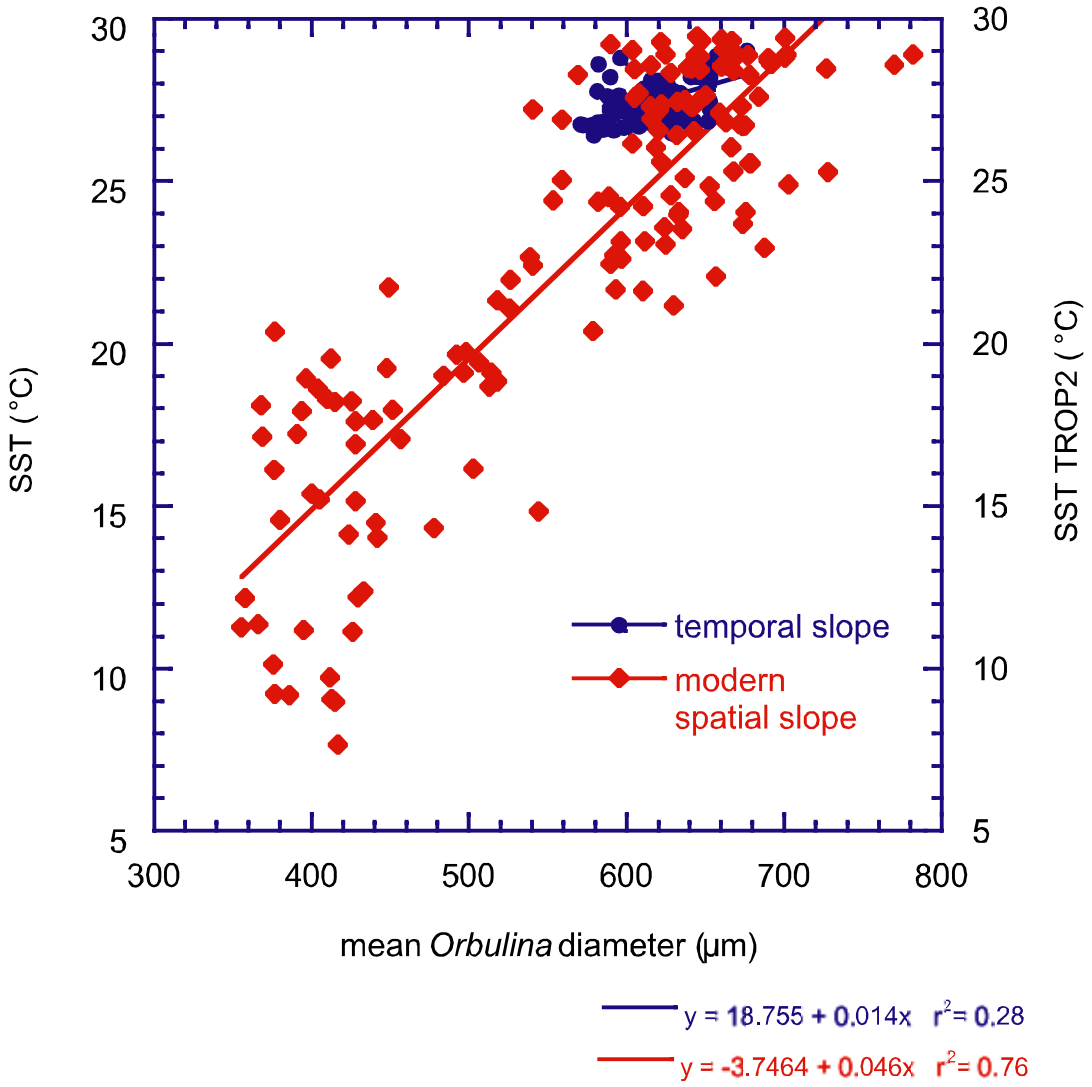

Figure 11 : Comparison of the modern spatial calibration, and the relation between the O. universa mean size diameter and the temperature inferred from foraminiferal transfer function TROP2.

Millenial-scale variability : application to core MD97-2134 **:**

The size of *O. universa* was investigated in the MD97-2134 Papua Gulf core which documents the last 40 kyrs (figure 12). This is the first high resolution record of changes in *O. universa* mean size. The mean diameter does not show any clear glacial/interglacial pattern as the MD97-2138 core already showed, and oscillated between ~550 and 700 µm. Even if the changes are weak in amplitude, they

seem significant because of the lack of noise in the signal. Three significant periods are present in the record as demonstrated by Multi-Taper Method spectral analysis (not shown). First a strong semi-precessional peak at 12.8 ka ; and also 3300 and 1900 years periods. These periods are close to these found in the East Asian winter monsoon dynamics of 4 kyrs and 1.8-1.5kyrs (de Garidel-Thoron et al., 2001).

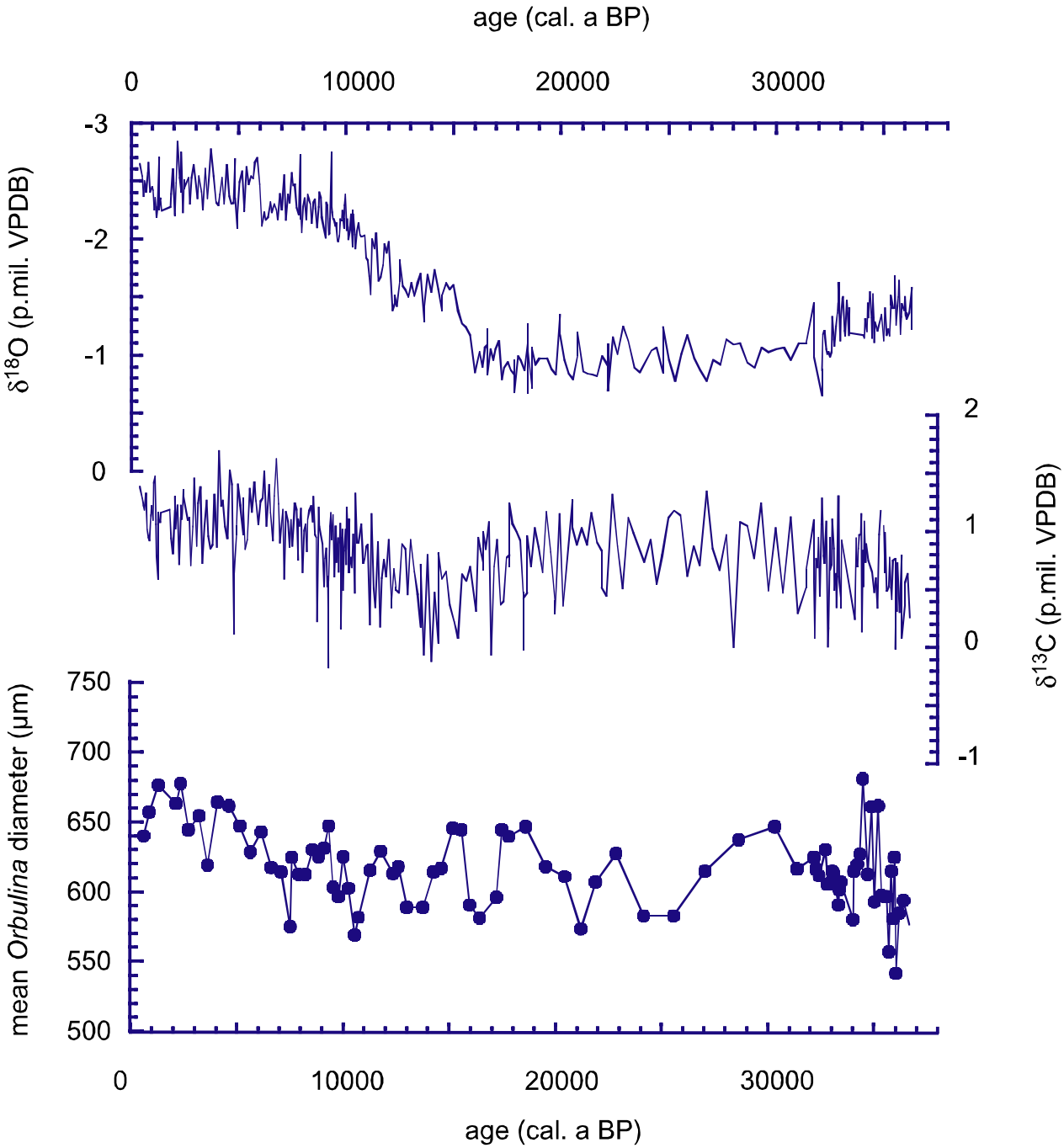

Figure 12 : MD97-2134 $\delta^{18}O$ and $\delta^{13}C$ of *Globigerinoides ruber*, and *O. universa* mean diameter (µm).

Discussion :

Geographic distribution of the different types of *O. universa* :

The two distinct types of *O. universa* defined from the inner porosity show an ambiguous geographic distribution (figure 13). Five of the 12 core-tops studied are composed of one type. Unfortunately; a maximum of 6 measurements has been performed, thus limiting the statistical robustness of the interpretation of the geographic distribution. Nevertheless, the type 2 *O. universa* (small porosity mode around 6 µm) are find mainly in the Western Pacific warm pool whereas the type 1 seem to be ubiquitous.

In the core of the WPWP, the samples MD38 and MD40 contain different types. We address the potential effect of a dissolution bias which should have affected the inner porosity by calculating the correlation coefficient between the depth of the samples and the relative abundance of the two types. This relation is close to 0 (r^2 = 0.03 for the 12 samples). The different types are not linked with dissolution, and thus cannot explain the difference between the MD38 and MD40 samples. A gradient in the sea surface density exists at the eastern edge of the Western Pacific Warm Pool (Delcroix and Picaut, 1998), confirming that the density could be an important factor monitoring the spatial extant of the different porosities.

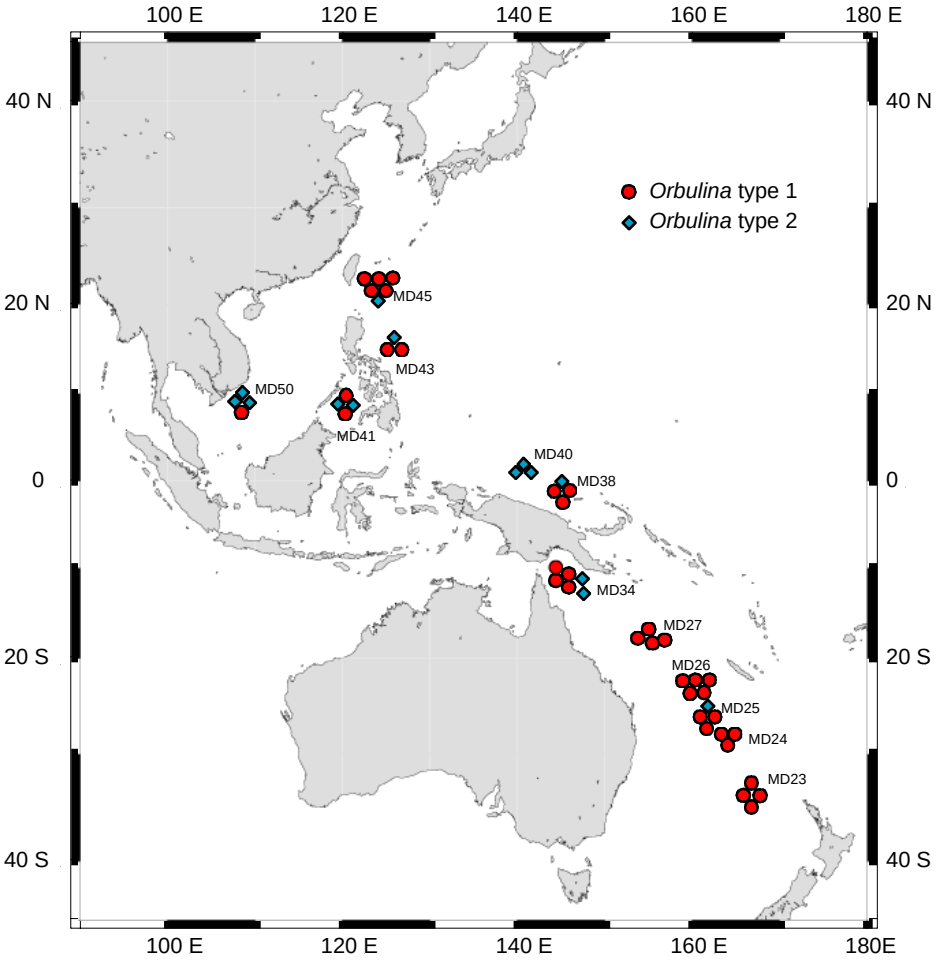

Figure 13 : Map of distribution of the two different types of *O. universa* defined from the inner porosity.

Morphometry and potential cryptic species of O. universa :

In this study, two different morphotypes can be separated from the inner test porosity. Two cryptic species in *O. universa* have been distinguished using DNA analyses by (Darling et al., 1997), whereas the extensive work of (de Vargas et al., 1999) distinguished three different cryptic species in the Atlantic ocean. These authors argue that each genotype corresponds to a typical morphology. The absence of a third morphotype in our study could indicate that either the porosity is not a valuable tool to distinguish this morphotype or that this morphotype has not been sampled in our study. We favour this hypothesis because we did not analysed any core-tops from highly productive areas. Similarly, (Darling et al., 1997) study does not include DNA analyses from upwelling areas, and found only two different genotypes. Our data clearly indicate that two morphotypes coexist in the Pacific ocean, but as long as coupled morphometric work and DNA analysis cannot be achieved on the same samples like as stated by (de Vargas et al., 2001) study, our hypothesis of polyphenetism linked to polygenotypes is still open to discussion. The geographic distribution of the two types of *O. universa* could be refined and thus should help to improve transfer functions by furnishing a quantified taxonomy.

Factors affecting the mean size of O. universa :

Previous studies based on core-tops and plankton tows show an increase of the diameter in association with warmer waters (Bé et al., 1973; Frerichs et al., 1972). However laboratory cultures indicate that for relatively high temperatures (>26°C), the relation between the sea suface temperature and the *O. universa* diameter is reversed (Bé et al., 1973; Caron et al., 1987). The range of the oscillations in the mean diameter of *O. universa* in the MD38 core is always above 580 µm, so at values where a considerable scatter can be observed in the modern calibration plot. Thus, we can try to deduce the other parameters influencing the size of the foraminifera. Among these factors, the concentration in nutrients in the water column, indispensible for the photosynthesis from which the symbionts of *O. universa* catch their energy, is considered as a major limiting factor of the planktonic foraminifera growth. This hypothesis was demonstrated in the cultures of *O. universa*. For example (Caron et al., 1987) demonstrated in cultures that both temperature and food availability exerce a strong influence on the mean shell diameter. To modelize this competing effect of food and temperature, we computed the substraction of the standardized SST inferred from planktonic foraminifera transfer function (de Garidel-Thoron et al., submitted-a) by the standardized Primary Production inferred from the relative abundance of *Florisphaera profunda* (Beaufort et al., 2001) in the MD38 core. These two time-series were prealably resampled at the same time interval than the *O. universa* mean size. The mean shell diameter oscillates in opposition to this effect (figure 14) : the shell size increases when temperature and PP, in the water column are high, but the size decreases when one of these two factors is lacking. These two parameters influence the size of *O. universa* with the same weight.

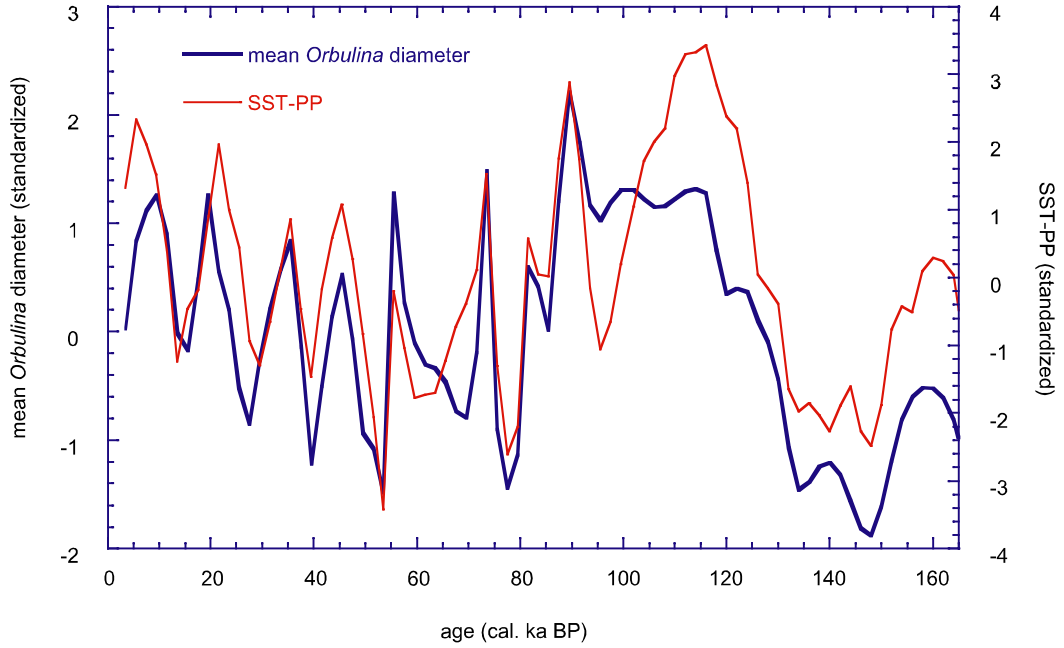

Figure 14 : *O. universa* mean size diameter (bold line) versus the standardized SST from TROP2 minus the the standardized Primary Production inferred from *Florisphaera profunda.*

This conjunct influence of temperature and food on the mean size of planktonic foraminifera has been already suspected by (Bijma et al., 1992). They studied three different core-tops in different areas which show very different signatures to the environmental conditions, and find that both nutrients and temperatures were affecting the mean size of *O. universa*.

This low-latitude effect of the nutrient concentration can also explain the difference between mean *O. universa* mean size and other paleoclimatic proxies as find by Malmgrem and Kennet studying mean size variations of *O. universa* in a deep-sea core from the Mexican Gulf (Malmgren and Healy-Williams, 1978). However, if the size is a very complex signal resulting from physical and trophic parameters, the porosity of *O. universa* seems to be a more adequate tool to study past changes in sea-surface hydrology.

Sea-surface density inferred from *O. universa* : test on glacial-interglacial gradient in the WPWP

The inner porosity, which has been succesfully calibrated to the sea-surface density could be used to reconstruct sea-surface salinity changes together with SSTs records. The inner porosity gave a higher density for the late glacial sample than for the Holocene one (table 3). This higher density during the late glacial is linked in part to the global change in salinity due to polar ice-caps, and to local changes in the SST and Precipitation-Evaporation bilan. In a first step we resolved empirically the late glacial salinity, by resolving the equation :

$$density_{glacial} = f(T_{glacial}, S_{glacial}).$$

$S_{glacial}$= 35.95‰ using $T_{glacial}$=27°C, inferred from the transfer function TROP2 ; and $density_{glacial}$=23.36.

To compare the glacial and the modern SSSs values, we have to substract the global ice-volume salinity change which is around 1.03‰, giving an estimate of the local change in salinity of :

$$\Delta SSS = (SSS_{Glacial} - SSS_{Holocene}) - 1 = + 0.45 ‰$$

We did not propagate the errors through the calculations, so this result should have to be interpreted cautionously. This estimate should not be biased by the different types of *O. universa* as the two samples have the same percentages of each type (table 3). This positive anomaly in SSS during the LGM indicates that the precipitation minus evaporation was reduced over the Western Pacific warm pool during the late glacial interval. This result is in agreement with other studies as recently reviewed by (De Deckker et al., in press) which compile all available records – continental and marine - that reveal dry conditions during the Last Glacial Maximum over the Western Pacific warm pool.

Conclusions :

We evidencized from SEM analysis of inner porosity in O. universa that its inner porosity size distribution is bimodal wih a small porosity (2-8 µm) and a large one (>10-15 µm). Two different types of O. universa can be separated from the smaller inner porosity. First one has a mode from 2 to 5 µm and the second one has a mode around 7µm. In core-tops sediments from the Western Pacific, these two different morphotypes coexist in the same areas, with a larger abundance of the type 2 in the equatorial band. In a sediment core, the two types can be find during the last climatic cycle. We suggest that these two morphotypes could correspond to the previously described cryptic species in O. universa. We speculate that the potential different genotypes could be distinguished in the downcore records using this porosity criterion.

The porosity percentage is correlated to the sea-surface density, making this tool a potential good proxy to reconstruct past changes in sea-surface hydrology. However, this proxy seems to be also affected by preferential dissolution of the more porous foraminifera. There is no correlation between the inner porosity and the mean size of O. universa, indicating that the mean size of O. universa is an independant proxy.

We reassessed the mean size of O. universa in function of the sea-surface hydrology. It appears that the SST is the main factor which influences the size of O. universa. In a sediment core from the Western Pacific, where the SST did not changed by more than 3°C during glacial-interglacial cycles, the mean diameter of O. universa seems to be influenced secondarly by trophic effects. It prevents the use of O. universa diameter as a direct proxy of SST changes, but makes it potentially suitable to detect strong changes in the nutrient availability when used together with a SST proxy.

Acknowledgements

We are thankful to D. Denis, C. Brocard and the team of the Laboratoire de Police Scientifique de Lyon for the S.E.M. analyses.

References

1. *Antoine, D., André, J.-M. and Morel, A., 1995. Oceanic primary production 2. Estimation at global scale from satellite (coastal zone color scanner) chlorophyll. Global Biogeochemical Cycles, 10: 57.*
2. *Bé, A.W.H. and Duplessy, J.-C., 1976. Subtropical convergence fluctuations and quaternary climates in the Middle latitudes of the indian Ocean. Science, 194: 419-421.*
3. *Bé, A.W.H., Harrison, S.M. and Lott, L., 1973. Orbulina universa d'Orbigny in the Indian Ocean. Micropaleontology, 19(2): 150-192.*
4. *Beaufort, L., de Garidel-Thoron, T., Mix, A.C. and Pisias, N.G., 2001. ENSO-like forcing on oceanic primary production during the late Pleistocene. Science, 293: 2440-2444.*
5. *Bijma, J., Hemleben, C., Oberhansli, H. and Spindler, M., 1992. The effects of increased water fertility on tropical spinose planktonic foraminifers in laboratory cultures. Journal of Foraminiferal Research, 22(3): 242-256.*
6. *Caron, D.A., Faber, W.A. and Bé, A.W.H., 1987. Growth of the spinose planktonic foraminifer Orbulina universa in laboratory culture and the effect of temperature on life processes. Journal of the Marine Biological Association of the United Kingdom, 67: 343-358.*
7. *Conkright, M. et al., 1998. World Ocean Atlas 1998 CD-ROM Data set documentation. 15, NODC, Silver Spring, MD.*
8. *Darling, K.F., Wade, C.M., Kroon, D. and Leigh Brown, A.J., 1997. Planktic foraminiferal molecular evolution and their polyphyletic origins from benthic taxa. Marine Micropaleontology, 30: 251-266.*
9. *De Deckker, P., unpublished. Orbulina universa in the Indo-Pacific ocean. .*
10. *De Deckker, P., Tapper, N.J. and van der Kaars, S., in press. The status of the Indo-Pacific Warm Pool and adjacent land at the Last Glacial Maximum. Global and Planetary Change.*
11. *de Garidel-Thoron, T., Beaufort, L., Bard, E., Sonzogni, C. and Mix, A.C., submitted-a. Glacial-interglacial sea-surface temperature changes in the Western Pacific warm pool inferred from planktonic foraminifera and alkenones. Paleoceanography.*
12. *de Garidel-Thoron, T., Beaufort, L. and Bassinot, F., submitted-b. Large Methane Gas Hydrates Releases during the last glacial stage. Geology.*

13. *de Garidel-Thoron, T., Beaufort, L., Linsley, B. and Dannennmann, S., 2001. Millenial-scale dynamics of the East asian winter monsoon during the last 200,000 years. Paleoceanography, 16(5): 491-508.*
14. *de Vargas, C., 2000. Evolution moléculaire chez les foraminifères planctoniques, Genève, Genève et Paris, 194 pp.*
15. *de Vargas, C., Norris, R., Zaninetti, L., Gibb, S.W. and Pawlowski, J., 1999. Molecular evidence of cryptic speciation in planktonic foraminifers and their relation to oceanic provinces. Proceeding of the National Academy of Sciences, 96: 2864-2868.*
16. *de Vargas, C., Renaud, S., Hilbrecht, H. and Pawlowski, J., 2001. Pleistocene adaptative radiation in Globorotalia truncatulinoides: genetic, morphologic and environmental evidence. Paleobiology, 27: 104-125.*
17. *Delcroix, T., Hénin, C., Porte, V. and Arkin, P., 1996. Precipitation and sea-surface salinity in the tropical Pacific Ocean. Deep-Sea Research I, 43(7): 1123-1141.*
18. *Delcroix, T. and Picaut, J., 1998. Zonal displacement of the western equatorial Pacific "fresh pool". Journal of Geophysical Research, 103(C1): 1087-1098.*
19. *Fofonoff, R. and Millard, R., 1983. Algorithms for computations of fundamentals properties of seawater. Unesco Technical Papers in Marine Sciences, 44: 1-53.*
20. *Frerichs, W.E., Heiman, M.E., Borgman, L. and Bé, A.W.H., 1972. Latitudinal variation in planktonic foraminiferal test porosity. Part 1. Optical studies. Journal of Foraminiferal Research, 2: 6-13.*
21. *Hecht, A.D., Bé, A.W.H. and Lott, L., 1976. Ecologic and paeoclimatic implications of morphologic variation of Orbulina universa in the Indian ocean. Science, 194: 422-424.*
22. *Imbrie, J. et al., 1984. The orbital theory of pleistocene climate: support from a revised chronology of the marine _^{18}O record. In: e.a. A.L. Berger (Editor), Milankovitch and climate. D. Reidel Publishing Company, pp. 269-305.*
23. *Le Calvez, J., 1936. Modification du test des foraminifères pélagiques en rapport avec la reproduction: Orbulina universa d'Orbigny et Tretomphalus bulloides d'Orbigny. Annales de Protistologie, 5: 125-133.*
24. *Lindstrom, E. et al., 1987. The Western Equatorial Pacific Ocean Circulation Study. Nature, 330: 533-537.*
25. *Malmgren, B. and Healy-Williams, N., 1978. Variation in test diameter of Orbulina universa in the paleoclimatology of the late Quaternary of the Gulf of Mexico. Palaeogeography Palaeoclimatology Palaeoecology, 25: 235-240.*
26. *Sholkovitz, E.R., Elderfield, H., Szymczak, R. and Casey, K., 1999. Island weathering: river sources of rare earth elements to the Western Pacific Ocean. Marine Chemistry, 68: 39-57.*
27. *Stuiver, M. et al., 1998. INTCAL98 Radiocarbon Age Calibration, 24,000-0 cal BP. Radiocarbon, 40: 1041-1083.*

28. *Wells, M.L., Vallis, G.K. and Silver, E., 1999. Tectonic processes in Papua New Guinea and past productivity in the eastern equatorial Pacific Ocean. Nature, 398: 601-604.*
29. *Yan, X.-H., Ho, C.-R., Zheng, Q. and Klemas, V., 1992. Temperature and size variabilities of the Western Pacific Warm Pool. Science, 258: 1643-1645.*

Partie III

-

Morphométrie des foraminifères et paléocéanographie

Chapitre 6 : Reconnaissance automatique des foraminifères planctoniques : étude préliminaire

En collaboration avec Philippe Dussouilliez.

Introduction

La classification des organismes est fondamentale pour toutes les applications de la paléontologie, de la paléoécologie à la géochimie. Cependant, la maîtrise de la taxonomie demande un long apprentissage de la variabilité intra-spécifique avant toute reconnaissance. L'automatisation de cette tâche permettrait de limiter ce temps d'apprentissage, et d'obtenir rapidement et avec reproductibilité des résultats.

Une méthode de reconnaissance d'images par réseaux de neurones (SYRACO pour Système de Reconnaissance Automatique de Coccolithes) a été développée au CEREGE par Denis Dollfus au cours de sa thèse (Dollfus, 1997; Dollfus and Beaufort, 1999). Cette méthode a été appliquée avec succès aux nannofossiles calcaires. Le taux de reconnaissance des coccolithes est actuellement d'environ 90% (Beaufort and Dollfus, submitted). Cette méthode est désormais employée en routine au CEREGE, et les premiers résultats ont permis d'obtenir des reconstructions de production primaire à très haute résolution (e.g. (Beaufort et al., 2001) – chapitre 4).

Le but de cette étude préliminaire est de tester la faisabilité de l'adaptation de ce système aux formes complexes des foraminifères planctoniques. La réussite d'un tel projet permettrait d'éviter les longues séances de « piquage » de foraminifères, d'obtenir des résultats reproductibles et de garder des images de chaque foraminifère piqué en vue d'analyses morphométriques. L'objectif final n'est pas d'obtenir une reconnaissance des assemblages strictement identiques à celle d'un taxonomiste, mais d'arriver à classer les foraminifères par groupes morphologiques, ces groupes pouvant correspondre à une ou plusieurs espèces. *In fine*, un tel dispositif permettrait de séparer automatiquement les foraminifères d'un groupe morphologique pour des analyses géochimiques (e.g. $\delta^{18}O$, Mg/Ca, ^{14}C). Cette méthode permettrait également de conserver une image de leur test avant leur destruction, ce qui permettrait par exemple de corriger de potentiels effets de dissolution (Rosenthal and Lohmann, in press). Enfin, nous avons vu dans le chapitre précédent l'existence d'une diversité cryptique chez les foraminifères planctoniques qui peut-être détectée par l'utilisation de la morphométrie. La reconnaissance automatique couplée à un système d'analyse morphométrique permettrait d'avancer vers une taxonomie quantifiée des foraminifères planctoniques, et de raffiner ainsi les fonctions de transfert.

Les tentatives de développement d'un système de reconnaissance automatique de microfossiles n'ont pour l'instant jamais abouti excepté SYRACO. A notre connaissance, deux études ont tenté de développer un tel système pour les foraminifères. En 1980, un premier système de reconnaissance

automatique par analyse des contours des foraminifères arrivait à un taux de reconnaissance de 45%, proche d'un classement aléatoire (Johnson, 1980). Une étude de faisabilité de la reconnaissance des foraminifères planctoniques a été plus récemment publiée (Liu-Yu, 1992; Yu et al., 1996). Cette étude proposait un certain nombre de nouvelles techniques d'analyse d'images, mais sans que celles-ci ne soient testées et validées sur des cas réels. Ces deux méthodes emploient des systèmes experts, c'est à dire que les images sont analysés par des algorithmes classiques comme l'extraction du contour extérieur, les transformées de Fourier sur le contour, ou l'analyse de la texture. Ces algorithmes qui peuvent être très efficaces pour des images normées comme les produits industriels, le sont beaucoup moins pour les objets naturels comme les foraminifères qui possèdent une large gamme de variations morphologiques et dont l'image peut être pertubée par des paramètres extérieurs comme par exemple la présence d'argiles résiduelles dans l'ombilic des foraminifères. Les réseaux de neurone sont par contre beaucoup moins sensibles à ce bruit de fond. Par exemple, SYRACO permet de reconnaître des visages éclairés et orientés différemment avec beaucoup plus de justesse que les méthodes classiques de traitement d'image (Dollfus and Beaufort, 1999). Les réseaux de neurone sont donc particulièrement adaptés pour la reconnaissance des foraminifères.

La taxonomie des foraminifères planctoniques est basée sur les critères morphologiques de la texture du test, de la forme et de la taille des loges, de leur arrangement en trois dimensions, et les caractéristiques du foramen. Les critères les plus déterminants nécessitent une vision tri-dimensionnelle des microfossiles. Cependant, pour une grande partie des espèces de foraminifères planctoniques actuels, la vision d'une seule face permet de classer rapidement le fossile. Dans cette étude nous faisons l'hypothèse que la définition d'une classe morphologique à partir d'une face pertinente correspondant la plupart du temps à la face ombilicale, permettra de classer les images dans des classes appropriées pour des applications en paléoécologie et géochimie.

Nous décrirons tout d'abord le dispositif expérimental qui a été développé au CEREGE pour permettre de saisir automatiquement les images de foraminifères. Ensuite nous décrirons l'architecture du réseau de neurones SYRACO. Enfin nous présenterons les résultats préliminaires de cette méthodologie appliquée aux foraminifères planctoniques avec des tests de reconnaissance sur les bases de données et sur la carotte MD97-2138. Cette étude préliminaire n'a pour but que de démontrer la faisabilité de l'automatisation de la reconnaissance des foraminifères.

Matériel et Méthodes

Système d'acquisition automatique des images de foraminifères :

Pour automatiser la saisie des images de foraminifères, en collaboration avec Olga Afanasieva et Philippe Dussoulliez, nous avons développé une platine motorisée composée de deux moteurs pas-à-pas sur laquelle est montée une coupelle micropaléontologique standard (figure 1). Le dépacement de

la platine est contrôlée par une carte IMPACK, et intégrée dans le logiciel SYRACO fonctionnant sous le sytème Windows NT. Les images sont saisies par une caméra standard CCD Grundig 768x576 pixels montée sur une loupe trinoculaire Zeiss STEMI2000-C équipée d'un éclairage annulaire par fibres optiques. L'interface du logiciel SYRACO permet de synchroniser le déplacement de la platine avec l'acquisition des images qui sont sauvegardées sous format TIFF. L'intégralité de la surface de la coupelle est prise en photo en environ deux minutes.

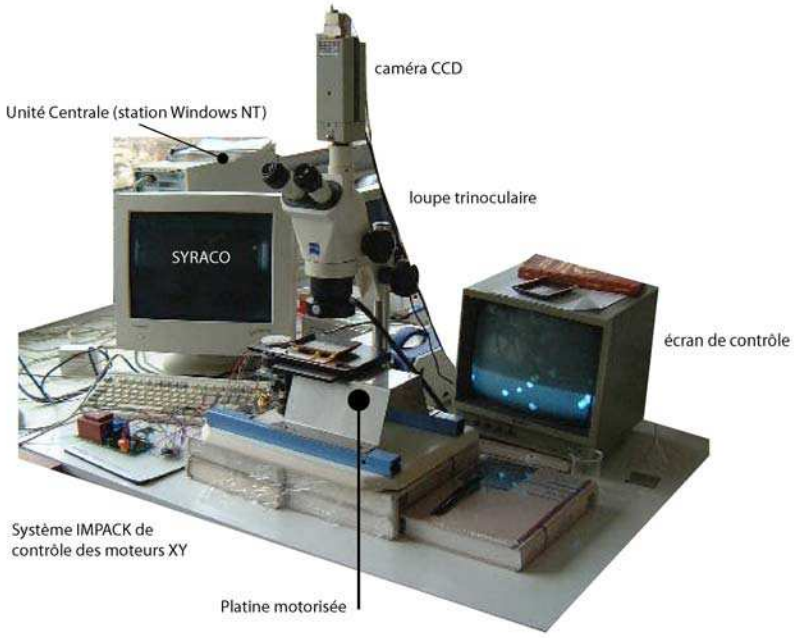

Figure 1 : photo du sytème expérimental d'acquisition automatique d'images de foraminifères.

Réseau de neurones

Le sytème SYRACO (pour SYstème de Reconnaissance Automatique des Coccolithes) est basé sur un réseau de neurones multicouches à rétropropagation (figure 2). L'algorithme du réseau de neurones a été décrit en détail par (Dollfus, 1997; Dollfus and Beaufort, 1999). Surimposé à ce réseau de neurones, se greffent des réseaux de neurones dynamiques qui ajustent et modifient la luminosité, l'angle, le contraste et la symétrie de l'image analysée, en analogie avec les traitements dynamiques que l'homme effectue pour reconnaître des objets. Ces réseaux de neurones supplémentaire, également basé sur un algorithme de rétropropagation permettent d'améliorer significativement la reconnaissance des objets analysés, et notamment des coccolithes (Beaufort and Dollfus, submitted).

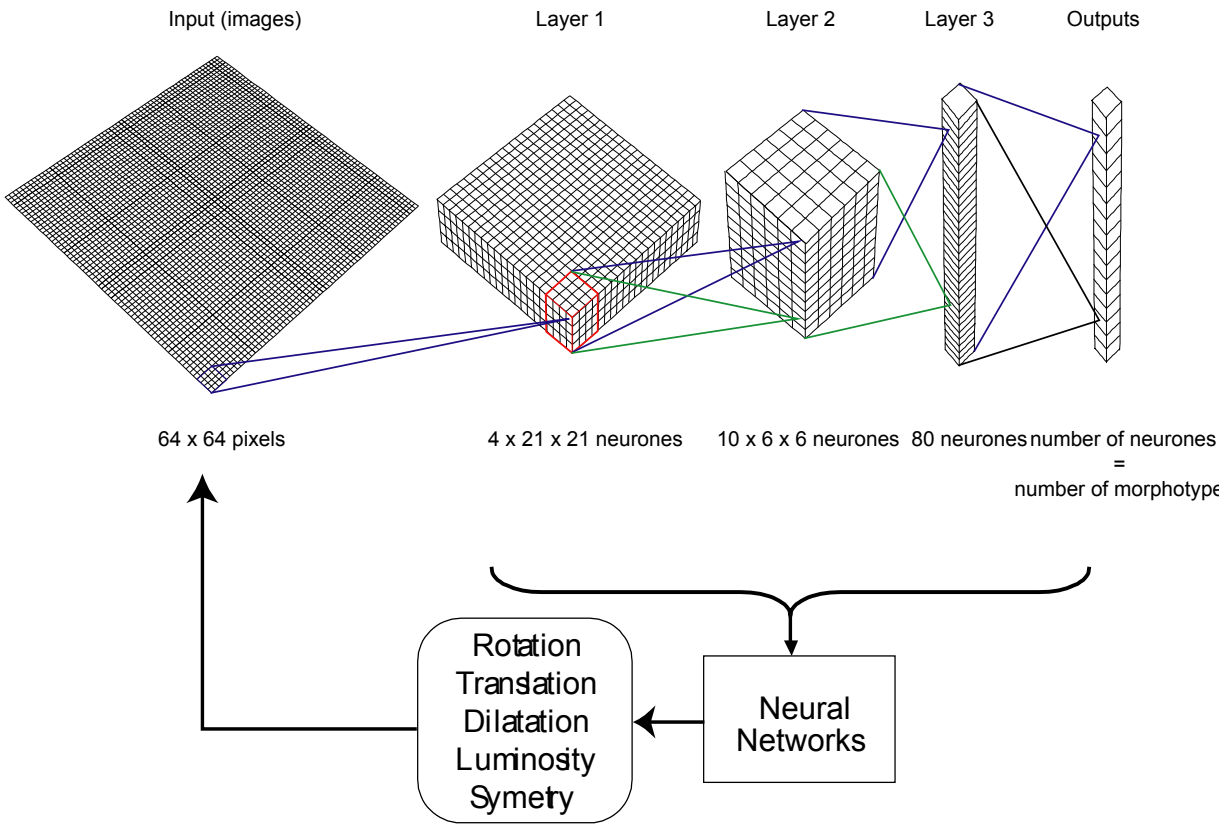

Figure 1 : Architecture du réseau de neurones de SYRACO (d'après Dollfus, 1997)

Base de données images d'apprentissage :

Les 16 classes morphologiques définies pour le réseau de neurones testé dans ce travail correspondent à la cinquième génération du réseau de neurones, les classes ayant été modifiées empiriquement en fonction des résultats des précédents apprentissages (tableau 1). La taille de chaque image est dans la configuration actuelle de SYRACO de 64x64 pixels. Chaque classe comporte envion 125 objets différents. Ainsi, la base de données d'apprentissage est constituée d'environ 2000 images de foraminifères planctoniques. Ceux-ci proviennent exclusivement de sédiments Pléistocènes du Pacifique ouest équatorial (carottes MD97-2134 ; MD97-2138 et MD97-2140 – tableau 2), expliquant l'absence dans notre base de données d'espèces de hautes latitudes. L'image d'entrée du réseau de neurones étant limité à 64x64 pixels nous avons fait le choix d'utiliser un grossissement qui privilégie l'intervalle granulométrique compris entre 200 et 400 µm ; limitant la reconnaissance des petites espèces ainsi que celle les plus grosses. Ce choix se justifie par le fait que cette gamme correspond aux plus grandes abondances de foraminifères adultes, gamme de taille dans laquelle sont piqués les foraminifères analysés en géochimie.

bou	fragment de loge sub-circulaire de globigérines/*Orbulina* de petite taille.
bri	*G. glutinata* et petites globigérines dont le test apparaît brillant
cir	fragment de loge de globigérines, face concave
cro	*G. calida et aequilateralis*
dbl	doublons de foraminifères
duo	*N. dutertrei* face ombilicale
dut	*N. dutertrei* face dorsale
hel	*G. truncatulinoides*
mas	*Globigerines « compactes » (conglobatus et certains conglomerata)*
pul	*Pulleniatina obliquiloculata*
str	objet brillant coupé suivant une ligne (artefact lié à la segmentation des images)
fer	*G. truncatulinoides* sur le côté
tri	*Globigerinoides sacculifer trilobus* (sacculifer sans sac)
fra	fragment de contour polygonal
men	globorotalia
rub	*Globigerinoides ruber* face ombilicale

Tableau 1 : Classes utilisées dans SYRACOforam

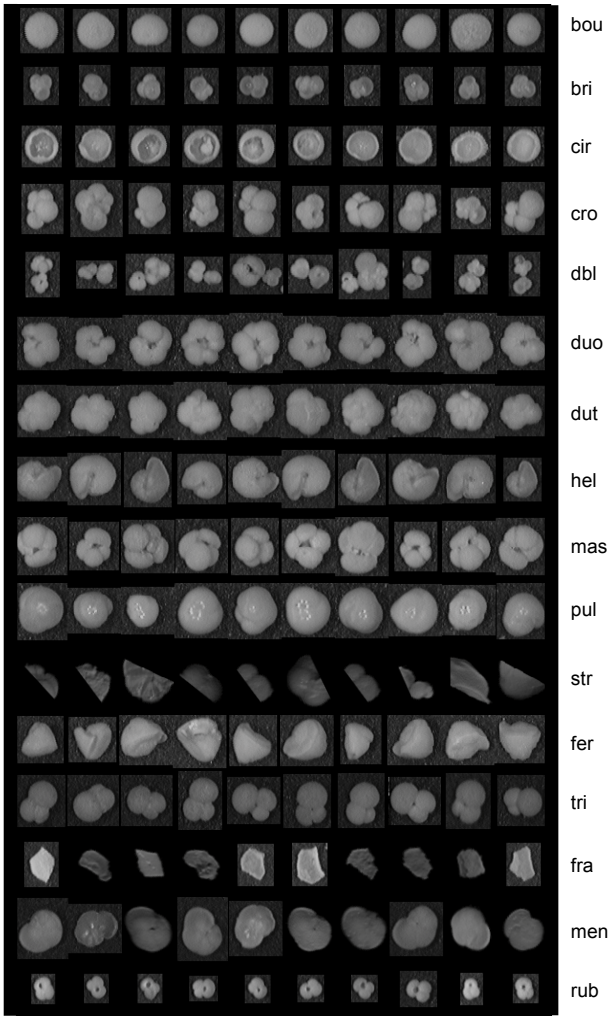

Figure 3 : Exemples d'images de la base de données d'apprentissage

Nom	latitude	longitude	profondeur (m)
MD 97-2134	9° 54.44 S	144° 39.65 E	767
MD 97-2138	1° 25.246	146° 14.20	1900
MD 97-2140	2° 02.586 N	141° 45.49 E	2547

Tableau 2 : Localisation des sédiments de carottes utilisés pour constituer la base de données d'apprentissage

Fonctionnement de SYRACO:

- Apprentissage :

Pendant la phase d'apprentissage, SYRACO va ajuster le poids des coefficients des neurones en fonction de la base d'apprentissage. Il faut en moyenne 250 itérations, c'est à -dire que la base de données doit être apprise 250 fois par le réseau de neurones, pour que celui-ci commence à reconnaître les classes de la base de données. Si le nombre de tours est trop important (>350 tours pour les foraminifères), le réseau de neurones ne reconnaîtra plus que les images de la base de données, et sera incapable de généraliser à d'autres images. La phase d'apprentissage du réseau de neurones testé ici a duré 300 tours, et le nombre d'actions était limité à 6.

- Reconnaissance :

Pendant la phase de reconnaissance d'images, le réseau de neurones va activer à chaque image traitée, un neurone de la couche de neurones de sortie en lui attribuant un poids. Sa valeur est comprise entre –1 et +1. –1 correspond à une image non classée ; tandis qu'un poids de +1 indique une très forte probabilité d'appartenance de l'image à la classe du neurone activé. La valeur du seuil au-delà duquel une image est attribuée à une classe donnée, est paramétrable sur SYRACO. Une valeur de 0.8 pour les foraminifères, offre un bon compromis entre les erreurs d'omission et celles de contamination. Toutes les images d'objets reconnus sont stockées dans des fichiers images qui compilent toutes les images de chaque classe pour un échantillon.

Résultats :

Pour tester l'efficacité de la reconnaissance du réseau de neurones, deux séries de test ont été effectuées. La première série teste une base de données d'images de foraminifères sélectionnées par un spécialiste, base de données différente de celle utilisée pour l'apprentissage du réseau de neurones. Ce test est biaisé par le fait que toute les formes et positions trouvées ne sont pas représentées dans une telle base de données ; et n'inclut pas le « bruit » contenu dans la coupelle micropaléontologique.

La deuxième série de test a été faite sur des images « brutes » saisies sous la loupe binoculaire, et inclut donc du « bruit » pour le réseau de neurones (formes non apprises, foraminifères benthiques, radiolaires, ptéropodes,…). La comparaison des résultats obtenus par le réseau de neurone avec un comptage de spécialiste est effectuée sur les mêmes images.

Deux types d'erreur peuvent fausser les résultats de la reconnaissance. Le premier type d'erreur est ce que nous appellerons « omission » qui correspond aux objets reconnaissables comme des foraminifères d'une des classes apprises par SYRACO mais qui ne sont pas reconnus du tout par SYRACO. Le deuxième type d'erreur, les « envahisseurs » qui ont un effet de « contamination », sont des objets qui sont mal classés par le réseau de neurones. La contamination par des objets qui correspondent à des classes apprises par le réseau de neurone, sera dite « contamination interne ». Dans le cas inverse, si les envahisseurs ne correspondent pas à des objets appris par le réseau de neurones, la contamination sera dite « externe ».

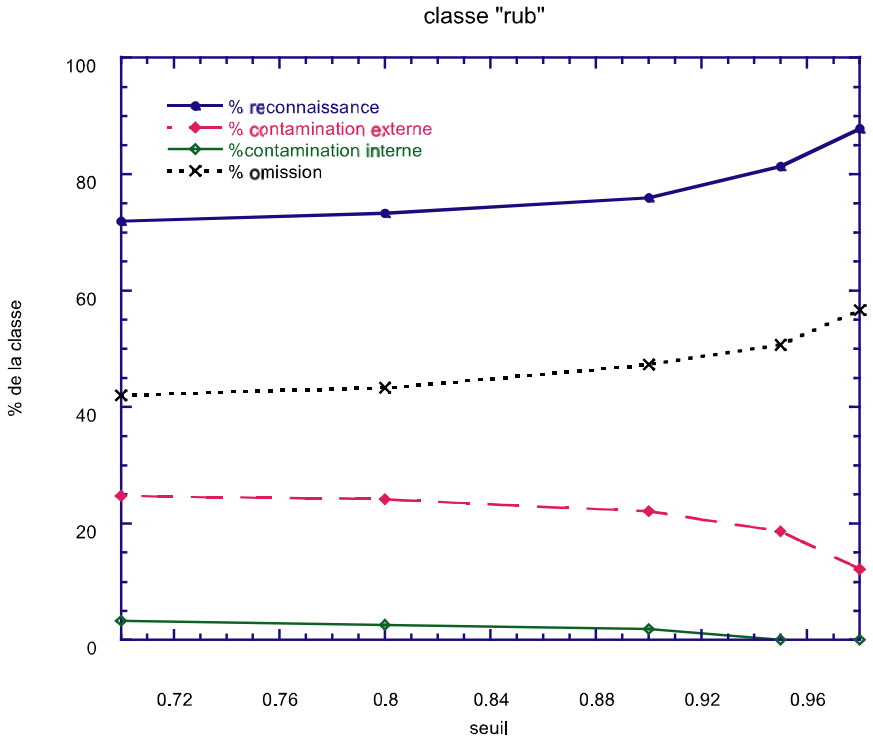

Figure 4 : Pourcentage types d'objets reconnus dans la classe « rub » en fonction du seuil de la couche de sortie

Tests sur une base de données :

La base de données images de test consiste de 40 images pour chaque classe définie, sauf pour la classe rub qui est constituée de 150 images, et 400 objets non définis lors de l'apprentissage, qui doivent permettre de quantifier la contamination « externe ». Sur cette base de données, les performances du réseau de neurones pour 5 valeurs de seuil de la couche de sortie du réseau ont été testées (figure 4). Ainsi, pour la classe « rub » on constate que le niveau de reconnaissance est très bon avec des valeurs comprises entre 80 et 90%, le maximum étant atteint une valeur de seuil de 0.98. En parallèle à l'augmentation de la performance du réseau de neurones, l'effet d'omission augmente en fonction du seuil. Le réseau de neurones est alors beaucoup plus sélectif. L'effet de contamination interne apparaît comme très peu important (<10%), tandis que les objets non définis dans la base de données introduisent des erreurs de reconnaissance plus conséquentes (aux alentours de 40 %).

Nous avons calculé les différents pourcentage de mesure de la qualité du réseau de neurones, en utilisant la valeur de seuil de 0.98, ce qui implique donc le meilleur pourcentage de reconnaissance possible, mais aussi une plus grande quantité d'individus de chaque classe manqués.

classe	bou	bri	cir	cro	duo	dut	fer	fra	hel	mas	men	pul	rub	tri
%reconnaissance	67	71	64	78	54	50	88	68	55	65	60	60	87.8	90
%omission	20	88	10	55	65	58	83	25	35	63	48	25	56.7	55
%contamination interne	18	0	3	0	18	5	0	10	25	0	10	7.5	0	2.5
%contamination externe	23	5	48	13	13	38	2.5	25	28	20	25	43	22.5	2.5

Tableau 3 : Pourcentages de reconnaissance, d'omission et de contaminations sur la base de données images pour une valeur de seuil de 0.98.

Pour une valeur de seuil de 0,98, la valeur moyenne de reconnaissance est d'environ 69%, celui d'omission est d'environ 50%, alors que les contaminations internes et externes ont des pourcentages respectifs de 7 et de 21 %. La disparité dans le pourcentage de reconnaissance est encore grand entre les différentes classes. Les objets de grande taille sont souvent les plus mals reconnus (men, pul, dut). Ceci est dû à la limitation de la taille de l'image d'entrée du réseau de neurones, qui n'englobe souvent pas la totalité du foraminifère. Les résultats de ce réseau de neurones sont déjà prometteurs, avec notamment d'excellents résultats pour les classes rub, tri et fer qui correspondent à des espèces de foraminifères couramment utilisés en géochimie.

Test sur échantillons « réels »:

Le seul moyen de vérifier la validité du réseau de neurone comme outil de reconnaissance comparable au classement d'un taxonomiste est de comparer les résultats obtenus par ce réseau de neurones avec les comptages « humains ». Dans cette étude préliminaire, nous nous somme focalisés sur la classe « rub » (de Globigerinoides ruber). Une série d'images de coupelles micropaléontologiques a été analysée par le réseau de neurones, et sur ces mêmes images nous avons comptés visuellement le nombre de foraminifères attribuables à cette classe (figure 5). Le seuil choisi pour ce test était de 0.7 afin de minimiser l'effet d'omission. Les comptages de SYRACO sont ceux bruts, non corrigés par un taxonomiste et sont donc très « contaminés ». Il existe une corrélation significative entre les comptages de SYRACO et les nôtres (r=0.93). Cependant, les comptages de « rub » obtenus par SYRACO sont beaucoup trop élevés, par rapport à nos comptages. Cette surévaluation est due à un effet de contamination lié à la faible valeur du seuil de la couche de neurones de sortie. Il est néanmoins notable que le taux de contamination semble constant dans l'intervalle étudié, comme l'indique la droite de corrélation, et qu'il est donc possible (même si ça n'est pas souhaitable) d'appliquer un coefficient de correction aux comptages de SYRACO pour obtenir les valeurs obtenues par un expérimentateur humain (toujours dans le même intervalle, car pour des valeurs inférieures à 40, la pente doit être beaucoup plus forte).

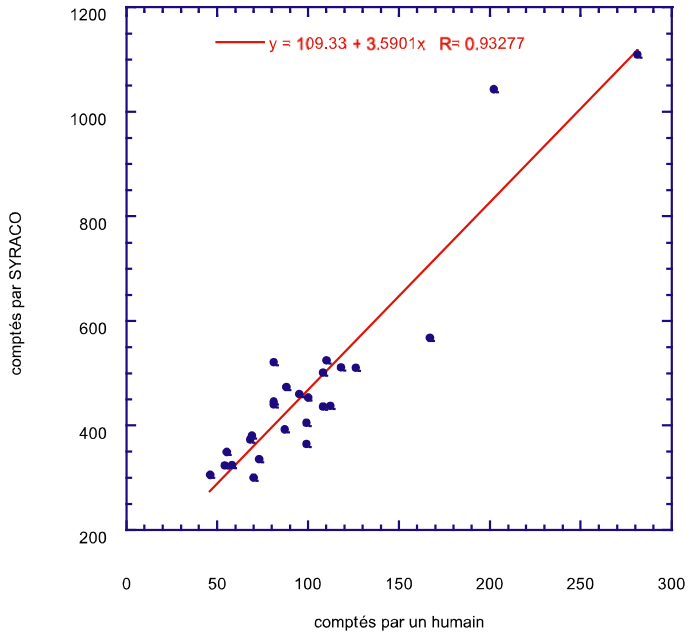

Figure 5 : Comptages bruts de « rub » effectués par SYRACO en fonction des comptages effectués sur les mêmes images par un expérimentateur humain.

Ainsi, même si la calibration est encore sommaire, l'application de réseaux de neurones peut-être envisagée pour des échantillons micropaléontologiques réels, non prétraités par un taxonomiste comme dans le cas des bases de données.

Nous avons testé l'utilisation de ce réseau de neurones sur la carotte MD97-2138 dont les résultats issus des comptages, et d'analyses morphométriques *d'Orbulina universa*, ont été montrés précédemment (chapitres 3 et 5). Les résultats de cette partie sont dépendants d'une calibration plus étendue. Les figures suivantes permettent d'illustrer l'utilisation potentielle de ce système de reconnaissance automatique de formes aux foraminifères. Ces résultats ont été, rappelons-le, obtenus à partir d'un réseau de neurones encore « primaire ».

Les comptages de « rub » effectués par SYRACO ont été comparés à nos comptages de *G. ruber*, dans lesquels 300 foraminifères sont triés et collés sur une lamelle micropaléontologique (figure 6). Les données de « rub » sont donnés en pourcentage de classes associées à des foraminifères non fragmentés. Les dynamiques des deux enregistrements sont tout à fait comparables, avec l'existence de 3 zones, dans lesquelles les abondances relatives possèdent les mêmes niveaux de base. Les valeurs d'abondance exprimées par SYRACO, n'ont dans l'état actuel de la calibration aucune valeur intrinsèque. Cette classe « rub » est envahie par des objets extérieurs à cette classe (figure 7). Il apparaît que la plupart des envahisseurs correspondent en fait à des ruber, mais dont la face spirale est visible. Ainsi cette contamination n'est pas critique pour d'éventuelles piquages en vue d'analyse géochimiques. En tout état de cause, la reconnaissance par SYRACO doit toujours être visuellement corrigée par un taxonomiste.

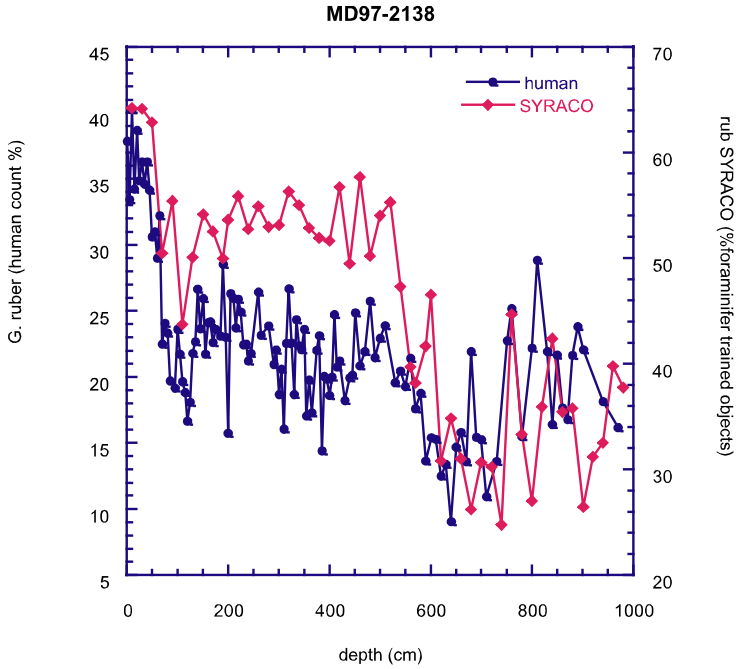

Figure 6 : Pourcentage de G. ruber (foncé) comparée au pourcentage de « rub »/tous les foraminifères non fragmentés comptés par SYRACO

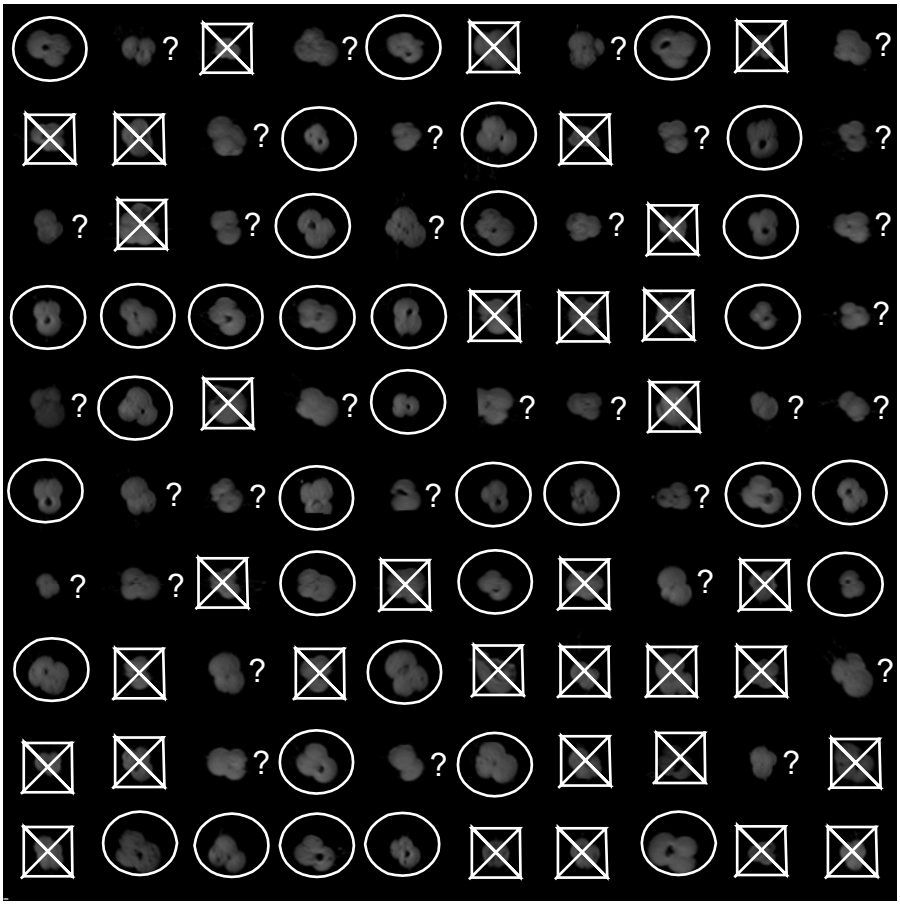

Figure 7 :Exemple d'image de sortie de SYRACO de la classe « rub » montre qu'à partir des images brutes, le classement par SYRACO permet d'obtenir de bons résultats. Les croix indiquent les onjets mal classés, les cercles ceux qui sont justement classés, et les points d'interrogation, les images pour lesquelles la probabilité que l'image soit un rub est élevée (échantillon MD97-2138 – 10cm)

Dans la même carotte, nous avons comparé la fragmentation des foraminifères planctoniques avec le comptage effectué par SYRACO des fragments de loges de globigérines « cir » (figure 8). L'index de fragmentation « cir » a été rapporté à toutes les classes correspondants à des foraminifères non brisés. De la même manière que pour « rub », une bonne correspondance existe entre les deux enregistrements, montrant qu'il n'est pas déraisonnable d'envisager le comptage automatique des fragments de foraminifère dans une carotte sédimentaire.

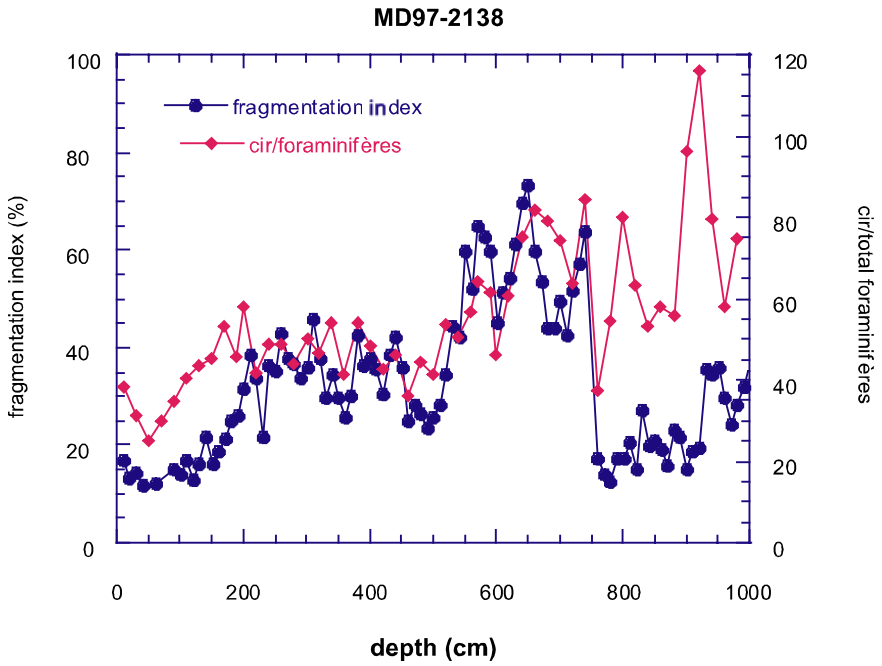

figure 8 : Pourcentage de fragments de foraminifère planctoniques (foncé), par rapport au pourcentage de fragments de type « cir »/foraminifères non brisés comptés par SYRACO

Discussion :

La reconnaissance de foraminifères par réseaux de neurones semble donc une voie très prometteuse pour les études en paléocéanographie. Avec le réseau de neurones que nous avons présenté, il est possible d'obtenir un très bon pourcentage de reconnaissance pour certaines classes, avec des valeurs proches de 90%. L'hypothèse qu'une vision en 2D permet d'obtenir des résultats pertinents est donc validée par cette étude préliminaire.

Ce système n'est cependant pas encore applicable aux carottes sédimentaires. Plusieurs améliorations permettront d'envisager son application. Ces améliorations ont trait (1) à la base de données d'apprentissage, (2) au logiciel utilisé, et enfin (3) au matériel employé.

(1) Base de données images :

La reconnaissance des foraminifères par SYRACO est dépendante de la base de données d'images de l'apprentissage. La contamination « interne » est beaucoup plus faible (4 à 10 fois) que la contamination « externe ». Pour réduire cette contamination externe, le meilleur moyen est

d'apprendre au réseau de neurones les classes morphologiques qu'il ne reconnaît pas. C'est en suivant ce principe que nous avons défini dans notre base de données les objets « str » qui correspondent aux bords des images saisies par SYRACO. L'ajout de cette classe a permis de limiter considérablement la contamination « extérieure », en cantonnant ces objets dans cette classe. Ainsi, l'ajout des classes de grandes tailles, mais aussi de classes liées aux foraminifères d'upwelling et de hautes latitudes permettra de considérablement renforcer la reconnaissance des foraminifères planctoniques.

(2) Logiciel :

- Le logiciel SYRACO utilise pour sa couche d'entrée des images de 64x64 pixels. Cette résolution était bien adaptée pour les coccolithes. Cependant, dans le cas des foraminifères, la reconnaissance pour les classes correspondant aux grands taxons est peu performante. Ceci est dû au fait que les images de ces classes sont tronquées par SYRACO, et ne représentent plus qu'une partie du foraminifère initial. Le passage d'une image de 64x64 à une image de 128x128 permettrait de résoudre ce problème. La base de données d'images que nous avons défini pourrait toujours être utilisée, et complétée par des images des grands foraminifères (*Orbulina*, *Globorotalia*…).
- Une deuxième piste qui permettrait de supprimer les contaminations qui sont parfois très grossières, serait d'ajouter à SYRACO, un petit module de morphométrie qui vérifierait si les invariants caractéristiques de chaque classe sont bien vérifiés pour chaque image. Un système analogue a été développé pour les coccolithes par Luc Beaufort.

(3) matériel :

- L'acquisition des images sur la platine expérimentale se fait sur une coupelle micropaléontologique classique. Celle-ci est recouverte d'une peinture à très faible réflectance. Malgré sa très faible réflectance celle-ci est encore forte. Cette réflectance introduit un très fort bruit de fond autour des images de foraminifère. Ce bruit de fond semble altérer sensiblement les reconnaissances. La solution adoptée actuellement a été de supprimer tout le signal en-dessous d'un seuil qui correspond à la bande du bruit de fond. Cependant, ce seuillage modifie légèrement le spectre des images. Il serait donc important de créer un support à très faible réflectance. Une possibilité serait de poser les foraminifères sur une lame de verre située quelques centimètres au-dessus d'un fond noir à très faible réflectance.
- L'augmentation de la résolution de la caméra permettra sans doute d'améliorer sensiblement ce sytème de reconnaissance de formes.

Le réseau de neurones actuel avec un seuillage élevé 0.98 permet de classer 90% de « rub ». De tels résultats impliquent que la faisabilité d'une « machine à piquer les foraminifères » est tout à fait raisonnable. (Johnson, 1980) avait décrit un système de tapis roulant associé à un cône rotatif sur

lequel tombaient les foraminifères. Ce sytème permet de séparer physiquement les foraminifères. Un tel système couplé à SYRACO permettrait de séparer les différentes classes de foraminifères.

Conclusions

Le système de reconnaissance automatique des coccolithes (SYRACO) a été adapté pour les foraminifères planctoniques. Une base de données préliminaire d'images de foraminifères planctoniques a permis de construire un réseau de neurones capable de reconnaître des foraminifères.
Les tests sur base de données indiquent que le pourcentage de reconnaissance moyen de ce système est d'environ 70%, avec certaines classes bien définies comme celle correspondant à la face ombilicale de G. ruber, qui sont reconnues à 90%. Les comptages effectués par le réseau de neurones et ceux effectués par un micropaléontologue sont significativement corrélés. Enfin, en utilisant le système expérimental de saisie d'images que nous avons développé, l'application de ce système à des enregistrements sédimentaires permet d'obtenir rapidement des résultats comparables aux comptages effectués par des expérimentateurs humains.
Nous suggérons plusieurs améliorations qui permettront de progresser vers une reconnaissance automatique des foraminifères, ce qui permettra d'accroître sensiblement la reproductibilité des résultats micropaléontologiques.

Références :

Beaufort, L., de Garidel-Thoron, T., Mix, A.C., and Pisias, N.G., 2001, ENSO-like forcing on oceanic primary production during the late Pleistocene: Science, v. 293, p. 2440-2444.

Beaufort, L., and Dollfus, D., submitted, Automatic recognition of coccoliths by dynamical neural networks: Marine Micropaleontology.

Dollfus, D., 1997, Reconnaissance de formes naturelles par des réseaux de neurones artificiels: application au nannoplancton calcaire [Ph.D. thesis]: Aix-en-Provence, Aix-Marseille III.

Dollfus, D., and Beaufort, L., 1999, Fat neural network for recognition of position normalized objects: Neural Networks, v. 12, p. 533-560.

Johnson, R.F., 1980, One -centimeter stratigraphy in foraminiferal ooze: theory and practice [Ph.D. thesis]: San Diego, University of California.

Liu-Yu, S., 1992, Reconnaissance de formes par vivion par ordinateur: application à l'identification des foraminifères planctoniques [Ph. D. thesis]: Nice, Université de Nice Sophia-Antipolis.

Rosenthal, Y., and Lohmann, G.P., in press, Accurate estimation of sea surface temperatures using dissolution-corrected calibration for Mg/Ca paleothermometry: Paleoceanography.

Yu, S., Saint-Marc, P., Thonnat, M., and Berthod, M., 1996, Feasability study of automatic identification of planktic foraminifera by computer vision: Journal of Foraminiferal Research, v. 26, p. 113-123.

Conclusions

L'analyse des microfossiles carbonatés du Pléistocène récent du Pacifique ouest nous a permis de quantifier la variabilité océanique (paléo-températures, paléo-productivités) de cette zone, et de la lier à la variabilité climatique.

Alors que cette zone était supposée être relativement stable au cours du temps, que ce soit à l'échelle glaciaire-interglaciaire, et à plus forte raison à l'échelle du millénaire, nous avons montré que son climat avait connu des changements significatifs dans le fonctionnement du sytème de mousson et dans celui de la circulation de Walker.

A l'échelle du millénaire, nous avons pu montrer grâce à un enregistrement à haute résolution que des changements rapides dans l'intensité de la mousson d'hiver Est-Asiatique soufflant sur la mer de Sulu ont eu lieu au cours des derniers 200 000 ans. La dynamique de la mousson d'hiver du Pacifique ouest équatorial est caractérisée par des fréquences proches de celles enregistrées dans les carottes de glace du Groenland, et indique l'existence d'une téléconnexion entre ces deux zones. Un cycle de 1500 ans, comparable aux cycles de Bond marque cet enregistrement, et celui-ci n'est pas influencé par le volume des glaces pôlaires. Nous avons suggéré que cette absence de modulation indiquait que le facteur forçant de cette dynamique n'était pas lié à un processus de hautes latitudes. Le (ou les) facteur(s) forçant(s) ces cyclicités reste(nt) indéterminé(s). Une telle dynamique pourrait être soit liée à des instabilités internes du système couplé océan-atmosphère, soit à un forçage externe. Un grand nombre d'études indiquent désormais que la variabilité d'insolation solaire séculaire est corrélée à ces changements, et pourrait ainsi être à l'origine des changements rapides du climat.

Une boucle de rétroaction positive dans le système climatique doit nécessairement amplifier le faible facteur forçant. Nous avons pu montrer grâce à un enregistrement isotopique à haute résolution, que des événements de dégazages catastrophiques de gaz-hydrates de méthane ont eu lieu au cours du dernier stade glaciaire dans l'océan Pacifique ouest. Nous suggérons que les dégazages que nous avons observés ne sont pas cantonnés au Golfe Papou au cours du dernier stade glaciaire, mais que la plupart des marges sédimentaires de basses latitudes sont susceptibles de relarguer des quantités au moins aussi importantes de méthane. Ainsi, de faibles variations de température de surface pourraient entrainer une dissociation thermale des clathrates de méthane des basses latitudes, et ainsi entrainer un réchauffement climatique. Même si ce scénario reste encore spéculatif, le nombre d'évidences de relargages de clathrates de méthane ne cesse de croître. L'analyse à haute résolution

d'autres enregistrements marginaux permettra de valider cette hypothèse. La température du Pacifique ouest est fondamentale dans la dissociation des clathrates, mais aussi pour la circulation atmosphérique globale.

Nous nous sommes donc attachés à reconstruire les variations de température au cours du dernier cycle climatique dans le cœur de la zone d'eaux chaudes du Pacifique ouest. La création d'une nouvelle fonction de transfert pour le Pacifique ouest, nous a permis de mettre en évidence l'existence d'un biais existant dans précédentes fonctions de transfert publiées, biais lié aux très grandes abondances de *Neogloboquadrina dutertrei* du Pacifique Est. Nous associons cette anomalie à la structure trophique unique dans la bande intertropicale de cette zone riche en nitrates et paradoxalement pauvre en chlorophylle (High Nitrate Low Chlorophyll area – HNLC), qui est sans doute liée au manque de micronutriments dans la colonne d'eau comme le fer. Grâce à cette fonction de transfert, nous avons montré que les températures de surface de l'océan Pacifique Ouest équatorial au cours des derniers 185000 ans, n'étaient pas descendues en dessous de 27°C, et n'avaient pas non plus dépassé les 29.5°C. Les résultats de cette méthode sont en accord avec ceux obtenus avec la méthode des alcénones. Cette gamme de température implique que la zone de convection atmosphérique « profonde » située au Nord de la Papouasie Nouvelle Guinée est restée une caractéristique relativement constante du système climatique global. Les variations de température de cette zone ont suivi des cycles liés à la précession des équinoxes.

Ces cycles sont également les moteurs de la variation de la profondeur de la thermocline dans les océans Indo-Pacifique. La conjonction de deux facteurs influençant la production primaire et donc la profondeur de la thermocline dans l'Indo-Pacifique équatorial a été mise en évidence sur toute la bande équatoriale de cette zone. Le premier est un effet climatique global qui influence uniformément la profondeur de la thermocline sur toute la bande équatoriale des océans Indien et Pacifique. Cette influence du climat global est associé aux cycles de l'excentricité et de l'obliquité. Un deuxième effet, caractérisé par la cyclicité de 23000 ans de la précession, oppose les profondeurs de la thermocline du Pacifique ouest équatorial de celles de l'océan Indien occidental et de l'océan Pacifique oriental suivant un mécanisme proche de l'ENSO. Ce fonctionnement de l'ENSO en réponse à la précession confirme les résultats de modélisations couplées océan-atmosphère du Pacifique.

La compréhension de l'influence de l'ENSO sur le climat global passe par la reconstruction des gradients de densité de l'océan Pacifique de surface dans le passé. C'est dans cette optique que nous avons essayé d'utiliser la morphométrie du foraminifère planctonique *Orbulina universa* comme marqueur de paléo-densité. Malheureusement, la

calibration et le test de cette méthode a permis de mettre en évidence que la taille moyenne de ces organismes est le résultat conjoint de l'influence des nutriments et des paramètres physiques de la colonne d'eau, et ne peut donc pas fournir d'indications environnementales valables pour le Pacifique ouest équatorial. L'analyse de la porosité interne de ces organismes semble être un marqueur beaucoup plus sensible de la densité de l'eau de mer, et en fait donc un marqueur potentiel très utile. Cette porosité nous a également permis de distinguer l'existence de deux morphotypes d'*Orbulina universa* dans le Pacifique occidental. Nous avons suggéré que cette diversité morphologique peut-être symptomatique d'une diversité spécifique cryptique chez cette espèce.

Cette hypothèse de diversité cryptique permettrait d'expliquer le caractère ambivalent de l'espèce *N. dutertrei* dans le Pacifique oriental par rapport au reste de la bande intertropicale. Le seul moyen de tester cette hypothèse serait d'étudier en parallèle la morphologie et le génotype de cette « espèce » dans le Pacifique Est. Les études morphométriques étant longues et fastidieuses, nous avons présenté une étude préliminaire sur la reconnaissance automatique des foraminifères par réseaux neuronaux qui montre qu'il est possible d'automatiser les comptages et les triages de foraminifères. Cette méthode permettra de progresser vers une taxonomie quantitative des foraminifères dans laquelle la diversité cryptique des foraminifères pourra être intégrée, et d'améliorer ainsi les reconstructions paléocéanographiques.

Annexe

-

Charbons et Production Primaire en mer de Sulu

Continental Biomass Burning and Oceanic Primary Production Estimates in the Sulu Sea Over the Last 380 kyr and the East Asian Monsoon Dynamics

accepted to *Marine Geology*

Beaufort, L.[1]*, de Garidel-Thoron, T.[1], Linsley, B.[2], Oppo, D.[3] and Buchet, N.[1]

1 CEREGE, Aix-en-Provence, France
2 University at Albany, State University of New York, Albany, NY, USA
3 Woods Hole Oceanographic Insititution, Woods Hole, MA, USA

Abstract

Coccolithophorid assemblages and micro-charcoal content were analysed in the giant piston core MD97-2141 recovered in the Sulu Sea (Philippines). They are use to estimate respectively the dynamics of the oceanic Primary Production (PP) and biomass burning in that area. Primary production in the Sulu Sea intensifies during the East Asian Winter Monsoon (EAWM) and therefore PP constitutes a proxy for EAWM dynamics. Most of the precipitation in the Sulu Sea region occurs during the East Asian Summer Monsoon (EASM). Because the intensity of biomass burning is related to dryness of the surrounding area, the sedimentary micro-charcoal content can be used as an inverse proxy for EASM intensity. Our results show that the EAWM intensifies during glacial times in agreement with previous studies. Precessional forcing appears to act directly on EAWN because of the early response of PP in that frequency band. The micro-charcoal record exhibits complex dynamics, which we attribute to the competing influence of long term El Niño Southern Oscillation (ENSO)- like forcing coupled with the glacial/interglacial cycle on EASM. These influences create an unusual frequency spectra with power around 30-kyr and 19-kyr attributed to the non-linear response to 100-kyr cycle (glacial) and 23-kyr (ENSO) cycle. A factor of 2 increase in the amplitude of the micro-charcoal variability is observed between 51 and 10-kyr BP. That could correspond to *Homo sapiens* biomass burning in the style of the fire-stick farming of the Australian Aborigines who occupied the vicinity of the Sulu area during that time. We also find common dynamics of EASM and EAWM on millennial time scales with a periodicity near 5.8-kyr.

Introduction

The monsoon climatic system is characterised by a seasonal reversal of the wind direction due to differential seasonal heating of the continents and oceans. In Asia there are two major monsoon systems: the Indian Monsoon and the East Asian Monsoon. Monsoon winds come from the north during boreal winter and from the south during boreal summer. The relationship existing between long-term (orbital scale) variability of these monsoons systems and the seasons has been difficult

to determine. The long term dynamics of the Indian Summer Monsoon (ISM) is well established from sediments tracers in the Arabian Sea (e.g. (Clemens and Prell, 1990)), where it produces upwelling that strongly imprints the quality of the sediments (Anderson and Prell, 1993). It appears that Arabian southern ISM decreases during glacial periods and is significantly influenced by the direct insolation forcing of precession (Prell and Kutzbach, 1992). The dynamics of the Indian Winter Monsoon is more difficult to resolve using oceanic sediments because in most places the southern monsoon shadows the winter monsoon imprints. However, in the Bay of Bengal (Duplessy, 1982) and (Sarkar et al., 1990) shown that winter Monsoon was stronger during the last glacial period. Chinese loess-paleosol sequences also provide good records of both summer and winter East Asian Monsoon dynamics (An et al., 1990; Liu, 1985). They indicate that the intensity of two monsoon seasons has varied inversely (Xio et al., 1999) similar to the Indian Monsoon. The relation between summer and winter monsoon is not yet known at lower tropical latitudes in East Asia an area where EL Niño Southern Oscillation (ENSO) may complicate the high latitude dynamics shown in the Loess sequence (Porter and An, 1995). In order to study the dynamics of both phases of the monsoon it is necessary to develop proxy-records of the two monsoon seasons from the same core. The Sulu Sea is well suited for such a study because of its unique geography (enclosed basin away from major oceanic currents) and because both phases of the monsoon have distinct meteorological effects in the basin.

The Sulu Sea (Figure 1) is located between the Asian continent and the “Western Pacific Warm Pool”(WPWP) where annual SST is above 29°C (Yan et al., 1992). The climate of the Sulu Sea is strongly influenced by the monsoons. The East Asian monsoon results from the different potential heating between the WPWP and the Asian continent. During the boreal winter, the main heating source is located in the ocean. The latent heat release associated with intense convective precipitation fuels meridional circulation. Tropical convection in the western equatorial Pacific is connected to the descending branch over the Siberian region, forming a strong local Hadley cell in the East Asian region (Zhang et al., 1997). The East Asian winter monsoon winds in the Sulu Sea result from the merging of the Northerly East Asian monsoon with the Pacific trades winds over the South China Sea (McGregor and Nieuwolt, 1998).

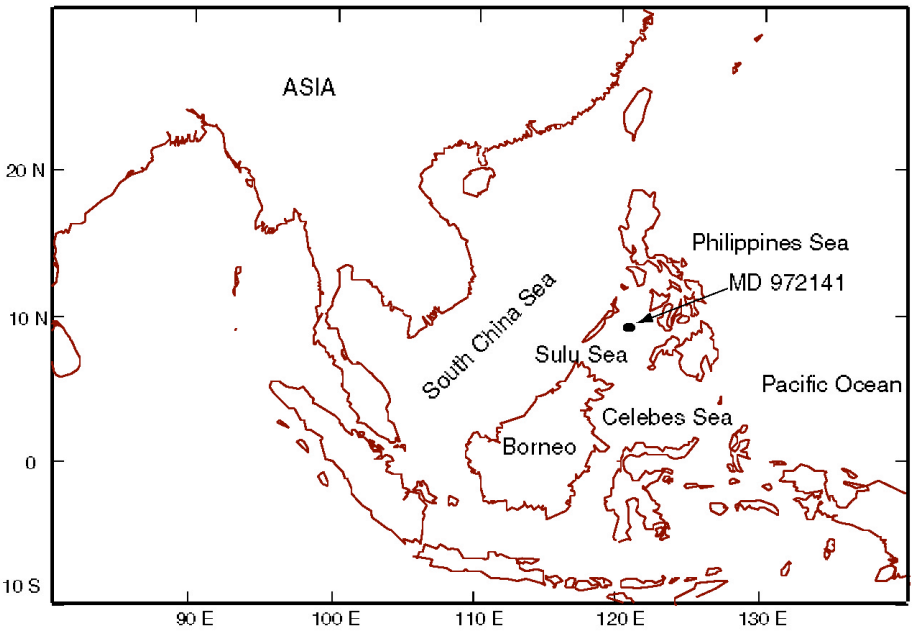

Figure 1 : Map indicating where core MD97-2141 was retrieved.

East Asian winter monsoon bursts during January to March (Figure 2) can induce blooms of coccolithophorids in the region (Wiesner et al., 1996). Primary Production (PP) rises correlatively with wind stress strengthening, because of the stronger mixing of the upper ocean (Figure 2) (Nair et al., 1989). Thus coccolith assemblages in the Sulu Sea record information on both paleoproductivity changes and also East Asian winter monsoon variations (de Garidel-Thoron et al., 2001). The winter monsoon corresponds to the dry season in the Sulu Sea where as the summer monsoon brings a lot of moisture to the Eastern Philippine Seas (Figure 2). Originating from the subtropical high region, the air incorporates moisture as it moves west above the WPWP and provokes rain when it arrives in the region of the Philippines (McGregor and Nieuwolt, 1998). Today, the summer monsoon humidity dynamics is strongly modulated by ENSO. For example, during ENSO events such as 1997/1998, the strength of the summer monsoon is reduced and rains are extremely weak. During these events, the surrounding islands of the Sulu Sea experience drought and intense fires due to reduced summer monsoon activity. Small charcoal particles from these fires (microscopic charcoal) are transported by wind and eventually fall into the sea. Down core records of microscopic charcoal may serve as a proxy for dryness and therefore for summer monsoon intensity.

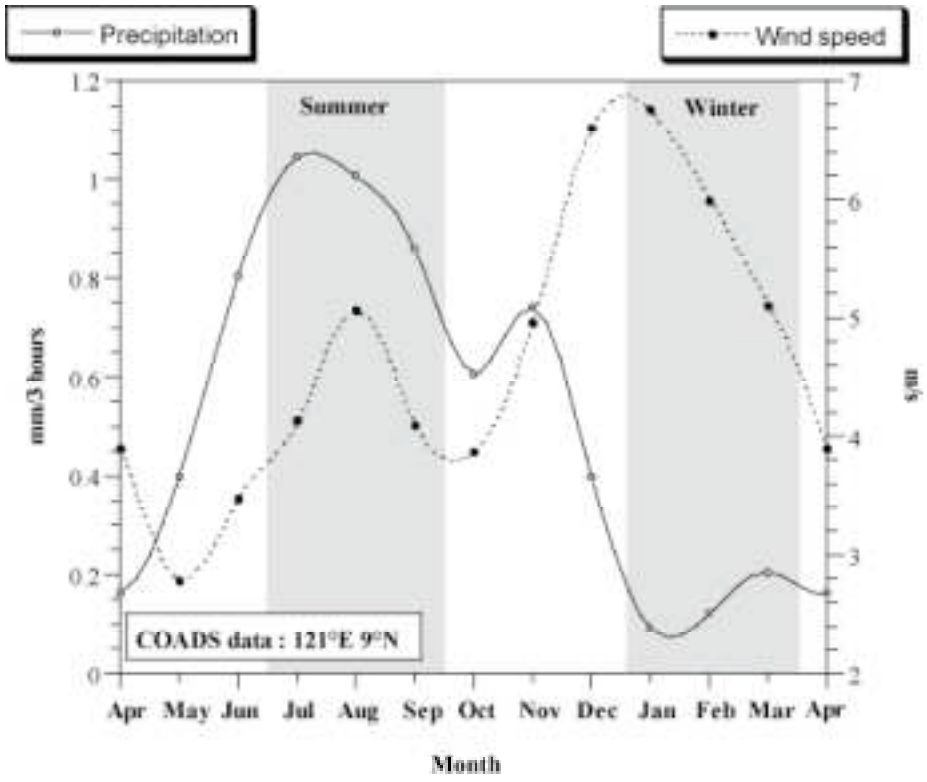

Figure 2: Monthly averaged of precipitation (solid line) and wind speed (dotted line) at the core location taken from COADS data-base.

Material

A 36 meter giant piston-core (IMAGES MD97-2141) (08°47'N-121°17'E - 3633m depth) was retrieved during the IPHIS-IMAGES III cruise of the R/V Marion Dufresne in May 1997 (Figure 1). The cores position is located in the vicinity of the ODP Site 769 (Linsley, 1996). The core is located on the Cagayan ridge which protects the site from downslope processes and is above the present lysocline depth (about 3800 m) allowing for good preservation of carbonates (Linsley et al., 1985; Miao et al., 1994). The sediments are composed predominantly of well-preserved nannofossil-foraminifera oozes and do not contain significant amount of detrital mineral.

Methods

Microscopic charcoal

About 2 grams of bulk sediment was sampled every 10 cm down the core. Carbonate was removed by adding 50 ml of 10N HCl. The residue was rinsed with de-ionised water and 50 ml of nitric acid was added followed by and addition rinsing. The remaining sediment was added to a beaker containing 100 ml of oxygen peroxide and soaked for 24 hours. This procedure dissolves pyrite and other hydroxides and opaque minerals such as hematite and leaves charcoal, which are the only dark particles left in the remaining sediment. The sediment was rinsed and filtered onto a cellulose membrane of .47 μm nominal porosity and 45mm in diameter. A portion of the membrane was mounted onto a slide with Canadian balsam. The slides were scanned with an

automated Leica DMRBE microscope and 100 view fields of 0.04 mm^2 were grabbed with a standard 756 X 582 digitising camera. With the light tuning of the microscope, all charcoal appeared darker than a given threshold. The number of pixels darker (darker) than a given grey level (light intensity) threshold were counted in each digitised image. The results are given as the total surface area (in mm2) occupied by dark particles (microscopic charcoal) per gram of sediment. This automated optical method provides reproducible results.

A limit of that method is that it is not possible to be certain that some opaque minerals were measured. For most of the peaks, we visually checked that they did not correspond to increase of non-dissolved pyrite but to higher concentrations of charcoals. In another oceanic core this method had been satisfactory compared with two methods for measuring the black carbon content in sediment based on chemistry (Thevenon et al., in prep.). An other limit of that method is interpretative and corresponds to the fact that some charcoals could had arrive by river discharged and not correspond only to an eolian input. Because the Western Pacific Marginal seas experience strong sea level variations, it is possible that fluvial detrital material varied considerably and that the record would reflect sedimentation variations rather than climatic dynamics. But (1) the core has been retrieved from a ridge and therefore protected from fluvial transport, (2) the Sulu Sea has relative steep margin and did not varied extremely in size during glacial-interglacial cycles, (3) the core consists of an homogeneous hemipelgic mud with no visible down core variations and (4) as we will see the micro-charcoal record does not follow a clear glacial-interglacial cycles.

Coccoliths

Counting :

The coccolith data and results have been published recently (de Garidel-Thoron et al., 2001). The core was sampled every 2 cm in the upper 6 meters allowing for a resolution of about 70-yrs and every 3-4 cm in the lower 30 m for a resolution of about 200-500 yrs. A smear slide was prepared for each sample, and at least 300 coccoliths were counted for each slide (mean 357 coccoliths) on a Zeiss Axioscop at a 1000 x resolution. Percentages of *Florisphaera profunda* (Fp) were computed using the following equation:

$$\%Fp = 100*\text{number Fp} / \text{total coccoliths}.$$

The 95% confidence interval for %Fp varies between ±2% and ± 6% depending on the percentage of Fp (Mosimann, 1965).

Primary Production Transfer function

Most of the coccolithophorid species live in near surface waters where light for photosynthesis is abundant. Phytoplanktons also require nutrients, and thus thrive where a shallow thermocline brings subsurface nutrients into the upper euphotic zone. In contrast, the coccolithophore *Florisphaera profunda* lives in the deep-photic zone where nutrients are relatively abundant although light is rare (Okada and Honjo, 1973). Where the thermocline is deep total primary productivity is low, and the dominant coccolith species in fossil assemblages is *F. profunda* (Molfino and McIntyre, 1990). As productivity increases, the relative abundance of F. profunda decreases. Thus, estimates of primary productivity (PP) are made from counts of the

relative abundance of F. profunda (%Fp) converted to PP using the following equation %Fp by PP = 316 * log (%Fp + 3) (Beaufort and Heussner, 1999; Beaufort et al., 1997). This equation derives from the fit of Indian Ocean core-top coccolith counts with modern productivity based on satellite chlorophyll (Antoine et al., 1996). The correlation between the estimated and observed productivity in the calibration data set is r = 0.94 and the standard deviation of the residuals is ±26 gC m-2 year-1. This transfer function has been shown to be reliable in Equatorial Atlantic (Henriksson, 2000) and Pacific Ocean (Beaufort, unpublished.).

Chronostratigraphy

The age model of the core includes twenty eight AMS ^{14}C ages (converted to calendar ages) on *Globigerinoides ruber* and *G. sacculifer*. Older ages were selected by of the planktonic foraminifera $\delta^{18}O$ curve (on *Globigerinoides ruber* test) to the SPECMAP stack (Imbrie et al., 1984). The age model is presented in further detail elsewhere (de Garidel-Thoron et al., 2001). Two ninth order polynomial regressions were used from the core-top top to 400 cm and from 440 to 920 cm on the ^{14}C ages and SPECMAP tie-points to smooth the sedimentation rate for the last 60 kyr. This smoothing is indispensable for the spectral analyses to avoid spurious peaks linked with sedimentation rates changes.

The average sedimentation rate is about 10.5 cm/kyr, with a maximum during glacial stage 2 of 34 cm/kyr. For example, the sedimentation rate during the stage 3 is about 30 cm/kyr that allows a 70 years resolution (2 cm sampling). A hiatus occurs between 30 and 22 kyr BP.

Time series analysis:

To extract the significant periodicities contained in the PP signal, we performed spectral analysis using Blackman-Tukey and Cross-Blackman-Tuckey provided in the package Analyseries (Paillard et al., 1996).

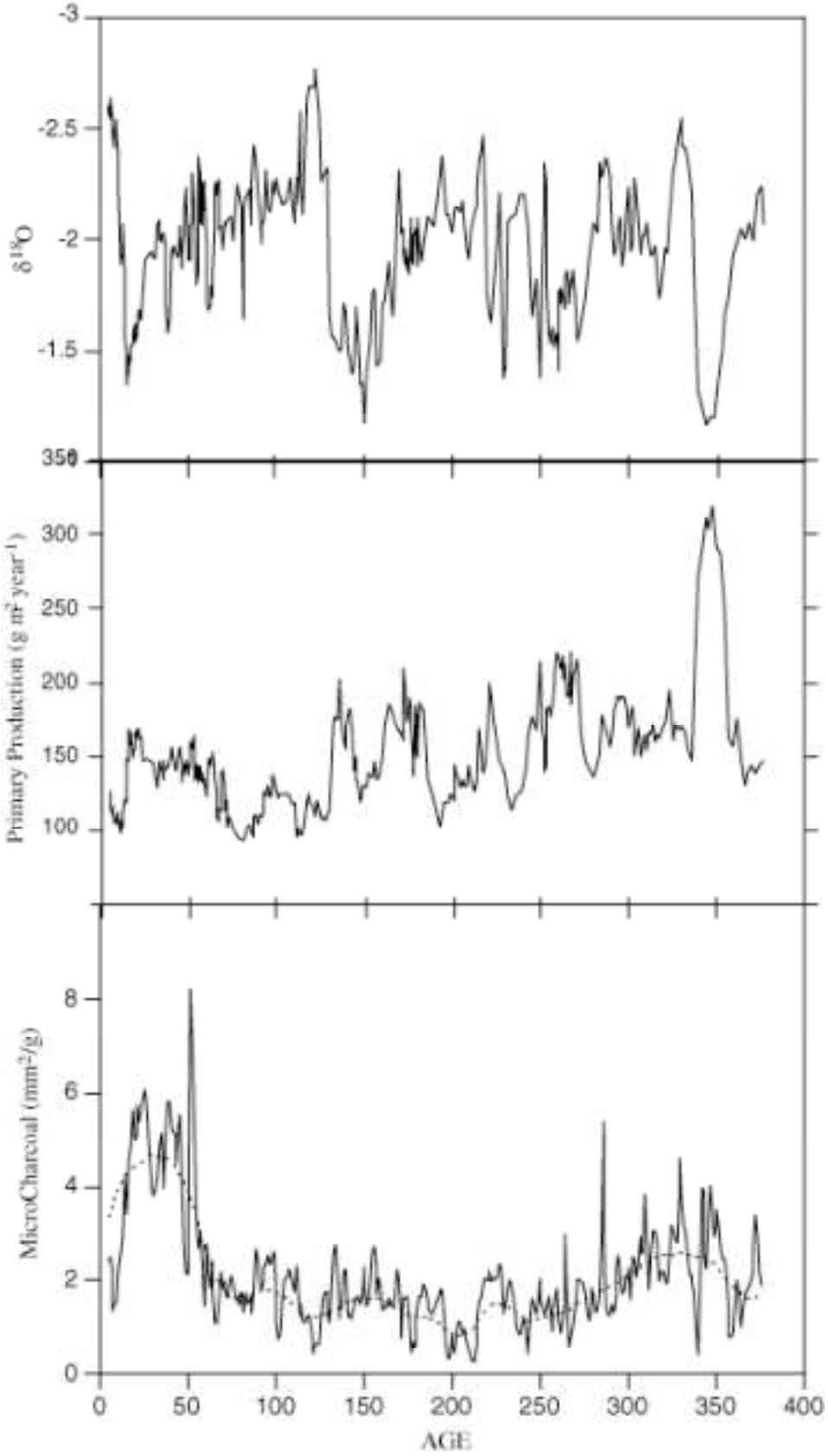

Figure 3 : Down core data : from top to bottom $\delta^{18}O$, Primary Production and micro-charcoal content. The dotted line in that latter graph correspond to the long trend of the series revealed by the first component of a Singular Spectrum Analyses (Vautard and Ghill, 1989)).

Results :

The present annual PP in the Sulu Sea is 148 $gC.m^{-2}.a^{-1}$ (Antoine et al., 1996) which is close to the average reconstructed PP over the last 380 kyr of 149 $gC.m^{-2}.a^{-1}$. The PP* oscillates during the last 380 kyr between 80 and 330 $gC.m^{-2}.a^{-1}$ (Figure 3). On glacial-interglacial time-scales, PP increases during glacial periods and decreases during interglacials (Figure 3). PP is moderately correlated (r^2=0.49) with the ice-volume curve (SPECMAP stack of (Imbrie et al., 1984)). This is shown by spectral analyses of the paleoproductivity record which contains peaks corresponding to the main orbital periods of Milankovitch theory (i.e. 1/100 kyr, 1/41 kyr and ~1/20 kyr) and confirmed by cross-spectral analyses between $\delta^{18}O$ and PP (Figure 4). The precession cycles are not well marked in the oldest part of the record (Figure 4B), certainly because of the unusual strength of Marine Isotope Stage (MIS) 10. Cross-spectral analyses indicate that PP leads $\delta^{18}O$ by 25° in the precession frequency band and lags by 39° in obliquity frequency band.

The absolute abundance of microscopic charcoals varies between 0.1 and 11 mm2/g. Flux of charcoal were also calculated. Flux and absolute abundance are strongly related. We discuss only absolute abundance, because flux data may be biased by discrete chronology and possible core disturbances that occurred during the piston-coring process (Thouveny et al., 2000). Micro-charcoals abundance increases during glacial periods, but does not correlate with $\delta^{18}O$ or PP. Only the long-term trend (see dotted line in Figure 3) shows recurrent increases during glacial times. There is an important increase starting at about 60-kyr BP and marked by the highest abundance of charcoal at 51-kyr BP. After this event the charcoal abundance remains high in comparison with older sediment. Before 60-kyr the average charcoal abundance is 1.75 mm^2/g and after 60-kyr the average is 3.96 mm^2/g indicating a doubling of the charcoal. Charcoal abundance decreased significantly during the last deglaciation, paralleling the $\delta^{18}O$ record. Between 380 and 300-kyr the charcoal abundance is relatively high with an average of 2.45 mm2/g. This long trend partly represents glacial/interglacial cycle, partly represent a non-cyclic trend. The main frequencies are a strong 29-kyr and a 19-kyr^{-1}, the latter related to precession (note the small 23-kyr^{-1} peak) (Figure 5).

* Data are accessible at http://www.cerege.fr and at ftp://ftp.noaa.ngdc.gov/paleo/

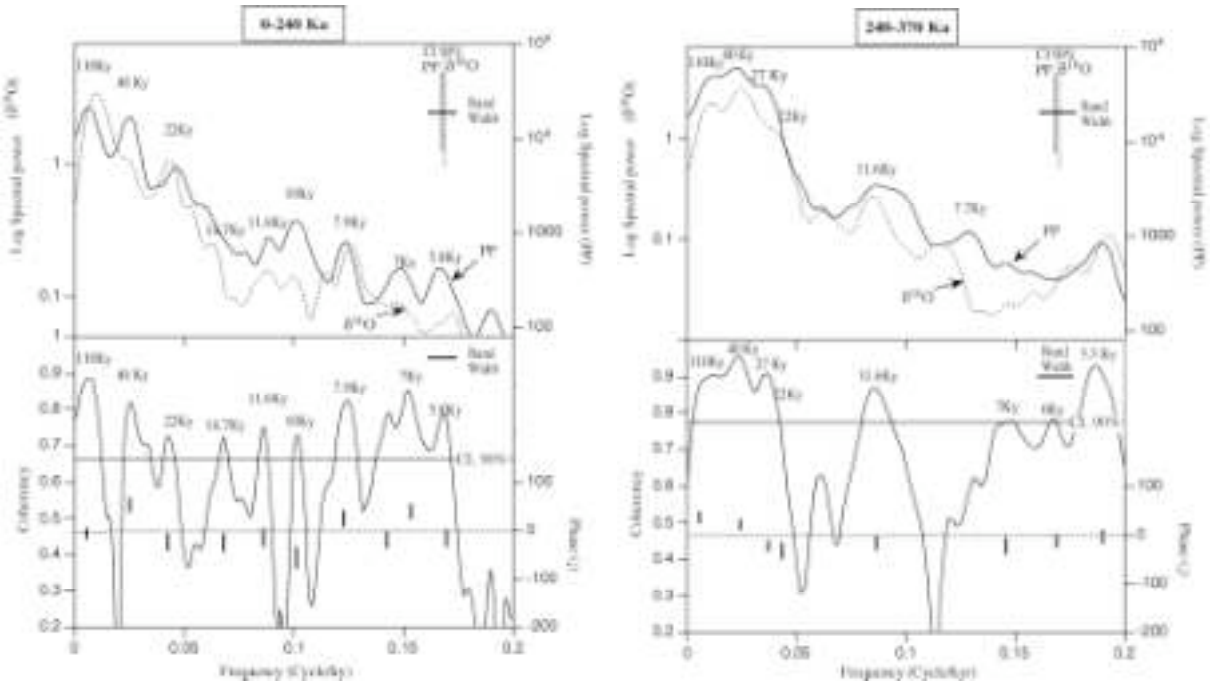

Figure 4 : Cross spectrum analyses of $\delta^{18}O$ and Primary Production form core MD97-2141. In the upper-panels are represented the Blackman-Tuckey of the records (dotted line : $\delta^{18}O$ and solid line PP), and in lower-panels are shown the coherency (line) and the phase (small vertical bars) when coherency is above 90% confidence limit. The length of these bars represents the 90% confidence interval for the phase. Analyses where performed between 0 and 240,000 years (A) and between 240,000 and 370,000 year (B).

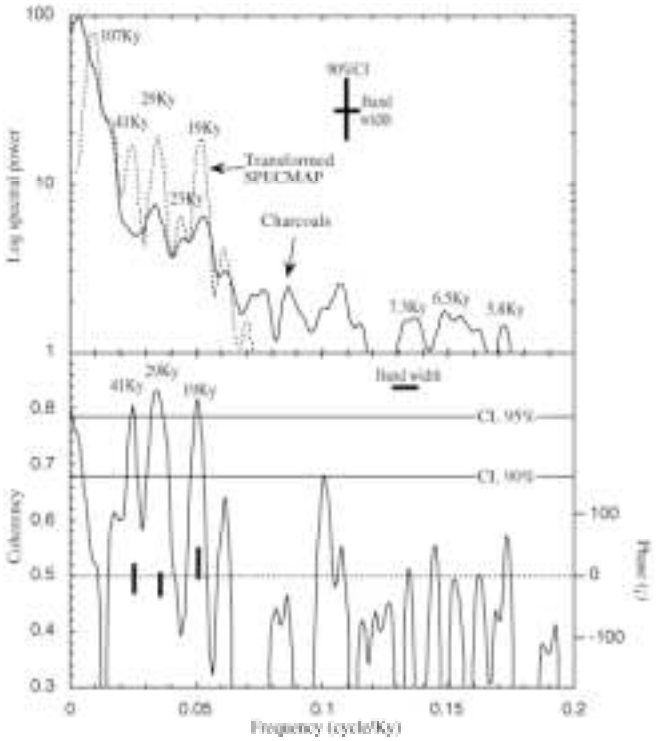

Figure 5 : Cross spectrum analyses of micro-charcoal series from core MD97-2141 and SPECMAP stack series transformed in a way which shift the phase of precession by 120° once by precession cycle (the series is shown in figure 6). . In the upper-panels are represented the Blackman-Tuckey of the records (dotted line : transformed SPECMAP stack and solid line micro-charcoal record), and in lower-panels are shown the coherency (line) and the phase (small vertical bars) when coherency is above 90% confidence limit. The length of these bars represents the 90% confidence interval for the phase.

Discussion:

Winter Monsoon Dynamics:

The PP is believed to respond to variations in winter monsoon dynamics (de Garidel-Thoron et al., 2001). This dynamic is clearly linked with the glacial-interglacial cycles and therefore implies some type of teleconnection between low and high latitudes. The strengthening and weakening of the Siberian high level pressure cell is often suggested to explain such a relationship between the North Atlantic and EAWM, a relationship that has been found also in Chinese loess records (Porter, 2001; Porter and An, 1995) and in marine records from South China Sea (Wang et al., 1999a; Wang et al., 1999b). A strengthening of the Siberian high in the cold northern continent during glacial times contrasted with the relatively warm tropical Indo-Pacific Ocean, reinforcing the winter monsoon (Wang et al., 1999a).

Changes in PP lead the $\delta^{18}O$ changes by 1600 yr in the precessional frequency band. This lead of PP is a common feature of the equatorial indo-pacific record (Beaufort et al., 2001). The opposition sign of PP records from the Western Pacific Warm Pool (WPWP) and the Eastern Equatorial Pacific and the Indian Ocean indicates that the thermocline is regularly rocking along the equator following insolation variations. That phenomenon corresponds to an ENSO-like mechanism equivalent to the present 2-6 year ENSO cycle but acting on a much longer time scale. Modelling results (Clement et al., 1999) suggest that precession-related variations of low latitude insolation produce cyclic variation of Walker Circulation strength and ENSO. ENSO and East Asian Winter Monsoon are linked. For example, (Wang et al., 2000) established a clear teleconnection between warm (cold) events in the eastern Pacific and the weak (strong) East Asian winter Monsoon. Strong winter monsoons are the response to colder than normal temperature in the Siberian highs and / or warmer than normal tropical SST. By analogy with the modern climate, long term variations of the Western Pacific Warm Pool (WPWP) SST related to the ENSO-like cycles may have had a strong influence on the East Asian monsoon.. In particular the weakening of the high convection cells located above the oceanic continent and the WPWP during El Niño events may have diminished the strength of the following winter monsoon. Lea et al., (2000) shown that WPWP SST variations precedes those of $\delta^{18}O$ by 3000 years. The lead of precession El Niño-like variability over global climate would explain the lead of winter monsoon on precession time scales. The lead of El Niño like variability vanishing at longer time scale (Beaufort et al., 2001), winter monsoon obliquity and eccentricity variability are in phase or lag global climate.

Biomass burning

Human impact: The micro-charcoal content is interpreted as related to the aridity of the surrounding terrestrial area of the Sulu Sea, but the long term variations show a peculiar trend with strong concentration of charcoal in MIS 2 and 3 between 51 and 13 year BP. These high concentrations are not reached in the other glacial periods (MIS 6, 8 and 10) and at the onset of the last glacial during MIS 4. Higher values in the last glacial than in the penultimate glacial are difficult to explain. A similar case is found in Australia and has been explained by intense anthropogenic fires (Kershaw, 1986), although other (e.g. direct) evidence has yet to be found

(Moss and Kershaw, 2000). The earliest *Homo sapiens* occupation in the Philippine Archipelago has been estimated at around 50,000 year BP (Fox, 1970) in the Tabon caves (in Palawan Island located north of the Sulu Sea) that yield artefacts. These artefacts as well as other found in Borneo (Niah in Sarawak) show little sign of any marked stone tool "evolution" until nearly 10,000 year BP (Harrisson, 1976). Early Holocene human skeletons from Malaysia, Tabon and Niah indicate strong morphological affinity with the Australian Aborigines (Matsumura and Zuraina, 1999). By 50000 yr Australian aborigines reached southwestern Australia (Turney et al., 2001) and they were also on the lands around the Sulu Sea until the beginning of the Holocene. These dates correspond surprisingly well with the high charcoal content in core MD97-2141 (51,000 to 12,000 years). At that time human did not practice agriculture, but they could have used burning for hunting and clearing the vegetation (fire-stick farming) as the Australian Aborigines did until the end of the XVIII century (Nicholson, 1981). The same type of culture may have existed around the Sulu Sea. The large and prominent peak of Charcoal at 51-kyr could mark the arrival of *Homo sapiens* around the Sulu Sea. Although the charcoal content in MD97-2141 increased by a factor of 2 after this event, the higher frequency variability is similar before and after 51-kyr. For instance the relatively low Holocene charcoal content is more diagnostic of wetter conditions during interglacials than on change of human habits. The "natural" summer monsoon dynamics is therefore the major mechanism responsible in the variability of biomass burning in that region.

Summer monsoon: Because most of the precipitation falls during the summer monsoon (Figure 2), micro-charcoal concentration is interpreted as an inverse summer monsoon proxy. The record indicates that summer monsoon was significantly reduced during glacial time. Pollen evidence suggests increased aridity in Australia and Indonesia (van der Kaars and Dam, 1995; van der Kaars et al., 2001; van der Kaars et al., 2000). A glacial weakening of the summer Indian monsoon has been also extensively described (Cullen, 1981; Duplessy, 1982; Gasse and Van Campo, 1994; Kutzbach, 1981; Prell and Curry, 1981; Prell and Kutzbach, 1992). Chinese loess also indicates lower summer monsoon in North East Asia (Porter, 2001; Xio et al., 1999). It appears that glacial weakening is a common feature of the Indian and Asian branch of the summer monsoon. However, our micro-charcoal data show that the link between summer monsoon intensity and glacial cycles is weak in the Sulu Sea, in comparison for example with the winter monsoon that exhibits a strong relationship with glacial cycles.

ENSO also strongly influences the intensity of the summer monsoon rain in that area: dry weather conditions prevail during El Niño events. On Milankovitch time scale model and data indicate that El Niño are more frequent during interglacial times (Andreasen and Ravelo, 1997; Beaufort et al., 2001; Bush and Philander, 1998; Fedorov and Philander, 2000). The strength of summer monsoon related to glacial cycles (Prell and Curry, 1981) and the long-term dynamics of ENSO (Fedorov and Philander, 2000) have an opposite influence on summer rains on glacial-interglacial time scale. That competing influence provokes a non-linearity between precession (insolation) and eccentricity (glacial /interglacial variations) expressed by the strong 30-kyr cycle revealed by the spectral analyses of the charcoal records.

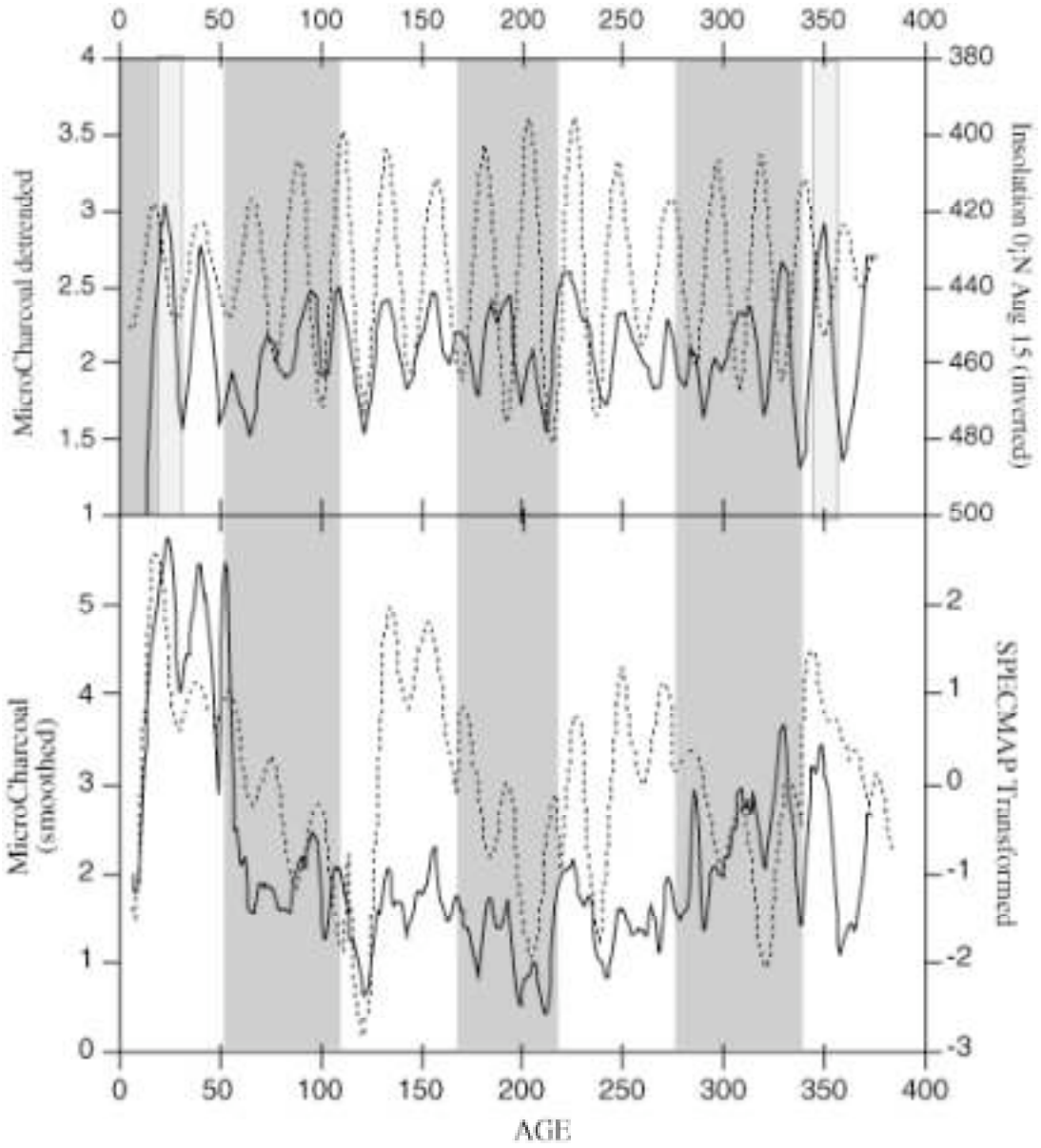

Figure 6 : **Upper panel** : Comparison of the micro-charcoal records (solid line), detrended by subtracting the long term variation represented in Figure 1 from the raw data , and insolation variation received at the Equator in August 15 (reverted scale). The two records are out of phase in the shaded parts (interglacials) of the record and in phase in the unshaded part (glacials) of the record. **Lower panel** : .Comparison of a smoothed (3 point running average) record of micro-charcoals and the SPECMAP stack transformed in the way that the its precession variations are inverted for the shaded part (interglacials) of the record. The secondary peaks of the two records are in phase.

A simple way to explain that non-linearity is to separate the 100-ky that we will call arbitrarily "glacial cycle" from the 23-kyr called a "precession cycle". In a glacial cycle, the summer monsoon strengthens (Prell and Curry, 1981) and El Niño is stronger (and/or more frequent) during warm phase (Fedorov and Philander, 2000). In a precession cycle, $\delta^{18}O$ warm phases lead strong monsoon by about 30° (Clemens et al., 1991) and strong El Niño by 150° (Beaufort et al., 1999; Beaufort et al., 2001; Beaufort et al., 1997). During the cold period of a glacial cycle, weak monsoons limit the amount of rainfalls in the Sulu Sea. Monsoon is therefore the "limiting factor". Changes in the summer monsoon induced by local insolation should increase the amount of rain.

In consequence, precipitation follows the phase of the monsoon of precession cycles during the cold period of a glacial cycle. During the warm period of a glacial cycle El Niño are more frequent and stronger and therefore ENSO constitutes the limiting factor for rainfall. During these periods changes in precipitation are following the ENSO phase of precession. Therefore, the phase in the precession band will shift once by 120° during a glacial cycle. This is what is shown in the upper panel of Figure 6, where the detrended charcoal record appears to vary between in and out of phase with low latitude insolation. Therefore, this suggests a phase modulation of precession by eccentricity. That induces a shift of energy from the 23 kyr period to periods of 30 and 19-kyr (1/100-1/23 = 1/29.9 and 1/100 +1/23 = 1/18.7). These frequencies are those observed in the charcoal spectra (Figure 5). To illustrate this hypothesis, in the time domain, we inverted the precession signal of the SPECMAP record for each interglacial period as in (Beaufort and Heussner, 2001) (Figure 6 lower panel). The relation between the smoothed charcoal record and this new series (SPECMAPtransformed) show a good phasing between the peaks. The cross-spectral analysis between the charcoal record and the transformed SPECMAP stack indicates significant coherency at periods near 30 and 19-kyr.

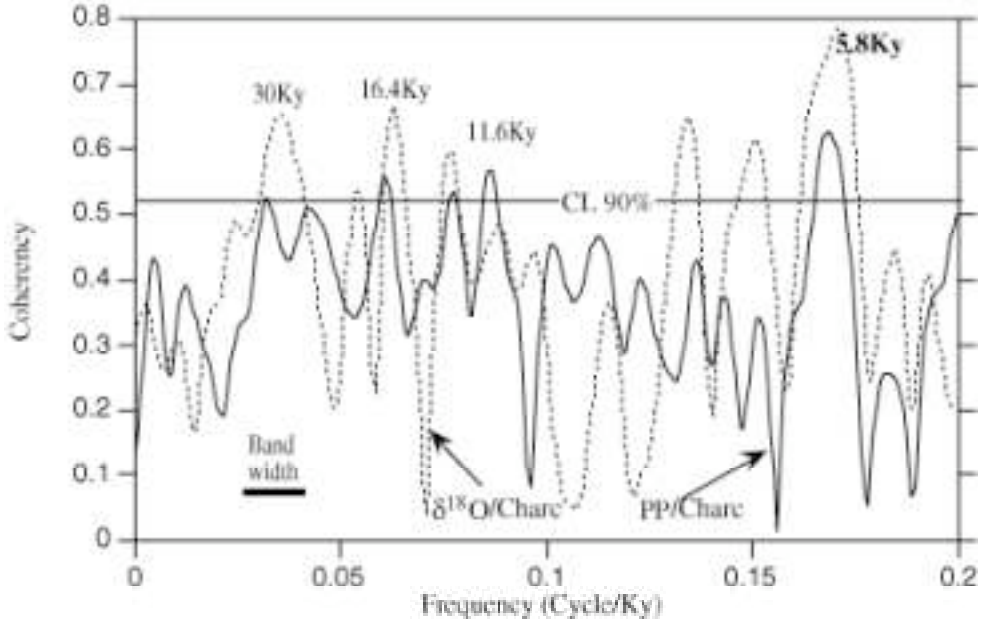

Figure 7 : Coherencies from two cross-spectral analysis computed between micro-charcoal and d18O (dotted line) and Primary Production (solid line) records from core MD97-2141.

On Milankovitch time scales, the charcoal record expresses the complex long-term dynamics of precipitation around the Sulu that are under the joint influence of the zonal dynamics of the ENSO and the meridional dynamics of the East Asian Summer, with the two mechanisms being out of phase.

Relation between winter and summer monsoons:

The micro-charcoal and Primary Production series have very little in common on long time scale. However on shorter time scale (suborbital) cross-spectral analyses reveal significant coherency between these records, in particular around 5.8-kyr (Figure 7). Although this pseudo-cycle is not stable in period and phase, it is always present. But it is not possible to discuss the charcoal

millennial dynamics without over interpreting the data, because of the low resolution of the charcoal record (10cm or about 1000 year –1000 yrs good enough to discuss 5.8!). The millennial PP variation from this core are discussed in detail in (de Garidel-Thoron et al., 2001). The 5.8-kyr period is interpreted as corresponding to the rapid response of winter monsoon to the northern ice sheet dynamics because these cycles increase during ice age and that they are of the same frequencies that those of Heinrich events.

Conclusions

Our results show that summer and winter monsoons in the Sulu Sea vary in opposition on most time scales because they have an inverse response to many climatic parameters.

1- Summer (winter) monsoon decreases (increase) during glacial time.
2- Present day climate shows that ENSO events positively influence winter monsoon winds (Wang et al., 2000) whereas decrease summer precipitation (e.g. 1997 ENSO event). Precession-induced long term ENSO variability (Clement et al., 1999) explains the opposite pattern of summer and winter monsoon dynamics in precession time scale and also the complex pattern of variability of the summer monsoon.
3- At millennial time scales, an opposition between the two monsoon dynamics is also observed at a pseudo-frequency of about 5.8-kyr^{-1}.

The two records do not appear completely opposite each other because winter monsoon dynamics is essentially driven by glacial/interglacial dynamics whereas the summer monsoon is more strongly influenced by ENSO cycles. The summer monsoon presents a strong non-linearity that dominates over glacial-interglacial cycles.

Homo sapiens might be responsible for the doubling of charcoal abundance after 51,000 years. Local biomass burning increased without changing the natural dynamics of fire frequencies that are under the direct influence of summer monsoon dynamics.

Acknowledgements :

The support of French MENRT, TAAF, CNRS/INSU and IFRTP to the Marion-Dufresne and the IMAGES Program was necessary to perform this work. Financial support from CNRS ECLIPSE program to L.B is acknowledged.

References

An, Z. et al., 1990. The long-term paleomosoon variation recorded by the loess-paleosol sequence in Central China. *Quatern. Internat.*, 7/8: 91-95.

Anderson, D.M. and Prell, W.L., 1993. A 300 kyr record of upwelling off Oman during the late Quaternary : evidence of the Asian Southwest monsoon. *Paleoceanogr.,* 8(2): 193-208.

Andreasen, D.J. and Ravelo, A.C., 1997. Tropical Pacific Ocean thermocline depth reconstructions for the last glacial maximum. *Paleoceanogr.*, 12: 395-413.

Antoine, D., André, J.-M. and Morel, A., 1996. Oceanic primary production 2. Estimation at global scale from satellite (coastal zone color scanner) chlorophyll. *Global Biogeochemical Cycles*, 10(1): 57-69.

Beaufort, L., Bassinot, F.C. and Vincent, E., 1999. Primary production response to orbitally induced variations of the Southern Oscillation in the Equatorial Indian Ocean. In: F. Abrantes and A.C. Mix (Editors), *Reconstructing Ocean History : a window into the future*. Kluwer Academic/Plenum Publisher, New York, pp. 245-272.

Beaufort, L., de Garidel Thoron , T., Mix, A.C. and Pisias, N.G., 2001. ENSO-like forcing on Oceanic Primary Production during the late Pleistocene. Science, 293(5539): 2440-2444.

Beaufort, L. et al., 1997. Insolation cycles as a major control of the Equatorial Indian Ocean primary production. *Science*, 278: 1451-1454.

Bush, A.B.G. and Philander, S.G.H., 1998. The role of ocean-atmosphere interactions in Tropical cooling during the Last Galcial Maximum. *Science*, 279: 1341-1344.

Clemens, S., Prell, W.L., Murray, D., Shimmield, G. and Weedon, G., 1991. Forcing mechanisms of the Indian Ocean monsoon. *Nature,* 353: 720-725.

Clemens, S.C. and Prell, W.L., 1990. Late Pleistocene variability of arabian sea summer monsoon winds and continental aridity : eolian records from the lithogenic component of deep-sea sediments. *Paleoceanogr.,* 5(2): 109-145.

Clement, A.C., Seager, R. and Cane, M.A., 1999. Orbital controls on the El Nino/Southern Osciallation and the tropical climate. *Paleoceanogr.,* 14(4): 441-456.

Cullen, J.L., 1981. Microfossil evidence for changing salintiy patterns in the Bay of Bengal over the last 20 000 years. *Palaeogeogr. Palaeoclim. Palaeocol.*, 35: 315-356.

de Garidel-Thoron, T., Beaufort, L., Linsley, B.K. and Dannenmann, S., 2001. Millennial-scale dynamics of the East Asian winter monsoon during the last 200,000 years. *Paleoceanogr.*, 16: 1-12.

Duplessy, J.C., 1982. Glacial to interglacial contrasts in the northern Indian Ocean. *Nature*, 295: 494-498.

Fedorov, A.V. and Philander, S.G., 2000. Is El Niño Changing. *Science*, 288: 1997-2001.

Fox, R.B., 1970. *The Tabon caves: archaeological explorations and excavations Palawan Island*, Monograph No. 1, National Museum, Manila.

Gasse, F. and Van Campo, E., 1994. Abrupt post-glacial climate events in West Asia and North Africa monsoon domains. *Earth Planet. Sci. Let.,* 126: 435-456.

Harrisson, T., 1976. The upper Palaeolithic in Malaysia (Malaya and Borneo) and adjacent areas: Gateways to the Pacific ? In: C. Serizawa (Editor), *Le premier peuplement de l'archipel Nippon et des Iles du Pacific: chronologie, paléogéographie, industries*. Union Internationale des Sciences préhistoriques et protohistoriques, Nice, pp. 12-27.

Henriksson, A.S., 2000. Coccolithophore response to oceanographic changes in the equatorial Atlantic during the last 200,000 years. *Palaeogeogr. Palaeclimatol. Palaeoecol.*, 156: 161-173.

Imbrie, J. et al., 1984. The orbital theory of Pleistocene climate : Support from a revised chronology of the marine d18O record In: A.L. Berger, J. Imbrie, J.D. Hays, G. Kulka and

B. Saltzman (Editors*), Milankovitch and Climate, Part 1*. *D*. Reidel, Dordrecht, pp. 269-305.

Kershaw, A.P., 1986. Climatic change and Aboriginal burning in north-east Australia during the last two glacial/interglacial cycles. *Nature*, 322: 47-49.

Kutzbach, J.E., 1981. Monsoon climate of the Early Holocene: climate experiment with the Earth's Orbital parameters for 9000 years ago. *Science,* 214: 59-61.

Lea, D.W., Pak, D.K. and Spero, H.J., 2000. Climate impact of late Quaternary Equatorial Pacific Sea Surface temperature variations. *Science*, 289: 1719-1724.

Linsley, B.K., 1996. Oxygen-isotope record of sea-level and climate variations in the Sulu Sea over the past 150,000 years. *Nature*, 380: 234-237.

Linsley, B.K., Thunell, R.C., Morgan, C. and Williams, D., 1985. Oxygen minimum expansion in the Sulu Sea, Western Equatorial Pacific, during the last glacial low stand of sea level. *Mar. Micropaleontol.*, 9: 395-418.

Liu, T., 1985. *Loess and Environment*. China Ocean Press, Beijing, 251 pp.

Matsumura, H. and Zuraina, M., 1999. Metric analyses of an early holocene human skeleton from Gua Gunung Runtuh, Malaysia. *Amer. J. Physic. Anthropol.*, 109(3): 327-340.

McGregor, G.R. and Nieuwolt, S., 1998. *Tropical climatology*. J. Wiley & sons, Chichester, 339 pp.

Miao, Q., Thunell, R. and Anderson, D.M., 1994. Glacial-Holocene carbonate dissolution and sea-surface temperatures in the South China and Sulu seas. *Paleoceanogr.,* 9(2): 269-290.

Molfino, B. and McIntyre, A., 1990. Precessional forcing of the nutricline dynamics in the Equatorial Atlantic. *Science*, 249: 766-769.

Mosimann, J.E., 1965. Statistical methods for the pollen analyst : multinomial and negative multinomial techniques. In: B.a.R. Kummel, D. (Editor), *Handbook of paleontological techniques*. W.H. Freeman, San Francisco, pp. 636-673.

Moss, P.T. and Kershaw, A.P., 2000. The last glacial cycle from the humid tropics of northeastern Australia: comparison of a terrestrial and a marine record. *Palaeogeogr. Palaeoclimatol. Palaeoecol.*, 155: 155-176.

Nair, R.R. et al., 1989. Increased particle flux to the deep ocean related to monsoons. *Nature*, 338: 749-751.

Nicholson, P.H., 1981. Fire and the Australian Aborigine - an enigma. In: A.M. Gill, R.H. Groves and I.R. Noble (Editors), *Fire and the Australian Biota*. Australian Academy of Science, Canberra, pp. 55-76.

Okada, H. and Honjo, S., 1973. The distribution of oceanic coccolithophorids in the Pacific. *Deep Sea Res.*, 20(4): 355-374.

Paillard, D., Labeyrie, L. and Yiou, P., 1996. Macintosh program performs time-series analysis. *Eos Trans. AGU*,, 77: 379.

Porter, S.C., 2001. Chinese loess record of monsoon climate during the last glacial-interglacial cycle. *Earth-Sc. Rev.*, 54: 115-128.

Porter, S.C. and An, Z., 1995. Correlation between climate events in the North Atlantic and China during the last glaciation. *Nature*, 375: 305-308.

Prell, W.L. and Curry, W.B., 1981. Faunal and isotopic indices of monsoonal upwelling : western Arabian Sea. *Oceanol. Acta*, 4: 91-98.

Prell, W.L. and Kutzbach, J.E., 1992. Sensitivity of the Indian monsoon to forcing parameters and implications for its evolution. *Nature,* 360: 647-652.

Sarkar, A., Ramesh, R., S.K., B. and Rajagopalan, G., 1990. Oxygen isotope evidence for a stronger winter monsoon current during the last glaciation. *Nature*, 343: 549-551.

Thouveny, N. et al., 2000. Rock-magnetic detection of distal Ice Rafted Debries: clue for the identification of Heinrich layers on the Portuguese margin. *Earth Planet. Sc. Let.*, 180: 61-75.

Turney, C.S. et al., 2001. Early human occupation at Devil's Lair, Southwestern Austrlia 50,000 years ago. *Quaternary Res.,* 55: 3-13.

van der Kaars, S. and Dam, M.A.C., 1995. A 135,000-year record of vegetational and climatic change from the Bandung area, West-Java, Indonesia. *Palaeogeogr. Palaeoclimatol. Palaeoecol.*, 117: 55-72.

van der Kaars, S. et al., 2001. Late Quaternary palaeocology, palynology and palaeolimnology of a tropical lowland swamp: Rawa Danau, West-Java, Indonesia. *Palaeogeogr. Palaeoclimatol. Palaeoecol.*, 171: 185-212.

van der Kaars, S., Wang, X., Kershw, P., Guichard, F. and Setiabudi, D.A., 2000. A Late Quaternary palaeocological record from the Banda Sea, Indonesia: pattern of vegetation, climate and biomass burning in Indonesia and northern Australia. *Palaeogeogr. Palaeoclimatol. Palaeoecol.,* 155: 135-153.

Vautard, R. and Ghill, M., 1989. Singular spectrum analysis in nonlinear dynamics, with applications to paleoclimatic time series. *Physica*, D35: 395-424.

Wang, B., Wu, R. and Fu, X., 2000. Pacific-East Asian teleconnection: How does ENSO affect East Asian Climate ? *J. Climate*, 13: 1517-1536.

Wang, L. et al., 1999a. East Asian monsoon climate during the Late Pleistocene: high-resolution sediment records from the South China Sea. *Mar. Geol.*, 156(1-4): 245-284.

Wang, L., Sarnthein, M., Grootes, P.M. and Erlenkeuser, H., 1999b. Milleninial reoccurrence of century-scale abrupt events of East Asian Monsoon: a possible heat conveyor for the global deglaciation. *Paleoceanogr.*, 14(6): 725-731.

Wiesner, M.G. et al., 1996. Fluxes of particulate matter in the South China Sea. In: Ittekkot J., Schäfer P., Honjo S. and D. P.J. (Editors), *Particle flux in the ocean*. J. Wiley & Sons, Chichester.

Xio, J.L. et al., 1999. East Asian mosoon variation during the last 130,000 years: evidence from the Loess Plateau of central China and Lake Biwa of Japan. *Quatern. Sc. Rev.*, 18: 147-157.

Yan, X.H., Ho, C.-R., Zheng, G. and Klemas, V., 1992. Temperature and size variabilities of the Western Pacific Warm Pool. *Science*, 258: 1643-1645.

Zhang, Y. et al., 1997. East Asian winter monsoon: results from eight AMIP models. *Climate Dynamics*, 13(11): 797-820.

RESUME :

L'océan Pacifique ouest équatorial, zone océanique la plus chaude du globe, est au cœur des cellules de circulation atmosphérique de mousson (méridienne) et de Walker (zonale). Les assemblages des foraminifères planctoniques, leur géochimie et leur morphométrie ainsi que les assemblages de coccolithophoridés nous ont permis de reconstruire la dynamique climatique de cette zone au Pléistocène récent
Nous avons développé une nouvelle fonction de transfert non biaisée par la structure des écosystèmes comme dans l'étude CLIMAP. Les températures de surface des derniers 185 ka reconstruites par cette méthode varient entre 27 et 29.5°C, en accord avec les estimations des alcénones. La convection atmosphérique liée à ces températures élevées a donc persisté au cours du Pléistocène récent. Ces températures sont modulées par les cycles orbitaux de précession qui forcent également à cette échelle de temps le balancement de la thermocline des océans Indo-Pacifique, suivant un mécanisme similaire à l'El Niño-Oscillation Australe.
A l'échelle du millénaire, la dynamique climatique rapide des cycles de Dansgaard-Oeschger des hautes latitudes est décelée dans les variations d'intensité de la mousson d'hiver Est Asiatique du Pacifique ouest équatorial. Cette mousson est marquée par un cycle de 1500 ans, indépendant du volume global des glaces, donc d'un forcage des hautes latitudes. Un rôle d'amplificateur des changements climatiques rapides est attribué à la dissociation thermale des clathrates de méthane des marges sédimentaires de basses latitudes. En effet, un enregistrement isotopique à haute résolution des isotopes du carbone démontre l'existence de dégazages catastrophiques de ces clathrates de méthane pendant le dernier stade glaciaire.

CLIMATE DYNAMICS IN THE WESTERN EQUATORIAL PACIFIC OCEAN DURING THE LATE PLEISTOCENE

ABSTRACT

The western equatorial Pacific warm pool (WPWP), warmest ocean area of the globe, fuels the meridian monsoon and zonal Walker atmospheric circulation cells. Using planktonic foraminifera assemblages, stable isotope geochemistry and morphometry, and coccolithophorids assemblages, we investigated past climate dynamics of this area during the Late Pleistocene.
We developped a new planktonic foraminifera transfer function which is not biased by the ecosystem structure like was the CLIMAP study. Using this method, the last 185 kyrs SSTs in the WPWP oscillated between 27 and 29.5°C, in agreement with alkenones estimates. The "deep" atmospheric convection over the WPWP was thus a stable feature of the Late Pleistocene climate. These temperatures appear to be modulated by the precession cycles which also force a rocking of the Indo-Pacific thermocline, following an "El Niño-Southern Oscillation-like" mechanism.
At millenial time-scale, the high-latitudes Dansgaard-Oeschger cycles were find in past changes in East Asian winter monsoon strength from the northern edge of the WPWP. A 1500 yrs cycle imprints this monsoon record, which is not ice volume modulated, and thus not driven by some high-latitude process. A potential climatic feedback is attributed to thermal dissociation of methane gas-hydrates from low-latitude sedimentary margins. Indeed, a high-resolution of carbon isotopic changes in the WPWP, exhibits the occurrence of large methane gas-hydrates releases during the last glacial stage.

DISCIPLINE : Géosciences de l'environnement

MOTS-CLES
Paléoclimat, océan Pacifique, microfossiles, températures de surface, production primaire, mousson, ENSO, Pléistocène

Centre Européen de Recherche et d'Enseignement de Géosciences de l'Environnement
Europôle Méditerranéen de l'Arbois – BP80
13545 AIX – EN – PROVENCE CEDEX 4 – FRANCE